Ingeniaritza Goi Eskola Teknikoa
Escuela Técnica Superior de Ingeniería
Bilbao

eman ta zabal zazu
Universidad del País Vasco
Euskal Herriko Unibertsitatea

TESIS DOCTORAL

Prediction of Moulds Wear in High Pressure Die Casting and Plastic Injection Moulding

/

Predicción del desgaste de moldes de inyección de plástico y aluminio

Presentada por:

D. Borja Zabala Igartua

en el

Departamento de Ingeniería Mecánica

de la

Universidad del País Vasco – Euskal Herriko Univertsitatea

para la obtención del grado de

Doctor Ingeniero Industrial

Dirigida por:

Prof. Dr. D. Franck Girot Mata

Dr. Amaya Igartua Aranzabal

Bilbao, Mayo del 2017

eman ta zabal zazu

Universidad del País Vasco
Euskal Herriko Unibertsitatea

Departamento de Ingeniería Mecánica

Escuela técnica superior de ingeniería de Bilbao

TESIS DOCTORAL

Prediction of Moulds Wear in High Pressure Die Casting and Plastic Injection Moulding

/

Predicción del desgaste de moldes de inyección de plástico y aluminio

Autor:

D. Borja Zabala Igartua

Dirigida por:

Prof. Dr. Franck Girot Mata

Dr. Amaya Igartua

Bilbao, Mayo 2017

ACKNOWLEDGMENTS

This work was developed within the European Project MUSIC (MUlti-layers control & cognitive System to drive metal and plastic production line for Injected Components, FP7-FoF-ICT-2011.7.1, under Contract nº 314145). I would like to thanks all the Music coordinator Nicola Gramegna from EnginSoft s.p.a, all the consortium partners, and especially the close collaboration of industrial partners MAIER S. Coop (Plastic Injection), Motultech-Baraldi (lubricant supply for HPDC), AUDI AG (collaboration in thermal fatigue Machine in HPDC), MAGMA Giessereitechnologie GmbH (collaboration in simulation of thermal fatigue), SAEN s.r.l. for supplying materials and for their kind suggestions. Also, we would like to thanks to Padova University, Prof. Franco Bonollo and Prof. Giulio Timelli for their kind collaboration specially for sending to IK4-TEKNIKER, 4 students to make a stage under my supervision to fulfil their Master Thesis on the subject of moulds wear: Valeria Scarpis, Matteo Peggiato, Tonino Cundari and Irene Bramati.

My training in modelling activity was also supported by Powerful EU project that was carried out during a period of 3 Months in the company AVL in Austria with the support from RENAULT Company.

I would like to thank my supervisors and all the laboratory colleagues from IK4-Tekniker that have contributed to the success of this work, offering personal and professional support.

Basic Data

- *Student:* Borja Zabala
- *Professor:* Dr. Frank Girot Mata, Dr. Amaya Igartua
- Project title: Prediction of Moulds Wear in High Pressure Die Casting and Plastic Injection Moulding / Predicción del desgaste de moldes de inyección de plástico y aluminio
- *Abstract*: High Pressure Die Casting and Plastic Injection Moulding are very cost effective and high production rate manufacturing processes. Both consist of introducing at high pressure, high temperature and high speed a fluid material that solidifies inside a mould. These moulds have to endure thousands of cycles on this aggressive media, which leads to a wear amount that limits the mould life, requiring repairing, as well as unexpected production stops. This involves high cost in maintenance and reparation. The damage of the moulds is ruled by different wear mechanisms. Some of them are common for both manufacturing processes like erosion and corrosion, while some others, are specific like abrasion in Plastic Injection Moulding and die soldering and thermal fatigue in High Pressure Die Casting. This doctoral thesis deals with all these wear mechanisms, setting protocols to simulate them at laboratory scale and studying the influence of different process parameters, in order to predict the wear of moulds.
- *Keywords*: High-Pressure-Die-Casting, Plastic-Injection-Moulding, Mould, Wear, Abrasion, Erosion, Corrosion, Die-Soldering, Thermal Fatigue, Modelling

Table of contents

1 Introduction 27

2 Literature review 33

2.1 Wear mechanisms in Moulds 33
2.1.1 Wear mechanisms in HPDC 33
2.1.2 Wear mechanisms in PIM 41
2.1.3 Summary of wear mechanisms 44

2.2 Wear mechanisms simulation at laboratory scale 44
2.2.1 HPDC wear mechanisms simulation at laboratory scale 45
2.2.2 PIM wear mechanisms simulation in laboratory scale 57
2.2.3 Discussion 62

2.3 Mathematical models applied to predict wear on moulds 63
2.3.1 Models for HPDC moulds wear 66
2.3.2 Models for PIM moulds wear 78
2.3.3 Summary of models for moulds wear prediction 80

2.4 Conclusions 82

2.5 Innovative aspects 83

3 Simulation of wear mechanisms at laboratory scale 85

3.1 Methodology 86

3.2 Thermal Fatigue in HPDC 90
3.2.1 Objective 90
3.2.2 Materials and methods 90
3.2.3 Results and discussion 97
3.2.4 Model assessment 106

3.3 Die Soldering in HPDC 108
3.3.1 Objective 108
3.3.2 Materials and methods 108
3.3.3 Results and discussion 112
3.3.4 Model assessment 118

3.4 Abrasion in PIM 119
3.4.1 Objective 119
3.4.2 Materials and methods 119
3.4.3 Results and discussion 122
3.4.4 Model assessment 127

3.5 Erosion in PIM and HPDC moulds 129
3.5.1 Objective 129
3.5.2 Description of the test devices 129
3.5.3 Results and discussion 131
3.5.4 Model assessment 134

3.6 Corrosion in PIM and HPDC moulds 136
3.6.1 Objective 136
3.6.2 Materials and methods 136

3.6.3 Results and discussion 138
3.6.4 Model assessment 142

4 Wear modelling implementation 145

4.1 Example of use in HPDC 148

4.2 Example of use in PIM 148

5 Conclusions 151

6 Bibliography 157

7 Acknowledgments 160

8 Annexed articles 161

8.1 Friction and wear of a piston ring/cylinder liner at the TDC: experimental study and modelling 162

8.2 On the nature of high pressure die casting die failures 184

8.3 Multiparametric study of Leidenfrost point and wettability of lubricants on HPDC dies 195

8.4 Evaluation HPDC Lubricant Spraying for Improved Cooling and Die Protection 209

Glossary

HPDC: High Pressure Die Casting

PIM: Plastic Injection Moulding

TGA: Thermo Gravimetric Analysis

DSC: Differential Scanning Calorimeter

EIS: Electrochemical Impedance Spectroscopy

HTMF: High Temperature Mechanical Fatigue

DOE: Design of experiments

LFP: Leidenfrost Point

CA: Contact Angle

HTC: Heat Transfer Coefficient

Ra: Roughness Average

Rp: Maximum Profile Peak Height

Rz: Average Maximum Height of the Profile

Ssk : measure of the asymmetry of the amplitude density curve.

SKu: is a measure of the peakedness of the amplitude density curve. For a profile with a Gaussian amplitude density curve SKu is 3.

SBi : Surface bearing index, This is the ratio of the RMS deviation over the surface height at 5% bearing area.

Deposition techniques:

PVD: Physical Vapour Deposition

CVD: Chemical Vapour Deposition

PACVD: Plasma Assisted Chemical Vapour Deposition

LTPVD: Low Temperature Physical Vapour Deposition

Plastics:

PVC: Polyvinyl Chloride

ABS: Acrylonitrile Butadiene Styrene

ASA: Acrylonitrile Styrene Acrylate

PC: Polycarbonates

PMMA: Poly(methyl methacrylate)

PA: Polyamide

RESUMEN EN CASTELLANO

En esta tesis doctoral se han abordado los principales mecanismos de desgaste que aparecen en los moldes de inyección de plástico y aluminio. Estos dos procesos de fabricación son muy eficientes, de producción rápida y efectivos en coste. Ambos consisten en inyectar a alta temperatura, presión y velocidad un fluido (plástico y aluminio respectivamente), en un molde cuya cavidad da forma a la pieza final tras el proceso de solidificación. Este molde tiene que aguantar cientos de miles de ciclos en este entorno agresivo, lo cual lleva a limitar la vida del molde debido al desgaste que sufren, requiriendo reparaciones y paradas de producción inesperadas. El desgaste de los moldes se genera debido a distintos mecanismos de deterioro. Algunos de estos mecanismos son comunes para los procesos de inyección de plástico y aluminio, como la erosión y la corrosión. Mientras otros son específicos de cada proceso, como la abrasión en la inyección de plástico reforzado con fibras o la adhesión del aluminio (die soldering) y la fatiga térmica, en la inyección de aluminio.

A lo largo del documento se propone una metodología cuyo objetivo final es generar modelos de desgaste gracias a los cuales se podría llegar a mejorar la capacidad de predecir la vida de los moldes y reducir los problemas que esto genera. Otros **objetivos** de esta tesis pueden listarse de la siguiente manera:

- Mejorar la comprensión de la naturaleza de los mecanismos de desgaste e identificar los parámetros que los influencian.
- Selección de los mecanismos de desgaste críticos que se deben predecir, y los parámetros que se deben analizar.
- Generación de protocolos de ensayo que posibilitan simular a escala de laboratorio los mecanismos de desgaste más representativos basados en ensayos previos en literatura así como nuevos desarrollos originales.
- Generar un diseño de experimentos para cada uno de los mecanismos de desgaste, que variando los parámetros que más afectan, hacen posible la generación de ecuaciones para modelizar el desgaste de moldes.
- Realizar los ensayos, generando datos experimentales consistentes, y analizar los datos y generar una selección de materiales, tratamientos superficiales y fluidos que mejoren la durabilidad del proceso.
- Generar los modelos predictivos a partir de los resultados experimentales, definiendo los rangos de parámetros en los cuales es aplicable, así como especificando la calidad de dichas predicciones.
- Aplicación del modelo a algunos ejemplos, mostrando como se utilizaría por parte de un diseñador de moldes o de un técnico de mantenimiento.

La estructura del manuscrito incluye tras la introducción una **revisión bibliográfica**, en la cual se han identificado los distintos mecanismos de desgaste de moldes, determinando su naturaleza y determinando los parámetros que afectan su aparición. Después se han analizado los equipos y **protocolos experimentales** que han sido utilizados para simular los mecanismos de desgaste a escala de laboratorio, para seleccionar los más apropiados para utilizar en esta tesis. Se han revisado también los **modelos matemáticos** disponibles en la literatura que han sido desarrollados para predecir la aparición y desarrollo de los fallos. Se han presentado unas conclusiones parciales acerca de esta revisión bibliográfica y se han resaltado los **aspectos más innovadores** de esta Tesis Doctoral respecto al estado del arte.

Después, en el capítulo tercero incluye el grueso del trabajo realizado acerca de cada uno de los mecanismos de desgaste seleccionados para ser estudiados, en el siguiente orden: **fatiga térmica, die soldering, abrasión, erosión y corrosión**. La fatiga térmica y el die soldering están referidos únicamente a la inyección

de aluminio, mientras que el apartado de abrasión únicamente a la inyección de plástico. Como la erosión y corrosión son mecanismos de desgaste comunes a los dos procesos, se ha realizado una experimentación y modelado comunes para ambos y se han presentado de una manera común. En este capítulo **se detallan los materiales y métodos usados, se describen y discuten los resultados experimentales, y se presenta el modelo creado.**

A lo largo de los capítulos 2 y 3, la **metodología** aplicada a los distintos mecanismos de desgaste para obtener los modelos, ha sido similar. Ha consistido en seleccionar las variables que más influencia tienen en el proceso, seleccionando posibles modelos para cada mecanismos de desgaste. Selección del ensayo a realizar para simular en el laboratorio cada uno de los mecanismos de desgaste, teniendo en cuenta la posibilidad de variar los parámetros de interés para generar los modelos. Realizar el diseño de experimentos para realizar los ensayos de cada mecanismo de desgaste variando los parámetros de interés. Creación del modelo, en general mediante el método multi lineal, generando ecuaciones que describen el comportamiento del desgaste en función de los parámetros. Se ha evaluado también la adecuación del modelo mediante el análisis de varianza del modelo, con el cálculo del coeficiente R^2 y la comprobación de que las suposiciones realizadas, normalidad y varianza σ^2 constante, son correctas.

En el capítulo 4, se han mostrado **ejemplos** de cómo se utilizarían estos modelos por parte de los usuarios de inyección de aluminio y plástico para la mejora de decisiones a la hora de diseñar el molde o planear las paradas de mantenimiento. En estos modelos pueden variarse las condiciones del proceso (presiones, velocidades, temperaturas), y predecir los ciclos hasta llegar a la aparición del fallo o hasta un desgaste inadmisible. Ya que estos modelos han sido generados a partir de ensayos de laboratorio, necesitarán de una calibración previa para mejorar la precisión de la predicción.

Finalmente en el capítulo 5 se han listado las principales **conclusiones** de este trabajo y los posibles pasos futuros. El documento incluye la lista de referencias incluidas en el texto, un anexo de los artículos publicados en revistas o presentados en congresos relacionados con la tesis, así como los agradecimientos a las entidades y personas que han contribuido a este trabajo.

La **fatiga térmica**, se ha puede asegurar que es creada debido a la repetición de un calentamiento muy poco homogéneo y un enfriamiento rápido del molde de inyección de aluminio. Los parámetros que se han identificado como más influentes en su aparición han sido algunas propiedades del material de molde (tensión de fluencia, módulo de Young, capacidad de deformación, resistencia al revenido…), evolución de la temperatura durante el ciclo en la superficie y hacia el interior de la superficie, así como concentradores de tensión geométricos y superficiales. En la literatura pueden encontrarse distintos tipos de ensayos utilizados para simular este fenómeno, diferenciados sobre todo por la forma en que se calienta la muestra a ensayar (inducción, mediante resistencias, baño en aluminio fundido, quemando gas natural…) y por la forma de enfriamiento (baño en agua, soplado de aire…).

En esta Tesis Doctoral, dos han sido los ensayos de laboratorio seleccionados para generar la información necesaria para los modelos. Uno de ellos es un ensayo innovador el cual no existía previamente en la literatura, basado en un calentamiento mediante inducción y un enfriamiento interior de circulación de un fluido y esprayado exterior, y capaz de realizar tantos ciclos como se requieran de una manera automática. Se ha validado la capacidad del banco para simular el ciclo térmico que aparece en los moldes, con los parámetros de ensayo puede generarse la aparición de grietas en el rango de los moldes de inyección de aluminio, hacia los 10000 ciclos. La creación de un modelo que conecte directamente los campos de temperatura del molde con los ciclos de aparición del fallo, es posible de realizar mediante la nueva máquina

de fatiga térmica desarrollada, aunque por el momento los datos generados son pocos para decir que la ecuación generada es fiable, y necesitarán de una mayor experimentación.

El estado del arte actual para la predicción de la aparición de grietas implementado en softwares de simulación del proceso de inyección de aluminio (capaces de calcular las temperaturas de pieza de aluminio y molde), consiste en el cálculo de las tensiones generadas por la distribución de temperaturas en la superficie y hacia el interior del molde. Con el objetivo de mejorar la predicción de los modelos basados en este cálculo de tensiones debidas al ciclo térmico, se ha utilizado un ensayo de fatiga mecánica a alta temperatura, que ha sido utilizado para generar curvas de fatiga que relaciona las tensiones generadas con los ciclos hasta el fallo. Esta curva generada es válida para materiales de tipo H11 y H13, trabajando en el rango de temperaturas de 300 a 500ºC, y un nivel de tensión entre 820 y 900 MPa. Esta aproximación ha sido utilizada para calcular mediante software el nivel de tensión aparecido en la placa de ensayo de la máquina de fatiga térmica, replicando el ciclo de referencia generado por la máquina. Algunas de las variables de enfriamiento han sido variadas, y se ha visto que el rango de aparición de grietas se espera aparezcan entre 6000 y 17000 ciclos. De entre los parámetros estudiados, se ha visto que la mayor influencia es debida a la intensidad del esprayado, mientras que otros parámetros estudiados tienen una influencia pequeña. Por ejemplo, la posición de los canales de refrigeración bajo la zona esprayada y un mayor diámetro del canal, mejoraría un poco la vida. Los canales más cercanos a la superficie tendrían también un efecto positivo en su vida.

Los principales aspectos innovadores de esta parte de fatiga térmica están relacionados con el procedimiento experimental de la nueva máquina de fatiga térmica, que genera un ciclo térmico muy similar a los que aparecen en el molde y posibilita el estudio de la relación directa de éste con la aparición de grietas. En cuanto a las curvas S-N (Wohler) que relacionan las tensiones generadas y los ciclos hasta el fallo, no es fácil encontrarlas en literatura. Siendo ésta, una manera de hacerlas disponibles para usuarios de software que requieran de dicha curva.

Los futuros pasos a realizar acerca de la actividad de fatiga térmica serán sobre todo continuar con la experimentación comenzada con la máquina de fatiga térmica. Los datos generados serán utilizados para validar el modelo de fatiga térmica generado. Esto puede hacerse tanto validando el método de cálculo de tensiones y uso de las curvas S-N, o generando directamente ecuaciones que conectan el campo de temperaturas y los ciclos hasta el fallo. La curva S-N generada, de los ensayos de fatiga mecánica a alta temperatura es también mejorable, generando más datos experimentales. Se ha observado que esta ecuación podría ser aplicable tanto a materiales H11 como H13 y en un rango de temperaturas de 300 a 500ºC, a una dureza de 43HRc, pero debería estudiarse más en detalle la influencia de diferentes microestructuras y durezas, así como distintos materiales y tratamientos superficiales. Tras la generación de las ecuaciones definitivas, éstas deberían de ser validadas o calibradas con el seguimiento del desgaste de moldes reales.

En el proceso de **die soldering** generado en la superficie del molde debido a la afinidad química entre el molde y el aluminio inyectado, se han identificado como variables más influyentes, la naturaleza y constituyentes de la aleación de aluminio, la naturaleza del material del molde, los tratamientos superficiales, las capas de lubricante, la rugosidad y las condiciones de operación (presión, temperatura y velocidad). Los principales ensayos utilizados en literatura para simular este fenómeno han sido revisados, y uno de ellos, el ensayo pin on disc, ha sido seleccionado con variaciones significativas. La principal variación consiste en el uso de un lubricante en el contacto entre aleación de aluminio y acero de molde endurecido H13, midiendo el tiempo de fallo de dicha capa protectora como el comienzo del die soldering, introduciendo como variables que influencian su aparición la temperatura, la presión, la velocidad y la química del lubricante depositada

como protector del disco de acero. Experimentando sobre el efecto de las variables significativas, se ha generado de un modelo de predicción del fallo. Los principales modelos existentes en literatura están basados en la temperatura crítica y el tiempo de exposición a dicha temperatura que generaría el soldering, aunque todavía este tipo de modelos no han sido validados con ensayos experimentales.

Dependiendo de las condiciones de ensayo, los ciclos hasta el fallo de "die soldering" pueden variar desde unos pocos ciclos hasta varios miles. Se ha mostrado que la temperatura es muy crítica, ya que tiene una influencia exponencial, y la presión juega también un papel importante (influencia logarítmica) en el fallo de lubricante y en el comienzo del soldering. Se ha visto también que una química y un índice de viscosidad del lubricante apropiado, mejora hasta 5 veces la resistencia al soldering, aunque el efecto de la velocidad, se ha visto que es despreciable. El coeficiente de fricción se ha medido mediante un ensayo pin on disc, el cual está relacionado con la capacidad del lubricante a facilitar el flujo del aluminio hacia el interior del molde y su comportamiento como agente desmoldeante.

La medida del espesor del lubricante y el comportamiento del lubricante en el ensayo termogravimétrico han mostrado la posibilidad de correlacionar distintas propiedades físicas con propiedades de lubricantes y con la aparición del die soldering en el ensayo pin on disc. El lubricante que generaba mayor espesor de capa y tenía mayor resistencia a la temperatura, mostraba también una mejora en la capacidad de prevenir el soldering.

La mejora de la mojabilidad del lubricante en la superficie del molde es posible reduciendo el ángulo de contacto e incrementando la temperatura Leidenfrost de éste. Se ha propuesto un procedimiento para mejorar la efectiva selección y optimización del lubricante. En primer lugar, se debiera seleccionar una combinación de lubricante y superficie de molde que minimice el ángulo de contacto, y como segundo paso, se puede maximizar la temperatura Leidenfrost mediante dos parámetros superficiales y 3 parámetros de lubricación. La configuración óptima consiste en acero H13 oxidado, lubricándolo con el lubricante estudiado "A", diluyéndolo al 3% y mezclándolo con agua dura y pulverizándolo con boquilla grande.

El principal aspecto innovador de la parte de "die soldering" es debida a abordar la problemática de la lubricación de los moldes de inyección de aluminio. Son varias las publicaciones en las cuales se resalta la importancia de la capa lubricante en la aparición del soldering, aun así son muy pocos los que han estudiado las propiedades de éstos. Los protocolos de ensayo generados en esta Tesis Doctoral pueden ser un buen primer paso para mejorar la selección y desarrollo de lubricantes para esta aplicación.

Los futuros pasos a realizar acerca del die soldering para mejorar la predicción estarían orientados a la ampliación de la experimentación a distintos lubricantes de inyección de aluminio (otros hidrosolubles, no hidrosolubles o incluso en forma de polvo), distintas aleaciones de aluminio y distintos tratamientos superficiales de molde (p.e. nitruraciones o recubrimientos PVD). Además puede ampliarse el estudio de parámetros (velocidad, presión y temperatura) comprobando la relación cruzada entre ellos. Otra mejora propuesta es la modificación de geometría de pin a uno esférico para evitar el efecto borde, teniendo siempre un punto de contacto. Por último, la predicción basada en el modelo del fallo de lubricante en el ensayo pin on disc, es muy distante de las condiciones reales de inyección. Por tanto hará falta una calibración de este modelo a partir de resultados reales de molde.

La **abrasión** del molde de inyección de plástico que aparece cuando el flujo del plástico reforzado con fibras es paralelo a la cavidad del molde, se ha identificado en la literatura que está influenciado de los materiales de plástico y molde, y de las condiciones de flujo (velocidad y presión). De una manera similar a algunas de las referencias bibliográficas revisadas, un ensayo tribológico tipo "block on plate" ha sido seleccionado para

simular este mecanismo de desgaste, y crear un modelo de comportamiento a partir de los resultados. La creación de este modelo es la principal novedad de este apartado, ya que la modelización del desgaste de moldes de inyección de aluminio se ha visto que está incluso menos avanzado que la de moldes de inyección de plástico.

Se han realizado ensayos "block on plate" a distintos niveles de presión y velocidad, donde el material de molde 1.2738 pretratado (HH) y no pretratado (BM), ha sido colocado como disco. Estos discos, han sido ensayados también con distintos tratamientos superficiales (recubrimiento TiN, Nitruración Sales, Nitruración Iónica, y electrolítico Ni-PTFE). El material de molde ha sido calentado a 100ºC para estar cerca de las condiciones de trabajo del molde. El bloque de material plástico de 4x4x4 mm^3 está realizado de material Poliamida reforzado con 25% de fibra (PA+25%FV) de vidrio para los ensayos de desgaste. También se han probado otros dos materiales plásticos (PMMA y PC) para evaluar la capacidad anti-adherente de las superficies a través de la medida de fricción en el ensayo. Estos dos materiales plásticos a pesar de que generan muy alta fricción, no generan un desgaste medible. La reducción de la fricción del PMMA y el PC mediante el Ni-PTFE ha sido la solución más efectiva. La reducción de la fricción de la PA+25%FV ha sido más efectiva mediante el TiN. Para la protección frente al desgaste, se ha visto necesaria para el uso de la PA+25%FV, y en este caso la Nitruración Iónica y el TiN serían las superficies más adecuadas. Se ha comprobado, que la resistencia al desgaste está muy relacionada con la dureza de la superficie, y por tanto el Ni-PTFE que es blando, no ha mejorado la resistencia al desgaste del substrato. La aplicación de los distintos tratamientos superficiales se comportaron de una similar tanto aplicados sobre el 2738HH como el BM. La aplicación de tratamientos superficiales ha aumentado sensiblemente la rugosidad de la superficie del molde, lo cual podría ser trasladado a un incremento de la rugosidad e influenciar el aspecto de la pieza final de plástico. La rugosidad medida en Ra, puede clasificarse de menor a mayor en el siguiente orden: substrato 1.2738 0,55 µm, Ni-PTFE 0,6 µm, TiN 0,7 µm, Nitruración Iónica 0,75 µm, Nitruración Sales 0,8 µm.

Los resultados de desgaste han sido utilizados para generar un modelo de predicción de desgaste en función de las variables estudiadas (presión, velocidad y dureza del material de molde). En cuanto a los resultados de fricción se ha visto que no son muy sensibles a variaciones de velocidad, mientras que el incremento de la presión reduce un poco los valores de fricción. La creación de un modelo de fricción no se ha visto que tenga sentido, aunque se ha preparado una tabla de valores de coeficientes de fricción para combinaciones de materiales de molde y plástico, para seleccionar las soluciones más óptimas.

Posibles futuros pasos podrían ser la mejora del modelo presentado, aumentando los rangos de presión y velocidad analizados, así como el estudio de otros plásticos con distinta composición de % de fibra de vidrio. La aproximación seleccionada para este mecanismo de desgaste está relativamente alejado de las condiciones reales del molde real, debido a que en el ensayo, el plástico está en un estado semi sólido. Queda abierta la posibilidad de crear en un futuro algún nuevo equipo que sea capaz de trabajar con plástico en condición de fundido. Similarmente a los demás mecanismos de desgaste, el principal paso de futuro estará relacionado con la validación y calibración del modelo de abrasión a partir de observaciones del desgaste en moldes reales, en zonas donde aparece este mecanismo de desgaste a distintas condiciones de presión y velocidad, y con insertos de distintos materiales. Tras la comparación del desgaste predicho y el real medido, se podría corregir la ecuación para ver cuantos ciclos de ensayo corresponden a ciclos de inyección mediante algún coeficiente.

La **erosión** es un mecanismo de desgaste identificado en la inyección de aluminio y plástico. Se ha visto que este tipo de mecanismo de desgaste está influenciado principalmente por las características del flujo

(velocidad y ángulo de impacto), cantidad de partículas duras en el flujo (relacionado con impurezas y la temperatura de flujo en inyección de aluminio y con el porcentaje de refuerzo de fibras en el caso de la inyección de aluminio), y también está influenciado por las propiedades del material de molde a la temperatura de trabajo. Por el contrario, la erosión por impacto de líquido no se ha considerado probable que aparezca en el molde en un periodo corto de plazo, la erosión por cavitación tampoco ha sido estudiada. El protocolo de ensayo Air Jet Erosion Test, basado en la norma ASTM G76, ha sido seleccionado para simular la erosión debida a las partículas duras, así como el ensayo de Gravelómetro basado en la ASTM D3170 para utilizar el material plástico reforzado como agente erosivo. Ensayos similares al primero, han sido previamente utilizados en la literatura para el desgaste de moldes, pero el gravelómetro, se ha utilizado por primera vez en la bibliografía, utilizando como agente erosivo el material plástico. Los modelos matemáticos para predecir el fallo de erosión han sido múltiples en literatura, aunque no han sido utilizados explícitamente para la predicción de este fallo en moldes.

La combinación de los resultados del Air Jet Erosion Test y el Gravelómetro han sido utilizados para crear un modelo de comportamiento respecto a la erosión común para la inyección de plástico y aluminio. Los parámetros que más influencia han presentado son la velocidad y el ángulo de impacto, así como la dureza superficial del material del molde. Los resultados en el Air Jet Erosion Test han mostrado que pequeñas diferencias en la microestructura y tamaño de grano, así como pequeñas diferencias en la temperatura de molde (ej. 75ºC), son despreciables respecto a la influencia del ángulo y velocidad de impacto. Se ha comprobado con el ensayo del Gravelómetro que los plásticos no reforzados no realizan un desgaste medible en la superficie del molde. De las soluciones superficiales ensayas ante la PA+25%FV, el recubrimiento TiN aplicado por PVD y la Nitruración Iónica se encontró que eran las más adecuadas para esta aplicación. Es también de interés comentar que la Nitruración por Sales, perdió con cierta facilidad la capa de combinación en el ensayo, pero la capa de difusión no se desgastaba apenas.

Los posibles futuros pasos para mejorar la predicción de la erosión en moldes, estarían sobre todo orientados a realizar la validación y calibración del modelo de erosión a partir de observaciones del desgaste en moldes reales, en zonas donde exista erosión con distintos ángulos de impacto, condiciones de flujo, y en insertos con distintas durezas. La metodología implementada, se podrá utilizar para desarrollar nuevos materiales o lubricantes que incrementen la vida de los moldes.

La **corrosión** es un mecanismo que aparece también en inyección de aluminio y plástico, debido a las duras condiciones de trabajo de los moldes (presencia de gases, humedad y alta temperatura). Diferentes ensayos (como la niebla salina o ensayos de polarización) han sido utilizados para simular este mecanismo de desgaste en el laboratorio. En esta Tesis Doctoral se ha utilizado la técnica Espectroscopia de Impedancia Electroquímica (EIS). Se ha utilizado como electrolito NH_4Cl al 1% de dilución, simulando los gases Cl_2 y el NH_3 que podrían estar presentes en un molde de inyección según el plástico inyectado. Los materiales de molde estudiados han sido H11 y H13 para la inyección de aluminio y los substratos 2738HH y 2738BM, con los tratamientos superficiales antes comentados, para la inyección de plástico. La principal ventaja de esta técnica es ser acelerada y a priori no es destructiva. A partir de estos resultados de corrosión en función del material del molde, se ha creado una tabla de coeficientes de seguridad para poder realizar una selección apropiada, prediciendo el fallo por corrosión respecto al fallo de un material ya conocido.

Se ha visto que la Nitruración de Sales aplicada sobre el substrato 2738HH proporciona una buena protección frente a la corrosión, pero tal vez debido a ser un tratamiento no demasiado homogéneo, no dio buen resultado cuando fue aplicado al substrato 2738BM. Además la resistencia a la corrosión se redujo con el tiempo de exposición al electrolito. Las siguientes opciones para alargar la vida a corrosión fueron el Ni-

PTFE (aplicado sobre cualquiera de los substratos), seguido del TiN (aplicado también sobre cualquiera de los substratos). En general, los tratamientos aplicados sobre el substrato 2738HH presentaron un comportamiento algo mejor que los aplicados sobre el 2738BM. Por el contrario, cuando se ensayaron los substratos solos, el 2738BM tenía una mayor resistencia a la corrosión que el 2738HH, y el H11 tenía mejor resistencia a la corrosión que el H13. Ambos, el H11 y el 2738BM tienen una menor dureza y tamaño de grano mayor que H13 y 2738HH respectivamente.

El recubrimiento TiN aplicado sobre el substrato de acero 2738HH resultó en la mejor solución global para la inyección de plástico reforzado con fibra de vidrio, generando el mínimo coeficiente de fricción de 0,4, y el mínimo desgaste de entre los ensayos de desgaste, y una resistencia a la corrosión relativamente alta, con un factor de seguridad 6 veces mayor que el acero de referencia 2738BM.

Como actividades futuras acerca de la corrosión, similarmente a los otros mecanismos de desgaste, se debería realizar una validación de la predicción con moldes reales. En este caso, una vez identificada la resistencia a la corrosión del material de referencia en un molde real, se deberían evaluar la durabilidad de moldes tratados para calibrar y validar los coeficientes de seguridad propuestos.

1 Introduction

High Pressure Die Casting (HPDC) is a single step and high production rate manufacturing process of light alloy castings. The resulting pieces have close dimensional tolerances and smooth surface finish. HPDC is a very cost efficient method, however, the maintenance and initial costs of the mould (around 20% of the total) [1] limits the competitiveness of the process seriously.

The maintenance cost limit is due to mould wear. A production of 100-300 thousand castings per die is a common series in high-pressure die-casting, although some dies fail even after 5000-25000 cycles. According to a questionnaire recently performed in the *StaCast* and *Music* European projects [71], about the 57% of the HPDC dies fail prematurely. Therefore, a better understanding of the wear mechanisms nature and the main parameters affecting them are needed.

During aluminium die-casting, molten aluminium is injected into the mould at temperatures of 670-710°C, velocities of 30-100 m/s and pressures of 50-80 MPa. Thus, the surface temperature of the die reaches around 400-450°C one second after metal injection and then the die cools to around 150-200°C due to the spray, giving a temperature variation of approximately 250°C throughout the casting cycle [2].

Die-casting dies are prone to surface damage, what influence the resulting casting quality or even force to stop the production process. Visual inspection of damaged mould allowed identifying the most common failure mechanisms (see figures 1 and 2). Even if they are connected to each other, a short list is commonly accepted:

1. Thermal fatigue: Cracks generated due to alternate heating and cooling of the die during the die-casting cycle. Involves two different failure types named heat checks and corner cracking.
2. Erosion wear: Loss of material due to mechanical interaction between surface and the casting fluid flow. An extensive erosion wear does not allow die soldering to develop. Involves three different failure types: liquid impingement erosion, solid particle erosion and cavitation erosion.
3. Die soldering: Intermetallic chemical and mechanical reactions in the die surfaces generating adhesion of the casting fluid to the die.
4. Corrosion wear: Diffusion or dissolution of the die in the melt.

There are less common catastrophic failures due to thermal shocks (gross fracture) or over-heating of die material, which causes instability of mechanical properties [3]. It is commonly used the term washout to refer a combination of mechanical and chemical wear, so contribution of erosion, die soldering and corrosion. Material washout is mainly observed in regions close to the ingate where high melt velocities are achieved.

The in-service tool life of a die can be prolonged with lower thermal gradients, i.e. lower stresses. These stresses can be reduced by a proper: (a) die design (without sharp edges or corners, and with adequate cooling channels distribution); (b) selection of die material and relative heat treatment, which enables higher resistance to heat checking and tempering during operation; (c) die manufacturing without surface deformation and temperature development during mechanical machining, grinding or electro-discharge machining, which cause phase transformations and residual stresses; (d) stress relieving heat treatment after die manufacturing; and (e) surface engineering techniques, such as PVD (physical vapour deposition) and CVD (chemical vapour deposition) coatings, weld cladding and functionally graded materials (FGMs) [4].

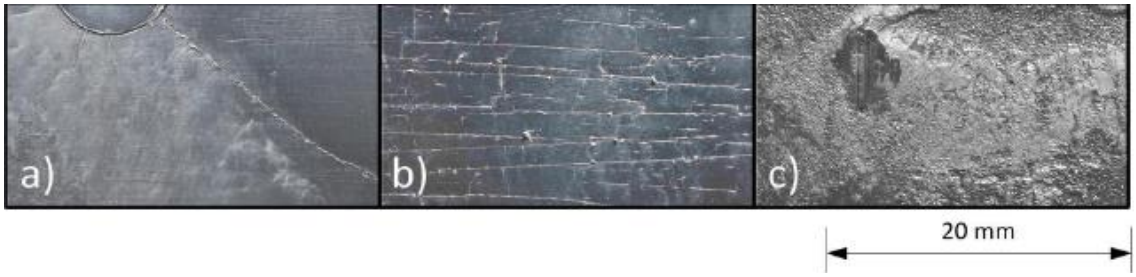

Figure 1. Detailed picture from tension cracks (a), heat checks (b) and washouts (c). [5]

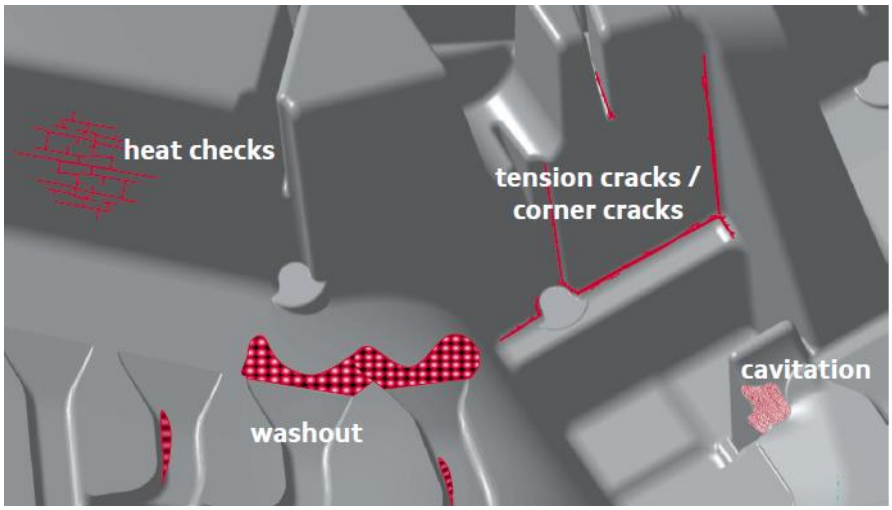

Figure 2. Schematic picture of the different damage in a die. [5]

Polymer Injection Moulding (PIM) is also a single step and high production rate manufacturing process, of plastic parts in this case, resulting in parts of very precise dimensions and geometries and low roughness's (Ra 0.2～0.025μm), and the initial cost of the mould is similar to the HPDC. The main problems of PIM are related to unexpected production stops, maintenance and reparation costs, or delays in delivery due to wear. The rising demands on quality (e.g. aesthetic requirements) and characteristics to fulfil of the injected parts can be solved by a correct design of the mould, optimizing the working conditions and the correct selection of polymer to be injected, but usually it is necessary to use additives in plastics to fulfil some requirements. Some of them can be:

- *Plasticizers*: to adapt to manufacturing process (elasticity, viscosity...)

- *Reinforcers:* long or short fibres, whiskers, grains, micro pearls...

- *Flame retardants:* there exist up to 5 different types of flame retardants

- *Colorants:* in the mass, not only for surface

- *Stabilizers:* for oxidation, UV photo-degradation

To resist the high injection pressures (>100bar) and temperatures (150ºC-300ºC) of the polymer with the additives represent a challenge for the materials of moulds. Particularly, when the polymer contains glass fibre reinforcements, which are very hard and abrasive generate noticeable wear in the mould. Other additives like TiO_2, used as white pigment can generate a similar failure as well [6,7]. This kind of additives,

depending of the flux conditions can lead to two different wear mechanisms, as showed in figure 3: erosion in mould regions where frontal impact of the plastic flux appears while abrasion mechanism is identified when flux is parallel to the mould surface.

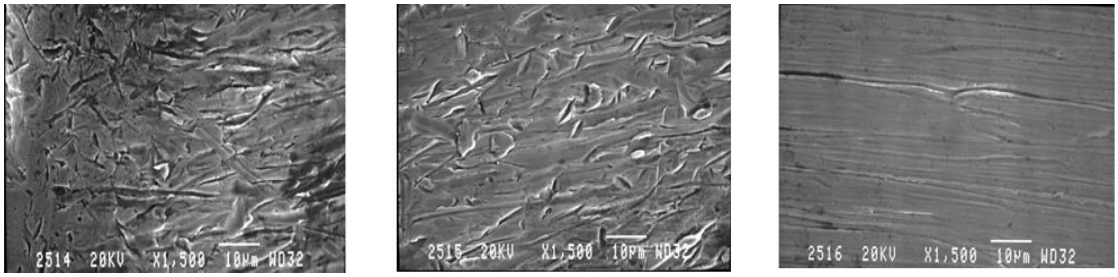

(a) (b) (c)

Figure 3: Microscope image of wear near a gate of a mould (a) erosion appearing by frontal collision in an edge (b) abrasion wear at 250µm from the edge and (c) 2 mm far from the edge [31]

The overheating of plastic material can lead to gas release resulting in a local corrosion of the mould. Regarding to molecular chains of polymers, Polyamide (PA) release NH_3 and Polyvinyl chloride (PVC) releases Hydrochloric acid (HCl). Additives like flame retardant usually contains halogens (F, Cl, Br) that can be highly corrosive [8, 9]. Other polymers could release other different acids [10].

Consequently the mould surface is deteriorated due to the different wear mechanisms reducing drastically the quality of injected parts. Any kind of wear of the mould surface can be copied into the injected part surface. The high aesthetic requirements of the parts are one of the reasons to make necessary to avoid any kind of wear scar in cavity surface. Figure 4 shows an example of a damaged mould. The appearance failures make necessary to stop the production, repair the die, and even to change the injected material and reset the injection process parameters. This problem supposes an over cost and a waste of resources (e.g. raw material, energy). To make possible an improvement, it is necessary to improve both the wear resistance and the wear prediction of the moulds.

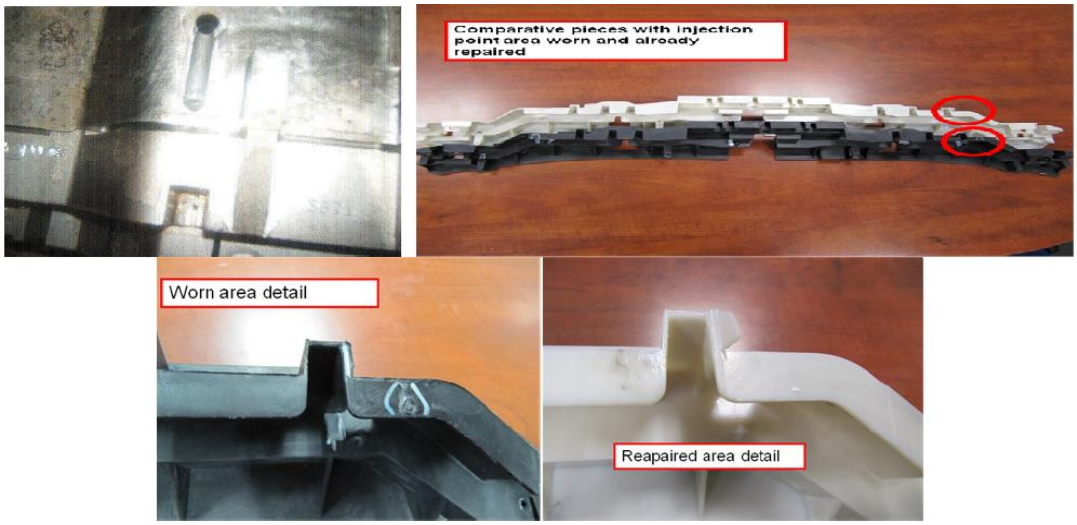

Figure 4: Damaged mould and wear scar copied into the part surface. The result after mould reparation and injected material change.

In the mould, the polymer molecules and fibres are normally oriented with the flow. While the cavity filling, when they are perpendicular to the flow, the speed for the extreme of the fibre or molecule in the centre is higher than for the extreme near the walls. This flow speed difference results in a shear that rotates the molecules and fibres until they are along the flux. In the centre where the speed is uniform they are not oriented as shown in figure 5.

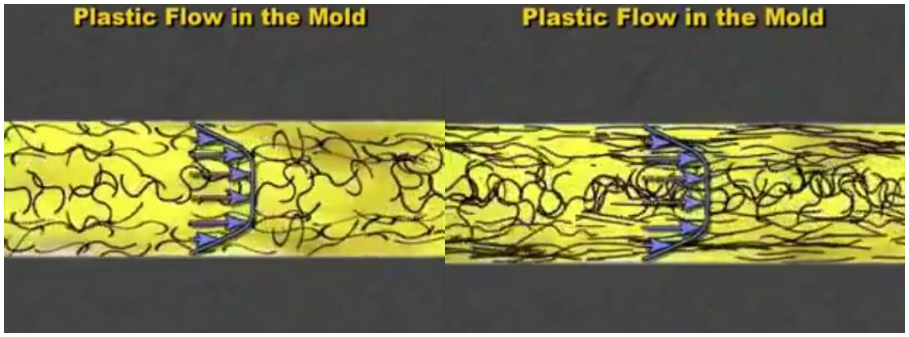

Figure 5: Plastic flow in the mould. The plastic in the centre flow the fastest. The plastic near the walls flow the slowest because their speed is reduced by friction with the mould surface

This shear rate is caused by the high speed applied to the polymer and the reduction of the speed due to the friction with the mould surface. This friction depends on the surface of the mould and the plastic nature making difficult the filling of the mould. To avoid incomplete filling makes necessary to increase the speed and pressure, generating high shear rate. These measures can lead to several problems in plastic parts as flow marks, burns or flashes. Friction between mould and polymer is a problem at the moment of part ejection as well, making the ejection difficult. The necessary ejection force will be higher resulting in ejection marks in the parts.

In this context, testing procedures need to be developed to evaluate the above mentioned phenomena of wear and friction adequately. Ideally, a test could be designed on an actual test die in a real die-casting and injection environment. Nevertheless, the risk of damaging an expensive and complex die, and the cost of interrupting production make this approach onerous. Consequently, it is necessary to find simple laboratory scale tests, that simulate as close as possible the actual production failure mechanisms and can get the result in a reasonable period of time, to evaluate different candidates and reach a better understanding about their behaviour.

It is important to take into account that PIM and HPDC moulds apart from high hardness and wear and corrosion resistance, must fulfil other requirements like good machinability, good dimensional stability, good polishing-ability and good weldability. In HPDC hot work tool steels like DIN 1.2343 and 1.2344 are acquired in annealed conditions that is hardened after machining. In PIM hardened 1.2738 is the typical steel that is machined, being applied sometimes different treatments like Nitriding or Coatings.

The presented problematic of HPDC and PIM have several points that are common:

- The mould is a key part of the injection/casting process. These moulds undergo a very similar process before they are ready for production: mould design, manufacturing, polishing, heat or surface treatment and set up testing. The cost and time that takes this process is very high.

- These moulds are worn due to the interaction with the fluid at high temperature that cyclically fill their cavity.

- This wear is the result of the action of different wear mechanisms.
- The wear mechanisms erosion due to the flow impact, corrosion due to the aggressive media and adhesion when the part ejection take place, are common to both processes.
- Other wear mechanisms are singular of each process, like thermal fatigue on HPDC and abrasion due to the fibres flow on PIM.
- The increase of knowledge of these phenomena, mitigate their consequences increasing the mould life and reducing the cost of the process, the time to setup the mould, the maintenance stops and reparation costs, achieving an improved competitiveness.

Substitution of a mould insert can cost up to 50,000€ and shutdown time of the die casting / injection machine approximately 3,000€/day. This document presents an approach to avoid this cost, through die lifetime prediction, which is the main objective of the study. To achieve this goal, some sub-objectives are set:

- Improve the comprehension of the nature of wear mechanisms and identify the parameters that rule the wear mechanism and influence the amount of the wear.
- Selection of the critical wear mechanisms that are intended to be predicted, and the related parameters that will be varied.
- Generation of testing protocols, that are able to simulate at laboratory scale, the wear mechanisms that will be studied. These protocols can be based on the ones that have been previously used in bibliography or newly developed testing procedures.
- Generation of a DOE (design of experiments) for each wear mechanism, that varying the most affecting parameters, makes possible the generation of equations to model the wear of moulds.
- Perform the tests, generating consistent experimental data, and analyse the data to perform a discussion of these results.
- Generate the prediction models from the experimental values, assessing the ranges of the values of the parameters in which the equation is applicable, as well as assessing the quality of this prediction.
- Application of the model to some examples, showing how can be used by a mould designer, and visualize how the kind of models would be useful in the future through implementation in software's.

In this document have been described the steps that have been followed to achieved these objectives. The structure of the manuscript includes this introductory chapter, a literature review, which includes the studies about the nature of wear mechanisms, existing test protocols simulating these wear mechanisms and mathematical models that have been developed for their prediction by different authors. Some initial conclusions from this review are detailed, and the innovative aspect of this study related to bibliography are highlighted. The chapter 3 includes the core of the work that have been done in this thesis for each wear mechanism in the following order: thermal fatigue, die soldering, abrasion, erosion and corrosion mechanisms. Thermal fatigue and die soldering are referred to HPDC, while abrasion to PIM. As erosion and

corrosion are common wear mechanisms for both process's a common testing and modelling approach have been selected and are presented together for both PIM and HPDC processes. In this chapter 3, the materials and methods used are detailed, the experimental results are described and discussed, and also the model created is presented. The chapter 4 summarizes all the created models, and it is described how the model might be used using case studies for HPDC and PIM, predicting the lifetime to failure for each wear mechanism in the moulds in both processes. Finally, chapter 5 includes the main conclusions and future steps. The document includes the list of bibliographical references, an annex of the articles published in journals or presented in congresses related to the thesis, and last but not least, all the persons and entities that have contributed to this work are acknowledged.

2 Literature review

The better understanding of the phenomena leading to moulds wear requires as first step to collect available information in literature. The information found is reported on three different points: nature of the wear mechanisms, different laboratory test to simulate these phenomena and current state of art on mathematical models applicable to simulation software tools.

2.1 Wear mechanisms in Moulds

The wear mechanisms of moulds are usually based on the industrial observation and are generally accepted in the form of the mechanism named before. Here, the main studies performed by different researches have been reviewed in order to be able to explain in detail the nature of the different mechanisms and the factors affecting their appearance.

2.1.1 Wear mechanisms in HPDC

The wear mechanisms appearing are classified as 4 wear mechanisms: Thermal fatigue, die soldering, erosion and corrosion.

2.1.1.1 Thermal Fatigue

Thermal fatigue cracking is a major mode of failure of hot working tool steel dies in die-casting and forging applications. In literature, two different failure groups have been identified ([3], [4], [11]): Heat checks and corner cracking.

HEAT CHECKS

Because of the large thermal gradients, during heating, the die steel surface is under compression and it is in tension during cooling. This leads to die surface cracks, which are popularly known as ‘heat checks’. The direction of cracking depends on which component of strain is dominant, but could exist a point in the die where there are two directions of maximum strain because of symmetry, thus the cracking can occur in both directions [3]. This phenomenon deteriorates the surface but can also initiate crack propagation, leading to gross failure of the die. An example of thermal fatigue cracks in a large transmission die is shown in figure 6:

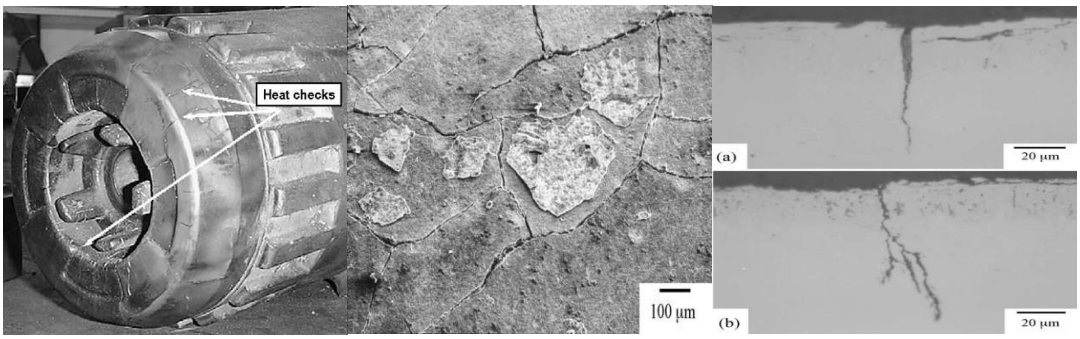

(a) (b) (c)

Figure 6. a) Cracks in transmission die [2], b) surface cracking detail [5] and c) polished cross-section revealing typical thermal cracks [5]

CORNER CRACKS

Cracks may appear in corners, in presence of sharp edges or abrupt transitions.

Corners are more susceptible to crack. At corners like in the figure 7b, cracking can take place in two directions, perpendicular to the edge, because of cyclic strain in direction 1, and along the edge (dotted line) because of cyclic strain in direction 2. In most of the laboratory tests, cracks perpendicular to the edges are observed more often.

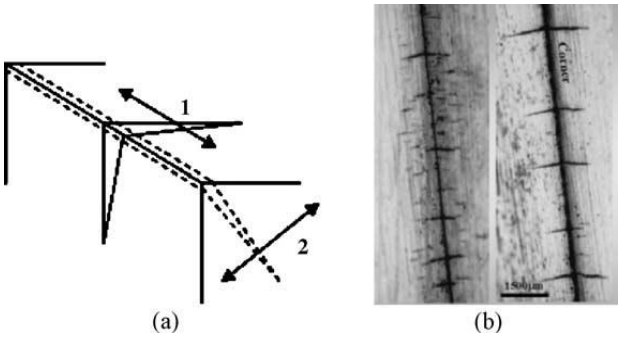

Figure 7. (a) Schematic of crack direction and stress direction and (b) corner cracking.[3]

In serial production dies, it is observed corner cracks, as shown in figure 8:

- In positive edges, they can be found just perpendicular to the edges.
- In negative edges, they can appear both along the edges and perpendicular to the edges.

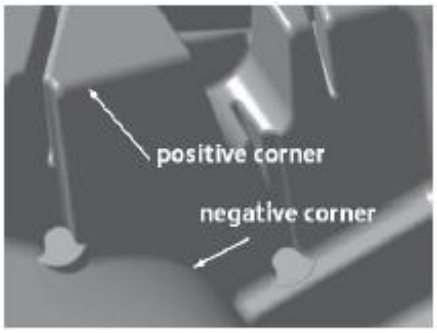

Figure 8.- Corner cracks observed in serial production dies. [12]

DEFECT GENERATION

The formation of thermal cracks can be divided into three stages; (1) nucleation, (2) initial growth, and (3) crack propagation. [4]

(1) The crack nucleation is associated with the accumulation of the local plastic strain in the surface material due to fatigue cycles. During the hot phase of the die casting cycle, high compressive stresses are produced in the surface material. The temperature in the surface is higher than in the bulk, subsequently the material does not expand homogeneously leading to deformations in the plastic region. In general, compressive stresses avoid crack nucleation and crack growth.

Instead, at working temperature a local plastic deformation occurs as a consequence of exceeding local material yield strength. During the cold phase of die casting cycle high tensile stresses are produced on the surface of the material, increased by their plastic deformation. When these stresses exceed the local yield strength and sometimes ultimate tensile strength of the surface material at working temperature, failure is produced.

Crack nucleation could be also due to aluminium alloy soldering to the mould surface, followed by the material washout, since it could produce sharp surface corners with subsequent stress concentration and crack nucleation.

(2) At cyclic loading, low cycle fatigue occurs, producing nucleation and initial crack growth (i.e not big enough to have influence of the melt introduction of crack surface oxidation). This behaviour could be simulated by classical low cycle fatigue Coffin-Manson equation or an equivalent one.

(3) Crack propagation is facilitated by cast material infiltration into the cracks, by oxidation (due to the presence of oxygen in high temperature environment) of the working surface and surface of the crack, and by softening of the tool material due to tempering or aging of surface layer.

- During the cold phase of the cycle, the presence of nitrogen and aluminium alloy inside the cracks increases the tension at the crack tip, causing the growth of cracks.

- The oxide layer has lower thermal expansion, higher volume and fragility than the mould material. Oxides may be formed from iron, aluminium, silicon, cobalt or nickel, in case of maraging steels.

- The undesired softening also affects to material yield strength causing rapid progression of the crack length to a depth of soft layer. Another reason for rapid crack length growth is the local stress relieve of areas along the thermal cracks, which delays the growth of adjacent cracks as larger, once propagate into the tool material.

INFLUENCING PARAMETERS

The main parameters that may affect the failure behaviour are listed as follow:

- *Material properties:* thermal expansion coefficient, thermal conductivity, yield stress, ultimate strain, Young modulus, resistance to tempering.
- *Die surface temperature and gradient into the die during cycle:* Depends on casting temperature, cooling channels temperature, spraying, mould design.
- *Stress concentrators:* due to the mould cavity geometry (corners) as discussed, but also at microscopic level (surface finishing) and also residual stresses.

2.1.1.2 **Erosion wear**

Erosion is a progressive loss of material from solid surface due to the mechanical interaction between that surface and impinging fluid flow, resulting in washout of the die surface. [16]

Erosion begins in the die with the physical removal of the lubricant and natural oxide film, but once the iron is exposed directly to the melt, it dissolves into aluminium (corrosion) or solidifies into an intermetallic compound. This is the onset of soldering. Experimentally it is difficult to pounder how much damage is due to erosion and how much is caused by soldering or corrosion, or to measure directly the erosion.

According to literature, three main mechanisms of erosion involved in die casting can be recognized: liquid impingement erosion, solid particle erosion and cavitation erosion.

LIQUID INPINGEMENT EROSION AND SOLID PARTICLE EROSION

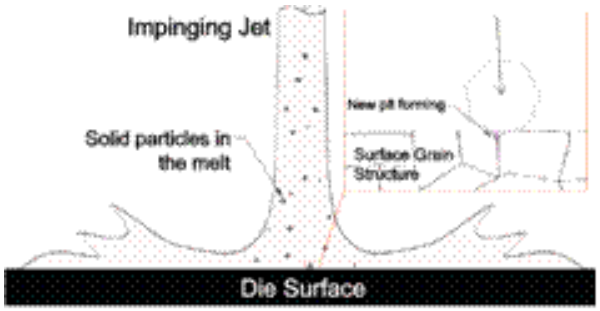

Figure 9. Representation of high angle impinging jet molten aluminium, and pit formation through erosive wear and local deformation [17]

Liquid impingement erosion has been defined as "progressive loss of original material from a solid surface due to continued exposure to impacts by liquid drops or jets"[18]. Sometimes the fluid can contain also solid particles that could increase the erosion rate (Figure 9).

Research on liquid impingement erosion have been conducted using liquid impact velocities much higher than the upper end of the filling velocities usually used in HPDC [19]. It could be expected a quadratic/cubic dependence between wear and velocity.

Erosion rate due to a continuous melt jet can be from one to five orders of magnitude lower than that due to the same quantity of liquid impinging at the same velocity but in the form of droplets.

Hardness is one of the key properties a material needs to resist this type of erosion, and the ingate is often the most damaged zone. H13 is the most popular and most versatile hot work tool steel providing a good balance of toughness, heat check resistance and high temperature strength in addition to moderate wear resistance. It may be used for tool temperatures up to about 540ºC and it is useful to examine the hardness of H13 and melt metals (silicon, aluminium) particles at temperatures relevant to die filling (30HRc *vs* <20HRc). In Figure 10, it can be seen the ranges of temperatures corresponding to mentioned hardness.

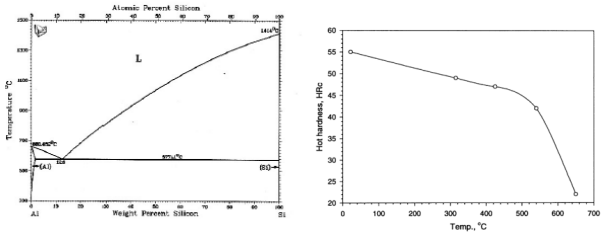

Figure 10. Evolution of hardness of H13 in function of the temperature and Al-Si phase diagram.[10]

Repeated impacts may result in erosion in a long-term through fatigue-like phenomena but it may require a long incubation stage for both impingement and solid particle erosion. Analysis based on existing theories on erosion has suggested that severe forms of liquid impingement and solid particle erosion are not likely to occur in HPDC, before soldering develops (short-term). However, the mechanisms of long-term erosion in HPDC are not well understood.[19]

CAVITATION EROSION

Any device handling liquid can be subjected to cavitation. Local pressure falls below saturated vapor pressure causing cavitation to occur. Resulting vapor bubbles collapse on surface material with high energy and heat. The casting metal vapor pressure could be around pure aluminium vapor pressure (2.42E-06Pa at 660°C [20]).

In HPDC, a sudden change of pressure is experienced due to melt flow direction changes generating pressure variations and cavitation. In figures 11, 12, 13 are represented some examples of these failures.

These phenomena (pitting, breakout, erosion and washout) may also occur on the high pressure side where the melt hits directly on the surface. [5]

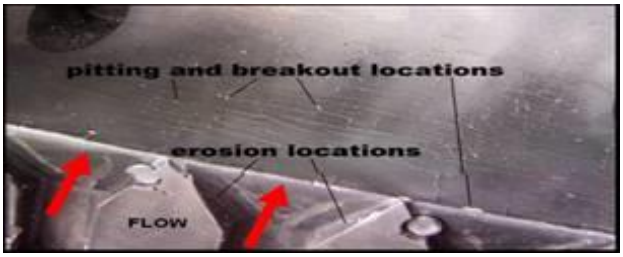

Figure 11. Breakout, erosion, and washout appears in the opposite locations of where they would be expected - on the low pressure side of the flowing liquid. [20]

Figure 12. Typical Cavitation phenomena in High Pressure Die Casting of Aluminium Dies [12]

Figure 13. Exhibited sheet or cloud and vortex cavitation effect [20]

Thermal fatigue can lead to breakout without incipient inertial cavitation, but breakout lead to heat checking of the die's surface [20]. The last can lead also to die soldering.

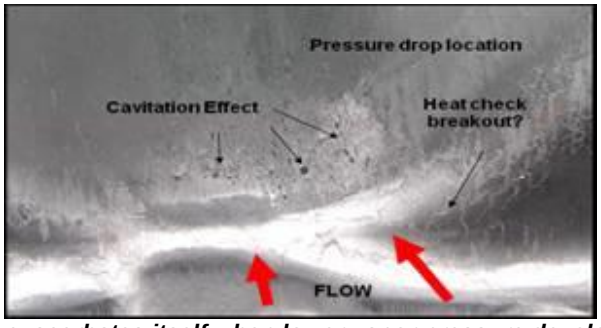

Figure 14. Cavitation effect exacerbates itself when lower vapor pressure develops from the disrupted flow patterns [11]. This kind of failure could be also related to washout [5]

INFLUENCING PARAMETERS

- Liquid impingement erosion and solid particle erosion:
  - *Flux characteristics:* droplet or jet sizes and impact velocities, angle of attack,
  - *Material properties:* die material properties at die working temperature,
  - *Amount of hard particles in the melt:* solid phases of the alloy and impurities.
- Cavitation: Flow characteristics and casting metal vapor pressure and Die material response.

2.1.1.3 **Die Soldering**

The losses from soldering do not provoke such an important damage to the die as for example large cracking, but affect the die casting production seriously due to the interruption for cleaning (remove chemically, re-melt or mechanically polished) and ejection problems (more force is needed to separate a soldered casting, or bent/broken pins).

Die soldering can be subdivided in two categories: mechanical and metallurgical-chemical.

Mechanical soldering takes place when sticking of the melt to the die happens after a few shots. Sticking is not related to any metallurgical-chemical reaction because there is not time/temperature to form intermetallic layers, but could be related either to high pressure or temperature, or to an error in the design of the mould. [13].

Metallurgical-chemical soldering is preceded by mechanical erosion since chemical interactions between the die and the melt are possible only when any protective skin layer separating the die surface from the melt (including iron oxide film and lubricant, or coating) is removed by erosion. Reactions between the melt and the die substrate are responsible for the die corrosion. These interactions could be due to the dissolution of iron of the die material into the melt or to the cast alloy elements diffusing into the die. As result, intermetallic layers are formed on the die surface like shown in figure 15.

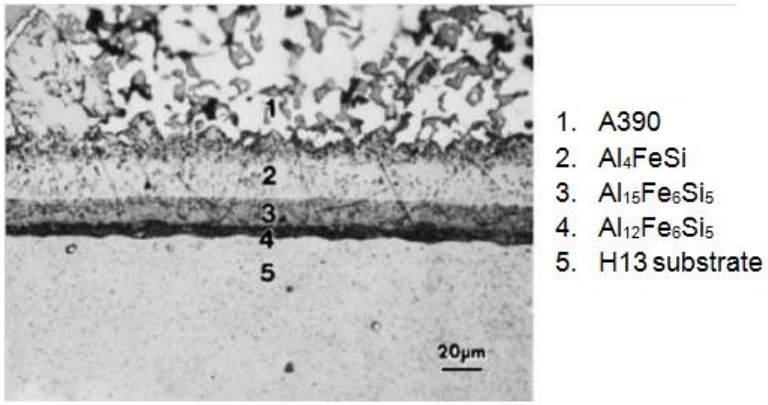

Figure 15. Intermetallic layers formed after dipping H13 steel for 2 hours in liquid aluminium (390) at 680 ºC.[14]

The resulting formation of a layer of the cast alloy that occurs on the interface is called soldering. The distinction between corrosion and soldering has its roots in the die-casting engineering practice. The term corrosion emphasizes the undesirable removal of the die material due to a chemical deterioration of the die surface, while soldering refers to the effect of adhesion (sticking) of cast material to the die surface.

Several approaches to the modelling of die soldering have been suggested in literature based in damaged moulds or laboratory tests at different temperature ranges, and most agree in that the diffusion processes on the die surface and the formation of the intermetallic layer play a major role in die soldering. Here, it is presented the most complete model found in literature, including both dissolution (corrosion) and diffusion (soldering) behaviour, explained in 5 stages, in the absence of an oxide layer. [14]

- Stage 1: During melt injection and solidification, diffusion of aluminium and iron atoms occurs to form $Fe_xAl_ySi_z$ intermetallic at the interface. Silicon changes the kinetic rate and the solubility of iron into aluminium.

- Stage 2: A new die casting cycle begins and fresh melt enters the die cavity. The driving force for diffusion is slightly lower due to the presence of previous intermetallic layer. There is enough driving force for the intermetallic layer to continue to grow. The driving force for dissolution in this stage is high but still lower than that for diffusion.

- Stage 3: In the next cycle, the thickness of the $Fe_xAl_ySi_z$ intermetallic layer reaches a critical limit, the driving force for diffusion has decreased to become negligible and the driving force for dissolution becomes the dominating force. The soldering dissolves in the melt.

- Stage 4: Mass loss has taken place on the die surface but is free of intermetallic layer. Driving force for diffusion increases due to loss of Fe_xAl_y to the melt but is still negligible compared to the driving force for dissolution. The driving force for dissolution decreases with increasing intermetallic thickness.

- Stage 5: The cyclic process of soldering growth and dissolution continues while the die surface continuously loses iron to the melt.

The interesting schematic illustration of the die soldering mechanism proposed by Shankar and Apelian is presented [15].

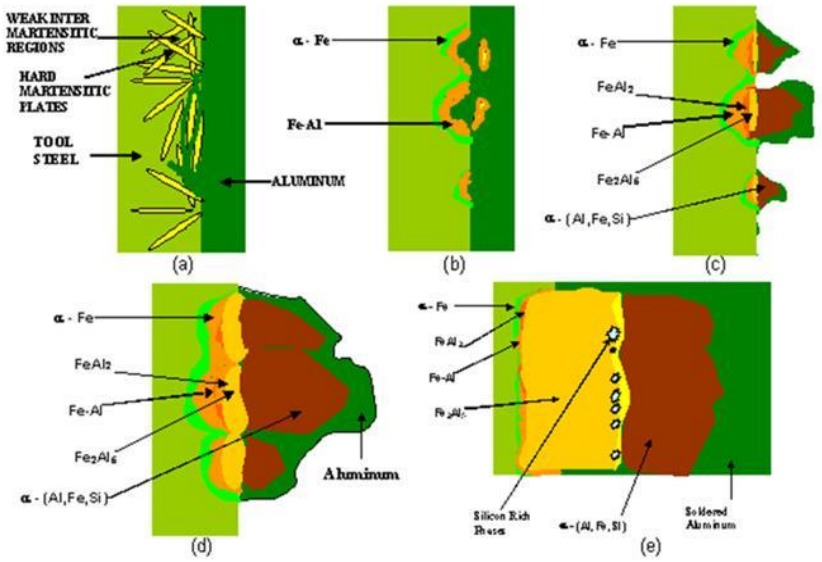

Figure 16. Modelling of die soldering [15]:
(a) Initial attack of the grain boundaries by aluminium to loosen up the hard grains and martensitic plates to cause pitting on the die surface.
(b) Formation of the iron-aluminium intermetallic phases inside the pits and around the broken grains close the die surface.
(c) "Pyramid' growth of the ternary -(Al,Fe,Si) phase on the pits over the -Fe_2Al_5. In addition, the pits expand laterally and in depth. Aluminium begins to stick after this layer structure is formed resulting in the beginning of soldering.
(d) Shows the growth of intermetallic layers and merging of neighbouring pits. Molten aluminium encounters the die surface only through the cracks and gaps present between adjacent pits.
(e) Straightening out of the pits and closing of the gaps between the adjacent pits. The ratio of the intermetallic layer thickness and the soldered aluminium is ~1:5. The reaction mechanism becomes very slow. Silicon is precipitated in the grain boundaries of the -Fe_2Al_5 phase and at the intersection boundaries between the two intermetallic phase layers.

INFLUENCING PARAMETERS

- Metallurgical-chemical Die Soldering:
  - Nature and constituents of *casting alloy*,
  - Nature of the *die material*, *surface treatments and roughness*
  - Die *Lubrication*,
  - *Operation parameters:* alloy and die Temperature, injection pressure and speed
- Mechanical Die Soldering: Pressure, speed, temperature, lubricant, alloy and die material nature

2.1.1.4 **Corrosive wear**

As explained in the previous paragraph, corrosion means dissolution of the die material in the melt. In literature soldering and corrosion are not always separated. Although the behaviour is already explained in the model of soldering it is important to clarify two aspects:

- The high temperature corrosion (or oxidation) is the formation of an iron oxide layer with no chemical reaction and is beneficial to protect the die from damage.
- The chemical (or electrochemical) corrosion is closely related with die soldering, and it could have also influence on thermal fatigue or erosion because of the changes of mechanical properties of the corroded die.

2.1.2 Wear mechanisms in PIM

In the introduction chapter the three wear mechanisms of PIM moulds have been defined as abrasion, erosion and corrosion, and their root cause have been described.

In fact for the tools working with polymers, it is widely referred that there are tribological phenomena that reduces the working life of them, like abrasive wear, adhesive wear, corrosion, galling or sticking [30].

In the interesting table 1, the specific tribological problems appearing on PIM tools are described, their causes and how could they be solved through surface treatments.

Type of problem	Appearance	Cause	Parts subjected	Possible solution by surface treatment
Adhesive wear	Galling, tearing and seizing, micro-welding, especially when lubrication is not used.	Relative movement of steel and/or metal surfaces in contact.	All parts in relative movement: cores, ejectors, die sets, steering elements.	Coating with PVD TiAlN or CrN coatings which results in rather low friction and very low adhesive wear especially when subjected to moderate or low contact pressures.
Abrasive wear	(a) Alteration of the finish of surfaces in direct contact to the plastic flow (roughening of very smooth surfaces and polishing of textured surface); (b) blunting of sharp edges; (c) in more severe cases changes of dimensions and shape.	Abrasive particles from fillers and dyes in the plastics.	All parts in direct contact with filled plastics, liquid or solid: screws, cavities, runners, gates, nozzles.	For mild and moderate abrasive wear: Nitrogen ion implantation. In more severe cases: PVD coating with hard wear resistant coating, e.g. 3 μm of the very hard TiAlN, or perhaps 5–10 μm of the medium hard but more ductile CrN.
Corrosive wear	(a) Pits at various sizes, changes of surface finish; (b) deposition of the corrosion products on the tool, often transferred to the products.	Corrosive gases or decomposition products from the plastics, hot corrosive exhaust products.	All parts in direct contact with the corrosive plastics or gases e.g. cavities, cores and especially the air outlets.	For air outlets, cavities and cores: re-alloying by chromium ion implantation for high corrosion resistance. For cavities and cores coating with protective PVD CrN.
Rather severe wear of soft tool surfaces	Mixture of abrasive and adhesive wear, often combined with corrosion (see above).	All above-mentioned causes, but wear is enhanced because of the softness of the tool material.	All parts made of soft tool materials, like Cu- and Al-alloys and non-hardened steel.	PVD coating with medium hard and ductile CrN protective layer.
Release problems	Finished products difficult or impossible to remove from the tool	(a) Inappropriate tool design etc.; (b) poor release properties of the tool material due to high affinity between the plastics and the tool material.	Parts in contact with the finished product: cores and cavities.	Changing surface affinity properties by nitrogen ion implantation, PVD coatings or by ion-implanting PVD coatings.
Accumulation problems	Build-up, accumulation and deposition of decomposition products from plastics on the tool	Affinity between decomposition products and the tool material. Can be enhanced by corrosion.	All parts on which the decomposition products can spread out.	As for release problems and corrosive wear.
Filling problems	The molten plastics does not fill the entire mould. The end products are defective.	(a) Inappropriate tool design etc.; (b) inappropriate process parameters; (c) high friction between plastics and tool surface.	Cores and cavities.	Coating with low-friction coating (type depending on plastics material).

Table 1. Tribological problems on PIM tools [7]

For the specific case of interest in this work, the mould cavities, there are only referred the abrasive wear due to the friction between the polymer flow and the mould surface and the corrosion. For the case of reinforced polymers, depending of the flux conditions can lead to two different wear mechanisms, as showed before in figure 3: *erosion* in mould regions where frontal impact of the plastic flux appears while *abrasion* mechanism is identified when flux is parallel to the mould surface.

This classification is based on the observation of the industry on the normal use of injection machines. For an exhaustive study of the fundaments of the wear mechanisms in HPDC, it has been widely used the approach of monitoring the evolution of the wear in an insert of a mould ([1],[33]) in a critical area. This insert can be extracted from the mould to analyse in detail in the laboratory. This approach has not been so widely used for plastic injection, but there are some interesting works ([31],[34]), where they get similar conclusions about the wear due to fibre reinforcements, being more severe in areas of impact erosion than in areas of abrasion wear. This approach has been used also by Silva et al. [35] where 3 samples were inserted in a mould where a part (fan for a car radiator) of Polypropylene (PP) with 30 % of glass fibre was injected. The samples were of two different types of TiAlSiN and a multilayer CrN/CrCN/DLC coating.

The experiment proposed by J. Bergstrom [31], justifies the mentioned difference between impact erosion and abrasion. A real scale machine was used for testing, where a mirror polished sample is introduced in a mould in a position in front of the gate from which the fibre reinforced plastic is injected Polycarbonate (PC) reinforced with 40 % glass fibre of 10-15µm diameter and 50-300 µm length), see figure 17. With the proposed sample geometry, the impact angle changes for its different areas (from the 45º in the leading edge where the flux is impacting, to the 0º in the side surface at 2 mm from the edge). Samples of different materials where tested.

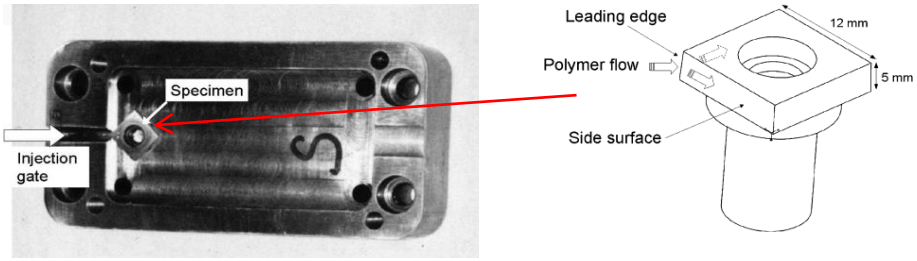

(a) **(b)**

***Figure* 17. Injection mould (a) and inspected sample (b) [31]**

In the SEM images shown in figure 3, it is possible to observe how the wear behaves in function of the impact angle of the fibres.

These wear mechanisms are defined as abrasive wear due to micro cutting and micro ploughing, and impact erosion of solid particles from plastic deformation and material removal. This behaviour will appear in the conditions tested in the aggressive injection conditions of high injection speed and pressures tested by J. Bergstrom [31], but also in the normal injection conditions in a less pronounced way.

From his conclusions it can be extracted that the phenomena depends, for the case of a polymer of interest, principally on: (i) location in the mould due to variable flux in a complex geometry, (ii) injection conditions and (iii) the mould material response.

This behaviour dependent on the fibre orientation is coincident with the conclusions obtained by Martinez-Mateo et al. [34], where the wear was maximized in the area where the fibres were less in order. Furthermore, they studied the influence of the hardness of the mould material, showing that a very high hardness avoids the surface damage. The way they quantified the wear was through the measurement of roughness of the final part (normalized samples were injected), as the reflection of the mould surface situation. 3D topography was acquired and the mean roughness was measured through the optical profilometer according to ISO 4287. For the case of low hardness, the wear rate was not linear. In the first

1000 injected parts the roughness increased remarkably from 0.46 µm to 1.18 µm, achieving the maximum at 2000 cycles, while at 3000 cycles the roughness achieved 1.02 µm. The injected material was Polybutylene Terephthalate (PBT) glass fibre reinforced at 50 %.

From studies of fibre orientation in a polymer flux [36, 37], it is possible to extract that in the area near to the injection point, the relative angle between the fibres and the mould surface is around 30º, even higher in corners and edges. Once the plastic is going into the mould, the fibres orientate along the flux, parallel to the surface, and according to the study of J. Bergstrom et al. [31], it is not much distance needed to appear this orientation (<2 mm).

From the study of Silva et al. [35] it can be extracted that when the mould is coated, the material response to the impact and abrasion is different. It is remarkable that coatings are reducing the wear amount in 25 y 58.2 times for the TiAlSiN y CrN/CrCN/DLC respectively, as it is possible to see in figure 18. The TiAlSiN does not present clear marks of wear (18a), while the CrN/CrCN/DLC (18b) shows small marks due to the partial elimination of the DLC. The reference steel (18c) shows clear marks of wear affecting the half of injected parts in comparison with the coated ones.

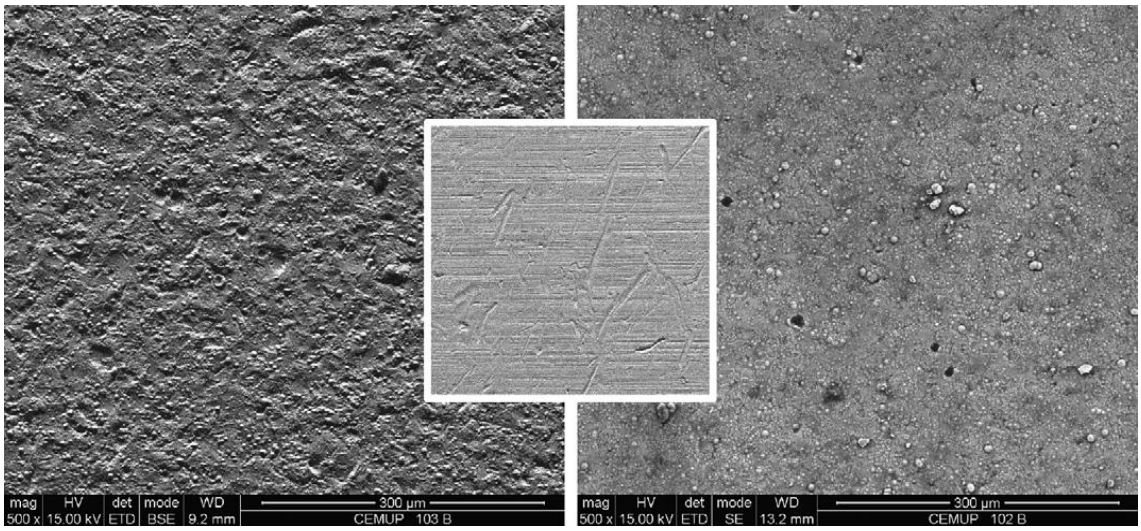

***Figure* 18. Morphology of the surfaces of a) TiAlSiN and b) CrN/CrCN/DLC for 90,000cycles and in the centre c) the reference steel for 45.000 cycles. All of them have the same magnification 500x. [35]**

The presented experiment is a step halfway between the real part and laboratory tests, and even being a very interesting approach, it is not sufficiently valid to split between the different variables in the wear. For this objective it is recommendable to search which tests in laboratory scale have been done to simulate wear in the mould as well as for the corrosion. The corrosion of the mould surface, depends on the type injected plastic. The overheating of the plastic material can lead to release gases, resulting in a local corrosion in the mould as for example the Polyamide (PA) can release NH_3, PVC chlorides generates HCl and other polymers can release different acids [10]. The additives that are in the plastic materials, like the flame retardants also contains halogens (Cl, Br, F) emitting the corresponding acids [8].

The wear mechanisms can have a combined effect, creating a synergy and the wear is enhanced when the material is subjected to corrosion, as checked by Dong-Cheng [10].

From an industrial point of view, it is necessary to highlight the problems that can be generated depending on the type of polymers that are injected. According to MAIER S.COOP experience, the main challenges to deal in function of the injected polymeric materials are the following:

- PMMA (Polymethyl methacrylate): this material may produce abrasion in the mould originating aesthetic defects due to it. Also flow lines are typical and welding lines can be very visible and difficult to control them. In addition this material often has high aesthetic requirements from end users.
- PC (Polycarbonate): very similar problematic to PMMA.
- PA (Polyamide) glass fibre reinforced at 30%: polyamide release gases such as NH_3 during the injection in the mould and produces wear due to their corrosive nature, as well as abrasion and erosion due to glass fibres sliding and impact. This leads to aesthetic defects in the parts such as flow lines and scratches.
- ABS: this material emphasize a lot any type of defects that may occur in the cavity: polishing defects, scratches, geometrical defects etc.
- PC+PET (Polyethylene terephthalate): it is not a friendly material to be injected, leading to restricted process parameters: is usual to present flow lines.
- ASA (Acrylonitrile Styrene Acrylate): it is a material that easily replicate the mould surface, and this property is very critical for aesthetic applications, since it copies every marks of mobile elements of the core.
- PP (Polypropylene): it has the same difficulty as ASA, in addition is very prone to have flashes and deformations.

Some of these surface treatments and plastic materials have been tested, and their response is described later in this document. In this chapter, it has been highlighted the influence of the injection speed and injection pressure, as well as impact angle of the fibres. Some dedicated studies have been performed in order to have a better insight on the influence of these parameters.

2.1.3 Summary of wear mechanisms

The main failure modes of the High Pressure Die Casting and Plastic Injection Moulding moulds have been defined according to most recent bibliographical data. It has been created a classification of terms and tried to explain the nature of them.

The HPDC wear mechanisms selected for simulation in laboratory scale have been Thermal Fatigue, Die Soldering, Solid Particle Erosion and Corrosion. For PIM, the selected wear mechanisms, such as Abrasion, Erosion and Corrosion have been simulated. As Erosion and Corrosion are common wear mechanisms for PIM and HPDC, for both process's a common testing and modelling approach have been selected and are presented together.

The main wear mechanisms have been simulated in the laboratory in order to build equations to predict lifetime and find the best solutions to increase the durability of the moulds. To perform an appropriate selection of tests protocols and models, a literature review of the of the test protocols at laboratory scale and models available in literature have been performed, as it will be shown in the next chapters.

2.2 Wear mechanisms simulation at laboratory scale

Ideally, a test could be designed on an actual test die in a real die-casting/injection environment. Nevertheless, the risk of damaging an expensive and complex mould, and the cost of interrupting production make this approach onerous.

The numeric and qualitative values of friction and wear obtained in any kind of tribological study, and in general laboratory scale studies, is always relative and depends strongly on test configuration, testing machine, working conditions or surface characteristic of tested materials.

This is explained because the experienced wear and friction by the materials is not an intrinsic property of them, but the response of a very complex system where two bodies interact. Therefore, the appreciation and conclusions described in this document are referred to the presented methodology and cannot be considered as totally proven until a validation of them is performed.

The target of the presented methodology is to use simple laboratory scale test to reproduce the main failure mechanisms of the moulds, using testing conditions as close as the actual production situation in order to get the result in a reasonable period of time.

2.2.1 HPDC wear mechanisms simulation at laboratory scale

2.2.1.1 Test devices for Thermal Fatigue

Once the steady state cycles of production are set, the mean temperature inside the mould is nearly constant around 200ºC. Nearer from the mould surface, where there is contact with molten aluminium, the temperature is more influenced by the different production stages. In fact, in the mould surface it is repeated a temperature cycle that lasts around a minute (like the production cycle of the aluminium part). This cycle starts at 200ºC, goes up to around 500ºC during the injection, the part is extracted at around 250ºC and goes down to around 100ºC when the spraying takes place, to go back to the initial 200ºC. The fatigue appearance depends on the time that takes place, to pass from one temperature to another, since it has a direct influence in the thermal gradients appearing in the die that can generate an inhomogeneous expansion of the material and higher stresses. The stages when injection and spraying take place are obviously when higher gradient and stresses appear, as shown in figure 19a.

The 4 key temperatures of the cycle are the next ones, as shown in figure 19b:

- T1: Initial temperature of the cycle, it ranges from 150 to 220ºC. It is mainly influenced by the internal cooling of the mould.
- T2: Maximum temperature of the cycle, that ranges from 450 to 500ºC. It is influenced by the injection temperature of the alloy, as well as the injection conditions.
- T3: Part ejection temperature ranges from 220 to 300ºC. It is influenced by the type of alloy as well as the part geometry and thickness.
- T4: Minimum temperature in the cycle after spraying, ranges from 80 to 120ºC.

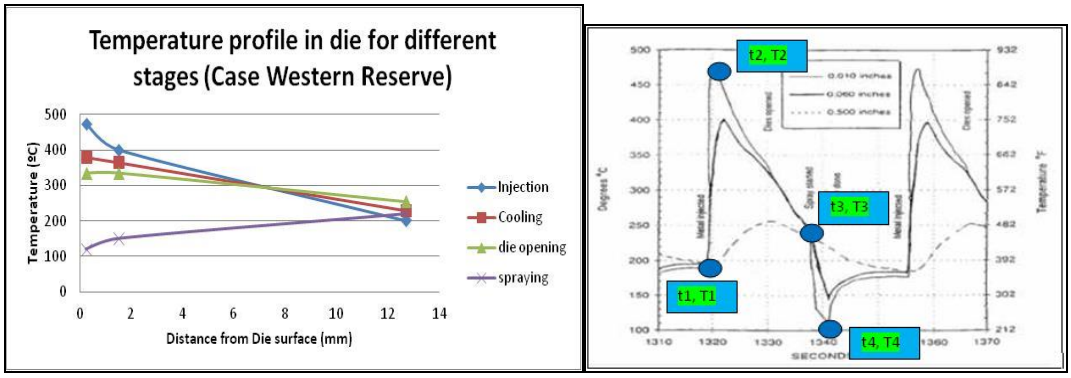

(a) (b)

***Figure* 19: Temperature profile from surface into the mould at the different production phases (a) and temperatures in the surface and into the surface during the cycle (b)**

To reproduce thermal fatigue at laboratory scale, several types of equipment's have been used to test samples of different geometries. A typical application has been HPDC, but it has also been addressed for other different applications (e.g. forging, hot forming). In bibliography there can be found devices based on heating with molten aluminium [3], resistance based heating [27], induction heating [11] or even natural gas [28]. The cooling is achieved by internal cooling of samples and/or directly in the surface by a jet or spray. It is important to note that there are two standards, ASTM E606 and ASTM E2368, which describe both the analysis for strain controlled thermomechanical fatigue testing, and for normal strain-controlled fatigue testing. Most of these methods have limitations when trying to reproduce the thermal gradients of the HPDC dies. Furthermore, it is not possible to study the influence of the main operation parameters, and have been mainly used to compare candidate materials and coatings.

To have an idea of how these kind of devices try to reproduce the fatigue phenomena, few of them are described in this document. The test device most focused in HPDC has been the so called "immersion test", where a sample of the die steel is heated in a bath of molten aluminium and cooled in a water bath. Depending on the author, it has different variations in sample geometries, temperatures, cooling conditions or cycle time [1, 3, 4]. An example of this device is shown in figure 20.

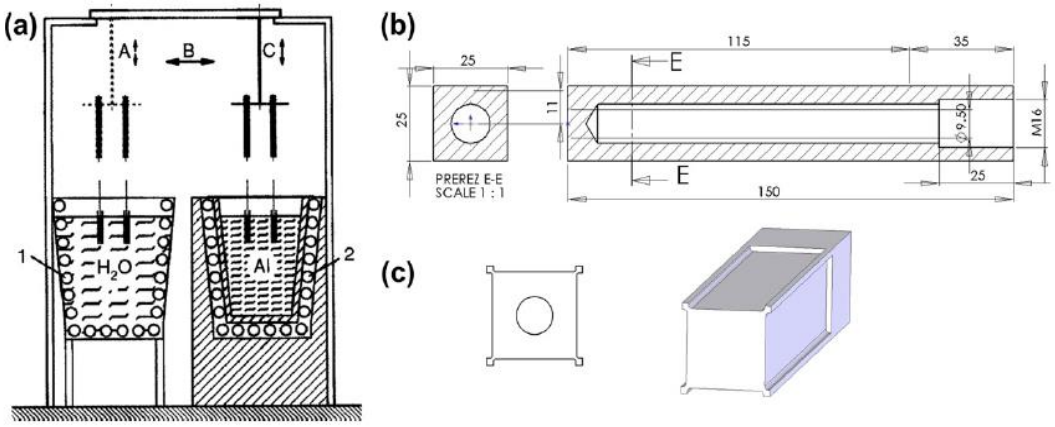

***Figure* 20: (a) Schematic of immersion test apparatus, (b) schematic of classic thermal fatigue test specimen, and (c) cross section of optimal test specimen [4].**

Temperature measurement can be performed using thermocouples, which are inserted in holes drilled to the different depths (for example at 1, 3 and 4 mm from the specimen edge in [4]).

After some seconds of immersion in the aluminium bath at around 700 ºC, the specimens must be air cooled for a brief time while moving to the bath of water or water-based lubricant. The test specimens can be internally constantly cooled with water. Then the specimens are moved back to the aluminium bath to repeat the cycle. The duration of thermal fatigue testing cycle can be around 20 s.

Thermal stresses during the immersion test are the consequence of thermal gradients between the surface and the centre of the test specimen. The highest thermal gradients will be obtained right after immersion of test samples into a hot aluminium alloy or a cold water-based emulsion. After a few seconds immersion, the thermal conditions stabilize, i.e. thermal gradients drop and consequently also the thermal stresses. During the immersion of samples in a hot aluminium alloy the surface stresses will be compressive, while during the immersion in cold water- based emulsion the surface stresses will become tensile.

The test specimens are subjected to a series of thermal fatigue cycles. For what concerns the outcomes of the immersion test, temperature transients at different locations of test specimen can be measured and used in computation of transient stresses performed by finite elements. The test specimens should be visually inspected every n cycles, for example 4000 cycles, in order to find surface cracks.

To compare the result, apart from the time to first crack appearance, two concepts are used for the evaluation of thermal fatigue resistance of die materials, i.e. "total crack area" and "average maximum crack length" [1].

"Total crack area" takes into account of all cracks contribution. Therefore, if a die's total crack area reaches a certain limit, the whole die fails. The area of a crack is defined by the square of crack length and the total crack area is the multiplication of the areas of all cracks.

"Average maximum crack length" is calculated as the average length of the longest crack of each of four corners of the test coupons. This is based on the assumption that if a single crack is big enough, the whole die is unusable.

Die Casting tools show small cracks (network) as well as bigger (leading) cracks after some time in use, due to thermal fatigue. Both are important to tool life. It has also been proposed [38] to use the scales of the figure 21 in order to give a combined grading using both network and leading crack values. The scales are used comparing the reference images with the die or testing sample. Give the grading from both scales and note the two gradings. These two combined readings give the degree of heat checking.

The evaluation of thermal cracks can be made visually or supported by techniques like penetrant liquids, magnetic particles or resins that replicate the die surface.

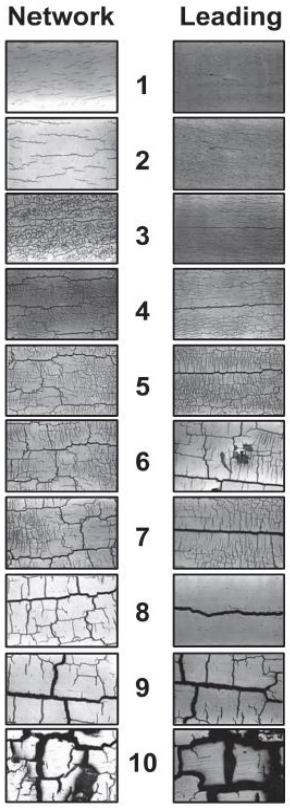

***Figure* 21. Photos of die surface crack patterns reproduced approximately 70% of actual size [38].**

The test concept for generating the thermal stresses by resistance based heating and water jet cooling [27] is shown in figure 22. Circular and hollow shaped specimen were applied for testing, using a thermocouple inside welded system. The outer testing part of the specimen was placed in a cooling chamber (figure 22 a). The cooling and emptying process was optimized by a pair of magnetic computer controlled valves. One valve controlled water quench and the other controlled the air compression to empty cooling chamber. The setup of test rig, without working jaws is shown in figure 22b and its positioning in the load cell is shown figure 22c.

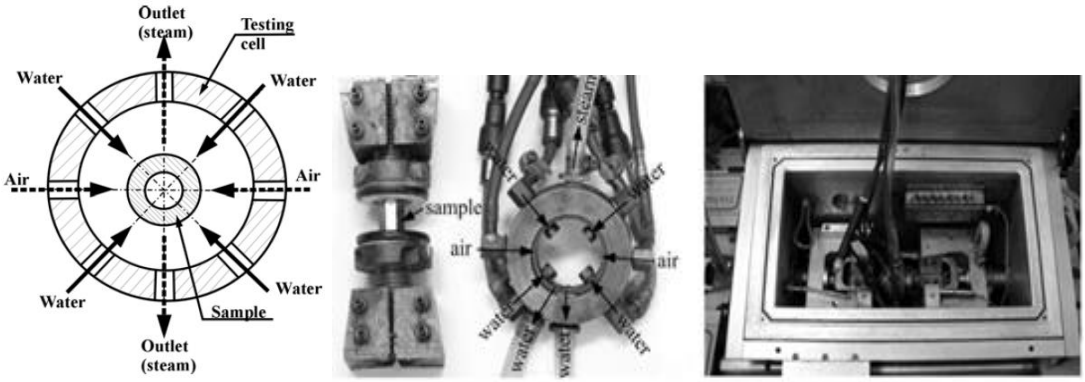

Figure 22. (a) Testing device with specimen, (b) Inserted test rig in the load cell (c) The cooling chamber with water quenched sample [27].

The combination of simultaneously controlled cooling and resistance heating of the specimen, greater thermal gradients in relatively thin specimen surface layer were achieved, while the remaining depth of the specimen kept approximately the same value. This reduced the number of cycles needed for crack nucleation and resulted in faster crack growth. With the possibility of generation various thermal gradient, the test can also simulate various thermal loading conditions in an applicative environment.

There are two main devices in literature with the objective of simulating the thermal stresses of HPDC dies heating with induction devices [39, 40].

The test rig of figure 23 from [39] uses an induction unit (25 kW, 3 MHz) that heats approximately 20 mm of the middle of the test rod. Continuous cooling is performed by circulating silicon oil or water through the specimen, and also externally with argon or air. It is of special interest that the surface strain of the sample is continuously recorded during the thermal cycling through a non-contact laser speckle technique. The applicability of the test is demonstrated on two hot work tool steel grades, hardened and tempered to different conditions, and heat cycled between Tmin 170 ºC and Tmax 600–850 ºC.

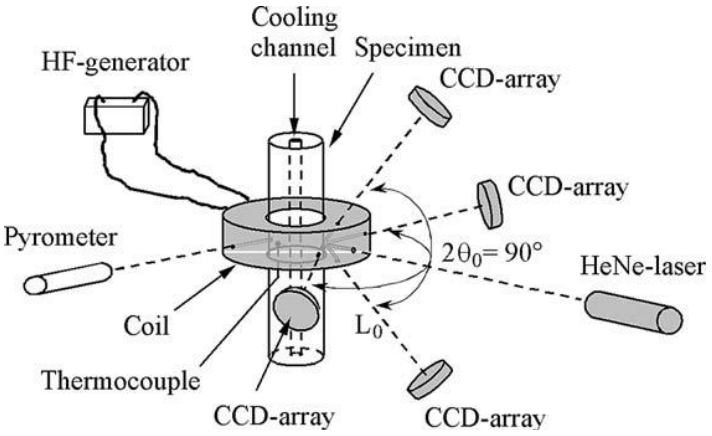

Figure 23. Schematic of the experimental set-up used for induction based thermal fatigue cracking tests in [39]

The other test rig based in induction heating is shown in figure 24. In figure 24a it is shown how the samples pass from the heating station (green colour) to the spraying station (bright blue) in a continuous movement, repeating the thermal cycle. The figure 24b shows the detail of the spraying station, where 10 nozzles are installed. The temperature is measured by an infrared system just after the heating and cooling stations. The cracking in the samples (of similar design as the ones of the immersion test), was demonstrated to be similar to the cracks appearing in the application.

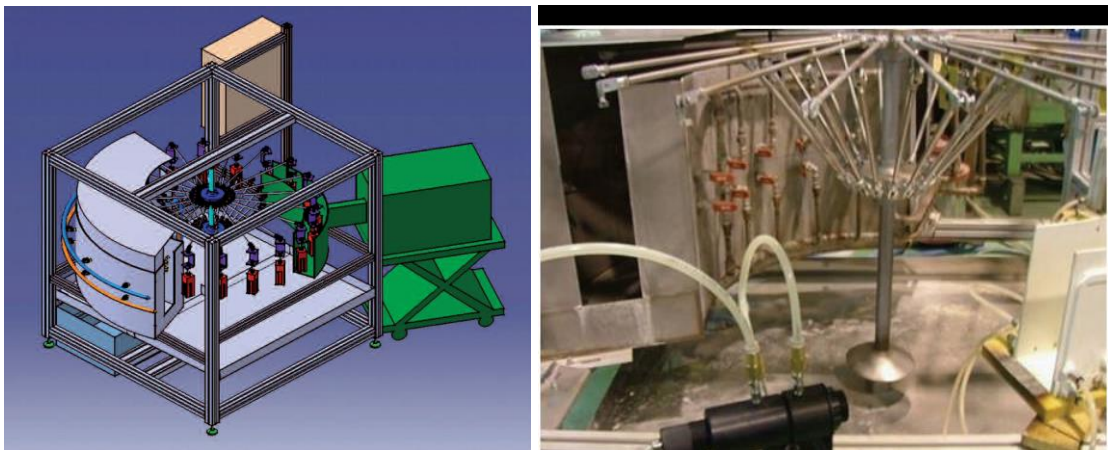

(a) (b)

Figure 24 Schema (a) and aspect (b) of the experimental set-up used for induction based thermal fatigue cracking tests in [40]

All these tests enable a controlled thermal fatigue testing at conditions relatively close to aluminium alloy die-casting thermal stress conditions. Nevertheless, the test specimens are not subjected to pressure and aluminium flows, unlike the die during die-casting, and it will generate some slight differences from the cracking appearing in the HPDC die surfaces. The figure 25 shows the thermal cycle in the surface of the different test devices, and it shows that they are fast enough to generate the inhomogeneous temperature to create thermal fatigue failure.

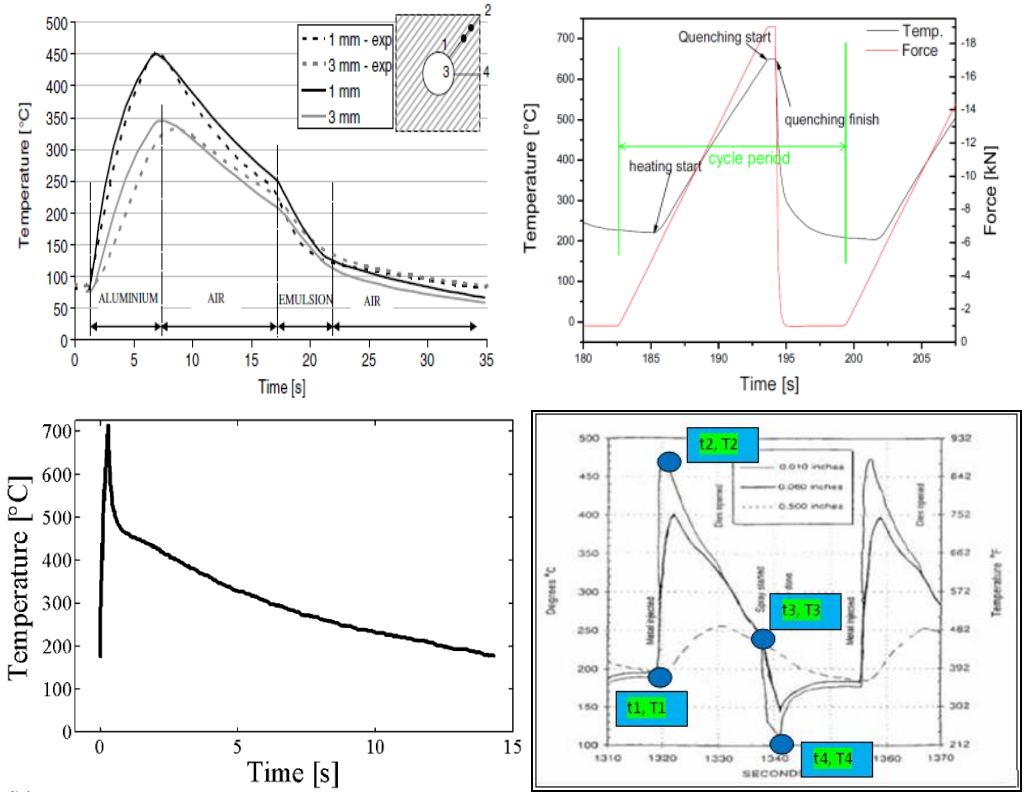

Figure 25 Temperature cycles of the different devices immersion test [4], resistors heating [27], induction heating [39] and the HPDC process

2.2.1.2 Test devices for Erosion

The main studies performed in literature about erosion up to now have been introducing core pins in a mould and test through cycles in a HPDC machine [1, 19, 33]. Even if the wear appeared in the surface will be a combination of all wear mechanisms, they were able to study the mass loss depending on multiple parameters.

As an example, figure 26 shows the "multiple-pin flat plate die" configuration with six test pins designed and fabricated in order to evaluate different materials or surface coatings and some different process parameters [33].

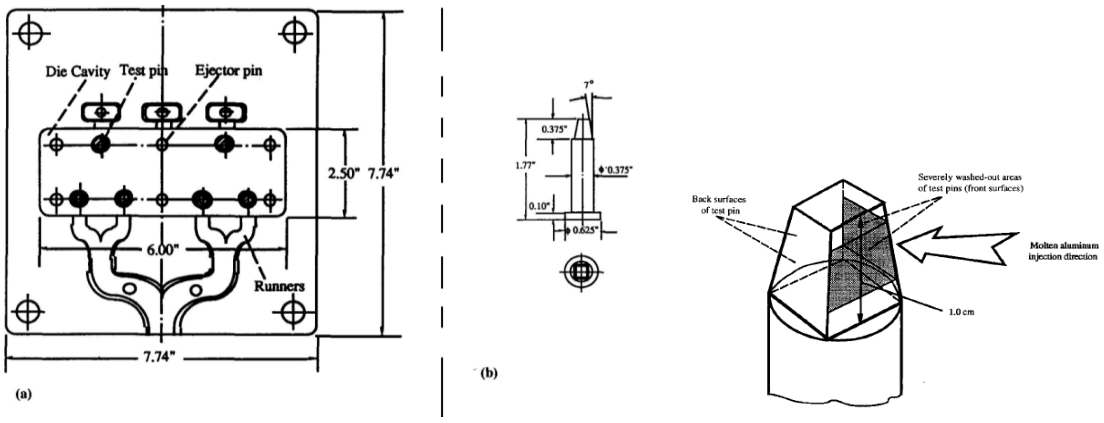

Figure 26 Dimensioned drawing of the multiple pin die [33]

Only the top edge of the pin shown in figure 26 is within the die cavity and is exposed to the molten metal. One of the reasons for choosing the multiple-pin design was their simplicity to assembly, disassembly, and measurement. In addition, a multiple-pin design allows the testing of several pins simultaneously thus providing multiple test sites for comparative evaluations.

These tests could be very long (>100,000 shots) and costly, because the wear is generated by a gradual loss of material. An operating procedure involving an extreme environment on the test was developed in order to accelerate wear effects in a reasonable number of shots. A pyramidal test pin designed with sharp corners was chosen to accelerate the erosive wear rate. These sharp pin comers will easily erode, solder, and exhibit heat checking along the edge within a reasonable time frame. A hypereutectic aluminium alloy, A390, with a high silicon content was selected to further accelerate the erosive wear. Since the silicon is very hard, A390 is more aggressive than other aluminium die casting alloys, which results in a higher abrasive wear rate for the die surface. Two major performance measurements selected for wear quantification were the pin weight loss and the edge profile change.

To test the erosion wear mechanisms, there are some standards that can be applied for the wear of moulds. For the solid particle erosion ASTM G76 is a reference, for liquid impingement erosion appear ASTM G73, ASTM G32 or ASTM G134, and for cavitation ASTM G32 y ASTM G134.

From the point of view of HPDC application there are mainly studies performed for solid particle erosion and cavitation erosion resistance. Liquid impingement erosion is not expected to appear in HPDC mould surfaces in the short term [19].

The erosion test rig shown in figure 27 was designed and built to perform the tests following the ASTM G76 by [41], with the objective of studying coatings that can be used to protect die casting dies. The abrasive particle used was angular silicon carbide (SiC) with a particle size of 420–450 µm. Tests were carried out using different impact angles (30°, 45°, 60° and 90°) with a particle velocity of 24±2 m/s and an abrasive flow rate of 0.7±0.5 g/min.

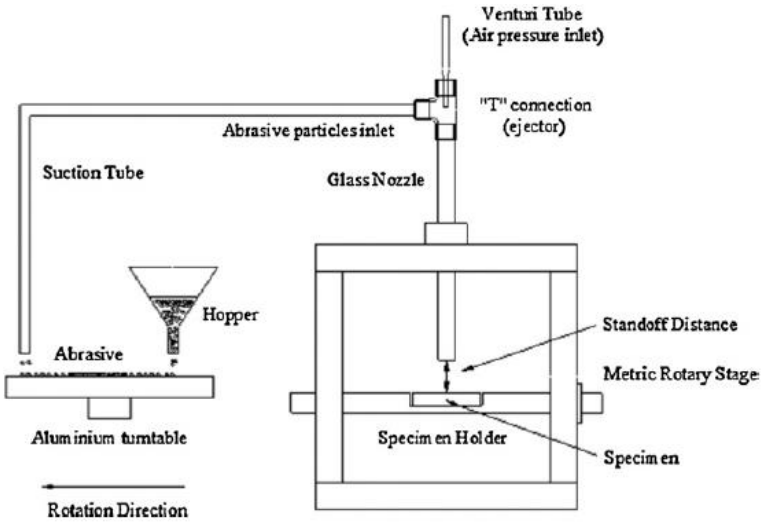

Figure 27. Schematic diagram of the erosion rig developed in [41].

The wear mechanisms identified were pitting and ploughing action at low impact angles ($\alpha \leq 45°$) due to sliding component commonly observed at these incident angles, whereas bigger craters, radial cracks and a more roughened surfaces were seen at angles near or at 90°. In addition, it was observed that the damaged

area was extensive in all of the cases at 30° and 45° reducing considerably the size of worn areas at 60° and 90°. The wear scars were characterized by an elliptical shape at 30° and 45°, which is a characteristic feature when the specimen are impacted at low-incident angles ($\alpha \leq 45°$) whereas a roughly circular was seen at 60° and 90°.

Similar test setup was used in [42], where aluminium balls instead of typical ceramic powder was used as eroding flow. The diameter of the ball was 3mm as defined by droplet size calculations. The frame was placed in a shot blaster which was used to fire aluminium balls at the specimens. In the frame, both flat and cylindrical specimens, made from H13 steel were tested.

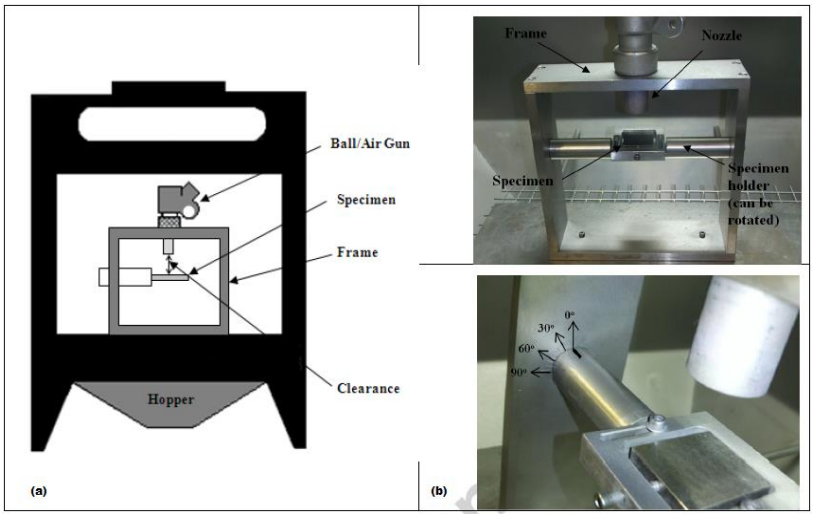

Figure 28. Test Arrangement: (a) Schematic of Overall Test Set-up (with cylindrical specimen mounted); (b) Test Surface Mounting Frame [42].

Different velocities were used and the setup was designed to be rotated to set different erodent impact angles as indicated in Figure 28b.

Flat specimens were tested at different angles and cylindrical specimens were tested centrally to the aluminium flow and in an eccentric position to cover a range of possible aluminium/die impact scenarios. It was concluded that the test method was a suitable approach to represent the erosion seen in aluminium casting dies, being the most representative specimen, the eccentric cylindrical one.

An investigation with a high speed video set-up to determine the impact rate showed that a very large number of balls would be needed to keep the impact rate high, so it was implemented a pulsed approach, i.e., once all balls are fired at the machine, it stops to recollect the balls and to re-fire.

The objectives of mentioned work was to set-up the testing approach; define the type erodent, the application protocol, determine the counter-face to mimic the variable geometry found in a die; in order to study the wear behaviour in function of the type of erodent, contact angle and velocity. The developed methodologies can be used to assess the wear behaviour of a surface treatment or coating in relation to the reference material.

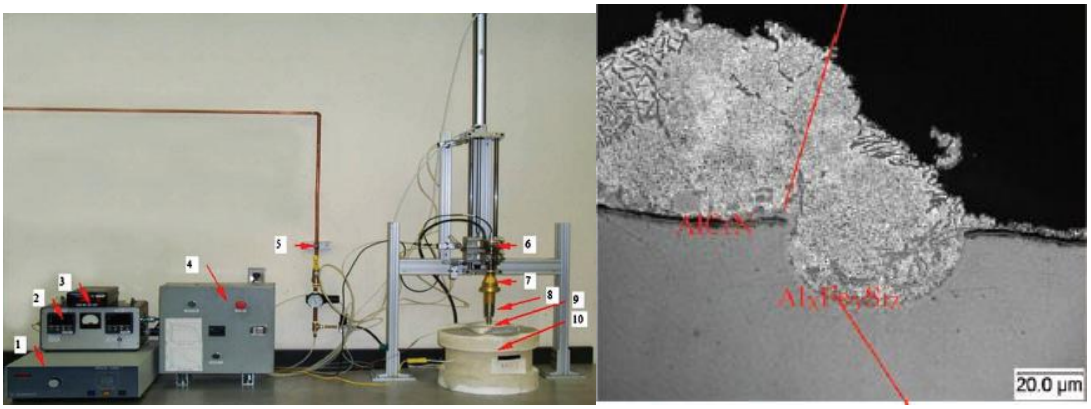

Figure 29. (a) Experimental system for accelerated die soldering test [43].
1: ultrasonic generator; 2: controller for electric furnace; 3: melt temperature indicator; 4: pneumatically operated device; 5: air inlet; 6: transducer; 7: booster; 8: horn; 9: core pin; 10: furnace
(b) results of intermetallic layer formed in the cavitation pit and remaining coating (AlCrN) applied on H13 material pin. Pin was subject to high intensity ultrasonic vibration

Figure 29a illustrates the apparatus built for the accelerated die soldering-**cavitation** test in [42]. It consisted of an ultrasonic generator, a transducer, an ultrasonic horn, an ultrasonic radiator/wave guide to transmit ultrasonic vibration into aluminium melt, and an electric resistance furnace. The ultrasonic radiator, 19 mm diameter and 127 mm long, was the pin to be tested. High intensity ultrasonic vibrations were applied axially to the pin made from coated and uncoated H-13 steel and relative speed between pin and molten aluminium resulted on 2 m/s. The intensity of ultrasonic vibration used in this experiment was so high that **cavitation** was generated in molten metal. The amplitude of the instantaneous pressure employed by the authors' experiment exceeded the threshold pressure since cavitation occurred in molten metal.

Figure 29b shows the cavitation pit formed and soldering formed in the surface for the case of a AlCrN coating applied on the H13 pin. The results indicate that tests under high intensity ultrasonic vibration accelerate die soldering and have potential for using as a rapid test to indicate performance in practice. The experimental results were in qualitative agreement with industry experience of the coatings examined.

2.2.1.3 **Test devices for Die Soldering**

In literature there are a lot of methods to simulate in laboratory conditions the die soldering mechanism or the interaction between melted aluminium and iron. Here it is presented a short list and description about these experimental methods.

Dipping test: this is a test that has been used in different articles [14, 15, 44]. In this test a sample (usually made with the die material) is dipped in melted aluminium kept in a fixed temperature. The melt is in stationary state and the sample is kept inside it for a fixed time (from minutes up to 2 days). In this test it is possible to change different parameters that affects the die soldering, for example the melt temperature (from 580 up to 750ºC, typically 680ºC), melt composition, die material, the presence die protective coatings, die roughness,... For evaluation of the test result, typically it is measured the mass soldered in the sample respect to the initial die material sample mass. It is also possible to eliminate the soldered aluminium attacking with NaOH, in order to measure the die material mass dissolved into the melt. In some cases instead of mass, the change of the pin diameter is used as reference for comparison. It is also quite usual to perform a cut of the sample to measure the intermetallic layers formed in the reaction of the steel with the aluminium. Figure 30 shows very well the structural of the test:

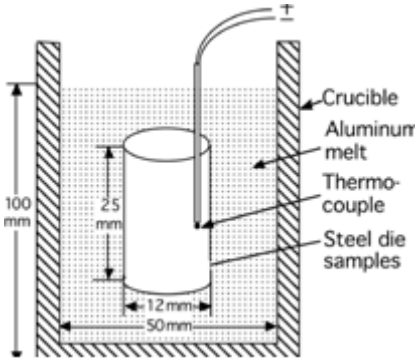

Figure 30: The image shows the experimental set-up of the rotation dipping test.[44]

This test neglects some physical variables that are present into the die during the HPDC process. For example the effect of the pressure applied or the speed of the melt is not possible to simulate. To try to reproduce HPDC process parameters, apart from the cavitation accelerated test presented before, some authors have created a rotational movement of the pin into melt [45,46].

Similarly to dipping test, another variant of this test has been to set a "diffusion couple" test [47], where a disk of die material is preheated at 350ºC, then aluminium melt is poured into the trough over the steel surface, and the system is kept a predetermined time in a furnace at 625ºC . In some cases, these authors half of the H13 steel surface was coated with a layer of white boron-nitride paste to prevent the aluminium from interacting with the steel substrate. This coated area of the surface was used as a reference point to measure the depth of attack on the steel surface by molten aluminium. Afterwards, die-soldered interfaces were metallographically examined.

Casting ejection tests: Molten aluminium has affinity for the steel surface, bare or coated H13 die steel. This affinity results in chemisorption and adhesion (welding) of aluminium on the pin surface. This adhered surface substantially increases the ejection force required to separate the casting from the die surface. A tribologically sound surface (well lubricated with no adhesion) will permit low force ejection of the casting. Adhesive strength between a die casting alloy and die steel is related to the soldering tendency of the two materials.

The approach presented in [49] consisted of solidifying a casting around a coated pin, and then, pulling the casting from the pin using a fixture mounted on a MTS machine. This force of separation is a measure of the adhesive tendency of the casting to the pin surface. A small crucible was used as a mould for the casting process. A measured amount of A380 was melted in this crucible and the coated pin was dipped to a constant depth. After a predetermined time, the melt solidified onto the dipped pin. This solidified cylinder (casting) was then pulled from the pin using a specially designed clamping mechanism, and the force of ejection was measured. They measured a maximum value of 200 MPa when the pin was plain H13, while it was reduced down to around 60MPa when the surface was Nitrided or coated.

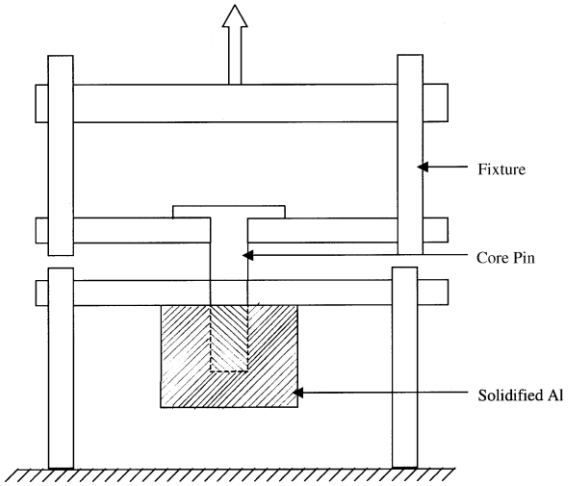

Figure 31: Schematic of the ejection test set up [49]

DSC test: Eduardo et al [48] have studied the die soldering mechanism with an alternative method that is called DSC (differential scanning calorimetric) test.

This test simulate the chemical interaction between the samples similarly to a "dipping test" or "diffusion couple" test, but inside a DSC machine, were the heat flow is controlled and measured, and an inspection of the endo or exothermic reactions, their onset temperatures, the activation energies, and the formed intermetallic compounds reactions is possible to perform through the heat flow measurements. For the test 5 mg sample was subjected to non-isothermal tests at four different heating rates (5, 10, 15, and 20ºC min−1) from room temperature up to 1000ºC. In order to produce samples compatible with the DSC technique, freestanding multi-layered films containing aluminium deposited on die materials or aluminium deposited on coated materials were prepared by physical vapor deposition (PVD), more specifically by Direct Current (DC) magnetron sputtering deposition. Before analysis, the DSC chamber was pumped down to pressures below 10^{-4} Pa, whereas during the DSC analysis, an argon flow (50 ml/min) was used.

Pin/Ball on disc test: This is a tribological test where a pin (in the studied case aluminium) is moved or rotated against a disc (die steel). All the system is in a temperature condition that is below the melting point of the materials, so the contact between the sample and the aluminium, is a solid state contact. With this test, it is possible to follow the wear mechanism that is due to the first interaction between aluminium and iron, and eventually study the effects of the presence of a lubricant film above the surface of the disc, as well as different coatings. Normally this test is used to investigate which is the wearing mechanism and the trend of the friction coefficient with the time.

In this experiment, the user typically has the ability to control and measure the applied normal load, unidirectional speed or oscillation frequency, and environmental parameters such as temperature, pressure, type of gas (vacuum, air, nitrogen, refrigerant, etc.) and presence of a lubricant. Both the normal and friction forces are measured with transducers. The pin holder is attached to a fixture that is allowed to deflect slightly; the transducer measures this deflection and converts it to a force. Performance is generally characterized by friction coefficient and wear rates (wear per unit time) determined by mass or volume loss.

This pin or ball on disc approach has been mainly used in the frame of aluminium hot forming application [50, 51], in order to simulate the adhesion of the aluminium sheet to the hot work tool steel, which doesn't differ too much from HPDC problematic. It is of special interest the publication [52], in which the wear

mechanism that was intended to simulate was the die soldering that occur in HPDC. High temperature sliding tests were carried out in a CETR UMT-2 tribometer with ball-on-disc configuration. Different die steel were located as disc, varying hardness (41 and 52 HRC). An AA2017-T4 aluminium ball (diameter 9.5 mm) was used as counterpart. Different test conditions varying sliding speed (0.025 and 0.05 m/s), load (8 and 15 N) and temperature (250 and 450ºC) were conducted in order to select the optimal test parameters to obtain aluminium adhesion on disc surface. 1400 cycles were performed in all tests in order to obtain measurable and reproducible wear rates that allow computing an average value of the tribological behaviour. Wear scars on disc surfaces were examined by means of optical confocal microscopy scanning electron microscope (SEM, ZEISS ULTRAplus) and energy dispersive X-ray analysis (EDX). The normalized wear rate ($K_{negative}$, in mm^3/Nm) was defined as the volume loss per sliding distance per normal load. An equivalent positive rate ($K_{positive}$) was calculated for stuck or piled up material with the same units. Coefficient of friction was acquired as well, as reference for adhesion appearance when the friction goes up.

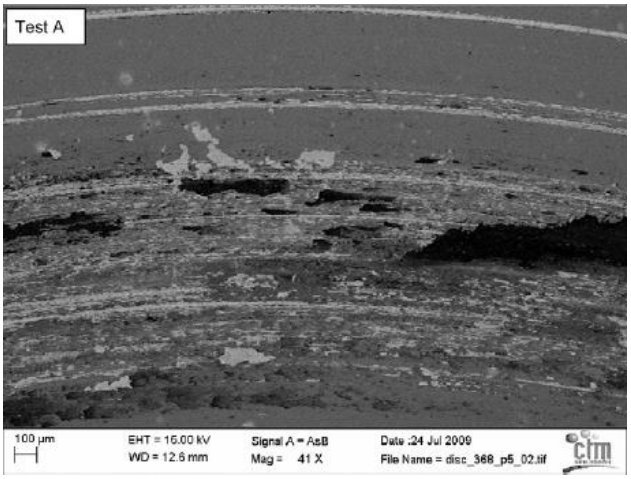

Figure 32: Backscattered SEM images of disc wear tracks with aluminium adhesion in ball on disc test [52]

Pin on die: the approach "multiple-pin flat plate die" shown in figure 26 for erosion case, can be used for the study of die soldering with the correct process parameters. The figure 33 shows the schema of the die used by [1] and carried out on a commercial UBE VSC 315 ton squeeze casting machine, using an accelerated test die with two core pins positioned side by side in front of the chisel gate entry to the die cavity. Experimental facility provided an opportunity to examine the test core pin at any intervals to observe the development of soldering and washout. The operating conditions chosen to accelerate the soldering and washout rate included: the use of an aggressive aluminium alloy A356 and melt temperature of 730ºC, special test pin was designed with flat plane and sharp corners facing the impinging. In order to accelerate the jetting velocity, the gate was designed to be 2.5mm in thickness and 50mm in width, and the test was performed without lubricant to enhance the adhesion.

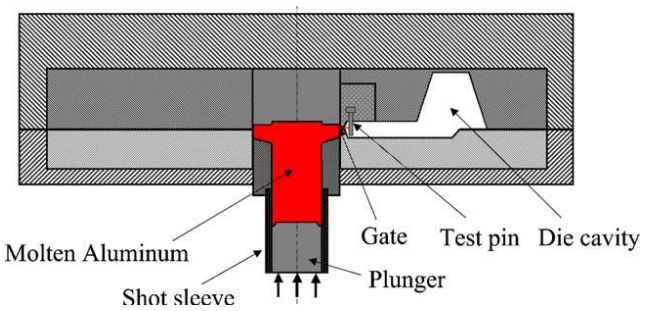

Figure 33. Schematic diagram of the accelerated test die used in [1]

This test simulates well the real conditions of temperatures, pressures and the environmental that occur inside a mould in a real process. As a drawback, it is difficult to control the value of the physical parameters with any consequent possibility to correlate the wear mechanism with a certain physical state. Another consideration is that it's an expensive test, because it requires all the HPDC system to carry out the test.

2.2.2 PIM wear mechanisms simulation in laboratory scale

In the 2.1.2 chapter of this document, some configurations of test pins installed on moulds of PIM for analysis of wear of materials in a semi-industrial conditions were referred. This approach, as for HPDC has the drawback of the need of PIM machine availability, dealing with a lot of injection cycles and its high cost. In this chapter, some different test devices that have been used in literature for the simulation of PIM moulds wear mechanism in laboratory scale are presented, which are spare. The main challenges of simulating the PIM mould conditions are the difficulty to deal with melt plastic and to generate a wear amount big enough that is possible to quantify.

This bibliographic analysis has been focused on the tests that try to simulate the behaviour of mould surfaces. There are some works in literature that are focused on other elements of plastic injection machinery (e.g. DKI [8]), but that it has been considered out of the scope of this work.

2.2.2.1 Devices based Abrasion standard tests

Different authors ([58],[59]) have used a modified system of the **ASTM G65-94 "Rubber Wheel"** to simulate the wear of mould materials, as well as PIM machine barrel and screw materials. Usually, this test is used to characterize the "scratch" wear resistance of metallic materials.

For this purpose, the modifications carried out on the standard device were the following: the rubber wheel have been substituted by a mould steel wheel. As abrasive, instead of sand, fibre reinforced polymer in raw condition in form of pellet have been used. The abrasive is fed into the gap between the wheel and sample from a hopper. The schema of figure 34 shows this test concept.

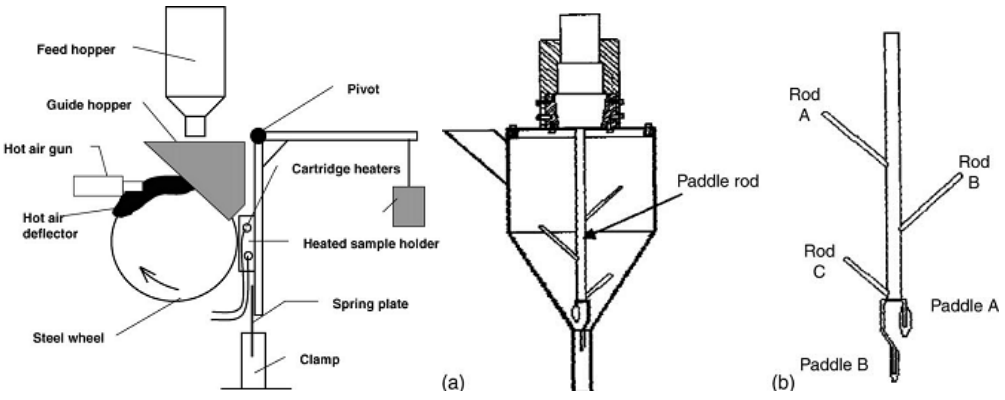

Figure 34. Schematic diagram of the test based on "rubber wheel" developed by [59]

The rim of the steel wheel was heated to the required temperature (above 250ºC) by hot air guns with ±10ºC accuracy. There were small grooves on the rim of the steel wheel in order to increase its ability to carry pelletized feedstock through the contact with the test sample and reduce the likelihood of metal–metal contact (according to the authors, less than 5% of the time is steel-steel contact, which could be reduced even

more). The design of the hopper was very key as well, in order to get a correct feeding of the plastic, and the system was adapted to feed also for long term operation (up to 3 hours at a 3 kg/h rate).

The sample holder was heated independently of the steel wheel by cartridge heaters. The sample was heated also to 250ºC±2ºC. The sample was held in a holder connected to a pivot-loading system that can press it against the rim of the steel wheel with a relatively small load (21.4 N). The sample was maintained at a small distance from the wheel under static conditions using a spring plate and the full-applied load is only transmitted to the granule as it passes through the contact. The contact pressure and duration can be changed by altering the applied load and wheel speed.

The wheel have a rotation movement of 84 rpm and a wear scar is produced at the contact point by a combination of abrasive wear from the glass filler and sliding wear from the plastic. At low temperatures, contact fatigue and impact were predominant, but at 250ºC, the abrasive wear was predominant. The wear analysis of the test was performed through mass and volume loss measurement (assuming that the wear scar adopts a cylindrical cap geometry). They also proposed a method to estimate, for the cases where the wear amount is not very big, through stylus profilometer Ra and Rp measurements before and after testing in the central line of the wear scar perpendicular to the sliding direction.

Because the wear depth D is very much smaller than the radius of the steel wheel, they used two different equations depending on circumstances:

- When there is not very much wear, the asperities in the wear scar are smoothed with respect to the untested profile and the roughness parameter Ra value tends to decrease. The wear depth D is given by: $D = Ra\ (initial) - Ra\ (final)$

- In the case where there is excessive wear, the roughness parameter Ra tends to increase slightly after the test and the previous method is no longer valid. However, another roughness parameter Rp, a measure of the displacement of the mean profile position from a line drawn through the highest peaks in the profile, can be used to give the wear depth D. If we choose a profile, which includes the regions outside the wear scar, the movement of the mean line gives an indication of the average recession of the worn surface during wear, and the wear depth will be given by: $D = Rp\ (final) - Rp\ (initial)$.

The **"Ball Cratering"** [6] shown in figure 35 is another system able to simulate the abrasive wear that have been used for PIM moulds materials and coatings. This is an abrasive test at micro-scale, where a DIN 100Cr6 standard steel ball rotates in an abrasive media against a sample of the mould material which is to be studied. TiO_2 small particle size (Ø 0.1–0.4μm), which is usually applied as a white pigment in injection plastics, suspended in water at 2.4% volume is used as abrasive. The rotation speed is 150 rpm and the applied load is 0.35 N.

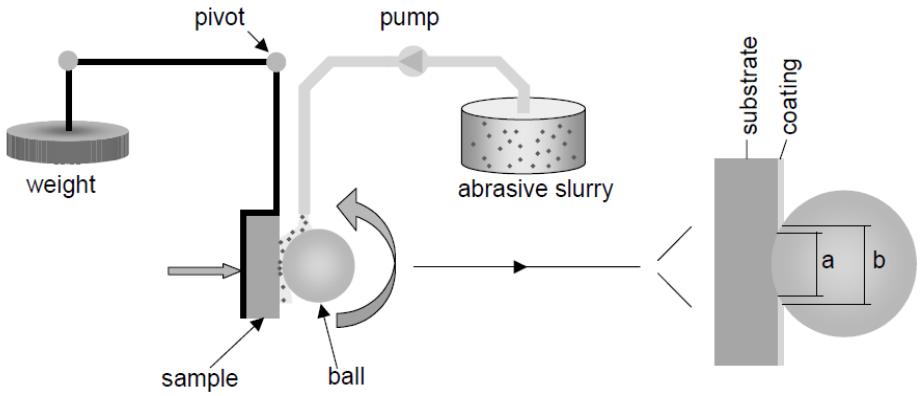

***Figure* 35. *Schematic diagram of the* "ball cratering" where a ball rotate at 150 rpm against a sample loaded (0.35 N) by weight [6]**

The authors showed that using the selected abrasive instead of the SiC angular particles, which are typically used in this test at 11.8 % volume water suspension, and are 2.4 times harder than TiO_2, led to different wear mechanism. This explained the much higher wear amount formed by SiC particles.

The test with SiC underwent rolling and grooving, while the wear mechanism with TiO_2 was always a rolling wear. The craters looked as if they were polished due to the applied mild abrasive test conditions. These mild conditions are due to the spherical shape and the small size of the titania rutile particles with relative low hardness compared to most of the tested coatings. The fact, however, that the wear mechanism remains the same for all tested coatings, enables comparison of abrasion resistance and ranking. They compared successfully 10 different coatings and different types of deposition methods (PVD, CVD, PACVD, LTPVD). After the test, the wear analysis was performed through the calculation of Archard wear factor [8] from wear volume measurement, taking into account that coating and substrate can have influence on it, since usually the coating was worn during the test.

The tribological test named "Block on Ring", is a device that was used by [56, 57] for the study of the wear of moulds (in this case aluminium and copper based alloys) generated by fibre reinforced plastics. The wear mechanism formed in the mould material was adhesive-abrasive, and in consequence they named the test protocol “adhesive dry wear test”. The surface suffered grooving and pitting due to the abrasive nature of the fibres and plastic material was adhered as well in the disc surface.

A disc of mould material (Ø35 mm and 10 mm thick) rotates at 200 rpm against a fixed a plastic block (20x15x8 mm), with an applied normal load of 500N. 15 minutes tests resulted in a wear amount, big enough to be quantifiable for a comparison study between different solutions. Mass loss due to the wear and friction measured during the test, were used for comparison purpose. The friction measured of the aluminium against the different plastics was 0.3-0.4 while 0.4-0.6 was recorded for the copper. Temperature measurements in the disc surface due to frictional heating were performed using a pyrometer, achieving 50-90ºC for the aluminium and 35-45ºC for the copper. Roughness measurements (Ra and Rz) were performed according to ISO 4287 standard in a profilometer to have an idea of the surface degradation.

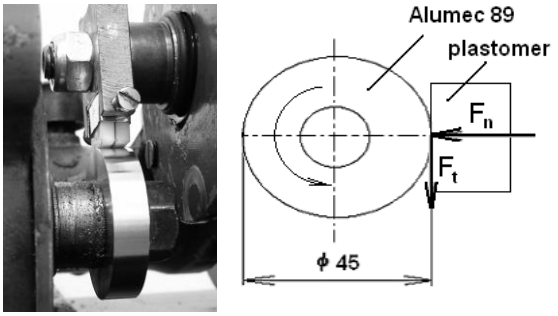

***Figure* 36. Aspect of the friction pair and schema of the test [32]**

2.2.2.2 Test devices for Corrosion

Most of the material corrosion failures are due to electrochemical attack, since the metallic materials contains free electrons that are able to generate an electrochemical cell.

The tests described in the bibliography to characterize the corrosion resistance, are mainly focused on uniform corrosion of different candidate mould material or coatings, but it is of interest to evaluate the corrosion potential due to pitting as well.

An example of corrosion test consist of introducing the mould material in a corrosive solution (5% HNO_3 - 1% HCl, or 10% CH_3COOH in [58]), and after certain immersion time, analyse the chemical wear, similarly to mechanical wear tests, measuring the mass loss and by surface visual analysis. The most common corrosion standard test is the "salt spray method" (ASTM B 117; using a solution of 2% NaCl in distilled water) [60].

Another approach to evaluate the corrosion behaviour is through the use of Potentiodynamic tests. The EG&G Princeton Applied Research [10] used a Potentiostat/Galvanostat Model 362A. The flat cell is a three-electrode setup consisting of the specimen as the working electrode, a saturated calomel electrode (SCE) as the reference electrode, and a platinum sheet used as the counter electrode. 3.5% NaCl solution was used as the electrolyte.

Potentiodynamic polarization was swept from -1000 to 1500 mV at a fixed rate of 1 mV/s. The potential variation generates a variation of the system current, making possible to calculate the parameters related to the kinetics of the electrochemical process. The obtained anodic polarization curve was used to calculate the pure corrosion rate (Wc). It was shown (figure 37) that the steel didn't suffer any passivation of the surface, and it was a continuous dissolution. The corrosion potential was -0.5V (SCE).

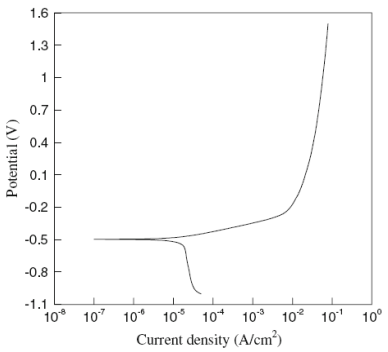

***Figure* 37. Polarization curve of the plastic injection mould NAK80 in a solution of 3.5% of NaCl [10]**

According to Faraday law, a corrosion current of 1mA/cm^2 is equivalent to a mass loss of 1.04mg/cm^{2}h for a steel of 7.8g/cm^3 and an atomic weight of 55.85. For the polarization curve, the current measured was 0.016mA/cm^2 and the corresponding mass loss by corrosion was 0.017 mg/cm^{2}h.

Apart from this technique, it is the possibility to calculate other parameters, like the open circuit potential, Electrochemical Impedance Spectroscopy (EIS) or the measurement of electrochemical noise. Electrochemical Impedance Spectroscopy is a technique particularly interesting to determine the corrosion mechanism. The corrosion resistance should never be considered a constant and absolute property, since it will always depend on the chemical composition of mould material, the corrosive agent and also the exposure time. These techniques can be used to screen the resistance of mould materials to corrosion in a certain media.

2.2.2.3 **Combination of erosion – corrosion**

In the bibliographic reference [10], apart from the measurement of corrosion resistance, it was considered the combination of corrosion and erosion as characterization test. It was seen that the synergy of the both mechanisms was between the 40 y 60% of the total wear amount. In any case the wear was very influenced by the particles speed and not much by the angle of attack or the size of the particles.

This corrosion-erosion test consists in samples of 80 x 25 x 3 mm^3 mould material, that are located in the specimen holder at different orientations respect to the flux, as shown in figure 38. It was carried out by using a rotating slurry wear tester as shown in figure 38a with the same electrolyte as that in corrosion test (3.5% NaCl) plus 20 wt.% of irregular Al_2O_3 particles. To analyse the synergism between erosion and corrosion, some weight loss tests in distilled water with 20 wt.% Al_2O_3 particles were also conducted to obtain the pure erosion rates.

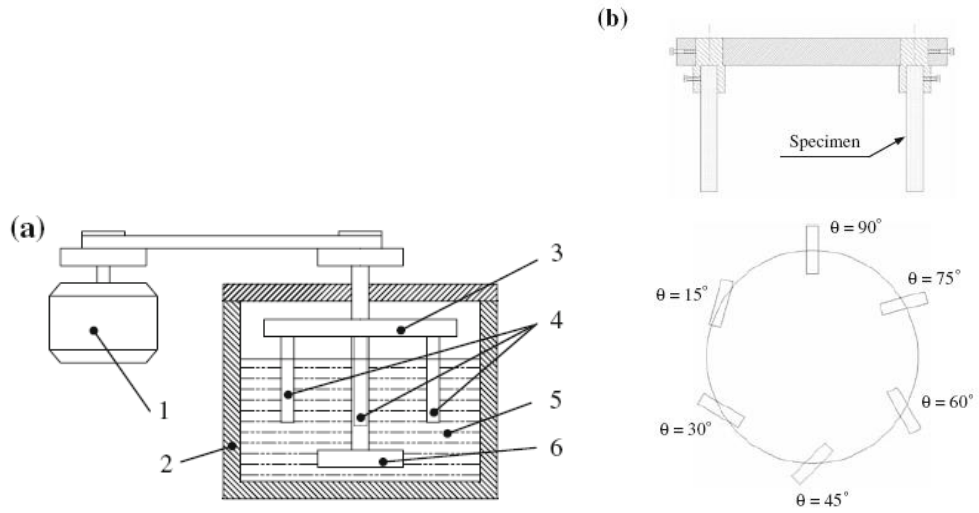

***Figure* 38. a) Schematic representation of the erosion–corrosion tester. (1) motor (2) slurry pool (3) specimen holder (4) specimens (5) slurry (6) stirring blade. b) Holding method and orientation of specimen [10]**

The test conditions used in the study are summarized in the table 2:

Slurry composition	20 wt% Al_2O_3 particles + 3.5% NaCl solution
Particle size range (μm)	S: 255–335, L: 530–625
Impact velocity (m/s)	4.2, 7.3, 10.4
Impact angle (°)	15, 30, 45, 60, 75, 90
Test duration (min)	120
Test temperature (°C)	20

Table 2. Parameters used for erosion-corrosion [13]

After the test, similarly to other wear tests, mass loss was used to quantify wear and surface analysis by SEM was performed to investigate the wear mechanism.

2.2.3 Discussion

Both HPDC and PIM consist of introducing at high pressure, high temperature and high speed a fluid material that solidifies inside a mould. The flux conditions that have to endure the moulds, with melt aluminium and plastics, is nearly impossible to simulate in simple laboratory devices in order to investigate the wear of moulds. As the damage of the moulds is ruled by different wear mechanisms, most of the authors approach is to try to build at laboratory scale, experimental procedures to simulate each wear mechanism separately. All of them have some limitations, but they are useful to have some initial conclusions of the nature of the phenomena and compare candidate materials. In this study it is also proposed a methodology based on this kind of simplified experimental tests.

For the simulation of thermal fatigue appearance in HPDC moulds, the different authors have tried to replicate the thermal cycle that the moulds endure in simplified samples. Three are the key aspect when comparing the different test devices available in literature: the way the surface is heated, the way the surface is cooled and the geometry and possible internal cooling of the sample. In bibliography there can be found devices based on heating with molten aluminium [3], resistance based heating [27], induction heating [11] or even natural gas [28]. The external cooling is achieved by introducing the samples in a bath of water or oil, or the surface is directly cooled by a jet or spray. The test samples are very varied, and in some cases developments were made to find an optimum sample geometry [4]. In this doctoral thesis, the machine that have been used to simulate the thermal fatigue of dies is a newly developed machine that is considered that outperforms all the devices used before in literature. This machine heats an internally cooled sample surface by induction, as fast as in HPDC process, avoiding the problems of dealing with molten aluminium like sticking and its influence in crack growth, and the external cooling is performed through spraying of water or water based lubricants, as it is made in HPDC processes. Additionally high temperature mechanical fatigue tests are performed to build fatigue curves that are needed to improve the existing models.

There are a lot of methods in literature that have been used to simulate in laboratory conditions the die soldering mechanism or the interaction between melted aluminium and iron. Most of them are relatively simple, like the so called "dipping test" or the "diffusion couple test" where a test sample of mould material and aluminium alloy usually in molten state are kept in contact at high temperature (between 550 and 750ºC) for a fixed time. Some variants are to leave the aluminium solidify and measure the strength necessary to separate the soldering, or set the two materials to react in a DSC machine where the heat exchange of the reaction (endo or exothermic) can be measured. For this study, a similar pin on disc approach proposed by [52] have been used, where relative speed, applied pressure or temperature can be changed. As novelty, a

lubricant have been applied between the mould steel disc and aluminium alloy pin, in order to evaluate the time to failure of the lubricant protection and start of soldering. This time of failure have been evaluated in function of the temperature, pressure and speed, and have been tested for different lubricants as well.

The simulation of erosion in the laboratory, it has been mainly performed for solid particle erosion with devices similar to the definitions of the ASTM G76 [41, 42], even if some studies were performed about cavitation as well [43]. The "multiple-pin flat plate die" proposed in [33], was performed in semi-industrial stage, and showed that at least at relatively low melt temperature, solid particles are embedded in the melt and is the ruling wear mechanism in die erosion in gate areas. Said that, in this study a test based in ASTM G76 have been used to simulate the erosive wear, using alumina powder as erodent. The main novelty of this approach has been to build a model from the experimental results in order to have a predictive equation of the wear. Furthermore, it has been built in order to be representative of the wear of PIM moulds as well. The erosive wear of PIM moulds has been also simulated with an innovative test where a mould material sample is subjected to the air jet erosion of plastic pellets, following the protocol based on the standard ASTM D3170. Using this second test, it has been possible to study the influence of different plastic materials on the wear of different mould materials.

The abrasive mechanisms that is generated in PIM mould surfaces due to glass fibres have been simulated before with, at least, the three different test protocols shown in this literature review. They are based in modification of standard tests, which is considered a good starting point. The "ball cratering test" is considered relatively far from the actual mould conditions, since even if the abrasive slurry was carefully selected, there is some influence of the metal-metal contact between the ball and the flat sample. The "rubber wheel test" is considered to be more close to the actual mould conditions, since the abrasive is the reinforced plastic in a condition near to fluid, since sample temperatures are quite high. In any case it is expected to have some component of the wear due to the metal-metal contact as well. In the "block on ring test", it is not this metal-metal contact drawback. In this doctoral thesis, a reciprocating pin-on-disc tribological tests has been selected, where the conditions are similar to the "block on ring test" but it has been tried to enhance the similarities to the PIM moulds through heating the mould sample to 100ºC. With this test it has been possible to study the influence of the pressure and speed, as well as different plastic and mould materials.

For the simulation of corrosion of mould surfaces, different techniques have been applied, as "salt spray methods" [60] or "potentiodynamic tests" [10]. In this study, Electrochemical Impedance Spectroscopy (EIS) has been selected as the most suitable test protocol. The main advantages are that is fast and non-destructive technique, being possible to evaluate the evolution of corrosion resistance with the time immersed in the corrosive electrolyte. Another key aspect is the selection of an appropriate electrolyte. Different electrolytes have been used in literature for PIM application (5% HNO_3 + 1% HCl, 10% CH_3COOH or 3.5% NaCl), but in this study 1% NH_4Cl has been selected. This selection has been done attending to the composition of the typical plastics used. It is likely that the NH_3^+ and the HCl^- that represent the selected electrolyte, appear in this application. It was also mentioned in literature [8, 9] that the fluorides and halogens (Cl, Br, F) could appear in the plastics due to additives like flame retardants, and they are somehow represented through the existence of Cl^- ion in the electrolyte.

2.3 Mathematical models applied to predict wear on moulds

Simulation software's for HPDC and PIM process's had a huge advance in recent years. One of the latest's area to be included is the wear prediction of moulds. In fact they are complex phenomena that need a huge amount of experimental data to be able to predict them.

From experimental results it is possible to obtain mathematical models that represent how the system is wearing in function of the different parameters, in order to have a tool that makes easier the selection of

different material candidates and makes possible the evaluation of future maintenance costs when the production of a new part is set up by mould makers.

Building this kind of wear models have been of interest for several tribological systems and subsequent wear mechanisms. Depending on the wear mechanisms, the most affecting parameters are different. R.G. Bayer in the book "wear analysis for engineers" [61] proposed a glossary of 88 different wear mechanisms that can appear depending on the tribological system. These terms have been frequently used by authors, not being always fully understood the difference between them. As an example, fretting term have been used for a kind of vibration of very small amplitude and high frequency, and also for a wear mechanism when a special kind of wear debris appears.

When it is intended to make the mathematic modelling of a specific wear mechanism, the bibliography proposes multitude of different equations, depending on different working conditions, material constants and other kind of parameters. For example for the erosion mechanism, once filtered to mature authors and equations with logical consistency, there were found by [62] at least 28 different equations. Each of them depends on different variables (density, hardness, speed...), up to the total 33 shown in table 3, that include material properties, thermodynamic quantities and other "engineering" variables. Furthermore, for example the speed, which would be expected to be elevated to a power of 2 due to the momentum of the particles, exponents cover a wide range from 2 to 5 (average about 3). Even if these equations are valid for the very specific case studied by the authors, it looks evident that it is missing the complete understanding of the involved phenomena.

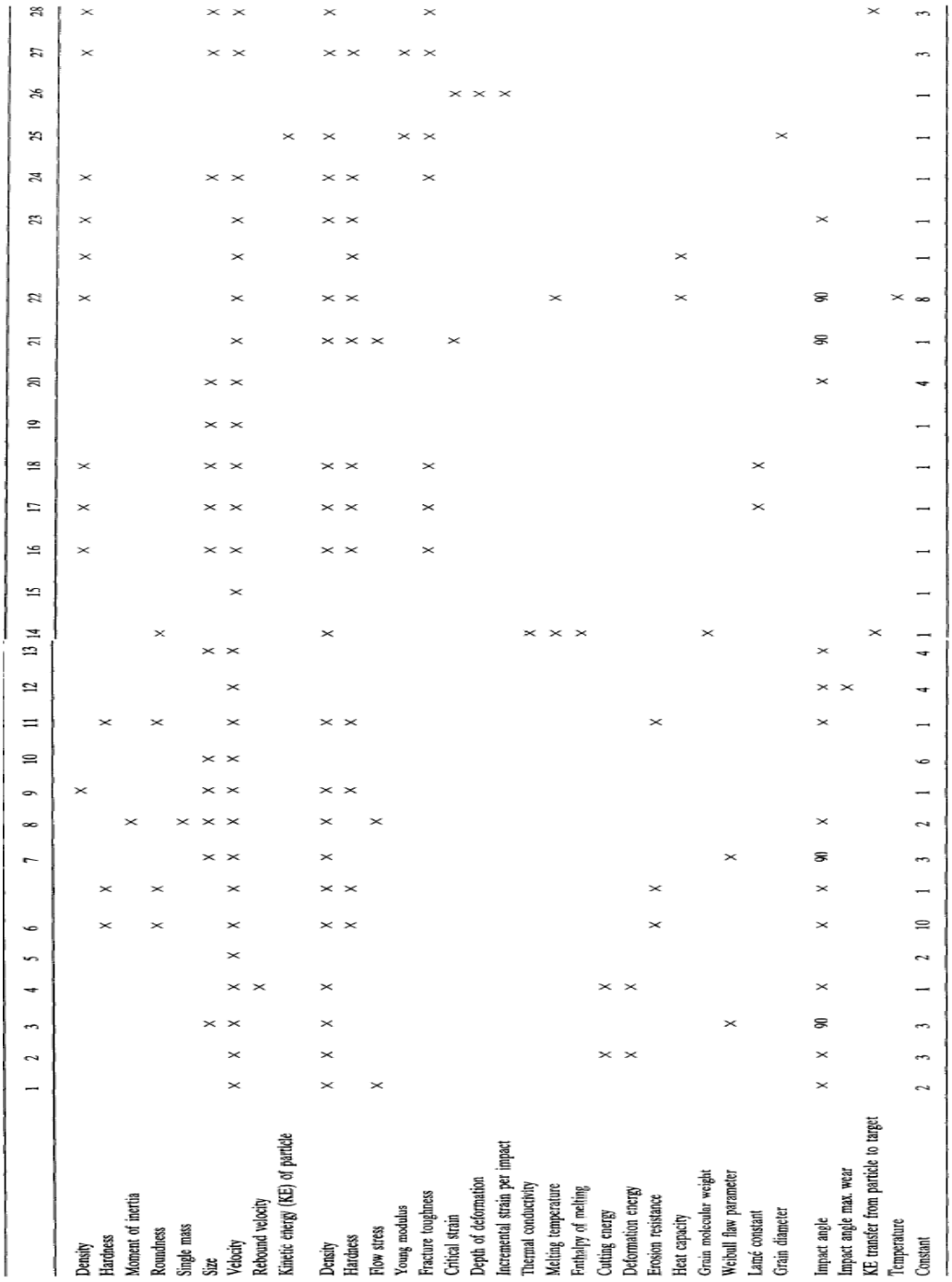

Table 3. Parameters selected in models for erosive wear (up to 1995) [62].

In this line, it is of interest the historic perspective about the emergence of wear predictive equations. H.C. Meng and K.C. Ludema [62] propose three different stages between 1947 and 1992, even if they are overlapped between them:

- Until 1970: Empirical equations: They are directly constructed with data taken from tests in which a few testing conditions were varied.
- 1970-1980: Contact-mechanics-based equations: They usually begin as models of a system, assuming simple relationships among working conditions. Some account is often taken of the topography of the contacting surfaces as well, in order to calculate the local region of contact. Many

of these equations are based on the assumption that a conventional material property (of the author's choice), usually Young modulus (E) or hardness (H), will be important in the wear process. An example of this type, is due to Archard [8], who published well in advance of the later "contact mechanics era".

- From 1980 to now: Equations based on material failure mechanisms: Authors appear to recognize that wear resistance is not an intrinsic property of materials and that mechanical properties chosen for mechanics purposes (e.g. for calculation of real contact area) may not apply directly. The earliest material phenomena studied include dislocation mechanics, fatigue properties, shear failure defined by slip line analysis and brittle fracture properties.

In conclusion, each tribological system, in any scale, needs a specific experimental simulation due to the following factors:

a) Material characteristics.
b) Dependency of the material characteristics in other factors like temperature or phase changes.
c) Dependency of the tribological characteristics on the applied load, speed, temperature and surface factors.

The paper shown in annex 1, which investigation was the embryo of this doctoral thesis, shows clearly how an optimally generated wear model (in this case, contact mechanics based equation), can lead to a good wear prediction. In this investigation, abrasion wear mechanism due to the friction and wear of a cylinder liner against a piston ring were experimentally studied in simulated laboratory tests, simulating the start/stop wear generated at the top dead centre, near the combustion chamber. The parameters which were controlled in these tests included oil type, lubrication starvation, surface finishing and surface coatings. The obtained experimental data were fed into a specific simulation model (AVL Excite-Power Unit). Comparison of experimental and simulated results yielded an error below 5 %.

2.3.1 Models for HPDC moulds wear

As stated before, HPDC moulds wear affects a lot the quality and final cost of the aluminium part. The different software developers for HPDC process simulation, are introducing the possibility of calculating the influence of mould design and the process parameters in their wear. As an example, some wear calculation results of the Music project [53], performed in the commercial software MAGMASOFT are presented here.

MAGMASOFT is in the cutting edge of this field, having already introduced modules for Die Erosion, Die Soldering and the latest developments were for Fatigue Die Life Time.

In the Music project, 65 different designs were simulated on new MagmaSoft Release 5.3. This optimization process included Die Erosion and Die Soldering calculations. Some results for Die erosion of ejector die in three different designs are shown in figure 39 where die erosion areas has been highlighted.

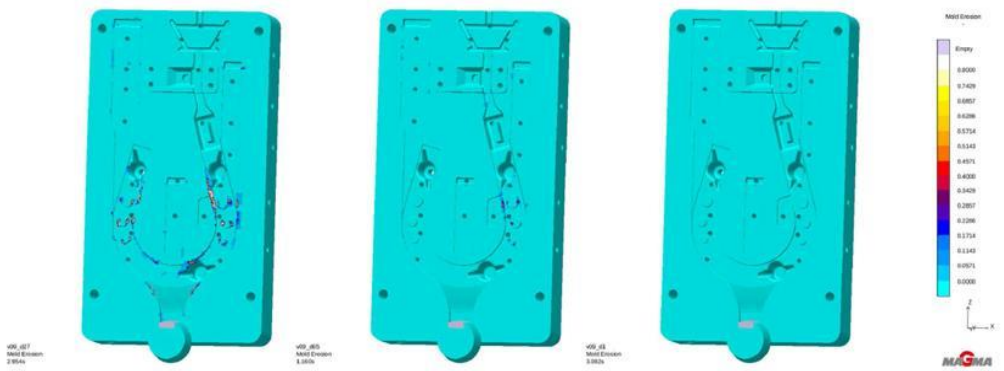

(a) **(b)** **(c)**

***Figure* 39. Results of Die Erosion in Ejector die for worst design (a), Reference design (b), Best design (c)**

The correlation diagram for die erosion of figure 40 had shown that the filling velocity was the main influencing parameter on die erosion. The detailed results of this investigation are presented later, in the chapter about erosion wear mechanism, now, it is shown the strong dependency on flux speed.

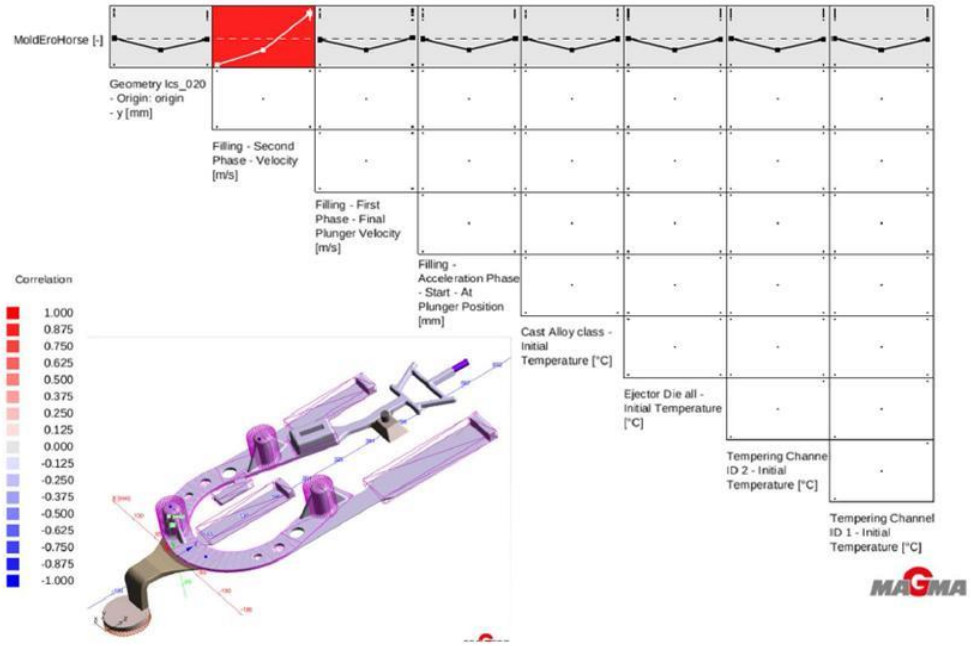

Figure 40. Correlation and main effect diagram for Die Erosion

Some results for Die soldering appearance areas also for three different designs are shown in figure 41.

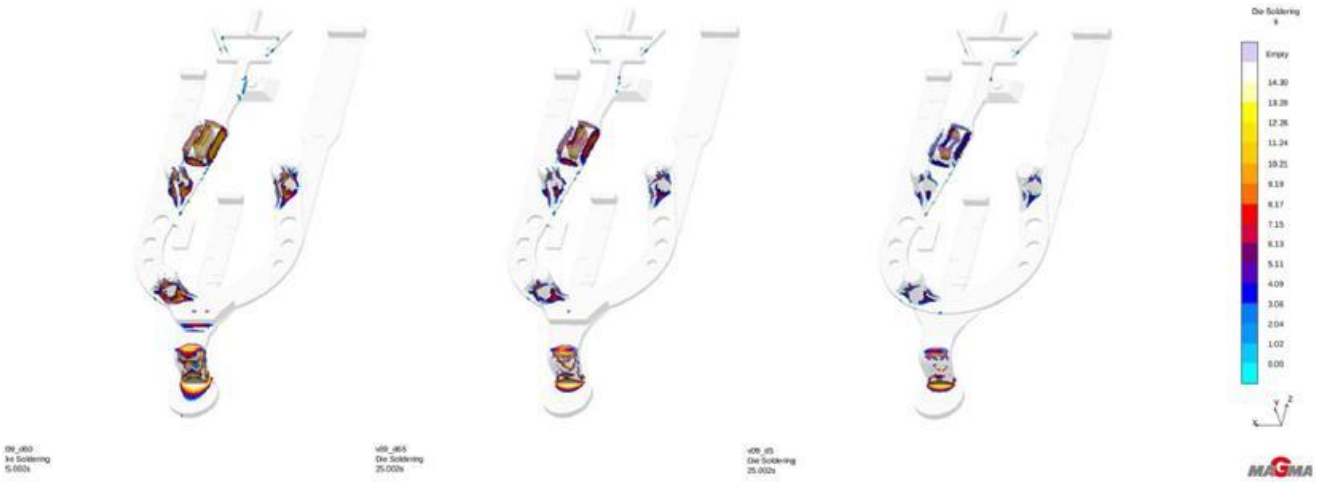

(a) **(b)** **(c)**

Figure 41. Results of Die Soldering for worst design (a), Reference design (b), Best design (c)

The correlation diagram for die soldering of figure 42 had shown that the die temperature, followed by cast alloy temperature were the main influencing parameter on die soldering. The results presented later in the document in the chapter about die soldering wear mechanism, also show this dependency on temperature.

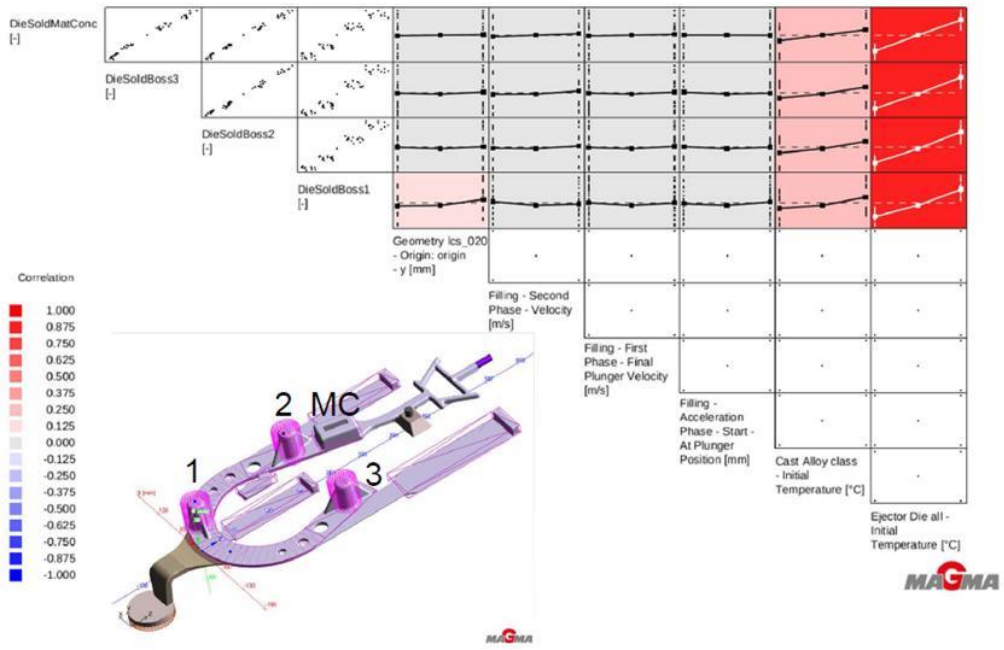

Figure 42. Correlation and main effect diagram for Die Soldering

The MAGMASOFT Fatigue Die life Time Module is based on stress and strain values calculation for the prediction of number of shots until crack initiation. Crack propagation and the number of shots until the surface quality of the cast part becomes insufficient, is not predicted. The concept of the workflow is represented on figure 43.

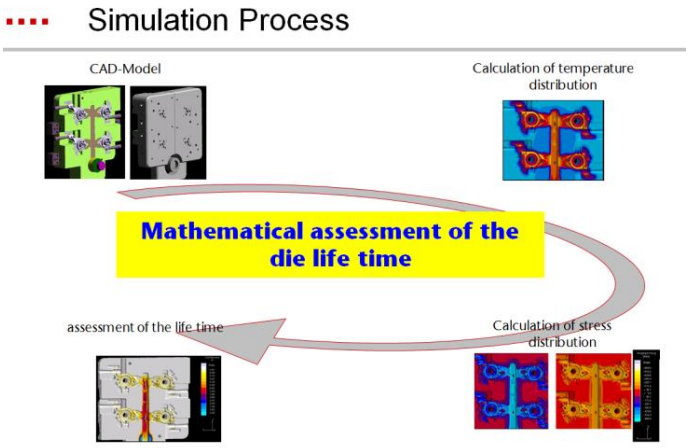

Figure 43. Simulation process for fatigue cracks appearance calculation

The module is capable of calculating the compressive stresses in the surface while heating and the tensile stress's in the surface while spraying, shown in figure 44. This calculation needs a fine mesh normal to the surface to be able to show the stress gradient (approx. 0.5 – 1.0 mm edge length).

The dependence of these stresses can be calculated in function of material properties like coefficient of thermal expansion, heat conductivity or the steel high temperature strength.

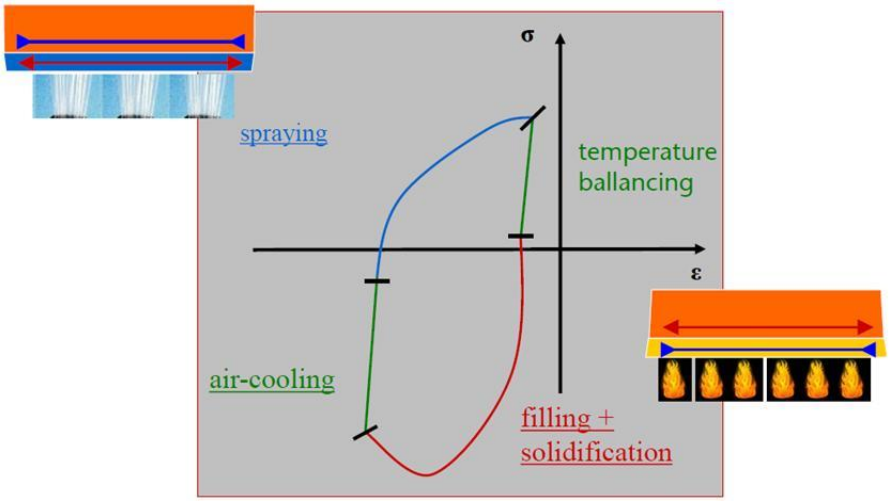

Figure 44. Stress amplitudes and corresponding temperature

The software is able to identify the most critical areas of the cracking appearance, as shows the example of figure 45. For the connection between the stress's and die lifetime is necessary to have the experimental data of Wohler (Stress-Number of Cycles) curves that has been generated by the High Temperature Mechanical Fatigue tests, described in the related chapter of this document.

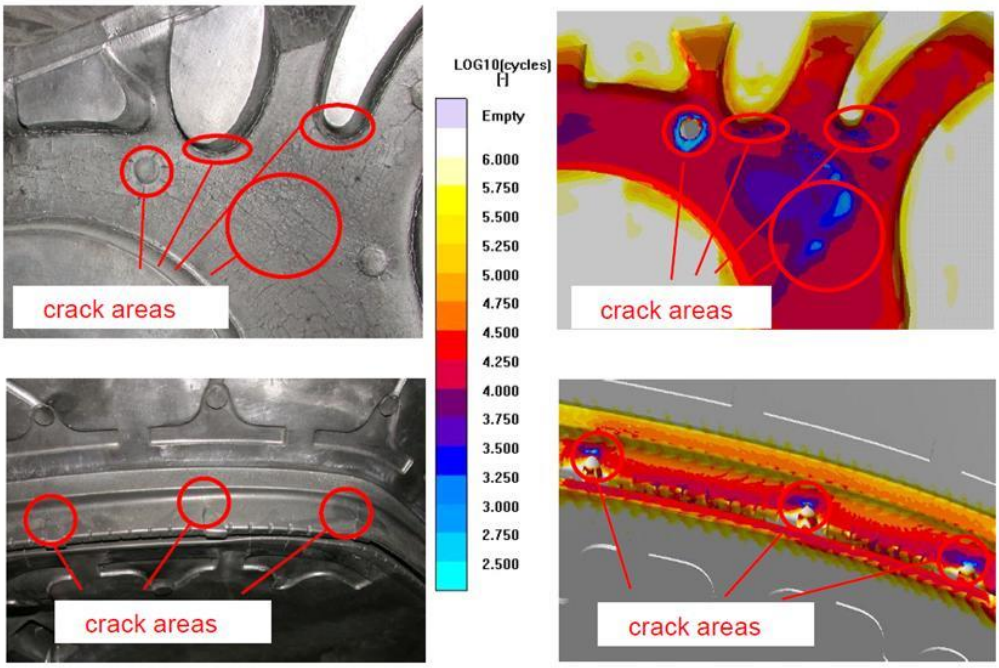

Figure 45. Example of comparison between real cracks and simulated lifetime

The models applied in commercial software's like MAGMASOFT are not available in open literature. Few authors have published in the open literature their research about finding equations able to predict the failures of the HPDC moulds. Most of them are presented in the following lines.

2.3.1.1 Thermal Fatigue models

The approach shown before applied in Fatigue Die life Time Module of MAGMASOFT, is similar to the commonly accepted procedures in fatigue analysis [29]. Once the thermal calculation of the die temperatures are calculated in a HPDC simulation software, the two key steps are the calculation of the stress and/or

strains generated due to the thermal differences in the mould material, and the equation that connect these stress and/or strains and the time to cracking appearance.

The first key aspect is possible through several software packages of Finite Element or Finite Volume Methods, once a correct model is built reliable calculations are expected [69]. The second one, needs to generate experimentally the knowledge to connect the stresses and the time to failure.

This approach was adopted by [2], temperature fields were acquired directly in situ in a HPDC die instead of performing simulations. Stress analysis from the steady state measured temperature of the die surface was calculated through a simple FEA model and the resulting stress fluctuation was applied to a fatigue equation for the die material, the predicted number of cycles for cracking to start was found to correlate well with observed die damage.

The measurements were performed with 2 thermocouples located in an insert in the shot plate. Apart from the temperature measurements, they also estimated the die surface temperature through the *Riemann temperature* calculation, which correlated relatively well with the measured values.

From the measured die surface temperatures, stress fluctuations were calculated, through a simple FE analysis in ABAQUS software. A column of 100, 0.2 mm elements was used to model the die surface using C3D8T elements (Coupled Temperature-Displacement Elements). A transient analysis was used to model the changing temperature trace with time. The simple column of elements used to model the die is shown in figure 46, the column of elements are restrained in the x and z axes, to replicate the bulk of the surrounding die material around the simplified model, but is free to move in the y axis, vertically. This model was used to calculate the resulting stress and strain from a temperature applied to the top surface of the model as indicated in the figure. This simplified method was used due to the fast calculation time and ease of change of parameters, such as the applied temperature trace.

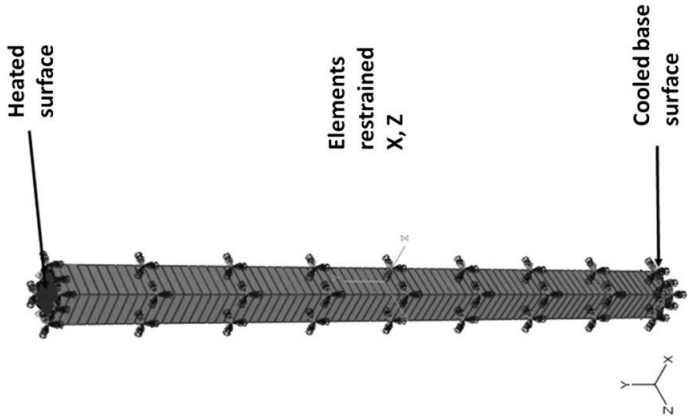

Figure 46. Column of elements used for the simplified stress analysis.

The figure 47 shows stress-strain calculated for a normal and interrupted die start, where it can be seen that the interrupted start shows a much greater fluctuation of stress than the normal start, indicating that the stress and strain fluctuations for the interrupted start will be greater than that of the normal start.

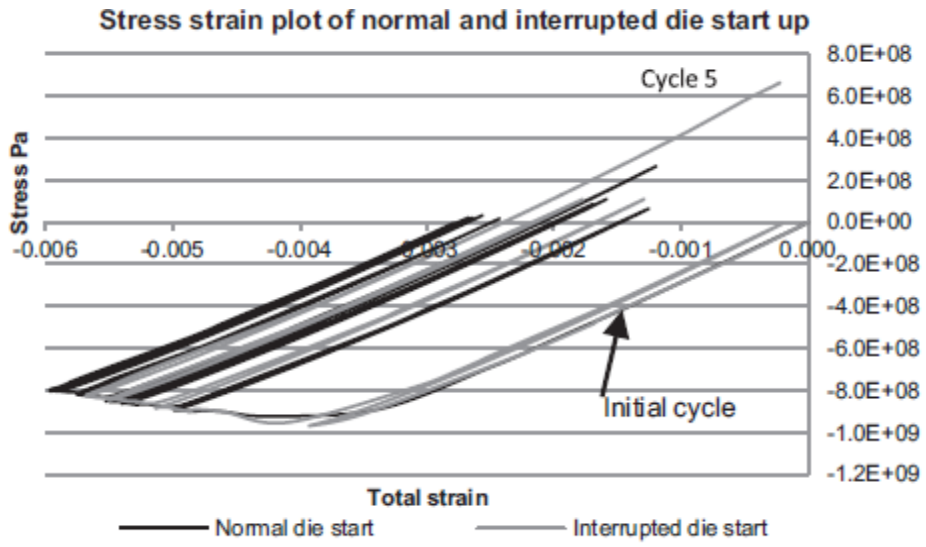

Figure 47. Graph showing a stress strain plot of the normal (black colour) and interrupted (grey colour) die start up.

The stress fluctuation was determined during steady state production and found to be, $\Delta\sigma$=842 MPa. This stress fluctuation was then placed into the following equation from [70] to determine the number of cycles before die cracking would occur.

$$\frac{\Delta\sigma}{2} = 1601 \times 10^{6} N^{-0.148}$$

The stress fluctuation of the standard cycle when applied to the fatigue life equation gave a predicted number of casting cycles consistent with the onset of heat check cracking observed experimentally on two different die casting shot plates.

Even better would be to be able to connect directly the calculated thermal differences with the cycles to failure, but this approach is more complex to set experimentally in order to be close enough to the thermal gradients of the application. Measuring accurately the generated temperatures in the test sample is quite difficult as well.

This approach was adopted by [63], where a model was built from an experimental results where a notched sample was heated in an oven to a certain temperature and cooled down in a bath of water. Thermal fatigue crack initial (TFCI) was identified as the moment when the crack length was of about 0.25 mm. The TFCI life of hot-work die steel was described by the following expression: $N_i=K(\Delta T-\Delta T_0)^{-2}$. This expression was derived according to the modified Manson–Coffin expression and the strain range caused by thermal stress.

According to this approach, for a particular steel, under given treatment conditions, there is a critical temperature ΔT_0 for TFCI life. When the specimen surface temperature change ΔT is less than ΔT_0, i.e. when $\Delta T<\Delta T_0$, under these treatment conditions the TFCI life of this steel tends to infinity, i.e. there is no thermal fatigue damage. K is a parameter related to the mould material.

In the publication [3], a model for predicting the thermal fatigue cracking using FEM software was developed. The general thermal fatigue equations are modified to model the cracking in die-casting and predict the number of cycles and regions more susceptible to such cracking, resulting in the following equation:

$$N_F = \left(\frac{C\varepsilon_f}{\alpha\,\Delta T - (1-\upsilon)\Delta\sigma/(E-\varepsilon_T)} \right)^{1/n}$$

In this paper, two models are discussed: (1) to determine the cracking direction, (2) to determine number of cycles to failure. The first model uses a stress based theory, whereas the second model takes into account the plastic strain. The plastic strain is calculated from temperature; stress and strain values obtained from FEM analysis and is used to calculate die life from modified Coffin Manson equation.

DEFORM 3D package was the FEM software used, where the thermal conditions were modelled using heat transfer environment for aluminium, air and water. Two graphs (temperature versus time and heat transfer coefficient versus time) are input in pre-processor corresponding to thermal cycle. Figure 48 shows the temperature and stress profiles for the simulation of a very simple hypothetical die (die: 12 in.×6 in., cavity: 3 in. × 2 in.) at three points, on the surface, 0.5 and 1.5 in. into the surface.

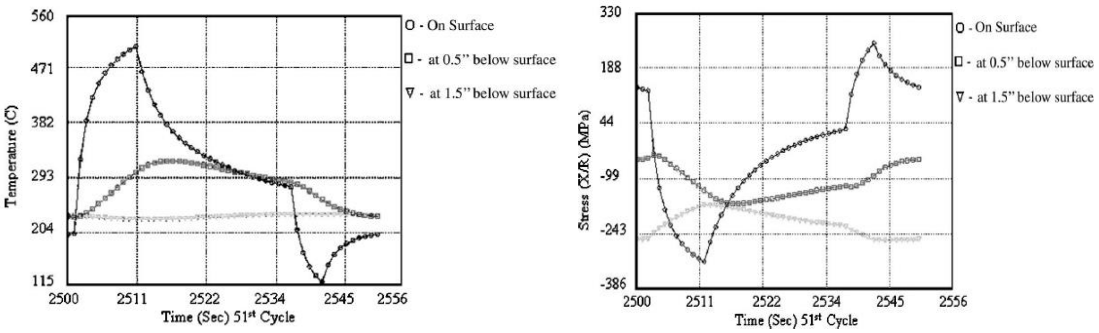

Figure 48. (a) Temperature profile and (b) stress profile (X-direction).

The simulation of the hypothetic die, at two different thermal conditions, applying the modified Coffin Manson equation led to increasing (by 100 ºC) the temperature and thermal gradient, the number of cycles decreased tremendously, which has been observed in die-casting industries. These predictions were to be further validated in real die castings. Some simulations were performed as well in some test coupons and the prediction of the direction of cracks based on the direction of principal stresses, where the direction of cracking would be perpendicular to the plane of maximum stress. The direction of cracking as predicted in followed the same trend as observed in the actual experimental run, so this approach was successfully validated.

2.3.1.2 Die soldering models

The very first soldering equation found in the bibliography was proposed by Hianliang et al. [64], which is an energy criterion for soldering:

$$\frac{A_r}{A_a} \geq \frac{2\gamma_\alpha}{\gamma_\alpha + \gamma_\beta - \gamma_{\alpha\beta}}$$

Where A_r = real contact area between die and casting
A_a = apparent contact area between die and casting
γ_α = surface energy of the casting
γ_β = surface energy of the die
$\gamma_{\alpha\beta}$ = interfacial energy between the casting and the die

This is based on the theory that the energy required to separate the soldering interface:

$$W_1 = A_r (\gamma_{\alpha+} \gamma_\beta - 2\gamma_{\alpha\beta}).$$

And the work required to divide the aluminium casting into two parts is:

$$W_2 = 2A_a\gamma_\alpha.$$

Alternately, the criterion can be expressed as:

$$\frac{A_r}{A_a} = \exp\left[-\frac{2c\rho(b_M + b_m)\Delta U}{2c\rho R(b_M T_M + b_m T_m) + R b_M c_d^2 \cos^2\beta P} + \frac{\Delta U}{RT_0}\right]$$

Where:
- A_r/A_a = ratio of real to apparent contact area between the die and the cast alloy
- ΔU = activation energy of interaction
- R = gas constant
- T_m, T_M = temperature of the melt and mold
- T_0 = critical temperature at which the bond is complete
- μ, β = casting velocity and angle to die surface
- c = specific heat of cast aluminum
- c_d = Darcy equation constant (~0.8)
- P = injection pressure
- ρ = aluminum density
- b_m, b_M = heat accumulation coefficient of the melt and mold

The complexity of this equation would certainly lead to questions about the nature of the results, especially with the number of difficult constants to determine.

In the research performed in [65], different approaches were tried in order to predict the soldering formation. All of them basically consisted in calculating in a commercial software (in this case MAGMASOFT) the time-temperature fields of die and casted part, identifying critical areas of the part and compare them with the appearance of soldering in these areas in real castings. It was proven that the temperature of the die (maximum, average) was a much better indicator of soldering than the temperature of the cast metal at the surface of the die. The user defined a critical time that the die was above a critical temperature, above which soldering would appear. An optimal critical temperature and the means to translate from a given time above that temperature to a severity of soldering were determined through the data mining approach. It was proved as well that the injection velocity had little or no influence in soldering, while influence of pressure was not possible to be studied.

One year later, appeared a new publication [13] about the use of the explanation of intermetallic layer appearance and growth phenomena due to diffusion, for implementation in a mathematical model. It is somehow an improved version of the approximation of the time about above a critical temperature presented before. This new model is able to calculate the intermetallic layer thickness growth, and the temperature through it. The figure 49 shows the inverse parabolic law used for the intermetallic thickness growth, for the case of 625ºC, that is in accordance with diffusion controlled process's as L=K*sqrt(t), where K is dependent of temperature and diffusing species.

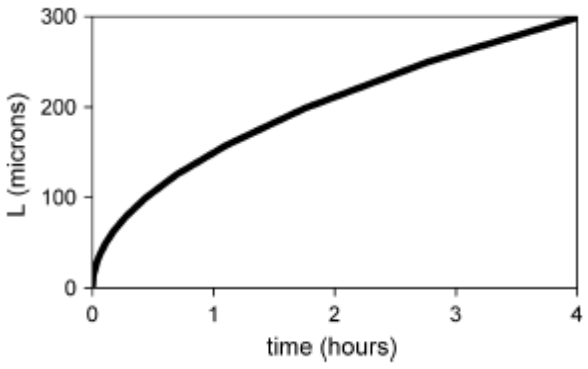

Figure 49. Thickness of the intermetallic layer, L, following the inverse parabolic growth formula, with the growth rate coefficient derived from the measurements. Such growth curve is typical for diffusion-controlled processes.[13]

The thickness calculated includes all intermetallic sublayers. As the growth is very dependent of the temperature, it is considered as a solution to the standard 1D diffusion equation, and after calculating the K as following equations in function of this diffusivity and the concentration of aluminium of the alloy cL.

standard 1D diffusion equation: $$\frac{\partial c}{\partial t} = \frac{\partial}{\partial x}\left(D(T)\frac{\partial c}{\partial x}\right)$$

experimentally measured rate constant: $$K = \sqrt{4D}\cdot \mathrm{erf}^{-1}(1 - c_L),$$

The intermetallic layer is assumed to grow only at temperatures higher than a certain cut-off temperature. It is assumed that this temperature is equal to the solidus temperature of the soldering alloy. Below D would be equal to 0. This means that over a die casting cycle only in the very first seconds are taking place soldering reactions.

The model takes into account that from the intermetallic layer thickness, it only will take place soldering if the temperature in this layer is above the temperature at which the last phase (eutectic aluminium rich phase) would remelt and solidify sticking to the aluminium part. From this assumption the bonding strength is calculated. Figure 50 schematically shows the interacting regions.

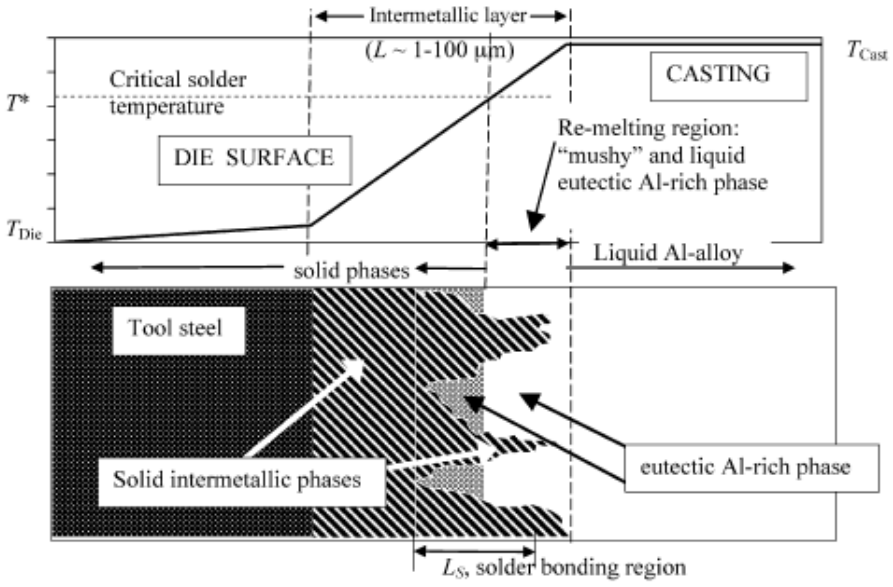

Figure 50. Schematic illustration of the intermetallic layer on the die surface and schematic temperature profile through the layer. The zig-zag interface between the Al-rich eutectic and the binary intermetallic phases provides the metallurgical solder bonding.[13]

In summary, the numerical model of die soldering includes the following five steps shown in figure 51.

1. 3D thermal analysis of the complete die-casting process until the approximately stabilized cyclic behaviour is achieved, obtaining the transient field T_{Die} (x,y,z,t) on the surface of the die and corresponding field T_{Cast} (x,y,z,t) in the casting.

2. Calculation of the 1D diffusion equation, obtaining the concentration of iron along the intermetallic layer.

3. Taking TDie (x,y,z,t) and TCast (x,y,z,t) as boundary conditions, 1D heat conduction through the layer is calculated to get the temperature field T(x,t) on it.

4. From the temperature field in the layer and iron concentration, diffusivity D and subsequent K are calculated. Afterwards the layer thickness is calculated for a number of cycles done.

5. The last step is to calculate the solder strength for a number of cycles. Inversely, it is possible to estimate the number of cycles to arrive to a critical solder strength that would be representative to a failure with the corresponding need of reparation.

One of the limits of this approach is the need of experimental work to have a reference of critical solder strength, as well as other different parameters and constants that have been taken from literature, or have been assumed arbitrarily.

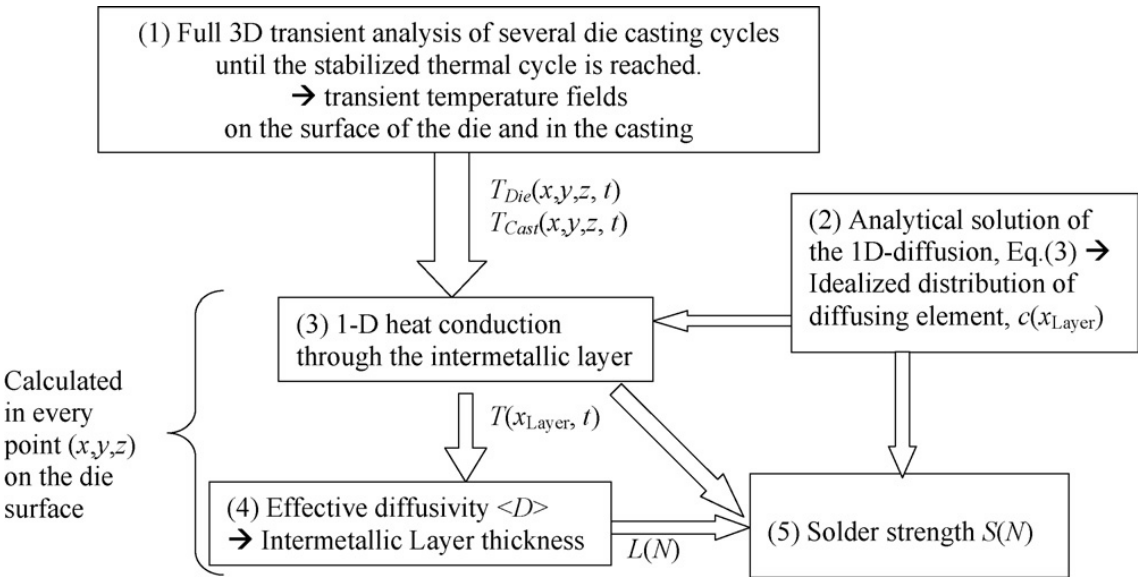

Figure 51. Flowchart diagram of the numerical implementation of the solder model. [13]

2.3.1.3 Erosion models

Even if several publications are available about die erosion in HPDC, none of them have generated specific equations. Nevertheless, it is possible to extract from these publications the importance of the different parameters on erosion. The literature has shown that the main factors are metal velocity, impact angle and metal temperatures [33].

The multiple pin erosion test shown before in figure 26, was used for the evaluation of these 3 parameters. The figure 52 shows the correlation between die wear profile distributions and velocity profile distributions along an edge of a wear pin. The wear and velocity ratios indicate the ratio of the wear and velocity at a location related to the maximum. FLOW - 3D based numerical model of the filling of the original pin layout was obtained to estimate the velocity at the different locations along the edge of the pins. The profiles of the pin edges facing the gate were measured by a comparator using 20x magnification.

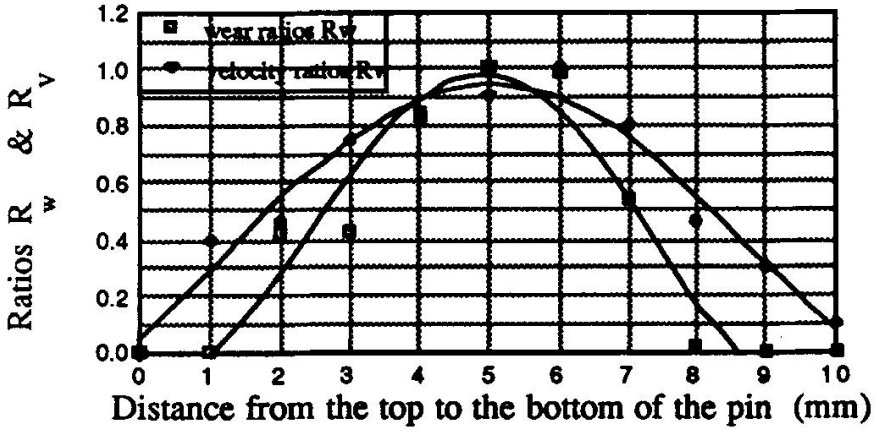

Figure 52 Correlation between die Wear Profile distributions and Velocity Profile distributions [33].

The erosive wear rate defined by the weight loss of the pins after 1000 shots is plotted against the attack angle of the molten metal in figure 53. As shown, the maximum wear rate occurs at an impact angle of approximately 72° degree. Previous studies have indicated that for impact of pure liquid, the impact angle at which maximum wear occurs is 90°. For solid impact, the tangential component contributes to erosive wear, and the impact angle at which maximum wear takes place is 45°. These results indicate that the aluminium metal is not completely molten, but is partially solidified. This work was to be completed with combination of other speed and temperatures.

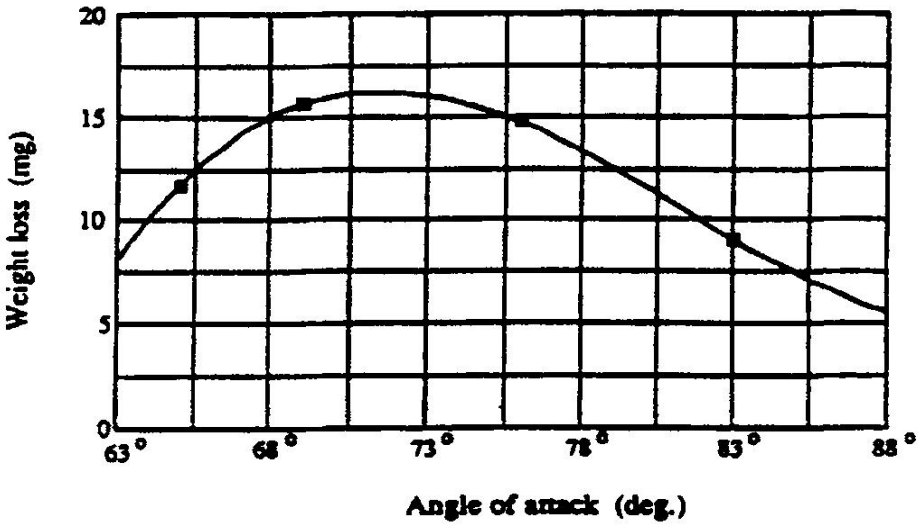

Figure 53 Dependence of Erosive Wear Rate on impact Angles of molten aluminium alloy [33].

Regarding the influence of melt temperature, in the same study as for velocity and impact angle, erosion wear tests were performed with aluminium alloy A390 at two different temperatures: 150° and 50°C superheat. The eroded profile of the pins is shown in figure 54, although qualitatively similar, are quantitatively quite different. The wear seen at the lower temperature is much greater than that seen at a higher temperature, even more when the pin material was nitrided. As the temperature decreases, the solid fraction and consequently the amount of solid particles in the melt increases. The impact of more solid particles on the pins at the same velocity thus causes greater wear at the lower temperature. Although the die

is likely to be cooler at a lower temperature thereby reducing metal diffusion, the increased wear due to the impact of more solid particles appears to be more significant to the overall wear.

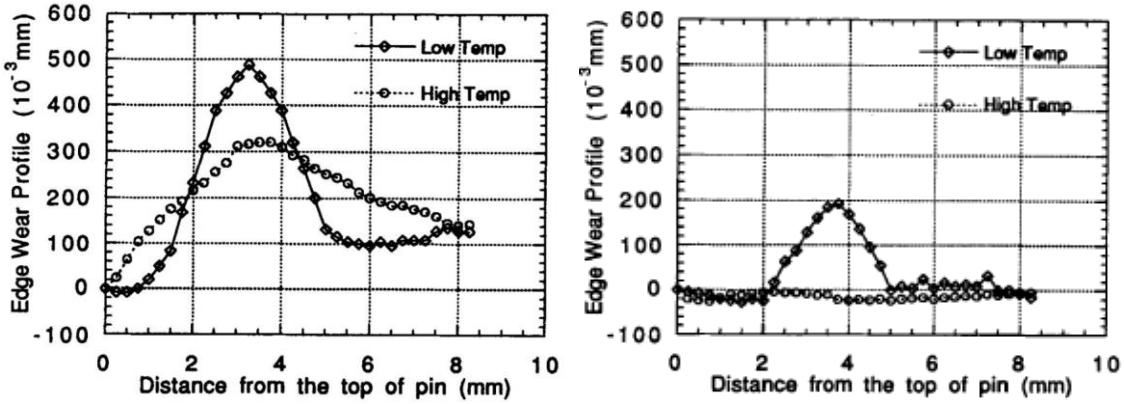

Figure 54 Dependence of edge wear profiles of H-13 (a) and nitrided (b) test pins on the temperature of molten aluminium alloy [33].

The behaviour of the materials when they are subjected to erosion tests is more complex than only influence of hardness. As it can be seen in figure 55, the impact angle influence in erosion is tightly related to the resilience of the material. Ductile materials have the lowest wear resistance to solid particle erosion at around 30º, while brittle materials at normal impact to the surface, at 90º.

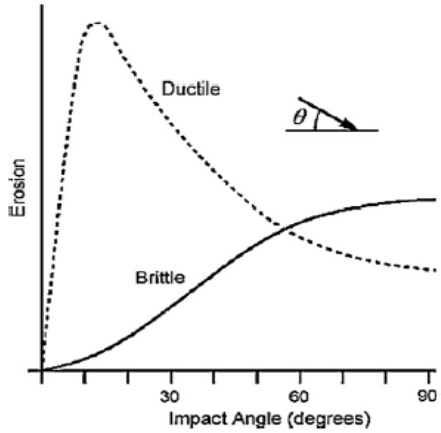

Figure 55: Erosive wear rates for ductile and brittle materials versus impact angle [68].

The investigations on wear behaviour of HPDC die materials in solid particle erosion tests [41, 42], confirmed this trend of ductile material being the highest wear between 40 and 45º. Regarding the influence of the particle speed in these studies, it was shown that particle speed was one of the most affecting parameters as well. In [42] where aluminium balls were used as erodent and the range of tested speed values was relatively small (10-20 m/s) impact angle was more influencing than speed. This may be because in most erosion works, the erodent are much harder than the counterface, whereas here it was the opposite. These results are shown in the following figure [42].

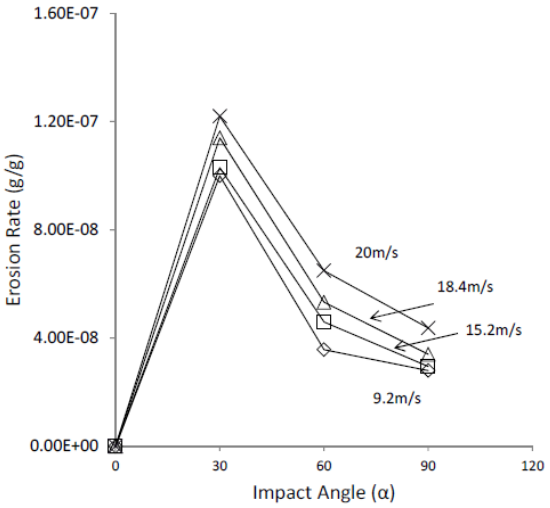

Figure 56: Specimen Impact Angle against Steady State Erosion Rate for Impact Velocities [42].

2.3.2 Models for PIM moulds wear

For the prediction of PIM moulds failure, very few studies have been published about the development of mathematical models. Two main publications have tried to create equations to predict the wear generated by glass fibres in mould surfaces. Their approach have been very different, and are explained hereafter.

The investigation of Bergstrom et al. [31] was based on the study of a supposed cylindrical glass fiber impact in a flat surface, shown in figure 57.

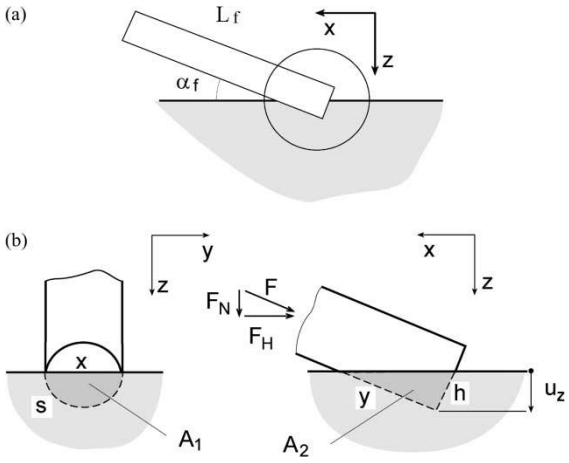

***Figure* 57. Model proposal and definitions of variables [31]**

The mathematical application of this model intends to calculate the width and depth of the wear scar generated by a fibre of L_f length and impacting at α_f angle in a material with a Vickers hardness (H). The injection conditions and the influence of plastic material are represented through the shear stresses transferred from the polymer melt to the fibre endings to indent the surface. This shear stress is affected by polymer viscosity, which as a non-Newtonian fluid, it is affected by the temperature and injection conditions (pressure, speed). It is supposed that the plastic flux is oriented along the fibre length.

The development is based on the application of force equilibrium shown in figure 58 to a fibre and calculate the strength applied to it, and equal it to the indentation resistance of the material:

$F_N=H^*(A1+A2)=2\pi\eta\gamma L_f r_f \sin\alpha_f$

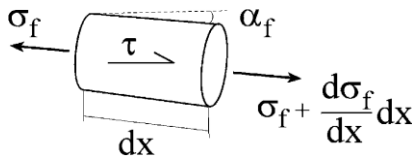

***Figure 58*. Equilibrium conditions. [31]**

Where A1 and A2 are function of the indentation angle α_f and indentation depth u_z and η is the viscosity of the polymer, γ the flux, L_f and r_f the length and radius of the fibre. Said that, according to the equilibrium equation, the indentation generated, only depends on the flux, for a fixed polymer and impact angle.

In the next figure there are shown the results of the application of the model for a mould and a reinforced plastic material. The indentation generated in the mould material in function of the shear rate is plotted for 4 different impact angles. In this publication full scale injection test were performed with different mould materials and observations of wear scars generated by the reinforced plastic had trends similar to the model.

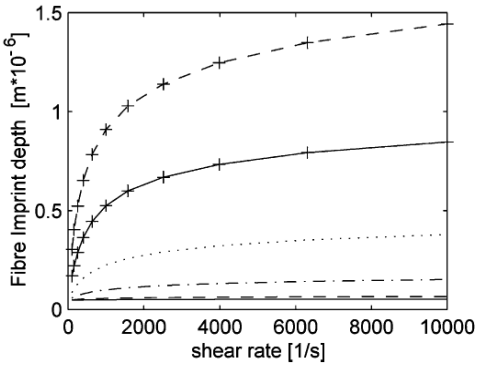

***Figure* 59. Model data, imprint depth as a function of shear rate for 4 different impact angles [31]**

Variations in the polymer flow orientation arising from corners and shape variations in the mould caused fibre orientations in relation to the die surface to alter in the experiments. It was shown in both experiments and model that for higher impact angles, the erosion was enhanced. For low range of flux values, small increments of flux have huge influence of wear, while for high range of the flux, did not have big influence on wear.

The biggest difficulty of these analytical calculations is to get a reliable value of the viscosity of the plastic (which will depend of the temperature and flux speed for a polymer) as well as a reliable value of the shear rate. The latter would be possible to calculate in a simulation software like Moldflow©, software which also provides material libraries, if measurements are not available.

Another limitation of this model it is that assumes that the fibre and the flux are aligned, which it is not always true for short fibres. In the experiments the wear resistance of the different mould materials was in accordance to the model, were higher hardness means lower indentation depth. Even though, this model is not able to take into account that some materials can have different phases (i.e. materials with carbides) or the cold hardening that suffers the material after the first indentations.

The second main publication that intended to create a model to predict PIM mould wear [66], was based on injection trials where an easy to machine, mould material (aluminium EN AW-6082 T4 and copper alloy ISO Cu Zn39 Pb3) was subjected to several cycles of polyamide 6 reinforced with 30% glass fibre injection. The behaviour of wear rate has been analysed by the study of the evolution of the surface parameters and

functional parameters in different points of the mould surface at different stages (at 200, 800, 2000, 5600, and 9200 injection cycles). For all this chosen experimental points, the special roughness parameters such as Ssk (Skewness), Sku (Kurtosis), mentioned in ISO 25178, and Sbi (Surface bearing index) according to EUR 15178N were obtained. It was found that the parameter Sku increase with the increment of the wear rate and an equation was generated from the experimental results. Simulation of the tangential and frontal flow of glass fibre was analysed in MoldFlow® at different areas of the mould to better understand the traces of wear scars. Figure 60 shows the flowchart of this methodology.

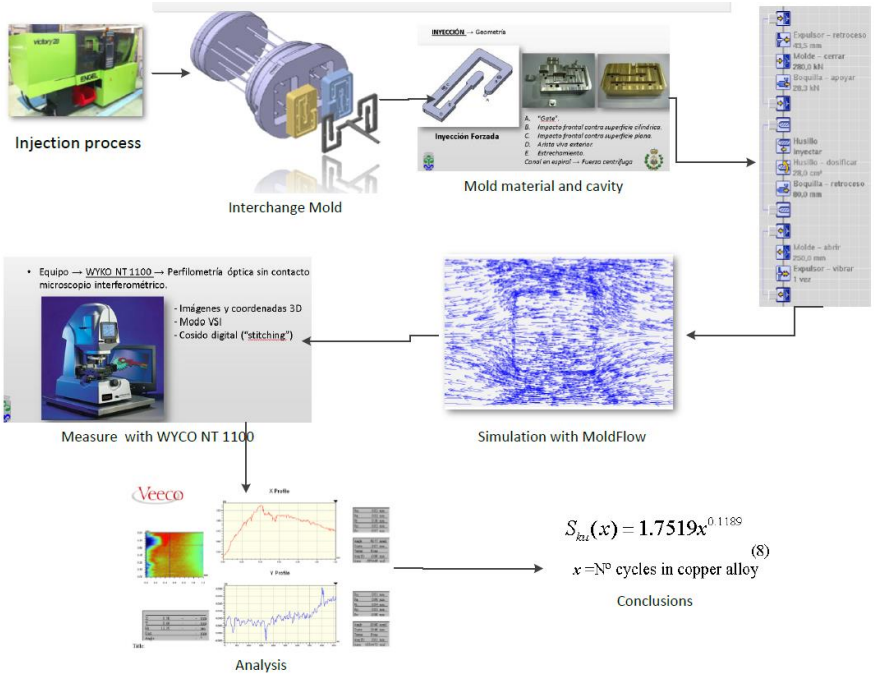

Figure 60. Flowchart diagram of the Methodology to measuring wear molds proposed by Pereira et al. [67]

2.3.3 Summary of models for moulds wear prediction

The different type of mathematical models available in literature build to predict wear are found to be mainly phenomenological (formed from suppositions and calculated from physical parameters, and validated from experimental results) or empirical (formed directly from experimental results, once selected appropriate variables that rule the wearing process).

It is found that each tribological system, needs a specific experimental simulation due the materials characteristics and dependency of their characteristics on different tribological parameters (load, temperature, speed, surface factors...). Once this is achieved, it is possible to build a model that predicts accurately the wear as demonstrated in the paper "Friction and wear of a piston ring/cylinder liner at the top dead centre: Experimental study and modelling" of annex of this document.

For the specific case of the wear of moulds, there are some options to calculate the wear of moulds in HPDC process simulation software's, while for PIM there are not these options available. These wear prediction modules have the drawback that as they are very recent developments, they are not very well validated and the models applied on them are not always available in open literature. The effort made by different authors in open literature have been reviewed, before selecting the approach to be followed in this work.

For the thermal fatigue prediction of HPDC moulds, the three main publications reviewed have been shortly described. The one of [63] was built from experimental results of a test performed with simple coupons,

building directly fatigue curves relating temperature changes (difference between maximum and minimum of the cycle) to cycles to failure. The models published by [2] and [3], connected the temperature changes and related strain and stresses through calculations, to apply stress and strain based fatigue equations respectively. The approach of [2] and [3] is similar to the one implemented in some commercial software's. Perhaps the approach from [63] does not represent very close the thermal conditions of dies, where temperature changes are quite different from the test used for building the equation. The approach [2] and [3] are based on a demonstrated [69] good calculation of the cycle temperature and stresses. The fatigue equations that connect the cycles to failures and the stress and strain variations they used respectively, are not fully validated nowadays for die materials at high temperature, at least in the open literature. In this work, a high temperature mechanical fatigue test have been used to build a model that connects the stresses appearing in HPDC die materials and the cycles to failure. Furthermore, it has been investigated the possibility to connect in a new device the thermal fields very close to the HPDC die conditions and the cycles to failure, which would be the ideal scenario but will take some years of experimentation to build the models.

For the prediction of die soldering phenomena of dies, also the three main publications reviewed have been shortly described. As stated before, the one from [64] is considered to be too complex and would certainly lead to questions about the nature of the results, especially with the number of difficult constants to determine. The one from [65] is considered much more rational, where from time-temperature field calculations on the surface in commercial software's, critical areas of soldering are identified, and critical residence time above a critical temperature would lead to soldering. These critical time and temperature are not public, and doesn't seem easy to generalize, even more taking into account that influence of pressure was not taken into account. The similar but much more advanced approach presented by [13] and based on the intermetallic layer growth, and the temperature in this layer to estimate the start of the soldering, seems promising. As a drawback, still needs huge experimental work to achieve reference critical solder strength, as well as other different parameters and constants that the model needs. In this work, an innovative approach has been used. It is commonly affirmed by all authors that while there is lubricant protection, soldering does not appear, while when temperature or pressure makes this layer to be washed out, soldering appears. In this work the influence of temperature pressure, relative speed and lubricant chemistry have been studied through a pin on disc lubricated test, and a model of its failure and start of soldering have been built.

For the prediction of erosion, even if the main parameters influencing the erosion of moulds have been identified in real casting conditions by [33], as well as different studies with laboratory tests of solid particle erosion [41, 42], no model have been built in literature for mould materials. These main influencing parameters have been identified as velocity of the flux, impact angle, melt temperature (related mainly to particles feature into the melt), and mould material characteristics. In this work a DOE has been performed in a test device similar to [41, 42], and it has been used to study all these key parameters and build this model. Furthermore, an innovative laboratory test have been developed to test different mould materials as well as different erodents. This second test procedure have been used to test different plastic raw materials as erodent from PIM moulds point of view, since this wear mechanisms is common for both process's.

The mathematical modelling of PIM moulds wear from literature is not as advanced as the one for HPDC moulds. The two references identified only tries to model the wear generated by glass fibres in mould surface. have been shortly presented in this document. Their approach was quite different. One of them [31] have built a phenomenological model, based on the indentation of fibres in a plastic flow. This model looks promising, since it correlates well with experiments performed in injection machines. Even though, it is still long way to be applicable on simulation software's, since the validation of the values predicted would need a

lot of injection tests and simulations of their conditions. The second publication, is an empirical model, constructed directly from results of tests performed in full scale injection machines. This model has been built for a specific mould with specific injection conditions, and relates the number of cycles performed with the roughness generated due to wear scars. This approach would need to perform a set of experiments in each of the moulds of interest in order to predict their failure. In this work, on the one side, it has been separated the study in the two wear mechanisms that are named by [31], erosion and abrasion. For the erosion, the procedure presented before that is common for HPDC and PIM have been performed. For the abrasion of PIM due to glass fibres, a model was built from the results of pin on disc tests performed, by a DOE varying speed, pressure, plastic and mould materials.

Regarding corrosion, even if some tests have been performed in literature, it was not found any try to model the moulds behaviour relative to corrosive wear. In this study the influence of mould material in the time to corrosion appearance have been modelled from the experimental results measuring corrosion resistance.

2.4 Conclusions

The main failure modes of the High Pressure Die Casting and Plastic Injection Moulding have been defined according to most recent bibliographical data. There is created a classification of terms and tried to explain the nature of them. It has been analysed how the main wear mechanisms have been studied in the laboratory in order to assess the lifetime and try to find the most appropriate material solutions to increase the durability of the moulds and dies. The tests from the literature have been defined to answer specific needs from the authors but there is a lack of standard tests. This experience in any case has been used as reference for the design of the test protocols to simulate the main failure mechanisms as detailed in Chapter 3.

The HPDC wear mechanisms selected for simulation in laboratory scale have been Thermal Fatigue, Die Soldering, Solid Particle Erosion and Corrosion. For PIM Abrasion, Erosion and Corrosion have been simulated. As Erosion and Corrosion are common wear mechanisms for both process's a common testing and modelling approach have been selected and are presented together for both PIM and HPDC processes.

For thermal fatigue, created due to thermal inhomogeneity of the die during the HPDC, the main influencing parameters were identified as some specific die material properties, evolution of die temperature in and into the surface during the cycle and stress concentrators. The experimental procedures used in literature are mainly differenced by the way they heat the samples to simulate the heating performed on moulds by the aluminium melt. In this study two different laboratory tests have been selected. One is an innovative test that have been validated to accurately simulate the thermal cycles of the dies, which did not exist before in the literature. The second one, a high temperature mechanical fatigue tests, have been used to create fatigue curves that relate stress and cycles to failure, to improve the existing predictive models based on the previous stress calculations from measured or simulated temperature fields.

For the die soldering, generated due to the chemical affinity between injected aluminium and the tool steel, the main influencing parameters were identified as the nature and constituents of casting alloy, nature of the die material, surface treatments and roughness, die lubrication, and operation parameters (pressure, temperature, speed). The main devices used in literature have been reviewed, and one of them, the pin on disc test have been selected, with significant variations. The main change was to use lubrication in the contact between aluminium and steel, and measure the time to failure of this protective film as the start of soldering, and the dependence of this failure with temperature, pressure, speed and lubricants chemistry. The main models present in literature are based in the critical temperature and residence time conditions that lead to start of soldering, which still need to be validated experimentally.

For the erosion that takes place in HPDC and PIM, was found that was mainly influenced by flux characteristics (impact angle and velocity), amount of hard particles (related to melt temperature in HPDC and glass fibre % in PIM) and mould material properties at working temperature. ASTM G76 has been

selected as the key test to simulate the erosion because of hard particles. Gravelometer test based in ASTM D3170 has been used as well in order to use the plastic material as erodent. The liquid impingement erosion was considered that is not very probable to appear in mould in the short term and was not included in the study. Cavitation erosion mechanism has neither been simulated. Mathematical models to predict erosion have been built in several applications (see table 3), but it has not been still applied to wear of moulds.

The abrasion mechanisms occurring in PIM when the reinforced plastic flux is parallel to the mould surfaces, has been found to be influenced by mould and plastic materials as well the flux characteristics (pressure and speed). Similarly to one of the references reviewed, a pin on disc test has been selected to simulate this wear mechanism, and a mathematical model has been built from these test results. The application of modelling for PIM moulds wear was not found to be as advanced as HPDC moulds wear, and the approach selected in this study is different to the two references found in literature.

The corrosion appearing both in HPDC and PIM mould, is due to the harsh environment the mould has to work (presence of gases, humidity and high temperature). Some standard tests has been used to simulate this wear mechanism in laboratory, and in this study one of them, the Electrochemical Impedance Spectroscopy (EIS) was selected using NH_4Cl at 1% dilution as the electrolyte simulating the Cl_2 and NH_3 gases that are usually in contact with the moulds. The main advantages of this technique is that is fast and non-destructive technique. From these results a model of the corrosion in function of mould material has been built, which was not applied before in the literature.

2.5 Innovative aspects

The main innovative aspects in this work are related both, to the experimental procedures used as well as the new models that have been built. Relatively few work have been published in the topic of moulds wear, and the multiple innovative aspects of this work are a small step forward in the increase of mould's life, with the aim of increasing the quality of the parts, reducing production stops, reparation and maintenance costs, and increase resource efficiency by reducing material scrap, the use of raw materials and energy consumption. It is important to highlight that this Doctoral Thesis has been performed in the frame of the EU Project MUSIC.

For the thermal fatigue, the main highlight is the use of a new machine concept for the nearly exact experimental simulation of the thermal cycle occurring in HPDC and its influence in the cracking appearance. Furthermore, it was identified a lack of the access to the fatigue curves necessary to predict the moulds failure in open literature, and this curve was built for a H13 and H11 material in a high temperature mechanical fatigue machine.

The simulation of die soldering appearance as the failure of lubricant protection is an approach never used before in literature. The measurement of the Leidentfrost effect, the thickness of the lubricant, the differential scanning calorimeter behaviour of the lubricant, showed the possibility to correlate different physical parameters with lubricant properties and mechanical die soldering appearance. The tests performed have been used to create a model.

The erosion failure have been simulated with two techniques. The first one, based on ASTM G76, has been similar to others used before in literature, and the main innovative aspect is to have built a model based on it. The second one, based on ASTM D3170, is the first literature reference in which plastic pellets are used as erosive gravel, even if the plastic is in solid state.

For the abrasion appearing in PIM, the pin on disc experimental rig used is not so far from others used before in literature, being the main innovative aspect the built of a wear predictive model from these results. Standard salt spray method and polarization curves have been used before for the simulation of corrosion in moulds.

In this study the Electrochemical Impedance Spectroscopy (EIS) have been applied for the first time to compare several mould materials. Furthermore, the test results have been used to create a model of corrosion appearance prediction.

3 Simulation of wear mechanisms at laboratory scale

Ideally, a test could be designed on an actual test die in a real die-casting/injection environment. Nevertheless, the risk of damaging an expensive and complex die, and the cost of interrupting production make this approach onerous.

The numeric and qualitative values of friction and wear obtained in any kind of tribological study, and in general laboratory scale studies, is always relative and depends strongly on test configuration, testing machine, working conditions or surface characteristic of tested materials.

This is explained because the type of wear and friction suffered by the materials is not an intrinsic property of them, but the response of a very complex system where two bodies interact. Therefore, the appreciation and conclusions described in this report are referred to the presented methodology and can only be considered as qualitative evaluation. The quantitative data can only be considered totally proven, when a calibration or validation in the real system is performed.

The target of the presented methodology is to use simple laboratory scale test, using testing conditions as close as the actual production situation in order to get the result in a reasonable period of time. In the next pages, the materials and methods employed are described, reporting afterwards some of the main results and discussing them, and the final model is assessed in order to be implemented in a future predictive software. This is repeated for each wear mechanism selected to be simulated.

3.1 Methodology

In this work, a similar methodology has been used to model the different mould failure mechanisms. The input variables of the process responsible for the changes in the wear of moulds are identified through experimentation, a model relating the response to the important input variables is created. This model can be used for wear reduction, maintenance scheduling or other decision-making process. The steps that have been considered were the following:

1. Selection of the most influencing variables and possible applicable model for each wear mechanism:

The first step has been to improve the understanding of the nature of the wear mechanisms generated in HPDC and PIM moulds. This work has been described in detail in the point 2.1 of this document and part of it, already published in the paper of annex 3 "On the nature of high pressure die casting die failures". This work resulted on the identification of the most important variables that should be considered when modelling the wear of the mould materials. It was also necessary to identify the different models available in literature and to consider how they can be fed from experimental test results. Once it was selected the kind of model to be used, the selection of the significant variables to build the models was made. This selection has been highlighted in the point 2.3.3 of this document.

2. Selection and development of the testing protocols for each wear mechanism taking into account the possibility of simulating the most influencing variables to build the selected models:

The test protocols selected to feed the models, were able to consider a wide range variation of the variables to create the models. In the point 2.2.3 of this document, it is a summary of the test protocols that have been used in literature. Some of the test protocols used in this work are similar to the ones used in literature, while others are fully original devices and testing protocols.

3. Design of the experiments for the testing of each wear mechanism

The testing variables have been modified according to the basics of the Design of Experiments theory [75] when it was possible, as a full factorial design with at least two levels in the range of each of the input variables. In the case of the erosion wear, dependences on speed, angle of attack, temperature, have been considered. In the abrasion wear, dependence on pressure and speed where taken into account. For the corrosion wear mechanism, it was a simple comparative experiment between the different surface candidates, since the modification of other variables was found very complex. The building of the fatigue curve, it was found that the model was ruled, mainly by a single factor (stress), and the test was designed to build a regression model equation based on least squares. Finally, in the die soldering model, the analysis was performed assuming that each of the variables (speed, pressure, temperature and type of lubricant) were independent variables and don't have interactions between them (this approach was made mainly due to limitations in resources, prevailing the interest to study different levels of a factor before the interaction between factors). The variables that are not of interest have always been blocked. The output variables have been cracking start for thermal fatigue, time to failure of die soldering appearance, friction and wear amount in abrasion tests, wear amount in erosion tests and the corrosion resistance in impedance corrosion tests.

4. Method to create the model from experimental results

Well-designed experiments can often lead to a model of system performance. Once the experimental design have been performed, the creation of the model was based on fitting response of curves, created from the experimental data. Generally speaking Multi-Linear models [75] have been applied, and in some cases, a

factorial design was applied to facilitate the data treatment (e.g. for Erosion and Abrasion wear mechanisms). This theory is based on the following hypothesis, which are reasonable for this case:

- The X_1, X_2… factors that control the response (pressure, temperature, speed… in this case), are independent between them.
- The response of the model (wear of mould in this case), is aleatory and follows the normal law Y~N (m, σ^2). Only the mean value "m" depends on the factors, while the errors are normally and independently distributed with mean zero and constant but unknown variance σ^2.
- The applied model is a linear combination of the factors:
  $Y = m + \varepsilon = \varphi(x) + \varepsilon$

  Where for example the function for the case of 3 factors in general would be:
  $\varphi(x) = \beta_0 + \beta_1 X_1 + \beta_2 X_2 + \beta_3 X_3 + \beta_{11} {X_1}^2 + \beta_{22} {X_2}^2 + \beta_{33} {X_3}^2 + \beta_{12} X_1 X_2 + \beta_{23} X_2 X_3 + \beta_{13} X_1 X_3$

  (Triple interactions and above, like $X_1 X_2 X_3$ are not usually considered because their physical interpretation is very complex).

  (To be able to calculate the coefficients, the following requirements are needed to fulfil: The number of different experimental values is at least equal or bigger than the number of β_{ij} to be calculated, and the maximum exponent of the factor is equal to the number of levels of this factor experimentally test minus one).

The β_{ij} coefficients of the model are estimated minimizing the Sum of Squares of the residual e_i (the residual e_i is the difference between the real response Y_i and the estimated response $\hat{Y}_i$ of an experimental point x_i). The coefficients that are not significant with a confidence above 95% are deleted and are not taken into account for the model.

For example in the case of the erosion wear mechanism, coefficients for the following equation were proposed:

$$\varphi(x) = \beta_0 + \beta_1 X_1 + \beta_2 X_2 + \beta_3 X_3 + \beta_4 X_4 + \beta_{22} {X_2}^2 + \beta_{12} X_1 X_2 + \beta_{23} X_2 X_3 + \beta_{13} X_1 X_3 + \beta_{14} X_1 X_4 + \beta_{24} X_2 X_4$$

After performing the analysis of variance it resulted in the following equation:

$$\varphi(x) = 427.02 + 77.41 X_2 + 280.47 X_3 + 62.13 X_2 X_3 - 176.46 {X_2}^2$$

The Xi factors are the physical parameters that have been varied in the test (impact angle, speed, temperature…) but that have been previously normalized to be working in the range between -1 and 1 in order to avoid numerical problems of the calculation. After the calculation of the coefficients the factors are converted again to the physical parameters, changing then the coefficient values, as can be seen in the example of wear equation for erosion test:

$W_{Hmax}(\mu m/h)$=-607.68+10.27ANG+12.09VEL+0.1ANGVEL-0.13ANG^2

It is also of interest to mention how equations were built when it was intended to combine the dependencies of the wear due to some parameters tested in one experimental device (speed, temperature and impact angle in the air jet erosion tester) and others in another experimental device (surface characteristic (hardness) in the gravelometer erosion tester). The wear equation coming from air jet erosion tester, was multiplied by a coefficient that was dependent of hardness. This coefficient is a unit when referring to the hardness of the reference material considered. For example in the air jet erosion tester, the reference material was 1.2738BM, while when hardness is increased this coefficient reduce the wear rate according to the hardness dependent equation, created from gravelometer results. The final equation looks as follows:

*Wear(µm/h)=(-607.68+10.27*ANG+12.09*VEL+0.1ANG*VEL-0.13*ANG^2)*(33.24-4.92*ln(H))*

5. Model adequacy checking:

The evaluation of the adequacy of the model is made through Variance Analysis of the model, obtaining determination coefficient R^2, which is the relationship between the Sum of Squares of the model and the Total Sum of Squares:

$$R^2 = \frac{\sum_{i=1}^{n}(\hat{Y}_i - \bar{Y})^2}{\sum_{i=1}^{n}(Y_i - \bar{Y})^2}$$

The nearer is this value from 1, the closer is the model from representing the reality.

Furthermore, the Plot of Residuals Versus Predicted Response (checking the assumption that σ^2 is constant), The Normality Assumption and Plot of Residuals Versus other Parameters are checked. These are subjective evaluations but commonly accepted. In the following picture, it is shown how these evaluations performed for the erosion wear mechanisms model. The normality assumption is valid whenever the plot versus residuals are reasonably aligned as they are in figure 44a. For the acceptance of the assumption that σ^2 is constant, the plot of residuals versus predicted response should not follow any kind of specific trend.

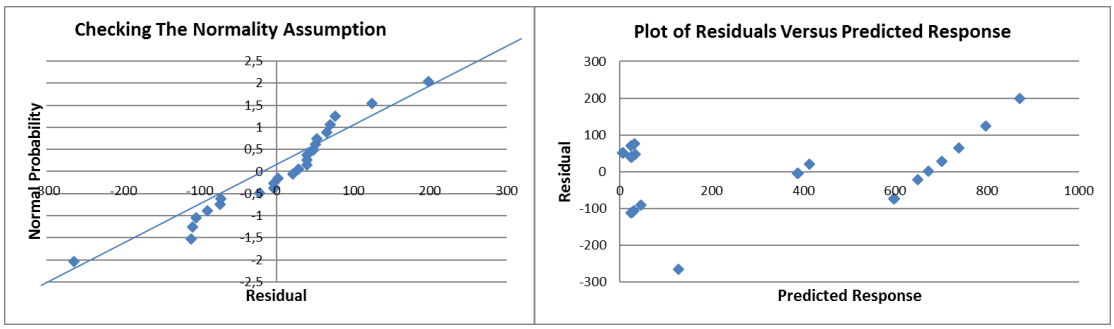

(a) **(b)**

Figure 61. Normality assumption (a) and σ^2 is constant (b) checking in the erosion model

6. Application examples of the model from a user point of view, and needs of validation and calibration of the model:

Once the equations are built, application examples have been created, which can be seen at the end of each of the chapters of each wear mechanism. In the chapter 4, it is described how the model might be used using case studies for HPDC and PIM, predicting the lifetime to failure for all the wear mechanism in the moulds in both processes. With these models, process parameters or surface material characteristics can be changed

in order to predict the time to failure and select the most efficient counter measurements to increase the lifetime and/or schedule the maintenance. After building the model, surface responses were built as well, as a useful tool for the optimization of process parameter, finding the combination that leads to the minimum wear.

Once a considerable experimental information has been collected and a definitive reliable model has been built, it should be validated or calibrated with real mould's wear monitoring. This would mean to calibrate the connection between the test conditions and mould conditions, for example each cycle of the test how many cycles' means in the real process. Even though, the prediction of the cycles to die soldering appearance is already in the range of durability of real moulds.

A suitable procedure for this step could be to track the wear evolution of real moulds at areas where for example erosion or abrasion mechanisms are present, and areas of different pressure and speed conditions, and with inserts of different mould materials. Afterwards, the wear amount predicted by the model and the wear of the mould should be compared. Similarly, speed and/or pressure could be calibrated. Afterwards this procedure should be iteratively repeated with mould observations.

3.2 Thermal Fatigue in HPDC

3.2.1 Objective

The objective of this chapter is to simulate the thermal fatigue wear mechanism that occurs in High Pressure Die Casting moulds at laboratory scale, to be able to evaluate the dependence of different parameters that influence their generation, and have a better insight of the phenomena to increase the lifetime of the moulds.

3.2.2 Materials and methods

3.2.2.1 Machine for simulation of thermal fatigue formation on HPDC moulds

As shown in literature review, several heating alternatives have been used in the literature to simulate thermal fatigue. The real thermal cycle that the test have to simulate, consist of heating up to around 500ºC and cooling down to around 100ºC as minimum temperature, while the mean temperature of the test sample is around 200ºC. In the EU Project Music [53], the suitability of the laser based heating (10 kW diode laser source of square shape) has been simulated based on finite element (FEM) calculation of the thermal field induced on the part, and some results are shown in figure 62. The results were considered satisfactory to simulate the HPDC heating an area of 50-70 mm square, achieving fast enough maximum temperatures around 500ºC. The regulation of the power could be useful to set a precise target temperature.

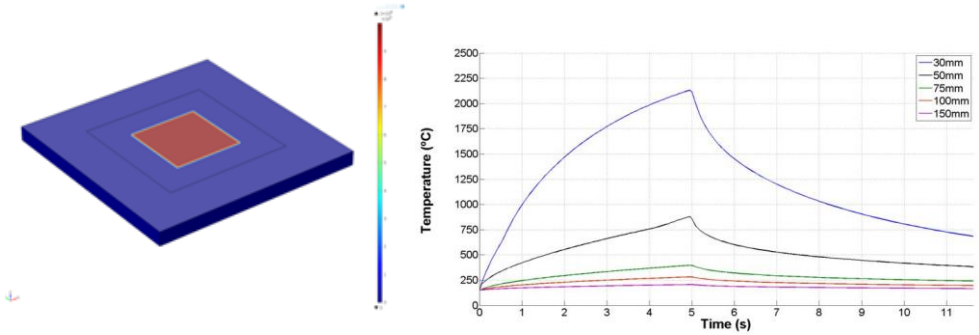

Figure 62. Example of an area of 100x100 mm² heated with laser (a) and temperatures achieved at 0.5mm below the surface (b)

A preliminary selection of the most suitable solution, left behind gas natural and resistance based heating because they were not fast enough to simulate the thermal gradients that takes place in HPDC. Regarding the laser heating, even if the simulation results were promising, it was discarded due to the high initial cost of the system and the uncertainty of the reliability of the system for continuum working on fatigue tests.

From the two other heating systems (melt aluminium and induction heating), two different testing machines were designed by IK4-TEKNIKER:

- The melt aluminium heating machine concept was similar to the existing in literature [1,3] were an alternative bath on molten aluminium and bath in water based fluid for cooling of small cylindrical samples were employed. The machine is presented in figure 63.
- The induction heating was a new concept of machine, based on alternative induction heating and cooling by a HPDC spraying system of an internally cooled test plate that simulates a HPDC mould. Their appearance can be seen in figure 64.

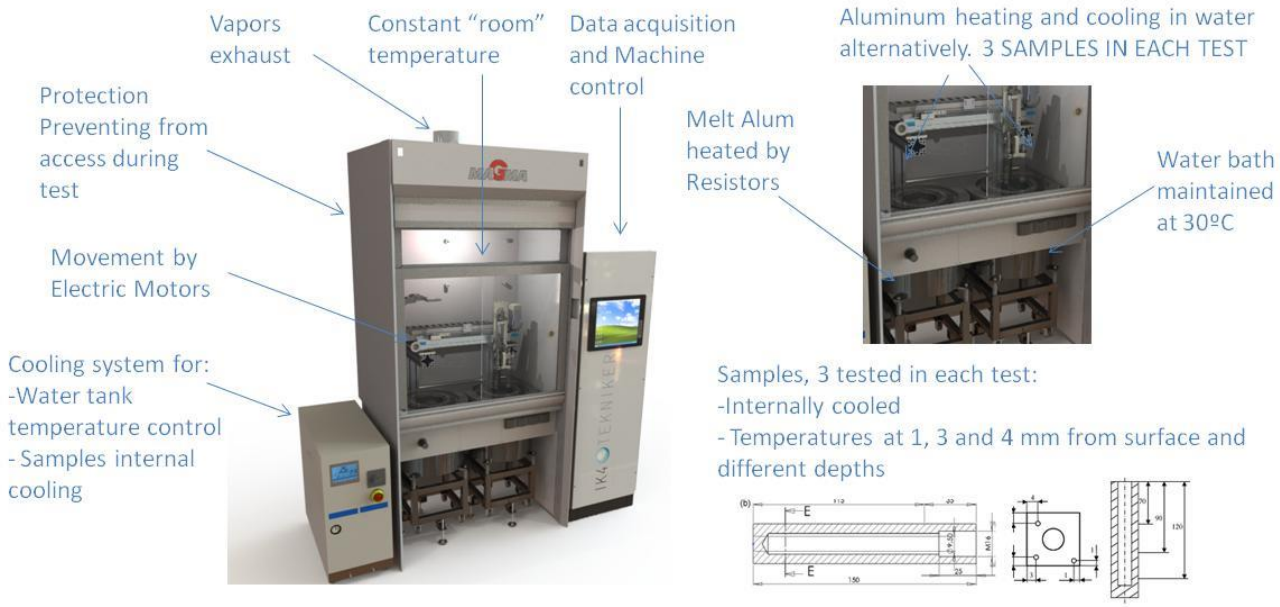

Figure 63. Machine design based on aluminum heating

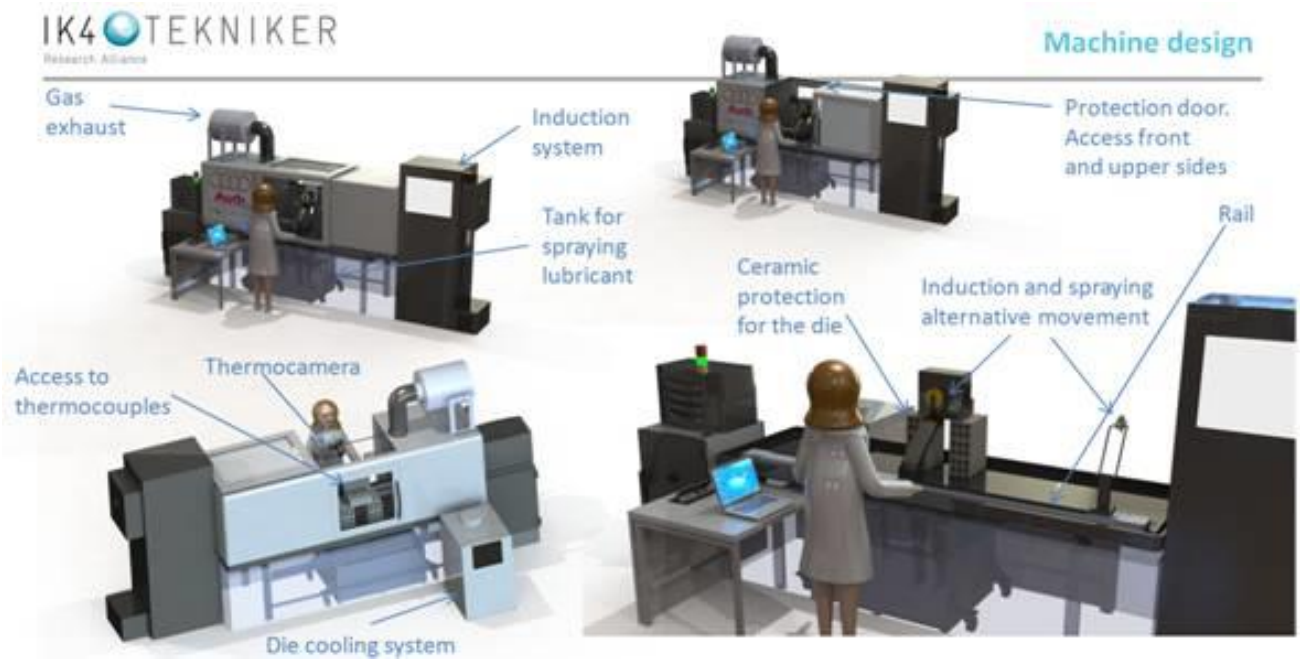

Figure 64. Machine design based on induction heating and spray cooling

The validity of the temperature profile generated by induction heating on the surface and below the surface of a steel plate like a die casting die (set with several thermocouples at different depths) was tested in the Music project [53] as well. This test plate and results are shown in figure 65. The heating through a medium frequency induction (13kHz) at 30kW for 0.8 seconds and 11.25kW for 4 seconds, led to maximum surface temperatures around 550ºC and gradients into the surface in the range of HPDC dies (375 and 280 ºC, at 2 and 4 mm depth respectively) and it was considered satisfactory to simulate the thermal fatigue.

(a) *(b)* *(c)*

Figure 65. Sketch of the plate manufactured (a), testing taking place (b), and temperature measurements (c)

The advantages and disadvantages of each systems to simulate thermal fatigue were evaluated, as shown in table 4. The final decision was that the best option for simulating the thermal fatigue of HPDC process was the induction heating based machine, mainly due to their higher flexibility of heating temperature, cooling and spraying possibilities.

INDUCTION HEATING	INMERSION HEATING (in Aluminium)
Parameters: **Die material, surface finishing, spraying, distance of cooling channels, heating**	Parameters: **Die material, surface finishing, few cooling parameters, limitations on heating**
Very high flexibility of heating application (Power, frequency, time, inductor geometry)	**Limited flexibility of heating** application (melt temperature, immersion time, melt of Zn, Cu)
Clean and **secure** heating	**Dirty** and **unexpected problems** could arise due to heating with Aluminum
Only **heating and oxidation influencing crack** nucleation and propagation	**Influence of heating, oxidation and aluminum inclusion on cracks** influence crack propagation
Very high flexibility on internal cooling (distance, flux, fluid type, temperature): **Like HPDC**	**High flexibility on internal cooling** (flux, fluid type, temperature)
High flexibility on external cooling through spraying: **Same as HPDC**	**Low flexibility on external cooling** through water tank bath
1 test – 1 sample	**1 test – 3 samples** (or even more)

Table 4. Evaluation of the testing machine designs.

Complete design of the Thermal Fatigue Machine, defining all the details of testing sample, cooling, spraying, heating, electrical and mechanical issues has been performed by IK4-Tekniker in collaboration with AUDI, a partner of the Music Project. The manufacturing of the Thermal Fatigue Machine was totally made at IK4-Tekniker, and the main elements are shown in figure 66.

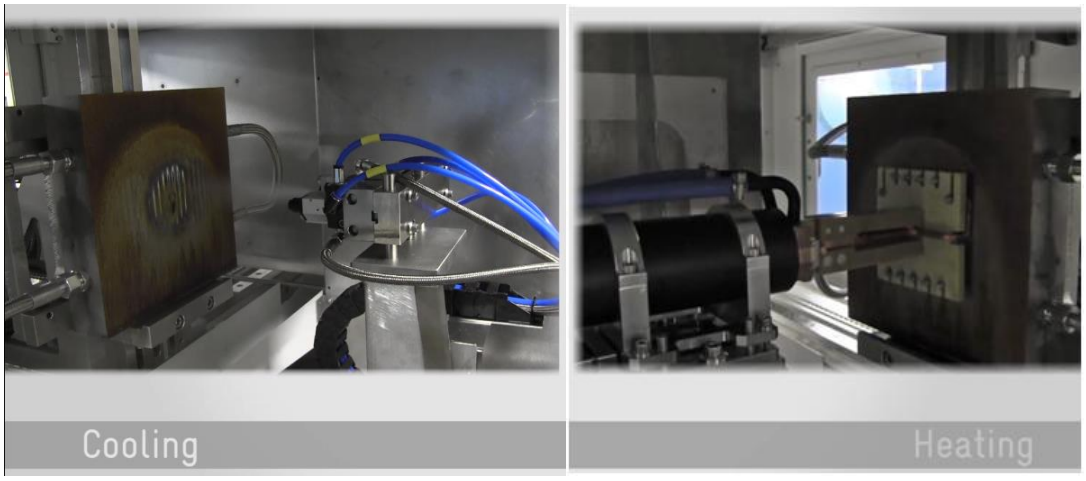

Figure 66. Thermal Fatigue machine manufactured in IK4-Tekniker for AUDI, simulating thermal cycles of HPDC that has been used for Music Project

The induction heating generator is a 70 kW medium frequency (13 kHz) device. The inductor coil was designed to heat as homogeneous as possible a circle of Ø 100 mm. Figure 67 shows the aspect of this coil and resulting heated area in the plate through a infrared thermo-camera image.

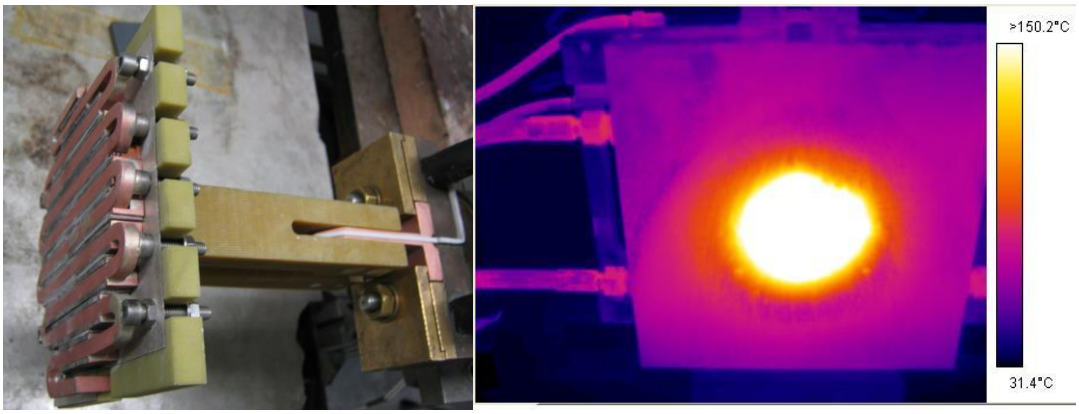

(a) (b)

Figure 67. Induction coil used to heat the test plate (a), and infrared thermal image of the plate after heating (b)

The test sample was a 43HRC hardened H13 steel plate of 300x300x63 mm^3. It was internally cooled through 2 cooling channels of Ø 12 mm by an oil medium at controllable temperature up to 160ºC. The inductor coil was installed at 2 mm distance from the steel plate surface.

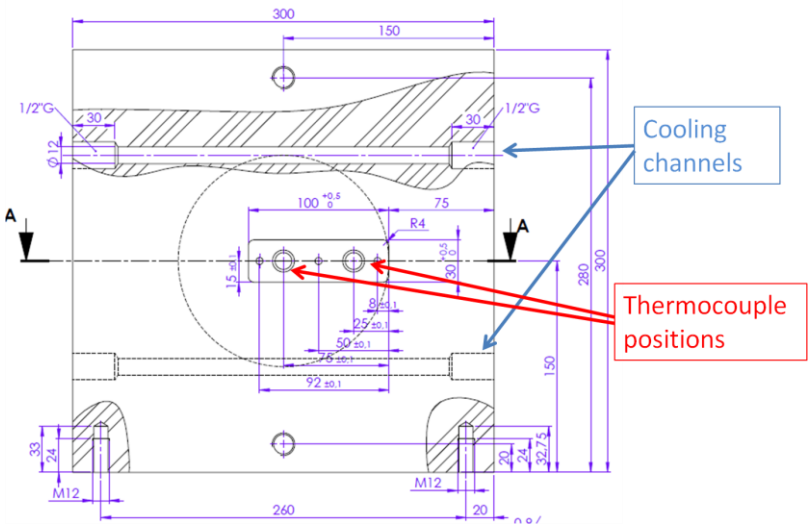

Figure 68. Design of the testing specimen for thermal fatigue test manufactured in IK4-Tekniker to simulate thermal cycles of HPDC that has been used for Music Project

The temperature was monitored through a multi-depth temperature measurement device designed by the company Electronics, partner in Music Project. The measurement system included K type thermocouples as sensing points in the surface, and at 1, 2, 4, 6 mm below the surface, which is shown in figure 69a. The readings of these thermocouples have highlighted that there is a huge temperature difference very near from the surface in both the heating and spraying cycles, as shown in figure 69b.

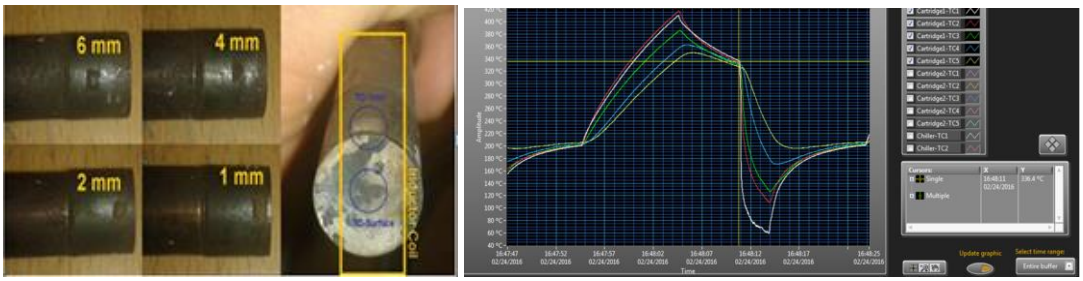

(a) ***(b)***

Figure 69. Aspect of the multi-depth sensor (a) and an example of temperature readings of them (b)

The external cooling was performed by an air -water external mixing system, where several parameters were variable (water pressure, air pressure, application distance, application angle, superposition of 2 nozzles), as shown in figure 70.

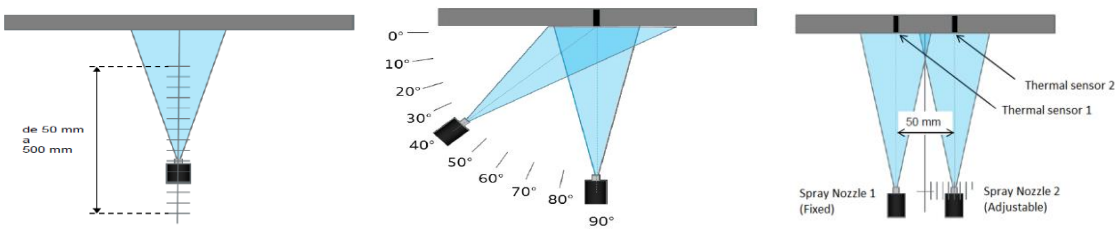

(a) (b) (c)

Figure 70. Possible variations of the spraying: (a) distance (b) angle (c) superposition of 2 nozzles

The machine is able to perform as many heating-cooling cycles as necessary, with any intervention of operators, in order to generate fatigue cracks. The test plate has to be inspected each n cycles in order to identify the crack appearance.

The applicability of resins to identify thermal fatigue cracks has been investigated on vertical HPDC mould surfaces on the Thermal fatigue machine test plates.

The replica resin curing time is very sensible to temperature, to cool down the mould to ambient temperature makes the operation easier and improves the quality of the replica. The fast curing at high temperature would make compatible for its use in a production. In contrast, it is detrimental for the quality of the replica. The resin may be cured under pressure, which is not so easy, when the surface is not flat.

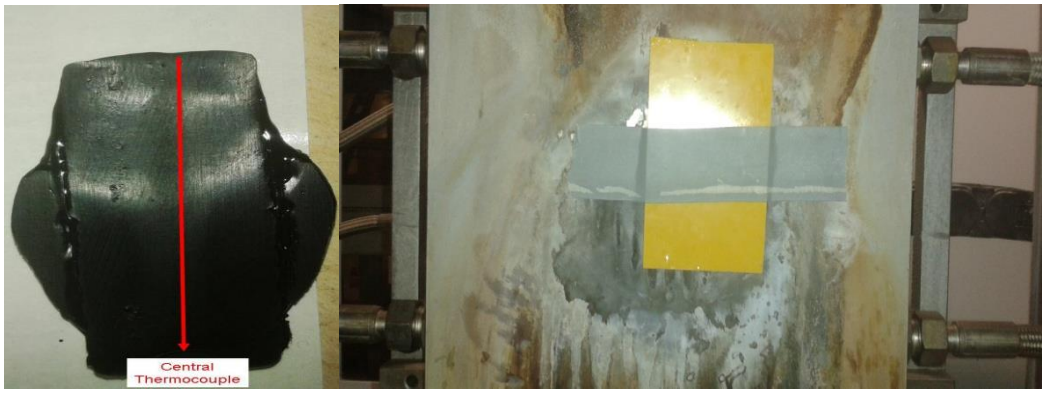

(a) ***(b)***

Figure 71. Result of a resin after cured and extracted (a) and curing process (b)

Afterwards, the replica can be checked in a microscope. The next figure 72 shows a result of the replica after scanning in a Confocal Microscope, where a crack depth around 30µm could be identified. It is suspected that image treatment could lose resolution of the system.

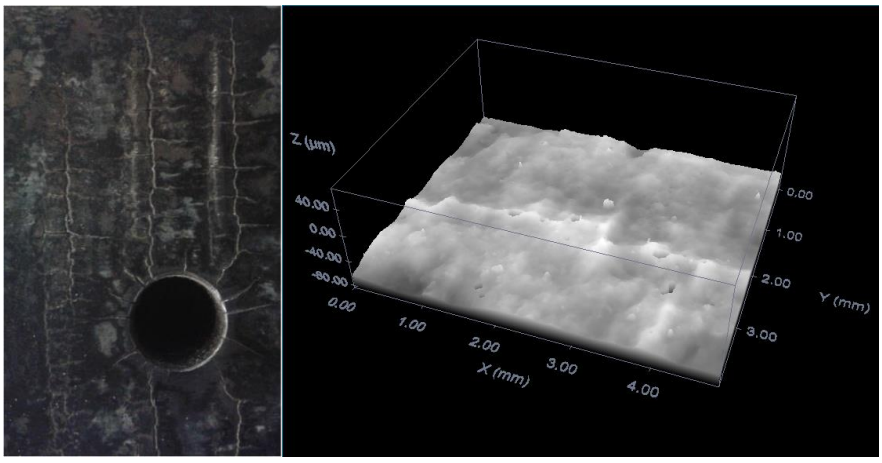

Figure 72. Cracks on the test plate (a) and Confocal Microscope image of a 4x6mm area of a crack (b)

3.2.2.2 **High Temperature Mechanical Fatigue testing machine**

The study of the Fatigue behaviour at high temperatures of the mould materials was performed using a testing device built based on ASTM E2368 - 10 (Standard Practice for Strain Controlled Thermomechanical

Fatigue Testing), that is shown in figure 73. This equipment consists of a computer controlled electromechanically operated loading device unit that can be operated as a constant load and a low cycle fatigue unit. The effect of chemical environment, temperature and pressure can be studied in this device.

The cyclic loading have been performed under strain control. The shape of the wave was sinusoidal type at a working frequency of 0.014 Hz. The strain and the temperature were varied and two different steel tested.

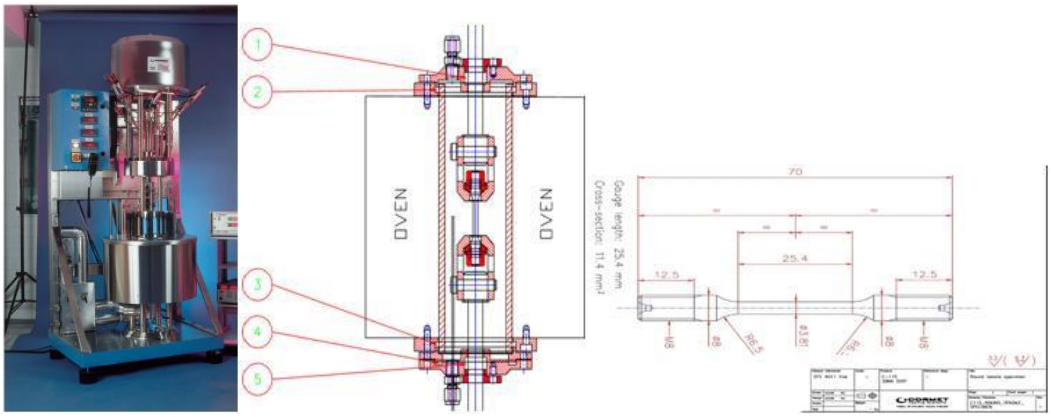

(a) ***(b)*** ***(c)***

Figure 73. Testing device picture (a), loading unit and heaters (b), sample sketch (c)

3.2.2.3 **Materials tested**

The selected 2 materials for the thermal fatigue studies were the typical HPDC hot work tool steels 1.2343 (H11) and 1.2344 (H13). For the fatigue tests (both Thermal Fatigue machine and High Temperature Mechanical Fatigue machine) the samples were manufactured and heat treated to 43HRC.

Two different type of steels, AISI H13 and H11, were selected for the study, since they are the most common die materials in HPDC [25]. The chemical composition was measured by optical emission spectrometer for both steels. Their composition is very similar as shown in Table 5; a small difference in the Vanadium content makes the H13 steel more resistant to wear and softening and it shows higher temperature resistance. Other properties that might have interest, like thermal conductivity (both around 28W/mºK) are very similar for both materials.

Steel		Si	Cr	Mo	V	Mn
H13	Nominal	1.00	5.10	1.35	0.90	0.40
	Measured	0.91	4.85	1.33	0.96	0.35
H11	Nominal	1.00	5.10	1.35	0.40	0.40
	Measured	0.99	4.90	1.20	0.31	0.40

Table 5. Measured (by optical emission spectrometer) and nominal (according to AISI) chemical compositions (wt.%) of H13 and H11 steels used in the study.

The microstructure of studied steels is shown in figure 74. Both have a martensitic structure, but the H13 has finer grains than the H11 one and the H11 steel has few carbides on its surface.

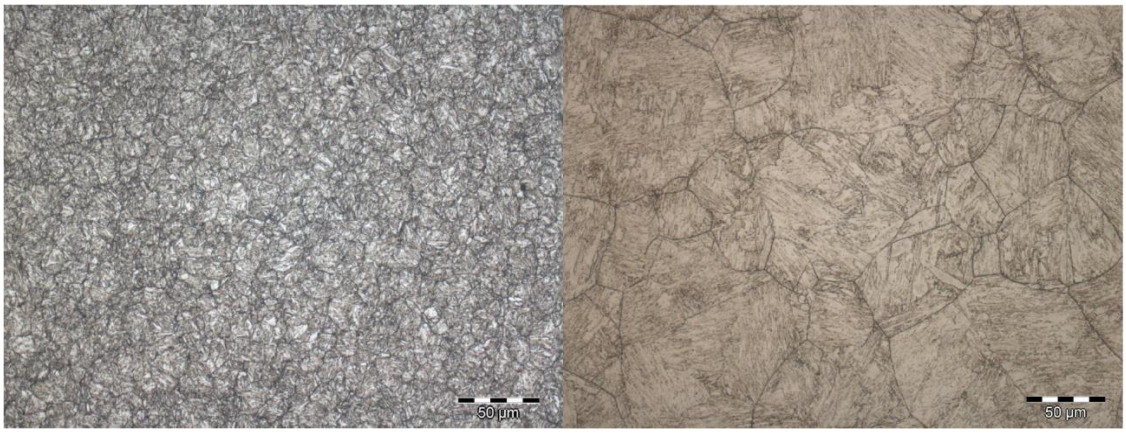

(a) *(b)*

Figure 74. Microstructures of (a) H13 and (b) H11 steel samples

3.2.3 Results and discussion

3.2.3.1 Effect of temperature and stress on Fatigue life in HTMF tests

In order to understand possible differences of both steels on their fatigue behaviour at high temperatures, tensile tests were performed at 300, 400 and 500ºC. The key properties selected for the evaluation were the yield strength, yield strain, maximum stress, final elongation, and young modulus (slope).

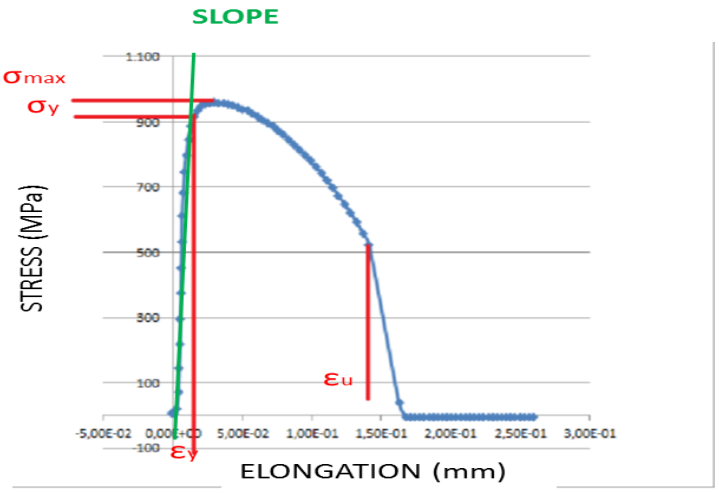

Figure 75. Tensile test key properties evaluated

According to literature [29] the effects of high temperature in properties that can affect fatigue are the following:

- The *tensile strength* is reduced but elongation increases
- *Young modulus* reduced: Less stress for the same deformation. It has to be kept in mind that Low Cycle Fatigue (what concerns this study) is expected to be ruled by deformation and not by stress like in High Cycle Fatigue.
- *Oxidation:* thermal fatigue is generated by an intergranular cracking in the surface. Oxidation is an intergranular effect as well. Its influence increases with time.
- *Creep:* Viscous behaviour at high temperature. Deformation increases for a constant stress. Fatigue resistance reduction and fatigue limit disappears. Creep temperature for these steels is around 580ºC, not being probably an influencing effect.

The results of tensile tests performed are shown in figure 76. The theory was confirmed, reducing the tensile stress, increasing the elongation and reducing the Young Modulus with temperature. The differences between H13 and H11 were not important (H11 has slightly higher deformation capability), consequence probably because both were heat treated to the same hardness. H13 is able to be heat treated to a higher hardness than the H11.

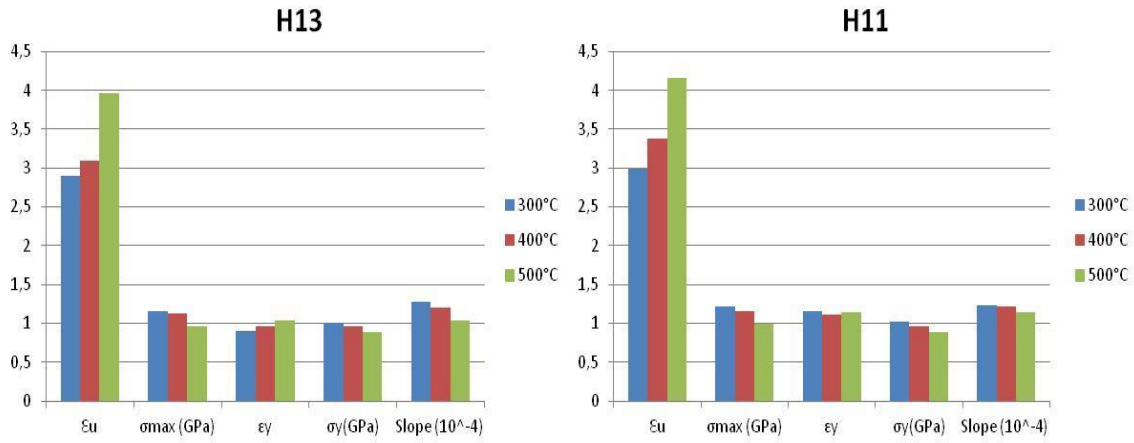

(a) ***(b)***

Figure 76. Results of H13 (a) and H11 (b) samples tensile tests at 300, 400 and 500ºC

High temperature tensile tests shown before in figure 76 are important to understand the mechanical behaviour of materials, but dedicated fatigue tests are necessary to support the thermal stress calculation in order to have a reliable thermal cracks appearance prediction.

The tests performed on the two steels H11 and H13 didn't show big differences between the two steels, what is reasonable as they have equal Hardness.

The influence of the temperature in mechanical properties have a combined effect as explained before. At lower temperatures, the Young Modulus is higher for the same strain. Thus, at 300ºC we are applying higher stress, but it also would have higher maximum stress for a lower maximum elongation. It has been found a good correlation between the stress and cycles to failure. This relation can be described as an equation shown in the next figure. The equation will be valid for a martensitic steel at 43HRC hardness:

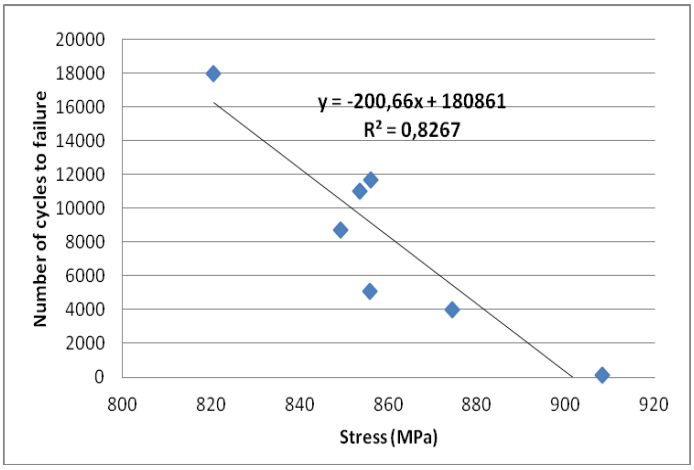

Figure 77 Cycles to failure for different stress level

This equation will be further validated making more fatigue tests as well improved using the data of results of Thermal Fatigue Machine.

3.2.3.2 Effect of different spraying and cooling parameters on thermal gradient in moulds

A model of the Thermal Fatigue machine testing plate was performed in MagmaSoft as shown in figure 78.

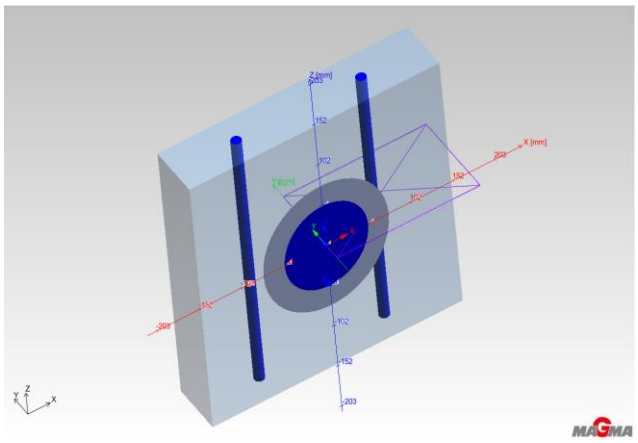

Figure 78. Model of the test plate performed in MagmaSoft

The temperature measurements of a reference cycle were replicated in order to have similar temperature profiles in the steel plate, shown in figure 79. Afterwards the resulting thermal stresses were calculated, and existing fatigue S-N (Wohler) curves were applied to estimate the time to cracking appearance.

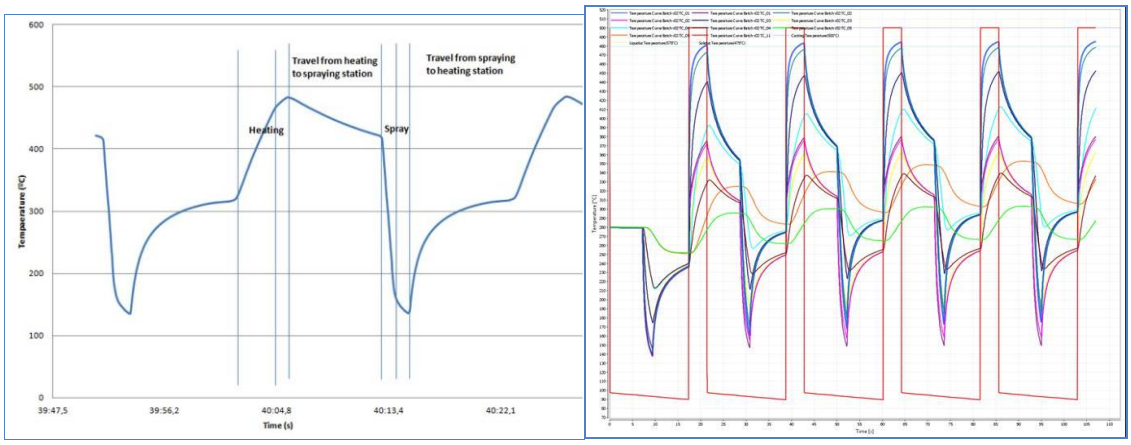

(a) ***(b)***

Figure 79. Cycle temperatures measured in Thermal Fatigue Machine (a) and cycle temperatures performed in Simulation (b)

With this procedure a DOE was performed, where cooling channel positions and spray intensity are defined through heat transfer coefficients (shown on figure 80). The parameter values were the next ones:

Cooling Channel

X-position: 75, 25mm

Y-position: 11.5, 31.5mm

Radius: 4, 6mm

Spray intensity: 5000, 10000 (default), 15000 W/m$^{2^{o}}$K

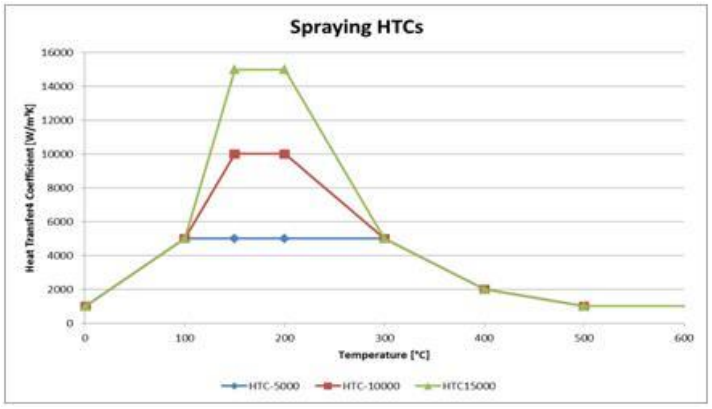

Figure 80 Spraying Heat transfer coefficients used on simulations

The DOE of fatigue life presented previously have been performed and the whole table of results and example of stresses appearance is shown in figure 81.

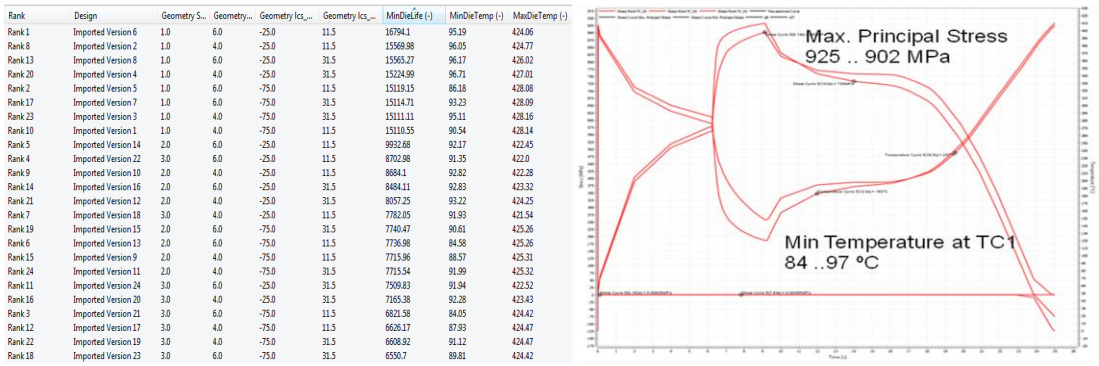

Rank	Design	Geometry S...	Geometry...	Geometry Ics_...	Geometry Ics_...	MinDieLife (-)	MinDieTemp (-)	MaxDieTemp (-)
Rank 1	Imported Version 6	1.0	6.0	-25.0	11.5	16794.1	95.19	424.06
Rank 8	Imported Version 2	1.0	4.0	-25.0	11.5	15569.98	96.05	424.77
Rank 13	Imported Version 8	1.0	6.0	-25.0	31.5	15565.27	96.17	426.02
Rank 20	Imported Version 4	1.0	4.0	-25.0	31.5	15224.99	96.71	427.01
Rank 2	Imported Version 5	1.0	6.0	-75.0	11.5	15119.15	86.18	428.08
Rank 17	Imported Version 7	1.0	6.0	-75.0	31.5	15114.71	93.23	428.09
Rank 23	Imported Version 3	1.0	4.0	-75.0	31.5	15111.11	95.11	428.16
Rank 10	Imported Version 1	1.0	4.0	-75.0	11.5	15110.55	90.54	428.14
Rank 5	Imported Version 14	2.0	6.0	-25.0	11.5	9932.68	92.17	422.45
Rank 4	Imported Version 22	3.0	6.0	-25.0	11.5	8702.98	91.35	422.0
Rank 9	Imported Version 10	2.0	4.0	-25.0	11.5	8684.1	92.82	422.28
Rank 14	Imported Version 16	2.0	6.0	-25.0	31.5	8484.11	92.83	423.32
Rank 21	Imported Version 12	2.0	4.0	-25.0	31.5	8057.25	93.22	424.25
Rank 7	Imported Version 18	3.0	4.0	-25.0	11.5	7782.05	91.93	421.54
Rank 19	Imported Version 15	2.0	6.0	-75.0	31.5	7740.47	90.61	425.26
Rank 6	Imported Version 13	2.0	6.0	-75.0	11.5	7736.98	84.58	425.26
Rank 15	Imported Version 9	2.0	4.0	-75.0	11.5	7715.96	88.57	425.31
Rank 24	Imported Version 11	2.0	4.0	-75.0	31.5	7715.54	91.99	425.32
Rank 11	Imported Version 24	3.0	6.0	-25.0	31.5	7509.83	91.94	422.52
Rank 16	Imported Version 20	3.0	4.0	-25.0	31.5	7165.38	92.28	423.43
Rank 3	Imported Version 21	3.0	6.0	-75.0	11.5	6821.58	84.05	424.42
Rank 12	Imported Version 17	3.0	4.0	-75.0	11.5	6626.17	87.93	424.47
Rank 22	Imported Version 19	3.0	4.0	-75.0	31.5	6608.92	91.12	424.47
Rank 18	Imported Version 23	3.0	6.0	-75.0	31.5	6550.7	89.81	424.42

(a) ***(b)***

Figure 81. Full table of results (a) and an example of stress result in the mould surface during the cycle(b)

The main conclusions from these results are highlighted in the next points:

- The range of minimum die life is estimated between 6000 and 17000 shots.
- The strongest effect on die life has the spray intensity, described by the used spraying Heat Transfer Coefficients (As shown by the correlation Diagram of figure 82 that underlines the strong effect of die spraying on die life). All the other considered parameters have minor effect.
- The position of the cooling channel below the spray spot improves die life a little bit.
- A larger Cooling Channel radius improves die life.
- Cooling channels closer to the die surface have positive effect on die life.

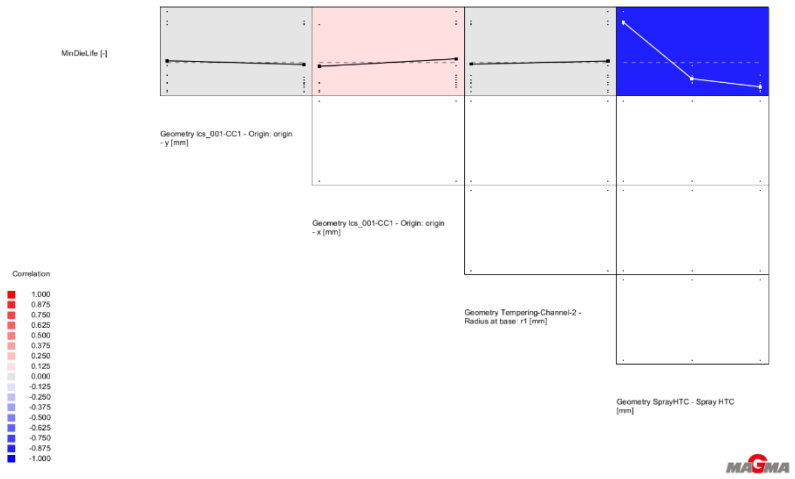

Figure 82. Combined Correlation and main effect diagram

These simulation results permitted a better decision on the test design for thermal fatigue machine tests, finally focused mainly on spraying, instead of cooling channels influence.

3.2.3.3 Relationship between thermal gradient and fatigue life of moulds

The setup of the test machine parameters, are related to intensity and application time of induction and spraying, and the temperature of the oil that goes through the cooling channels. The figure 83 shows an example of selected parameters for a test.

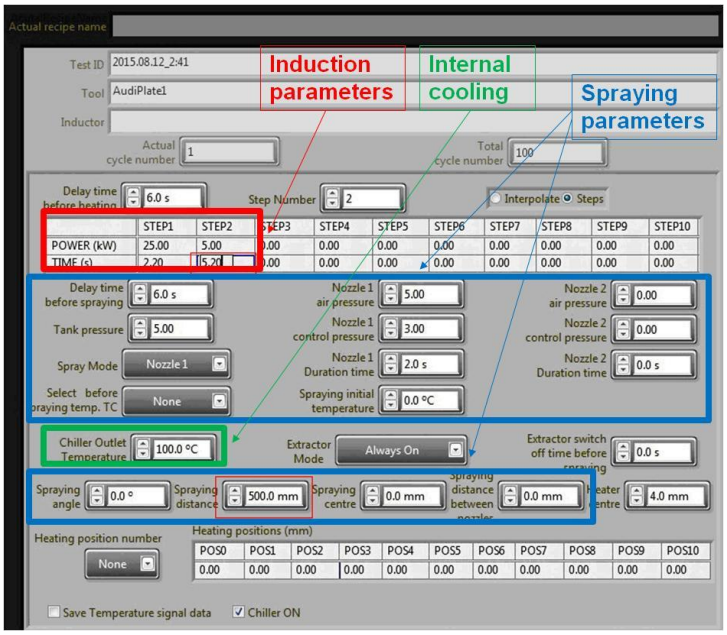

Figure 83. Test parameter selection view in thermal fatigue machine software

The induction heater parameter selection shows a two-step heating. First a 25kW applied through 2.2 seconds, and a second step of 5kW for 5.2 seconds. This second step, being shorter or longer was intended to simulate the influence of thinner or thicker wall aluminium parts, in order to heat deeper the test plate. The temperature of the oil in the example of the figure is 100ºC. The spraying was performed with an unique nozzle, with fluid and air pressure of 5 bar, applying it for 2 seconds, perpendicularly (0º) and centred, and at a distance of 500 mm to the surface.

The set-up of the tests consisted of making several short tests checking the temperatures in the surface and below the surface (see a cycle as example in figure 84). Maximum temperatures around 450ºC were set for all the cases, with variations in the temperature inside the surface and before spraying, while minimum temperatures in the surface depended on the spraying configuration.

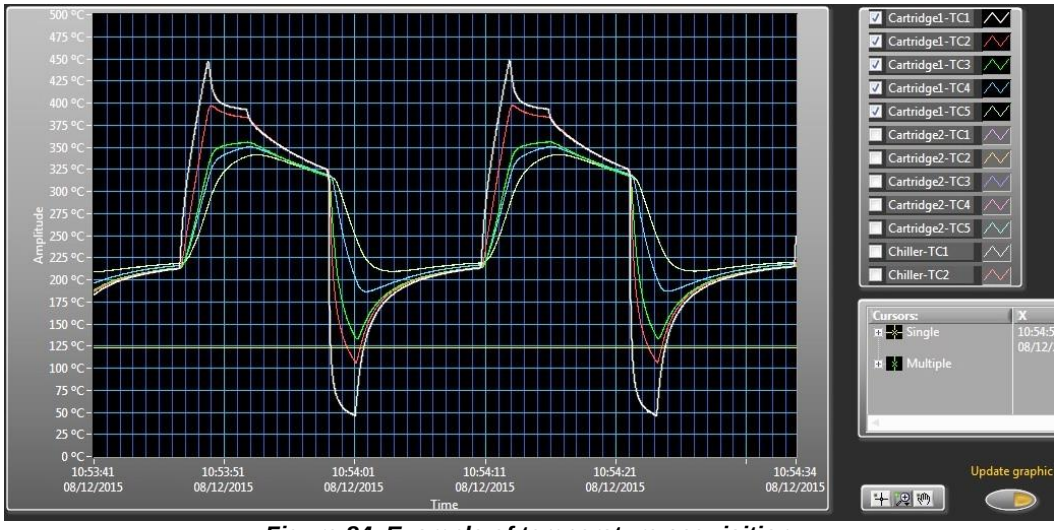

Figure 84. Example of temperature acquisition

As evaluation parameters were considered gradients in the surface and into the surface that are calculated as shown in next figures 85 and 86. About the temperature in the surface, there are of special interest the maximum and minimum temperatures of the cycle and the difference between them (DeltaT), as well as how fast is heated and cooled the surface (Gradient in the Surface). Regarding the temperature into the surface, the maximum gradient during the cycle (in ºC per mm of depth into the surface) was evaluated.

Tmax	463,59
Tmin	115,9
DeltaT+ (ºC)	240,16
DeltaT- (ºC)	-218,79
DeltaT (ºC)	347,69
GradSurf+ (ºC)	79,8
GradSurf- (ºC)	-61,62
GradSurfC (ºC)	141,42

Figure 85. Extreme temperature values in the surface

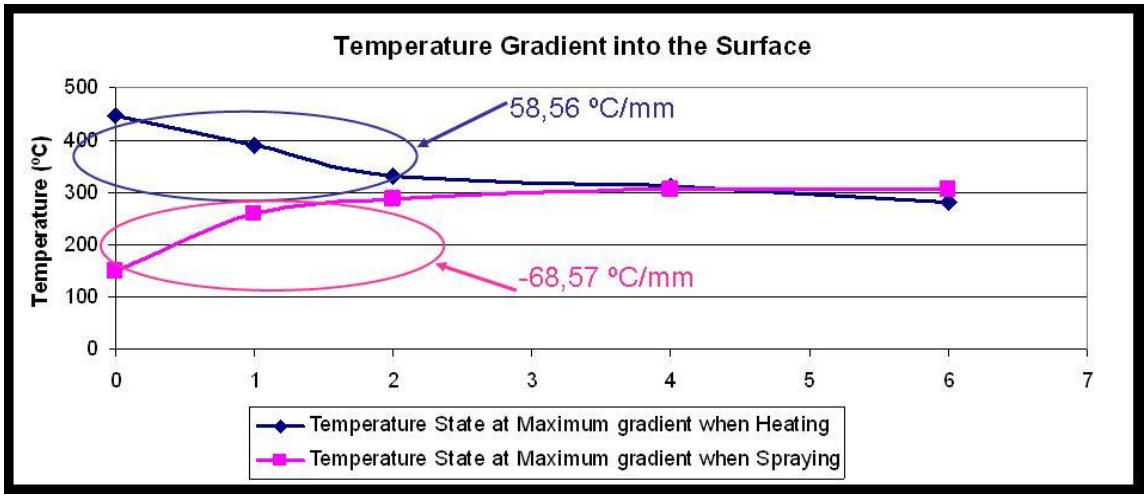

Figure 86. Temperatures into the surface in the maximum heating and gradient value (blue) and in the maximum spraying (pink)

During the first 1000 cycles, surface was inspected each 200 (200, 400, 600, 800, 1000 cycles). Afterwards was inspected at 1500, 2000, 3000, 4000, 5000, 7000, 9000, 11000, 13000, 15000.

The tested block number 1 was simulating thick walled castings heating and had the spraying very near (100mm from surface, what lead to a cooling area of 35mm diameter). It started cracking at 400 cycles in an area above central point and at 3000 cycles in more parts of the heated area of 100 mm diameter. The small cooling area resulted in an overheating far above the measuring point that might have been the reason of the early cracking.

The tested block number 2 was simulating thin walled casting heating and the spraying very far (500mm from surface, what lead to an area of 176mm diameter). It started cracking at 400 cycles as well, and evolved into a grid of cracks in some areas of the heated plate. The figure 87 shows the detail of the crack appeared in the two tests performed.

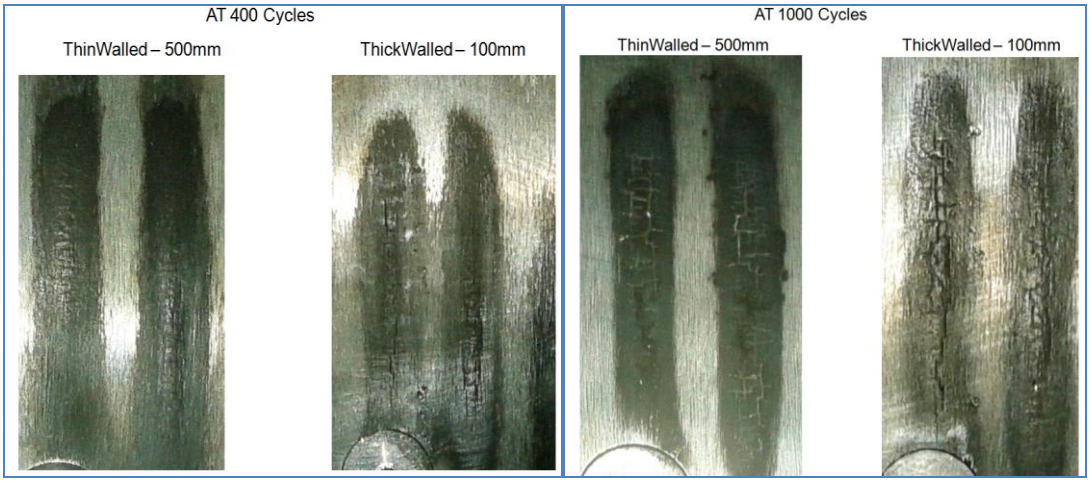

Figure 87. Cracking on test plate surfaces at 400 and at 1000cycles for the two tests

The applied heating power was very fast (2.2 seconds at 25kW and 3.2 and 5.2 at 5kW for thin and thick walled respectively) and resulted in a lack of homogeneity of induction heating as clearly can be seen in figure 88 for the example at 3000 cycles. The main issue of this inhomogeneity is that, there is a higher uncertainty of thermocouple measurement during induction heating.

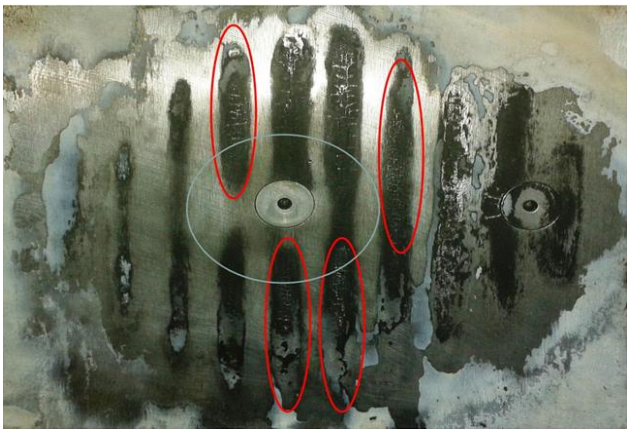

Figure 88. Cracking on thick walled plate surface at 3000 cycles

From these two tests the following conclusions were extracted to improve the protocol:

- The heating of the inductor coil was not homogeneous and looked as stripes like.
- The maximum temperature of the induction heating is below 1 mm, but the affected depth is much higher. The thermocouple measurements (at surface, 1mm, 2mm, 4mm, and 6mm) confirmed this behaviour.
- The heating is very dependent of inductor coil geometry, distance of application, power and some trials are needed to get a fast heating by induction to correlate with HPDC and get a failure at 10000 cycles, range at which cracking appears in typical dies.
- One way to avoid the stripes and get an homogeneous heating, is to heat very slowly, to have time to transfer the heat through the surface, avoiding such high stress generation while heating, and getting more influence of the stress's during spraying.
- The spraying would be better to make in a fixed distance at which the cooled surface area will be similar to the heated one. Afterwards the setup can be made to study different spraying water pressures and different temperatures before spraying (e.g. 300ºC and 250ºC)

From these initial lessons learnt, new testing was prepared. This time the set up was searching a slower and more controlled heating. The time for heating was fixed for 10 seconds, and 2 levels of power were set, in order to achieve two different temperatures before spraying: 300 ºC (9.1 kW) and 350ºC (9.8 kW). The most aggressive condition lead to appearing of cracking when checked at 2000 cycles, while the less aggressive did not appear after 25000 cycles. The crack length evolution was monitored from 2000 up to 15000 cycle, where nearly doubled the crack length from 16.4 mm up to 28 mm. The heating was much more homogeneous avoiding the overheated stripes.

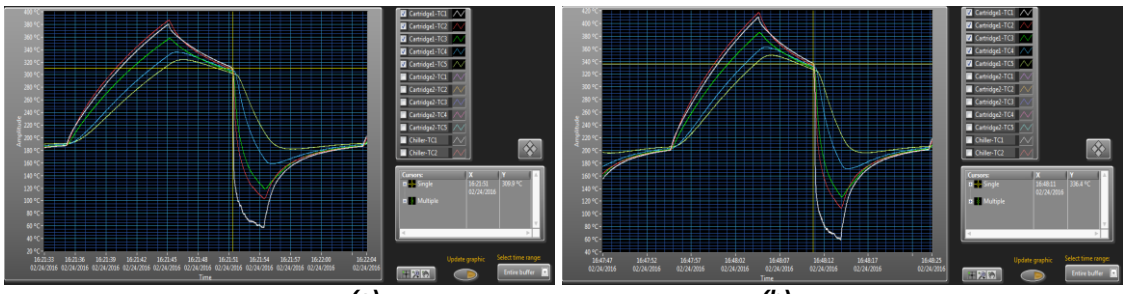

(a) ***(b)***

Figure 89. Thermal cycle performed when heating 10 seconds at 9.1 kW (a) and 9.8 kW (b)

It has been considered proved that the test procedure of the thermal fatigue test is able to simulate both the cracking appearing in HPDC dies and the temperature fields in the dies. The testing conditions can be tailored to reproduce a typical durability of the mould of 10000cycles.

These latest results, of slow heating (10 seconds at 9.1 and 9.8kW), are sparse. Even though, assuming that the cracking appearance is linear, that the test at 9.1 kW was to start cracking few cycles after the latest checking at 25000 cycles, a model can be created from these two data. As there are just 2 data, it is not possible to evaluate the quality of the model through the analysis of variance. The analysis have been made using as two possible factor that rule the cracking appearance: the maximum gradient during the cycle (in ºC per mm of depth into the surface during spray cooling since while slow heating nearly no gradients appear) and the accumulated temperature difference during the cycle, as the sum of the temperature difference while heating and temperature difference while fast spray cooling.

In the future, when more data are created this model can be fine-tuned, and depending on the analysis of variance of the two suppositions (cracking ruled by thermal gradient or accumulated temperature difference), the approach that leads to the best R^2 coefficient can be applied. In any case both models could be useful for

a Design or Maintenance Engineer. If the data available for him are the temperature differences during the cycle and he has no idea about the thermal gradients into the surface, the model based on temperature differences would be more useful, even if its quality would be lower than the one based on thermal gradients.

The curves showed in the figure below lead to the following equations:

$$N\ (cycles) = -338.24*TG + 55441$$

Where

TG: thermal gradient (in ºC per mm of depth into the surface during spray cooling) measured in the mould or calculated from simulation in MagmaSoft or other software's (valid for thermal gradients between 90 and 160 ºC per mm of depth).

$$N\ (cycles) = -377.05*\Delta T + 192787$$

Where

ΔT: accumulated temperature difference during the cycle, as the sum of the temperature difference while heating and temperature difference while fast spray cooling, measured in the mould or calculated from simulation in MagmaSoft or other software's (valid for temperature differences between 445 and 505 ºC).

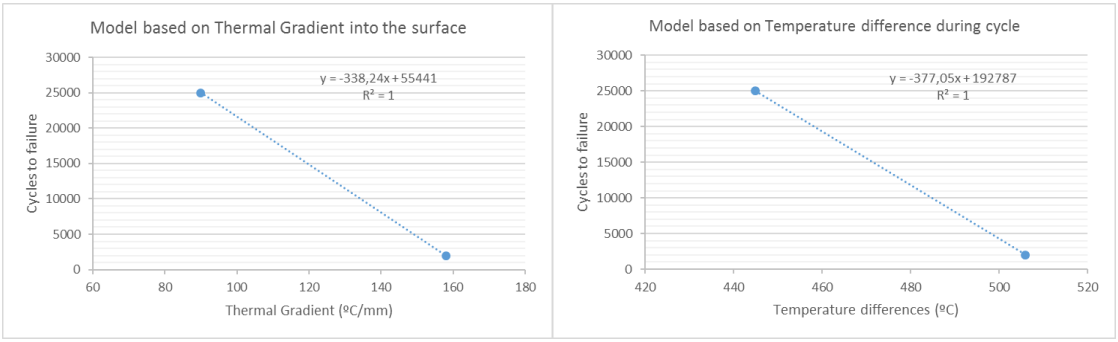

Figure 89. Thermal Fatigue curves based on thermal gradients into the surface (a) and based on temperature difference during the cycle (b)

3.2.4 Model assessment

For the thermal fatigue prediction in the mould the approach proposed here is, once the thermal stress is previously calculated in a HPDC process simulation software like Magmasoft, the fatigue curve generated in this work is applied to estimate the cycles to failure. For each material, it would be necessary to re-study the equation, that for H11 and H13 at 43 HRC have been generated from the experimental results, as the following one:

$$N\ (cycles) = -200.66*S + 180861$$

Where

S: thermal stress calculated from simulation in MagmaSoft (tested from 820 to 900 MPa, and valid for die temperatures between 300 and 500 ºC)

Analysis of variance of the model: $R^2=0.8267$

As an example the final user, could calculate as explained the thermal stress's in different critical areas and check the cycles to failure with this equation. For example for a value of 840MPa thermal stress, would lead to 13763 cycles to failure. This estimation has been considered reasonable taking into account stress levels and failure appearance in HPDC process's.

3.3 Die Soldering in HPDC

3.3.1 Objective

The objective of this chapter is to simulate the die soldering wear mechanism that occur in moulds of High Pressure Die Casting at laboratory scale, to be able to evaluate the influence of relative speed, the pressure, mould temperature as well as the mould material characteristics or alloy material characteristics, and have a better insight of the phenomena. As the formation of a protective lubricant film is key to prevent the soldering formation on mould surfaces, dedicated tests to investigate the performance and suitability of lubricants have been performed, and included in this chapter. A big part of this

3.3.2 Materials and methods

3.3.2.1 Materials

Five different lubricants for HPDC applications have been used for this study, supplied by the Company Motul-Baraldi in the form of concentrated lubricant and named A, B, C, D, E hereafter. The lubricants are generated from a concentrated solution composed by a 20-30% of an anhydrous part that is usually diluted in water once time more with a rate from 1:50 to 1:100 [23]. The active part, made of a blending of oils, polysiloxanes, polymers and many additives, gives the main characteristics to the film that forms on the die cavity after water vaporization. Together with the anhydrous part, there are the emulsifiers, normally surfactants, which have the aim to join the oil and water and to increase the filming power on the die [24]. Based on the typical classification of Metal Working Fluids, the B, D, E lubricants could be classified as semi-synthetic family, since they contain mineral oil with a viscosity index around 90, while the A, C lubricants as synthetic ones, that have a viscosity index around 180. These are estimated viscosity values of the base lubricants since the viscosity of the mixture is not measurable. In fact, when the products are dried they result in an inhomogeneous material consisting in solid parts and different liquids immiscible each other. The A and C lubricants offer a very high releasing power for average to big weight castings. The B lubricant is particularly indicated in the case of thin walled components with a low weight, and the D and E lubricants for any kind of diecast parts.

The reference dilution was 1:50 (2%) but other ratios were studied as well. The surface tension of lubricants diluted at 1:50 was measured according to the ASTM D-971-99 standard. The dilution were made mostly with tap water (7.52 ºdH German grade, 53.6 mg/l Ca^{+2}, <1 mg/l Mg^{2+}) and artificially generated hard water (17.9 ºdH, 96.8 mg/l Ca^{+2}, 18.7 mg/l Mg^{2+}).

Table 6 shows the measured surface tension values for the studied lubricants. It is important to highlight that these HPDC lubricants at such a small dilution rate as 2% reduce the water surface tension from 72mN/m to around the half of this value.

Lubricant	Surface Tension (mN/m)
A	48.7
B	53.2
C	35.1
D	33.9

E	31.5

Table 6: Measured surface tension of lubricants at 2% dilution ratio

Two different type of steels, AISI H13 and H11, were selected for the study, as the most common die materials in HPDC. The description of their characteristics is presented before in the chapter 3.2.2.3 about the materials used for thermal fatigue studies.

To simulate the ageing effect of die lifetime, the H11 and H13 samples were put in a furnace at 600ºC for 5 hours. This procedure led to an oxidized surface, but the microstructure was inspected and remained as shown in previous pictures. The hardness differences were in the range of measurement errors.

Surface roughness of an actual HPDC die was inspected with SAEN collaboration, partner from EU Project MUSIC, at different surface finishing stages: after electrical discharge machining operation, after milling operation by two different milling tools (tool "a" and tool "b"), after polishing operation and a used die surface after 15000 castings in two different die zones (the ingate where the flow is smooth and another where the flow is turbulent). The results are shown in Table 7.

Surface finishing stages	Ra (μm)
After EDM (Electrical Discharge Machining)	2.02±0.04
After EDM and milling (Milling tool "a")	1.22±0.07
After EDM and milling (Milling tool "b")	0.80±0.12
After EDM. milling and polishing	0.66±0.07
Used die. 15000 castings (Ingate zone. Smooth flow)	0.88±0.11
Used die. 15000 castings (Turbulent zone)	0.91±0.12

Table 7: Roughness at different surface finishing stages of HPDC dies, including difference of two milling tools, and influence of lifetime measured in two regions of the Die.

The Ra values of laboratory samples used for the study ranged between 0.02 and 1.8μm. The oxidation had little or no influence on the surface roughness. The surface energy measured for the H13 and H11 samples are very similar as shown in Table 8. Oxidation had a very different influence on the surface energy of die steels, i.e. increasing the H11 surface energy but reducing in the case of H13. This behaviour could be related to the fine microstructure of the H13.

Surface	Surface Energy (mJ/m^2)
H13	39.87
H13 oxidized	23.27
H11	40.68
H11 oxidized	46.25

Table 8: Surface energy of as received and oxidized H13 and H11

3.3.2.2 Goniometer for Contact Angle and Leidenfrost Point Evaluation

Experimental measurements were carried out by a SURFTENS Universal Goniometer shown in figure 90, which was used for the determination of the Leidenfrost Point (LFP) as well as the Contact Angle (CA) and the surface energy measurements. The approach of this study is similar to the one from literature [21], and its main advantage compared to other devices is the capability of measuring both LFP and CA.

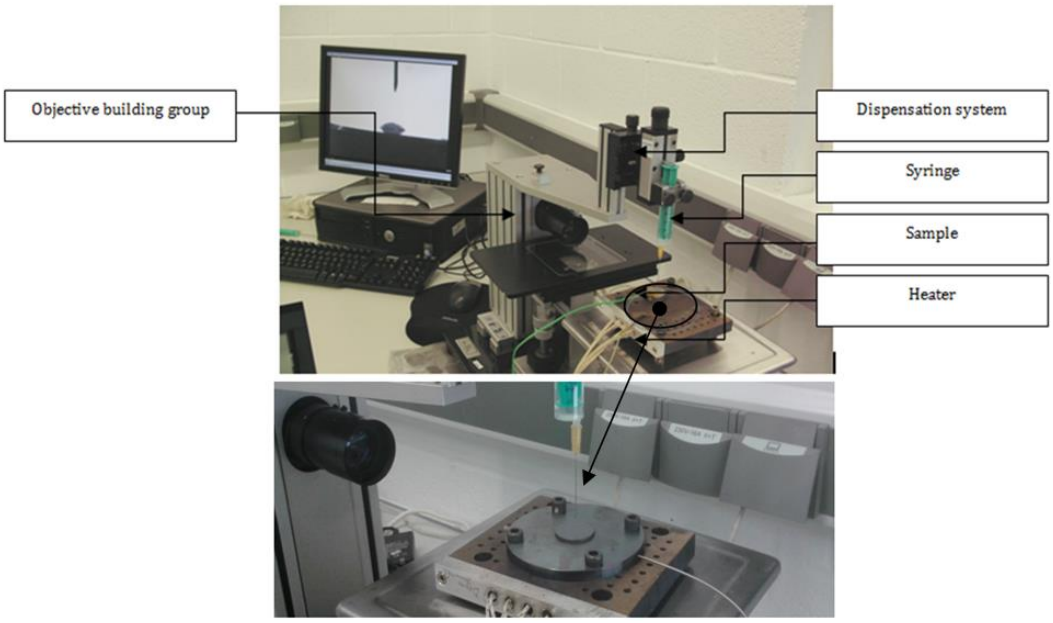

Figure 90. The universal goniometer modified © IK4-TEKNIKER to carry out high temperature measurements.

The equipment is composed by a fixed structure with an objective building group, an illumination unit and a droplet dispensation system, which was used with two different nozzle diameters: 0.5 and 0.9 mm. The sample is located in a heater based on resistances, fixed to a mobile structure. In order to check the temperature, a K-type thermocouple is placed into the sample and connected to a control unit.

The criterion used in the present work to identify the LFP was to increase the temperature progressively, in order to identify the temperature when the film boiling regime starts. A screening of the lubricant impact behaviour at the surface was recorded. After each droplet falls to the hot surface, the sample rotates to carry out the following test in a fresh area that it is not contaminated by previous lubricant droplets.

The same system is used to evaluate the Contact Angle (CA). When the droplet falls from the dispensation system into the surface, automatic measurement and data recording of CA is made from identification of 5 points of the droplet shape figure 91, and it is reported a value as the mean given by the data acquired during 30 seconds. Each measurement was repeated at least 4 times. The heating device was used to heat the surface at 25, 50 and 80ºC, respectively, in order to evaluate the CA at different temperatures.

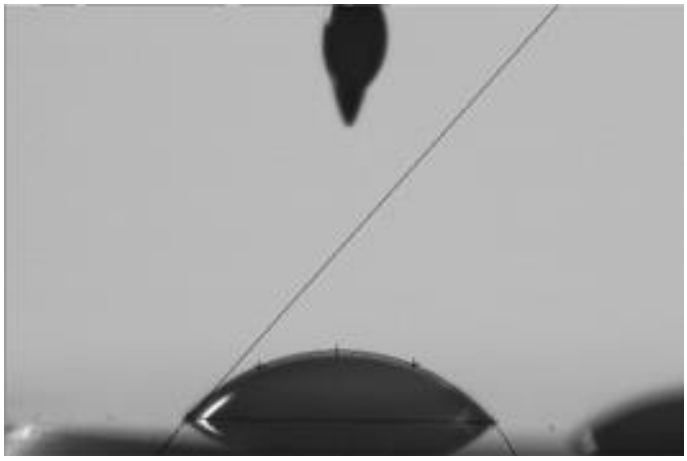

Figure 91. The contact angle calculation through 5 points measurements.

3.3.2.3 Pin on Disc tests for evaluation of lubricant protection film life

A reciprocating pin-on-disc test, where a cylindrical pin of aluminium EN-AC-43500 is forced to move against a mould material in AISI H13 steel disc, has been used for evaluating the performance of lubricants to prevent soldering and as release agent.

To create good conditions to simulate the presence of the lubricant film on the disc surface, a procedure to create a lubricant coating on the disc surface has been set up, based on resistance heating. About 1 ml of pure lubricant was progressively deposited on the H13 surface at 130ºC, resulting in a homogeneous and well distributed lubricant film.

The machine used is a SRV©. The testing temperature is selected as close as possible at HPDC die surface. A low temperature condition (~365ºC) has been selected to study the phenomena in a range of temperature that is equal to the average surface temperature in real HPDC process, and a higher temperature (~450ºC), which is the maximum value of the die temperature during die filling.

The basic normal load and sliding speed selected to reproduce the wear mechanism were 50 N and 25 Hz. The stroke was kept constant at 2 mm. To investigate this effect, different level of pressure and speed were considered: 20-50-125-200-300 N and frequencies of 10-25-35Hz.

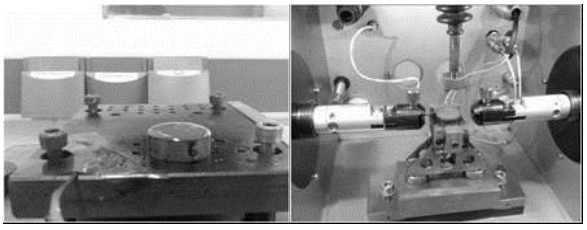

(a) (b)

Fig. 92. (a) Preparation process of the sample with a ''coating'' of the lubricant and (b) sample that is ready to start the pin on disc test

In order to evaluate the effectiveness as release agent, the stable initial value of friction was considered. As output for die soldering prevention, the time to lubricant failure has been identified to be a good indicator of lubricant effectiveness. The failure is measured when the friction coefficient rises from the stable value of 0.1-0.2 to a value of around 1 of friction coefficient.

3.3.2.4 DSC-TGA tests for lubricant thermal behaviour evaluation

Two typical chemical tests usually used to investigate the behaviour of the lubricants in function of the temperature and time have been used. The first is the Thermogravimetric (TGA) test and the second the Differential Scanning Calorimetry (DSC) test. In the TGA, the mass loss related to a degradation mechanism of the sample is recorded and in the DSC tests, it is recorder the heat flow that corresponds to the reaction mechanism.

This test has been made with a pure lubricant with an initial mass equal to 40 mg. Different lubricants have been tested to evaluate the effect of the temperature in lubricant degradation.

The range of temperatures investigated in the dynamic thermal test were from 50 up to 700°C. The heating rate was 10°C/min using N_2 atmosphere. Isothermal tests have been performed in the range from 350 to 425ºC.

Figure 93. Lubricants ready to be tested in the DSC/TGA test

Figure 94. DSC result in an isothermal testing conditions (a), dynamic testing conditions (b)

3.3.3 Results and discussion

3.3.3.1 Evaluation of lubricant filming formation: Leidenfrost effect and Contact Angle

Tests to search LFP were carried out with liquids diluted in soft water, both for H13 and H11 samples. The results are reported in Figure 94.

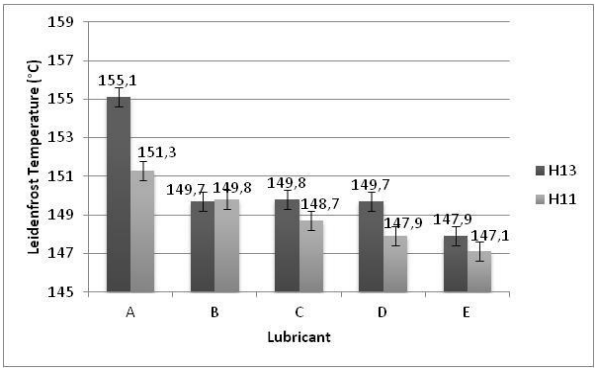

Figure 94. The LFP for soft water-based lubricants on H13 and H11 die materials.

The differences between lubricants, on the value of LFP, are probably due to the different formulations and additives. For both die materials, lubricant A has the highest LFP and lubricant E has the lowest LFP, while B, C and D are similar. The LFP is typically higher for H13 for most of the lubricants.

Regarding the CA values for different lubricants, shown in Figure 96, there is a wide range of values from almost 70º to below 15º depending on lubricant and surface temperature. It is shown, a reduction of contact angle when increasing the temperature, but not all lubricants reduce their values in the same way. The synthetic lubricants A and C, have less differences in contact angle at different temperatures with both steels, H13 and H11. This is probably due to their higher viscosity index due to their synthetic nature that means a lower dependence of the viscosity with the temperature. All the semisynthetic lubricants have a similar behaviour.

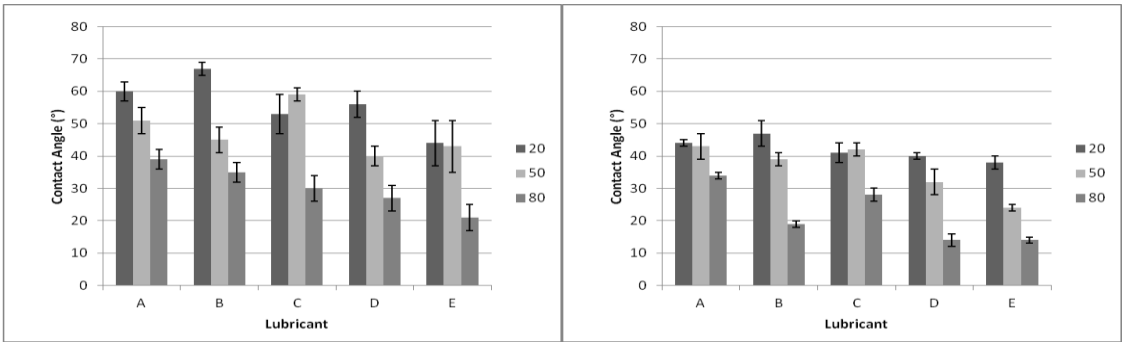

(a) ***(b)***

Figure 95. The CA at 20, 50 and 80°C on (a) H13 and (b) H11 steels

The trend of these curves highlight that the LFP decreases with the decrease of contact angle (CA). An explanation for this phenomena could be that a less wettable liquid has less contact area with the surface, but its weight is the same. Thus, the higher pressure makes necessary a thicker vapour layer to sustain the droplet, then this layer will be created at higher temperature.

A study of the different variables that affect LFP and CA was carried out being explained in detail in the Paper of the annex "Multiparametric study of Leidenfrost point and wettability of lubricants on high-pressure die-casting dies". The main results achieved are summarized below:

- The variation range of the LFP for all the studied cases is in the range 140-165ºC. These differences are significant for HPDC.
- The variation range of contact angle for all the studied cases is in the range 15-70 degrees; the repetitions show up to 5 degrees of deviation.
- The lubricant ranking of LFP for all the cases shows: highest value for A, lowest value for E and in the middle similar values for B, C and D.
- The higher the temperature, the lower is the contact angle. In general the lubricant CA values at 80ºC present a similar behaviour to temperatures near LFP.
- The CA decrease is less pronounced for some lubricants. The synthetic lubricants A and C, have a lower variation of CA with temperature, probably due to the higher viscosity index of their base oils in his type of lubricants.
- The lubricant ranking of CA, even if it is not the same ranking for the 3 tested temperatures, is similar to the LFP ranking. In fact, more hydrophobic combinations (higher contact angle) tend to have higher LFP.
- The LFP and CA for H13 are a bit higher than H11 probably due to their finer grain microstructure.

- The hardness of the water used for the formulation of the lubricant has some influence in the LFP for both steels H13 and H11. In general, the harder the water, the higher was the LFP being this behaviour especially significant for lubricants C and D.

- Oxidized surfaces show higher LFP, since the oxide layer, has a lower thermal conductivity that promotes surface temperature protection.

- A higher lubricant percentage (1-3%) leads to higher LFP. Above 3%, it is not observed further increase.

- Rougher surfaces have higher LFP both for H13 and H11 steels, but the CA variation depends on the type of steel and their microstructure. In the H13 with a finer microstructure, the contact angle increases with the roughness, they present a hydrophobic behaviour and it seems to fulfil Cassie's model [55] where the liquid doesn't penetrate the roughness. The H11 seems to follow the Wenzel's model [55] range where liquid penetrates in roughness grooves, and the contact angle decrease when increasing the roughness.

- Higher droplet size shows higher LFP, in line with prediction from We number [54]. Wettability seems not to be influenced by droplet size, being the droplet size, a parameter that could play a good role trying to maximize LFP, keeping low the contact angle.

- Die cast lubricants get lower surface tension, CA and LFP values than water. The droplet of the lubricant flattens after impact and then it evaporates, while water evaporates without an increase of surface contact.

- The combination of several factors make synergic the improvement, increasing further LFP. An increase of 25ºC in LFP relative to the reference, were achieved combining a high droplet size 0,9mm diameter, with 3% of lubricant A, diluted on hard water, on an oxidized sample, with high roughness.

3.3.3.2 Evaluation of lubricant effectiveness: time to film failure in pin on disc tests and thermal behaviour in DSC-TGA, and related film thickness

The lubricant behaviour and its tendency to be washed from the steel surface depend on many factors such as: pressure, speed, temperature and surface conditions. The main parameter that affects this tendency isn't a physical variable but it's a chemical parameter. The chemical composition (especially the amount and typology of additives) describes the desorption tendency of the lubricant.

The figure 96 show some of the results that could be identified in the pin on disc results. The time to failure ranking of lubricants was similar to the one of LFP being from highest A (C292H) followed by C (C015H) and D (C30), while B (C178H) and E (C073H) where the worst. The time to failure ranking of lubricants was similar to the one of LFP. The table 9 shows these results, being A lubricant, the one that lasted more followed by C and D, while B and E where the worst.

	A	C	D	E	B
Time to Failure (cycles)	39750	21625	16025	6500	5000
COF (-)	0.167	0.166	0.177	0.155	0.187

Table 9. Time to failure and friction coefficient of the different lubricants in the pin on disc tests at 50N, 25Hz and 365ºC

Regarding the physical parameters, as shown in figure 97, Temperature was the most important parameter (as exponential dependence), followed by Pressure (logarithmic dependence), while the speed didn't show a

huge influence. In the same figure, how the time to failure is evaluated from the friction curves is shown with black arrows.

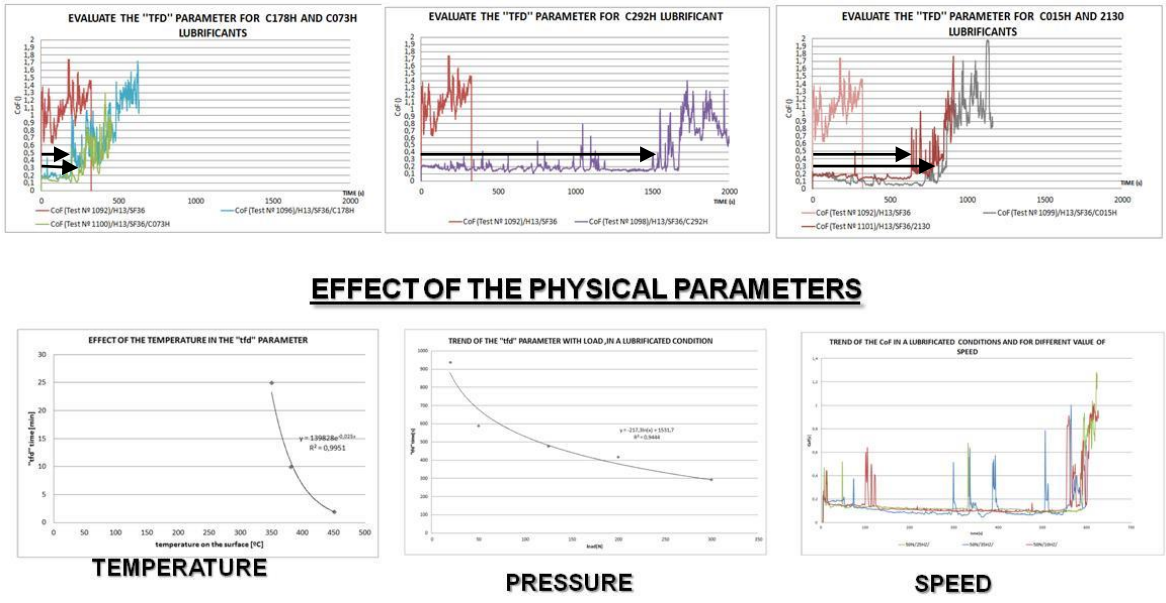

Figure 96. Results of lubricant film failure in pin on disc tests

With the results of the investigation of the lubricant behaviour, an equation to predict the life of the lubricants in terms of its tendency to be washed from the surface of the iron's disc has been built. This law is a simple result of an application of a best fitting process. It' based on these two assumptions:

- The speed has a negligible effect on the loss of the lubricant protection
- The pressure, the temperature and chemical composition haven't a reciprocal interaction.

The equation obtained from experimental data is described below, and its surface response for one lubricant is shown in figure 98:

$N(cycles)= 27.1*10^{6}*exp(-0.0198*T)-5432.5*Ln(P)+ 7587-6149*K$

Where:

T: Mould maximum surface temperature in ºC

P: Pressure in the mould surface

K: depending on lubricant (see next table 10)

Lubricant type	K
A	1
B	4,49
C	1,96
D	2,68
E	4,48

Table 10. Coefficients for die soldering equation

Analysis of variance of the model: R^2=0.6147

The quality of the model has been represented by the R^2 coefficient. Even if the coefficient has been found very high, it has to be into account that the experimental data are very sparse and that has been assumed that the pressure, the temperature and chemical composition haven't a reciprocal interaction. In the next figure it is shown the equation for the pressure and temperature independently.

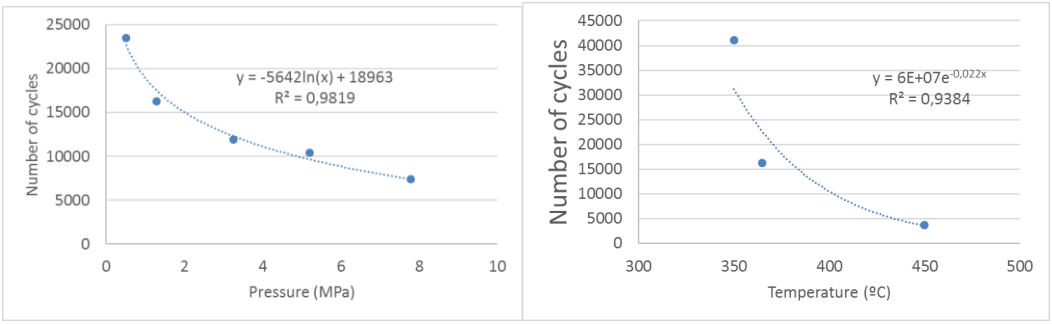

(a) ***(b)***

Figure 97. Fitting curves time to failure represented independently for Pressure (a) and Temperature (b)

Regarding the physical parameters, as it is shown in the response surface created from experimental results shown in figure 98, temperature was the most important parameter (as exponential dependence), followed by Pressure (logarithmic dependence), while the speed didn't show any influence. This is in accordance with Fick diffusion law, which also rules die soldering mechanism [13].

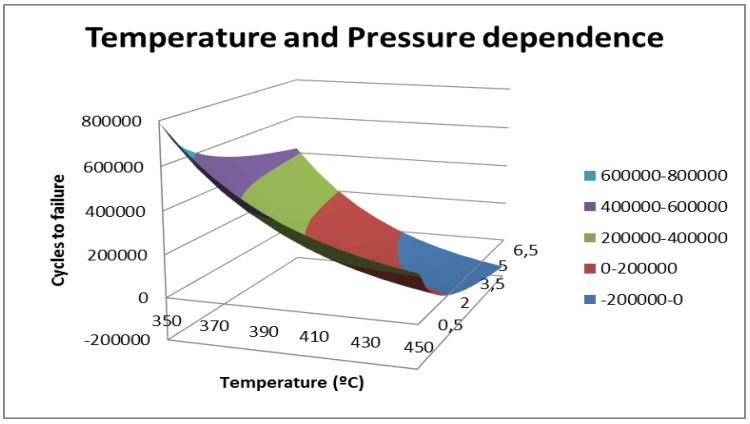

Figure 98. Surface response of time to failure for the A lubricant in function of the Temperature and Pressure.

It has been observed that the main element that affects the degradation mechanism of the protective film is the temperature; it leads to an increasing desorption tendency of the lubricant and a chemical degradation of it. These two aspects have been studied with another chemical test, the TGA test. This TGA test has been divided in two different parts: the isothermal and thermal dynamic tests. The first one has the scope to evaluate the effect of the time in ageing at high temperature conditions, and the second one, has the aim to evaluate the effect of the temperature.

The dynamic tests have shown that the lubricant has a very high initial degradation (at 100°C) because of their evaporation process. This degradation doesn't carry on until 375°C; above this temperature there' s a

high degradation process that causes a complete degradation of lubricant above 475°C. In this degradation process there is a difference between the different lubricants.

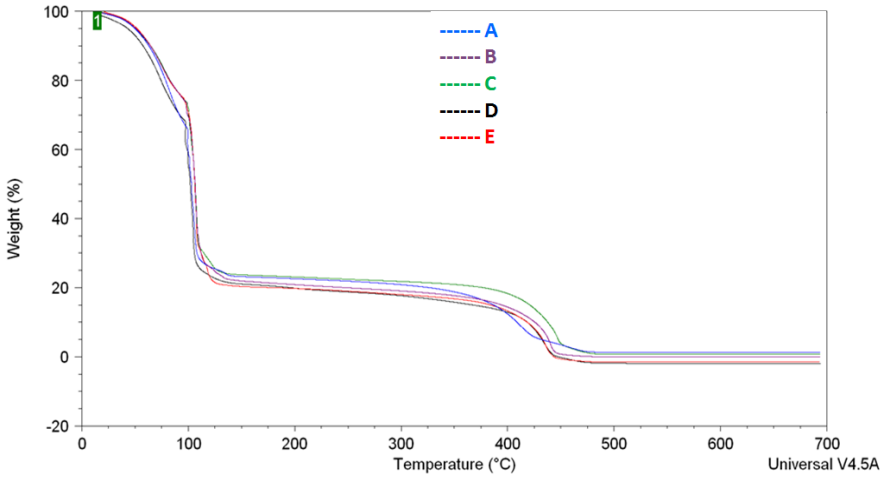

Figure 99. Results of non-isothermal / dynamic test of the 5 lubricants

The isothermal tests of the lubricants have been carried out at 350°C and at this temperature, after 3.5 hours, the degradation process isn't complete. At 425°C the total degradation of the lubricant appears after about 30 minutes of test. The ranking of degradation process in isothermal tests and dynamic tests was the same, film thickness measurements also show the same ranking (see figure 100).

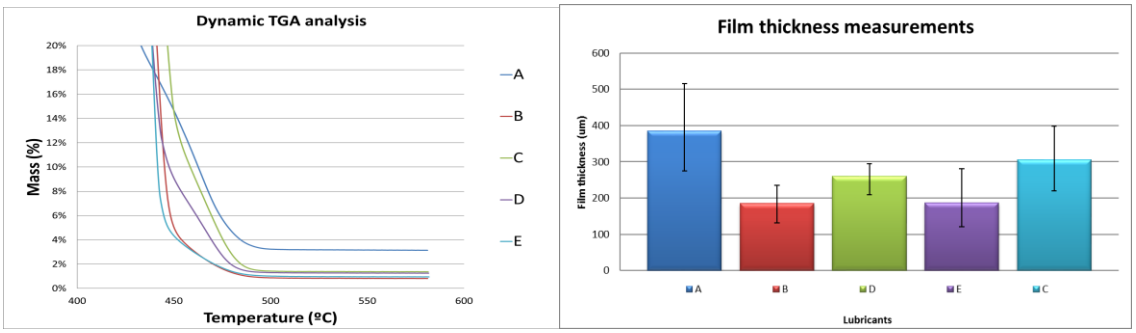

(a) ***(b)***

Figure 100. Isothermal DSC-TGA tests at 425ºC result of lubricants (a) film thickness measurement results (b)

Good correlation was found between filming capacity (Leidenfrost Point, Contact Angle stability, film thickness), TGA of lubricants (thermal behaviour) and Time to failure during frictional tests. The best lubricant is the A (C292H) followed by the C (C015H), both lubricants contain in their formulation synthetic oils with a high viscosity index**.** Lubricants B (C178H), D (C30), and E (C073H) in this order follow in the worst performance ranking. The next table 11 shows the summary of the key properties measured.

Property	A	B	C	D	E
LFP (ºC)	155.1	149.7	149.8	149.7	147.9
CA (º)	60	67	53	56	44
DS_failure (cycles)	39750	5000	21625	16025	6500
COF (-)	0.167	0.187	0.166	0.177	0.155
TGA (ºC)	478	450	472	465	447

Film Thickness (µm)	385	185	306	260	187

Property	Explanation of the value
LFP (ºC)	Leidenfrost point of lubricant diluted at 2% measured in the test protocol with H13
CA (º)	Contact angle of lubricant diluted at 2% measured in the test protocol with H13
DS_failure (cycles)	Time to failure by die soldering in the tribological test
COF (-)	Coefficient of Friction measured in the pin on disc tribological test
TGA (ºC)	Temperature at which lubricant mass below 5% of initial mass in non-isothermal TGA test
Film Thickness (µm)	Film thickness measured in the test protocol of depositing 1ml in a ø24 mm hot steel sample

Table 11. Summary of the main properties measured in the study

3.3.4 Model assessment

Several tests have been performed and information gathered in the activity related to die soldering prevention, especially through an effective lubrication, creating a protective film that prevents the part sticking to mould surface through die soldering formation.

To predict the time to failure of the protective film and start of die soldering formation, the following equation already defined can be implemented:

$N(cycles)= 27.1*10^6*exp(-0.0198*T)-5432.5*Ln(P)+ 7587-6149*K$

Where:

T: Mould surface temperature in ºC (between 350 and 450ºC)

P: Pressure in the mould surface in MPa (between 0 and 7 MPa), Pressure value is necessary to calibrate to convert from HPDC pressure range to the ones measured on the tests.

K: depending on lubricant (see table 10).

Analysis of variance of the model: $R^2=0.6147$

As an example of use of this equation, if cleaning/maintenance work is planned to be made each 5000 cycles, the benchmark would be to achieve these cycles in the equation. For the example, if the surface temperatures are around 400ºC and the pressure level on surface is relatively low (let's say 1 MPa for the equation) any kind of lubricant even the E or the B would achieve these 5000 cycles without problems. Instead if the surface temperatures will achieve 450ºC, only the A lubricant would arrive to 5000 cycles without any sticking problems, while for all the rest the cycles to failure would be very low. If the temperature would be around 425ºC also lubricant C and probably lubricant D, would prevent the sticking as well.

3.4 Abrasion in PIM

3.4.1 Objective

The objective of this test is to simulate the abrasion wear mechanism that occur in moulds of Plastic Injection Moulding at laboratory scale, to be able to evaluate the influence of relative speed, the pressure, mould temperature as well as the mould material or surface treatment characteristics, and have a better insight of the phenomena.

3.4.2 Materials and methods

The abrasion test is performed by the Universal Micro-Tribometer represented on figure 101, a general purpose reciprocating movement tribometer that can be used for testing of ferrous and non-ferrous metals, plastics, ceramics, paper, composites, thin and thick coatings, as well as of solid lubricants, lubricating fluids, oils and greases, in different configurations such as Pin on Disc, Ball on Disc or Block on Ring. It can work in a wide range of normal forces, movement stroke and speed, or temperature. During the test, the applied normal load and the evolution of generated friction force are recorded.

Figure 101. Universal Material Tester (UMT3 of CETR)

The selected configuration have been Block on Plate, where a 4x4x4mm block, injected by Maier S. Coop., is static while have a reciprocating sliding movement against a moving flat surface that is a disc of mould steel manufactured by Tekniker. Several of the discs were surface treated also by Maier.

The testing conditions were selected in order to simulate, as close as possible the PIM moulds failure mechanisms. The mould material sample was heated to usual mould working temperature of 100ºC. The plastic temperature was measured in static conditions in contact with the mould, achieving almost the same temperature as the mould temperature. In dynamic conditions (while testing) it is not possible to measure the plastic temperature in the contact, but is expected to be near the plastic melting point, simulating a similar behaviour as in PIM.

In the following figure 102 there are shown the temperature evolution due to friction between different plastic and mould materials in a “Block on Ring” configuration test [56, 57]. In this case the test started at

ambient temperature and the temperature raised between 15 and 30 ºC depending on the plastic material when the mould material was copper, and between 40-70ºC when the mould material was aluminium.

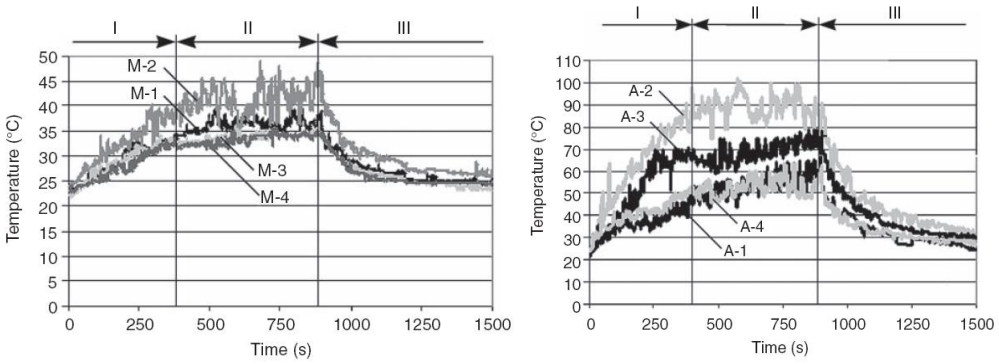

(a) *(b)*

Figure 102. Temperature evolution during the block on ring test, due to the frictional heating of copper (a) and aluminium (b) alloys for 4 different plastic materials [56, 57]

The melting temperature depends on the nature of the plastic material. The following table 12 shows the limit temperature of different plastics before degradation starts. Showing the temperature rise due to frictional heating of [56, 57], it is not expected to achieve this limit temperatures.

Type of plastic	Maximum Temperature
PMMA	280ºC
PC	280ºC
PA+30%FV	300ºC
ABS	250ºC
ASA	270ºC
PC/PET	280ºC

Table 12. Maximum temperature before degradation occurs of some candidate plastic materials

Contact pressure between the two bodies due to the applied normal load was selected in the range of PIM injection pressures (8-18 MPa) and the sliding speed as PIM injection speed range (20-50mm/s). To have this speed range, the movement stroke was kept constant at 8 mm, while frequency was modified.

Wear tests were performed mainly on PA+25%GF, since the rest of the plastics didn't generate measurable wear. These wear tests were performed at different pressure and speed conditions with all the different surface solutions. The wear tests were performed during 4 hour testing.

Friction tests were performed at single testing conditions of 8MPa and 20mm/s, with a duration of 5minutes. For some cases where the pin wear was very high, the test was stopped slightly before. They were performed at all the 3 plastic materials against all the surface combinations.

The materials used for the testing have been:

- *Plastic material:* PA+25%GF, PMMA, PC

- *Tool Steels:* 2738BM, 2738HH

- *Surface treatments:* Salt Nitriding, Ionic Nitriding, TiN, Ni-PTFE

After the tests, the wear was evaluated by mass loss measurement in a high precision balance (accuracy down to 0.00001g) as well as wear depth measurements in a Confocal Microscope as shown in figure 103.

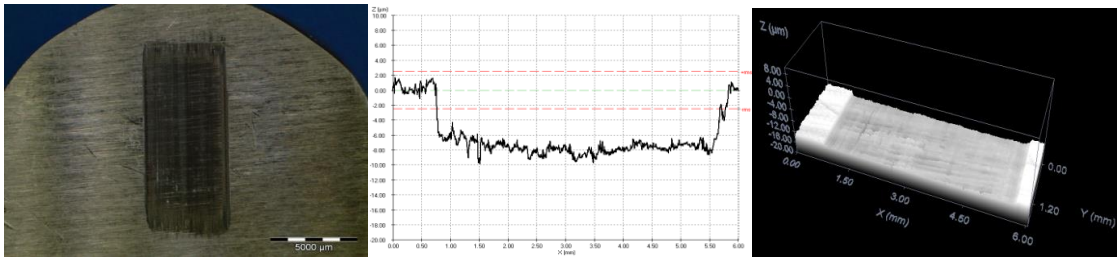

(a) ***(b)*** ***(c)***

Figure 103. Sample after wear test (a), cross section of the wear scar (b) and 3D image of a section of the wear scar (c) of Confocal Microscope.

SEM measurements were also performed for the cases that were necessary.

For the case of PA+25%GF plastic tests, it was checked that the pins had similar fibre orientation and same fibre percentage (25±1%). The procedure for fibre inspection was based on organic material evaporation in an oven at 600ºC for 2hours.

Hardness of the different mould surfaces were measured by Vickers durometer and Fischerscope H-100 for thin films. The order from higher to lower hardness was: TiN, Ionic Nitriding, Salt Nitriding, Ni-PTFE, 2738HH and 2738 BM. The next table 13 shows the values, as well as the roughness values. Regarding roughness, all the surface treatments increased the roughness of the substrate.

SURFACES	HARDNESS (HV)	ROUGHNESS, Ra (µm)
2738 HH	275±3.5	0.55
2738 HH + Ionic Nitriding	753±38.9	0.75
2738 HH + Salt Nitriding	586±12	0.8
2738 HH + Ni-PTFE	382±7.2	0.6
2738 HH + TiN	1592	0.7
2738 BM	266±2.1	0.55
2738 BM + Ionic Nitriding	861±37	0.75
2738 BM + Salt Nitriding	513±27	0.8
2738 BM+ Ni-PTFE	321±13.9	0.6

Table 13. Hardness and Roughness measurements of the different surface solutions

The two steels 2738 HH and 2738 BM microstructures were also investigated. They showed both a Tempered Martensitic structure, but 2738BM shows a sorbobainitic aspect while 2738HH present a sorbitic aspect. 2738BM showed grain size number of 4-5 while 2738 HH of 9-10. The next figure 104 shows their microstructure.

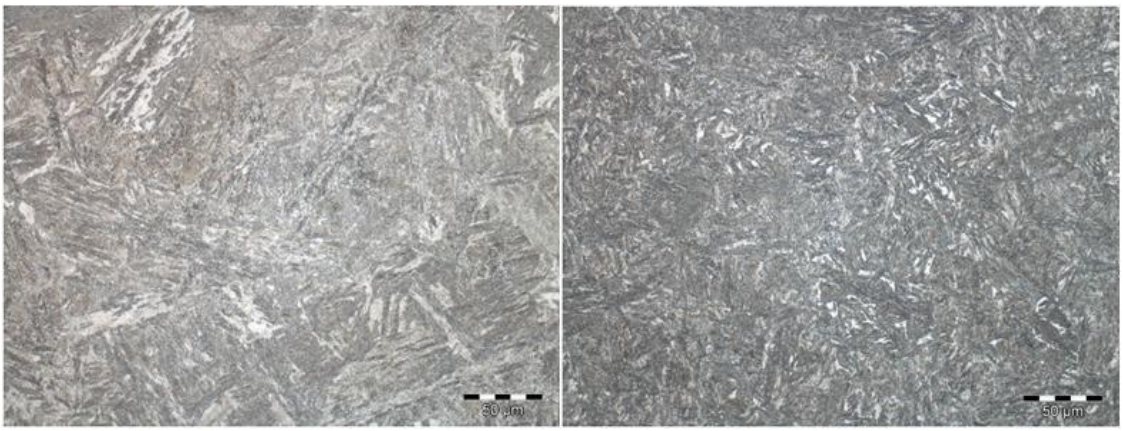

(a) ***(b)***

Figure 104. Microstructure of 2738BM (a) and 2738HH (b) steels

3.4.3 Results and discussion

3.4.3.1 Effect of injected plastic on friction coefficient

Regarding the wear of the moulds through abrasive mechanism, it was found that PMMA and PC, even if they generate very high friction with mould surfaces, they don't create measurable wear. Instead the fibre reinforced Polyamide that exhibited low friction, generated measurable wear in most of the surfaces. This will be analysed in detail in 4.4.3.2.

Regarding the friction, PMMA and PC had very similar friction against all the different surfaces, with a friction coefficient around 0.8, while PA+25%GF had a friction coefficient around 0.5 as can be seen in figure 105.

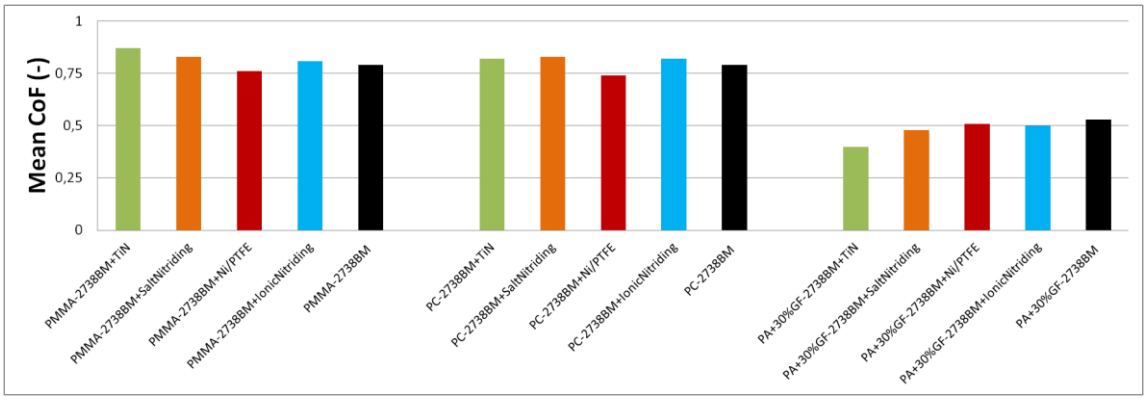

Figure 105. Mean friction coefficients of the different surfaces against PMMA, PC and PA+25%GF

For the case of PMMA and PC, only Ni-PTFE was effective reducing friction compared to the substrate, while the rest of the surface treatments had higher friction. In figure 106, it can be seen that at the beginning

of the test, Ni-PTFE starts with a coefficient of friction of 0.4 for the PC and 0.6 for the PMMA instead of the 0.8 afterwards. This result make sense due to the use of PTFE as anti-adherent in several applications.

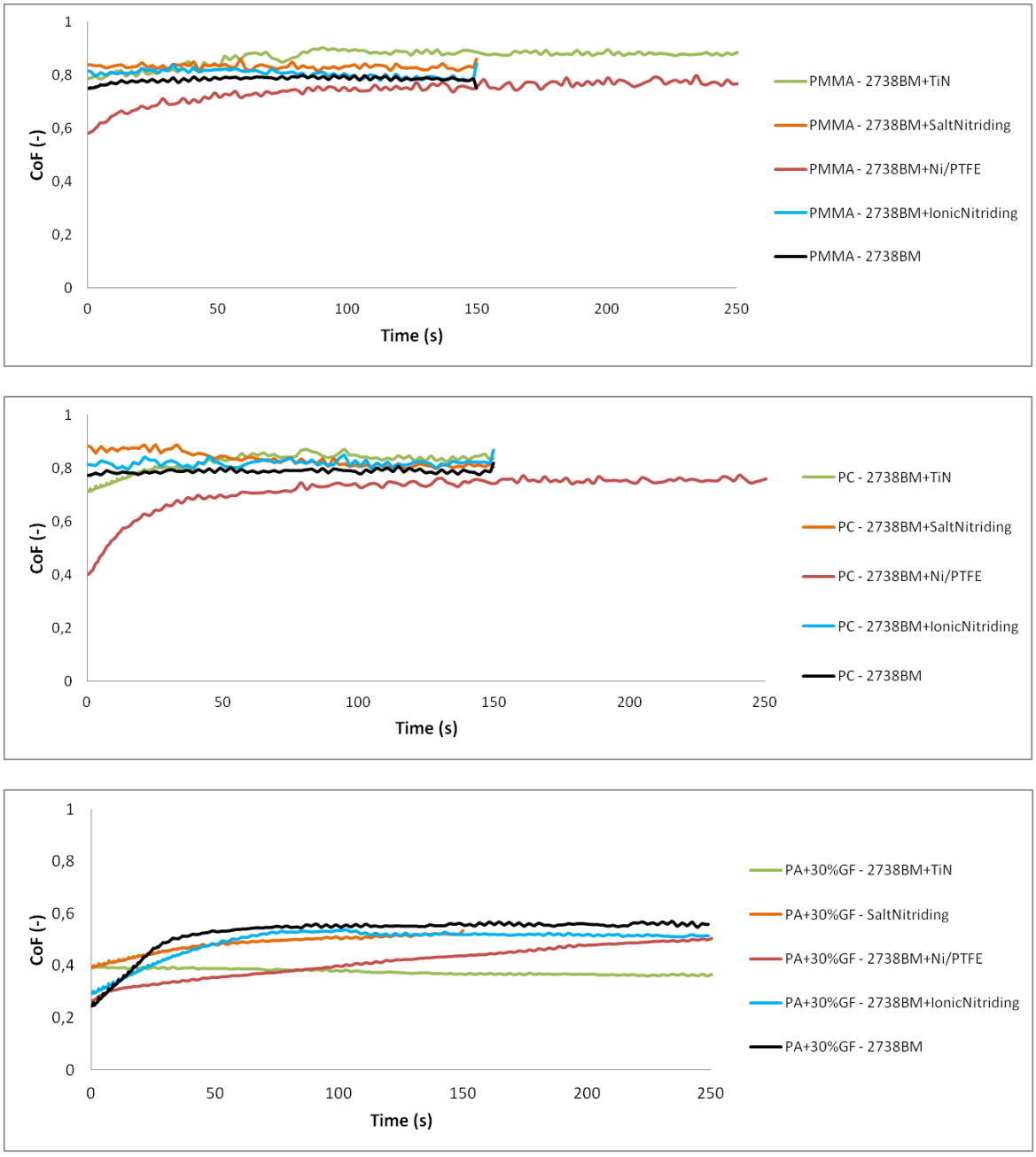

Figure 106. Friction coefficient evolution during the tests of the different surfaces against PMMA, PC and PA+25%GF

In the case of PA+25%GF, Ni-PTFE was not so effective. For this case TiN was the most effective probably due to their higher hardness, reducing down to 0.4 the mean CoF instead of the 0.53 of the 2738BM substrate. This is probably due to the wearing process that is taking place in the test against the fibre reinforced plastic.

3.4.3.2 Effect of mould material and surface treatment on abrasive wear

Wear tests were performed on PA+25%GR plastic against all the different surface treatments applied on the two different substrates. Due to the application of thermal treatment on 2738 BM to transform to 2738HH, the 2738HH showed higher wear resistance than the 2738BM. The Ni-PTFE treatment on 2738BM does not improve the wear resistance of the base material. It was less wear resistant than the substrate itself, reaching the substrate in some areas, along the wear track as shown in figure 107.

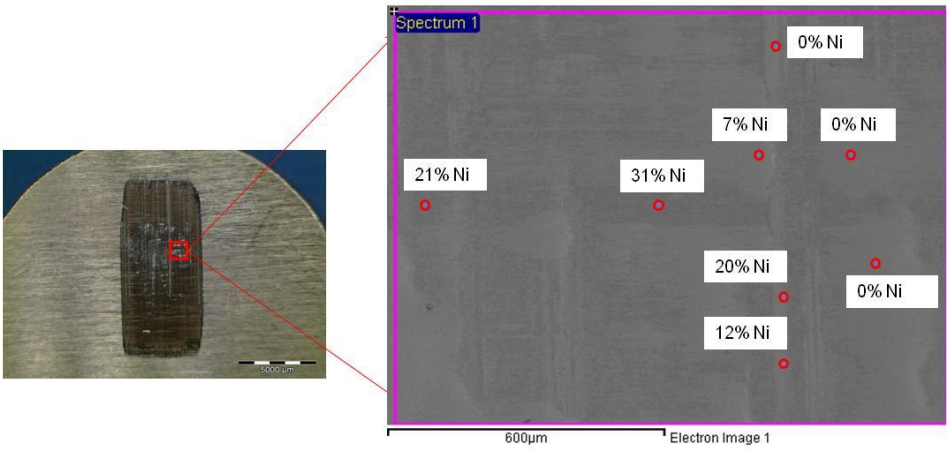

Figure 107. SEM measurement for checking the remaining Ni-PTFE coating at wear scar

Salt Nitriding presented more abrasive wear than the Ionic Nitriding. Salt Nitriding had around 4 µm depth and around 0.35mg of total wear amount while Ionic Nitriding below 1 µm and not measurable in mass lost. Both TiN and Ionic Nitriding were the only surfaces that didn't show any wear after the 4 hour tests. This behaviour can be explained by the higher hardness of the surface treatments. The application of the different surface treatment behaved similarly applied in any of the two substrates. Figure 108 shows the mass lost for all the surfaces in these tests.

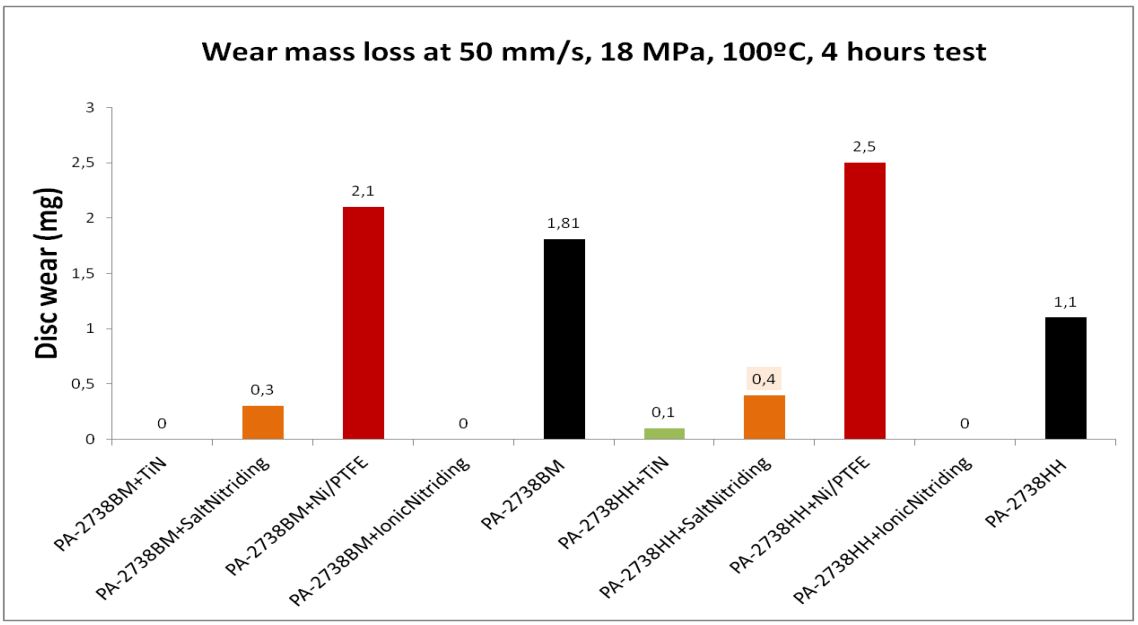

Figure 108. Wear mass loss of the different surfaces against PA+25%GF after wear tests

The figure 109 and 110 shows the wear depth measured in Confocal microscope for two of the surfaces, the salt nitriding and the Ni-PTFE surfaces, both applied on 2738BM surface. The wear depth was practically constant all over the wear scar, around 4 µm for the Salt Nitrided surface and 8 µm for the Ni-PTFE surface. These wear scars lead to 0.3 mg and 2.1 mg respectively.

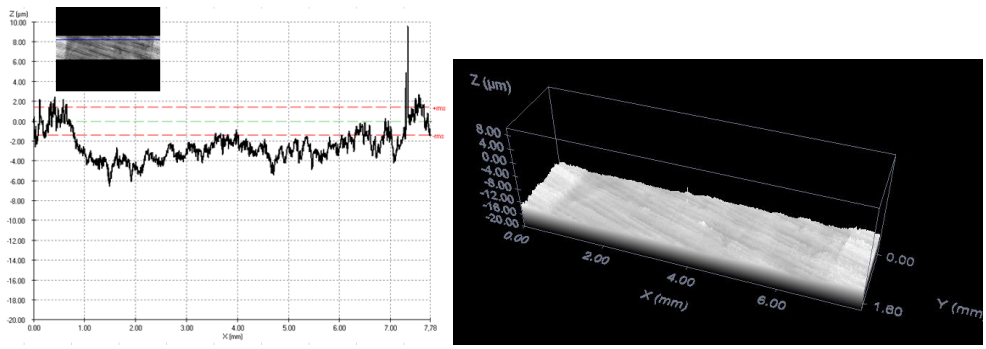

Figure 109. Cross section and 3D view of the wear scar of Salt Nitriding applied on 2738BM substrate after the wear test

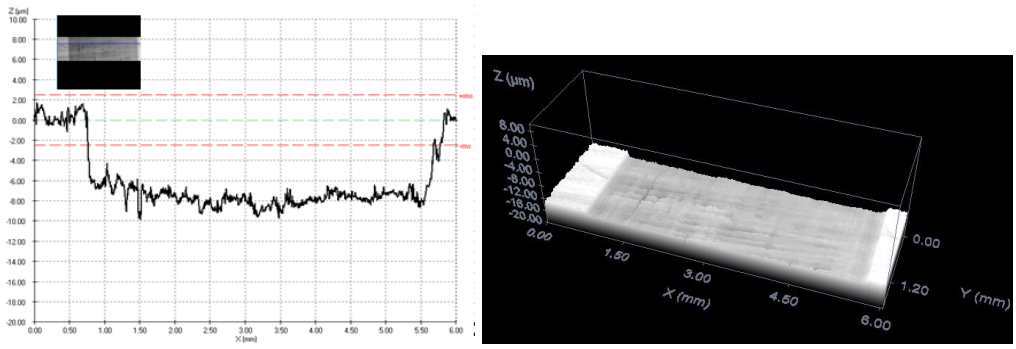

Figure 110. Cross section and 3D view of the wear scar of Ni-PTFE applied on 2738BM substrate after the wear test

The dependence between mould material hardness's and resulting abrasive wear is shown in the figure 110a. The correlation was better when applied only to both substrates and both nitridings, figure 110b, since it looks like above a hardness of 800 HV1 it is hardly possible to make scratches on mould surface.

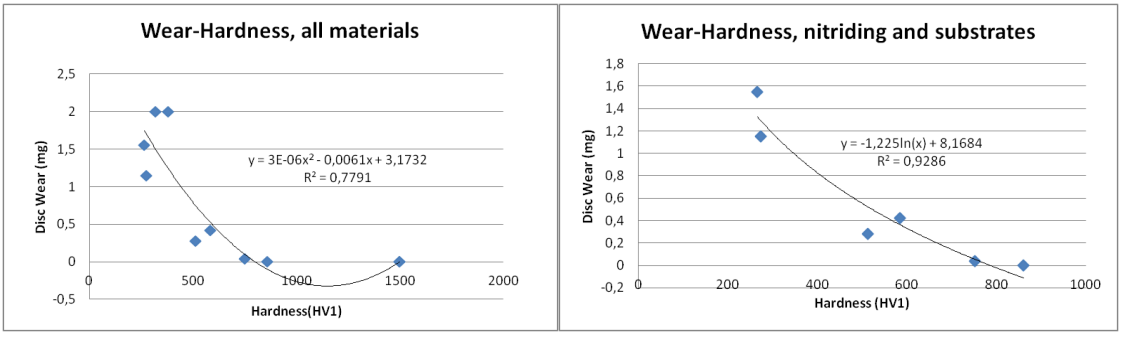

(a) ***(b)***

Figure 110. Correlation between Hardness and wear during the tests for all the surfaces (a) and only for both nitridings and both substrates (b)

3.4.3.3 Influence of different injection parameters on abrasive wear

Wear tests were performed at all the 4 extreme testing conditions of pressure and speed, for 2738BM substrate against PA+25%GF. The results show that both speed and pressure are critical for modelling the wear of PIM moulds as can be seen in the figure 111.

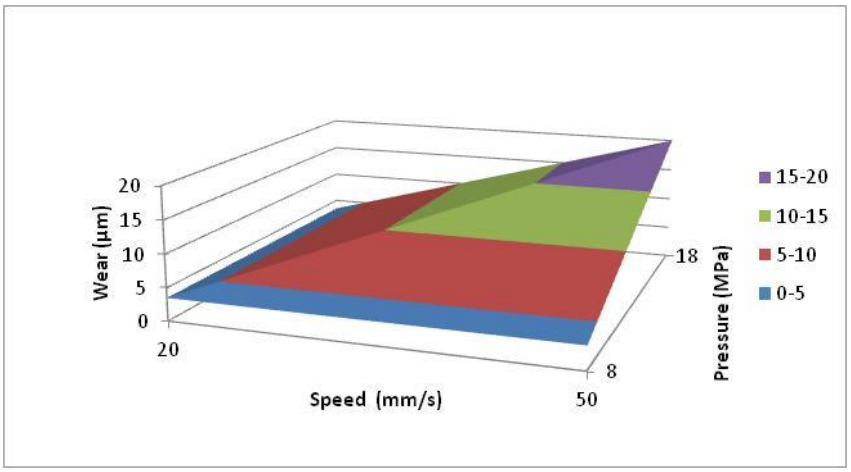

Figure 111. Surface response of wear tests dependent on pressure and speed

This dependence on both parameters can be written in an equation as follows:

Wear (µm)= 12.3-1.1P-0.44v+0.055Pv.

Where:

Speed range measured 20-50mm/s

Pressure range measured 8-18MPa

Regarding the friction coefficient, its values were not so sensible to the change of pressure and speed conditions as shows the results of figure 112, about the tests of the PA+25%GF against the 2738BM. These tests were performed at 8 and 18 MPa, and 20 and 50 mm/s. The 2738BM disc temperature was 100ºC, except one that was tested at ambient temperature.

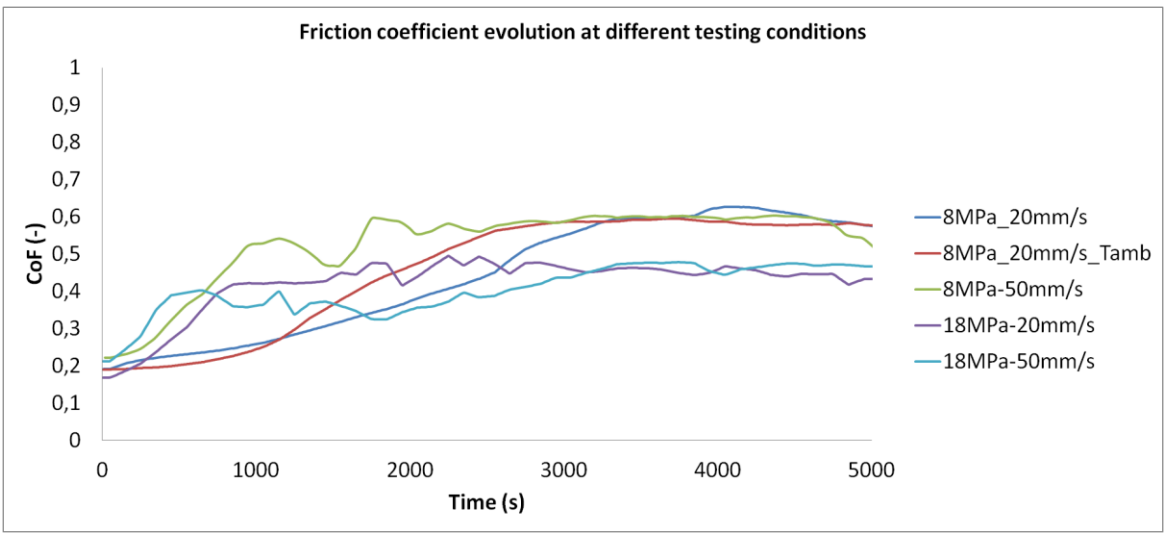

Figure 112. Friction coefficients evolution during the tests of the PA+25%GF against the 2738BM substrate at different testing conditions

It seems that it is independent of sliding speed, and descend slightly with the increased pressure. It was observed that the testing temperature was not so influencing in the final friction coefficient value. The slight reduction of the friction coefficient when increasing the pressure, was also found for other mould materials, as can be seen in the table 14.

Test condition	2738 BM	TiN	Ionic Nitriding	Salt Nitriding	Ni-PTFE
CoF-Mean (PA)-18MPa	0.44	0.37	0.38	0.39	0.42
CoF-Initial (PA)-18MPa	0.17	0.37	0.22	0.37	0.44
CoF-Mean (PA)-8MPa	0.53	0.40	0.50	0.48	0.51
CoF-Initial (PA)-8MPa	0.25	0.4	0.28	0.39	0.27

Table 14. Table for friction coefficient for different test conditions and surfaces

3.4.4 Model assessment

The small differences regarding friction makes no sense building a model on these results. In any case the results can be set in a software as a table for consulting how to reduce the friction when problems related to it are expected (part ejection problems or high shear stress's).

Material combination	CoF (-)
PMMA-2738BM+TiN	0.87
PMMA-2738BM+SaltNitriding	0.83
PMMA-2738BM+Ni/PTFE	0.76
PMMA-2738BM+IonicNitriding	0.81
PMMA-2738BM	0.79
PC-2738BM+TiN	0.82
PC-2738BM+SaltNitriding	0.83
PC-2738BM+Ni/PTFE	0.74
PC-2738BM+IonicNitriding	0.82
PC-2738BM	0.79
PA+30%GF-2738BM+TiN	0.40
PA+30%GF-2738BM+SaltNitriding	0.48
PA+30%GF-2738BM+Ni/PTFE	0.51
PA+30%GF-2738BM+IonicNitriding	0.50
PA+30%GF-2738BM	0.53

Table 15. Table for friction coefficient values consultation

Regarding wear, it makes sense to build a model that has taken into account both the injection parameters and mould material hardness, for glass fibre 25% reinforced PA plastics. The resulting model that combines both results can be written as follows:

$$Wear\ (\mu m/h) = 5.0918 - 0.0597P - 0.0262v + 0.0031Pv - 0.8128\ln(H)$$

Where:

P: *Pressure in MPa* (applicable from 8 to 18MPa, below not expected any wear. Pressure value is necessary to calibrate, to convert from PIM pressure range to the ones measured on the tests)

v: *Speed in mm/s* (applicable from 20 to 50 mm/s, below not expected any wear)

H: *Hardness in Vickers,* HV (applicable up to 900HV, above, it is not expected any wear)

Analysis of variance of the model: $R^2=0.9811$

The application of the model is shown in the in next table 16. It is supposed that in each cycle the filling time is 5s, so the wearing process takes place for this time.

Pressure (MPa)	Speed (mm/s)	Hardness (Hv)	Wear rate (µm/cycle)	Wear at 50000 cycles (µm)	Cycles up to 100 µm
18	50	200	1.65E-03	82.7	60467
15	35	200	8.34E-04	41.7	119935
8	20	200	3.89E-04	19.4	257393
8	20	800	0.0	0.0	∞
18	50	380	9.29E-04	46.5	107619
18	50	550	5.12E-04	25.6	195388
18	50	800	8.88E-05	4.4	1125922

Table 16. Examples of wear model application

The use of this tool from a final user could:

- *Predict the cycles to arrive to an unacceptable wear (i.e. 100 µm):* if the working pressure in a mould area is 18 MPa and the Speed of 50 mm/s for a common mould material of 200 HV, the mould would need reparation at 60467 cycles. If the Surface is improved to 380 HV the cycle number would be around 107619, while if the surface hardness is 800 HV, the cycle number would increase to 1125922 cycles. Additionally to a 800 HV surface, if the Pressure is reduced to 8 MPa and the speed to 20 mm/s the mould would have no signs of abrasive wear.

- *Predict the wear for a production cycle of 50000 cycles:* If the cycle number of production is known, the wear can be calculated and decide if it is acceptable or not, depending on the mould area and part requirements. If the working pressure is 15 MPa and the speed 35 mm/s, the wear would be 41.7 µm, what might not be acceptable for an aesthetic area of a part.

3.5 Erosion in PIM and HPDC moulds

3.5.1 Objective

The objective of this test is to simulate at laboratory scale, the erosion wear mechanism that occur in the moulds. Two applications have been considered:

- High Pressure Die Casting moulds due to the solid particles on the melt,
- Plastic Injection Moulding due to the glass fibre reinforcements,

The influence in the erosion wear of the process parameters such us the flux speed, the impact angle, mould temperature as well as the mould material characteristics, will be studied to have a better insight of the phenomena.

3.5.2 Description of the test devices

3.5.2.1 Air Jet Erosion tester

Air Jet Erosion Tester TR-471 of Ducom Instruments shown in figure 113, is designed to characterize properties against erosion of different materials or coatings. The testing procedure is based on ASTM G76-95.

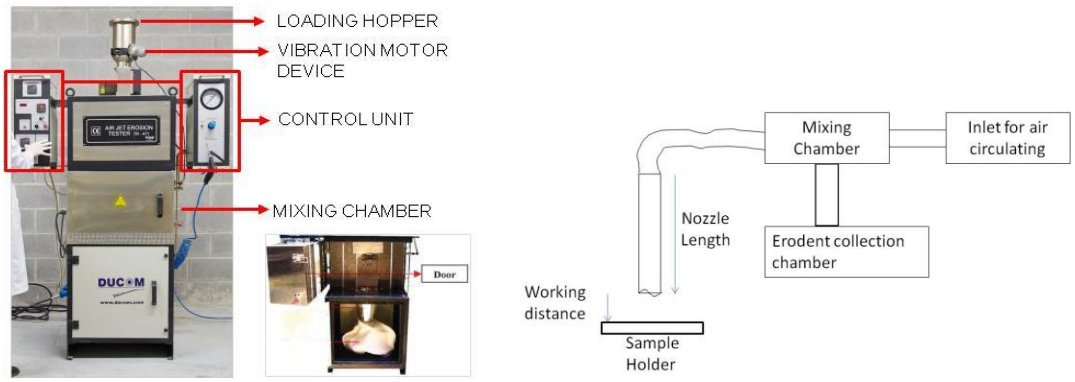

Figure 113. Air Jet Erosion Tester TR-471 machine and working scheme

In this tests a sample of 25x25x5 mm^3 receives the impact of an Alumina erodent (standard is 50 µm diameter alumina, that can be seen in the figure 114) on compressed air flow at specific testing conditions. Parameters like particle speed(m/s), discharge rate of erodent(mg/min), sample temperature and sample exposition time to the erodent can be varied.

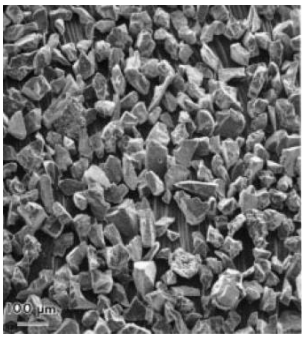

Figure 114. Micrograph of abrasive alumina 50 µm particles

The studied parameters have been particle speed (32, 64 m/s), sample temperature (25, 100ºC), impact angle (15, 45, 90º), and mould material (2738BM and 2738HH), keeping the rest of parameters fixed. The surface of the samples is grinded to have better analysis of the wear scar in the microscope.

The wear is measured by a Confocal Microscope, measuring the maximum wear depth at the three axis of the wear scar and making the equivalence of the wear scar to a semi-ellipsoid as shown in figure 115.

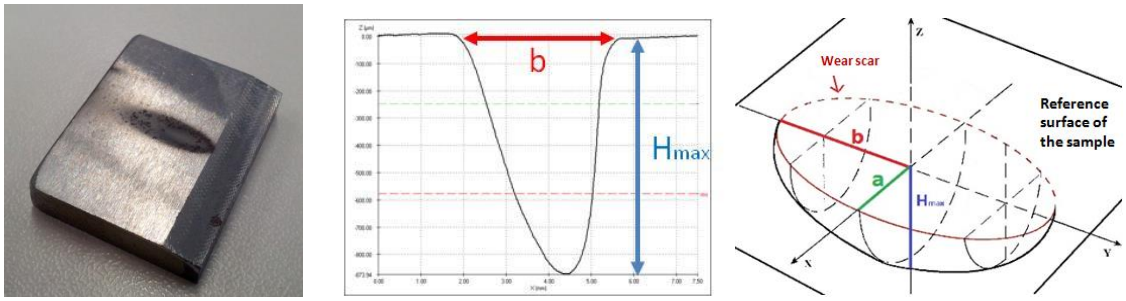

(a) ***(b)*** ***(c)***

Figure 115. Tested sample (a), confocal measurement (b), equivalent ellipsoid (c)

3.5.2.2 **Gravel-o-meter**

The gravelometer has been designed and constructed by IK4-TEKNIKER to evaluate the resistance of the mould material and coatings to chipping caused by the impact of gravel or other flying objects. Air pressure is used to project the gravel. The test sample is weighted before and after the test in order to compare the amount of material loss. This test has been designed according to the standard ASTM D3170, and pellets (PIM raw material) is used as the gravel.

The plastic gravel is charged in a tank and from there it is discharged in the supply hopper thanks to a vibratory feeder. The pipe of the gun has a hole with diameter of 5 mm. And the target is positioned at 350 mm (See figure 116). The gravel is recollected after each series of test to be re-used. The metal samples have square geometry of 50 mm x 50 mm. 5 discharges of 6 kg of raw material each time are performed.

The wear is quantified by mass loss measurement in a high precision balance (accuracy 0.00001g).

Figure 116. Gravelometer test layout

The materials used for the testing have been:

- *Plastic material:* PA+25%GF, ABS, PMMA, PC

- *Tool Steels:* 2738BM, 2738HH

- *Surface treatments:* Salt Nitriding, Ionic Nitriding, TiN, Ni-PTFE

3.5.3 Results and discussion

3.5.3.1 Effect of mould material and surface treatment and plastic type on erosive wear for PIM

Four different plastic materials were tested in against 2738BM to check their erosive power in the Gravel-o-meter test. It is clearly shown in figure 117 that the tests all over the 5 discharges that the fibre reinforced plastic is much more erosive than the rest of plastic materials. All the other 3 plastics have a combination of mild erosion and adhesion.

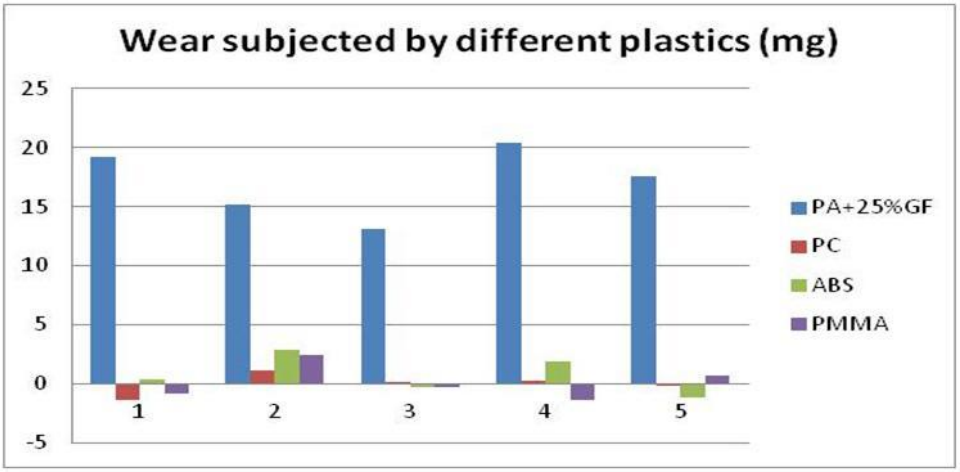

Figure 117. Wear subjected on 2738BM samples by different plastics

The different surface solutions were tested against PA+25%GF. They performed similarly to the abrasive tests, being the ranking from best to worse exactly the same. TiN and Ionic Nitriding are the most adequate surface treatments. It is interesting to remark that the Salt Nitriding underwent most of the wear in the first discharge, and progressively less in the rest of the discharges, as shown in figure 118. This is probably because the nitriding treatment is not homogeneous in the surface being two different layers (white layer and diffusion layer) of different properties. The white layer is brittle and it disappears in the first discharge batch.

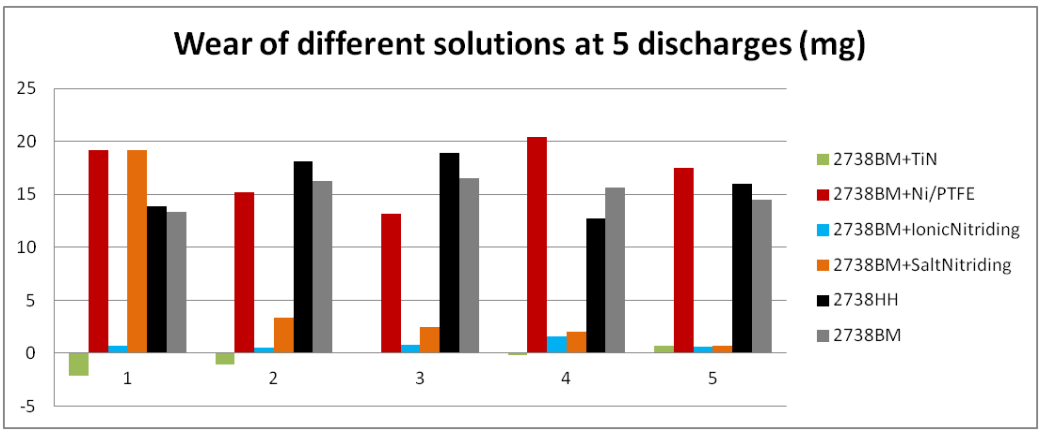

Figure 118. Wear subjected on 2738BM samples by different plastics

The correlation between mould material hardness's and resulting wear has been similar to the abrasive wear results as shown in the figure 119a. The correlation was better when applied for the surfaces not including TiN, figure 119b, since looks like above a hardness of 800HV1 it is hardly possible to erode the mould surface.

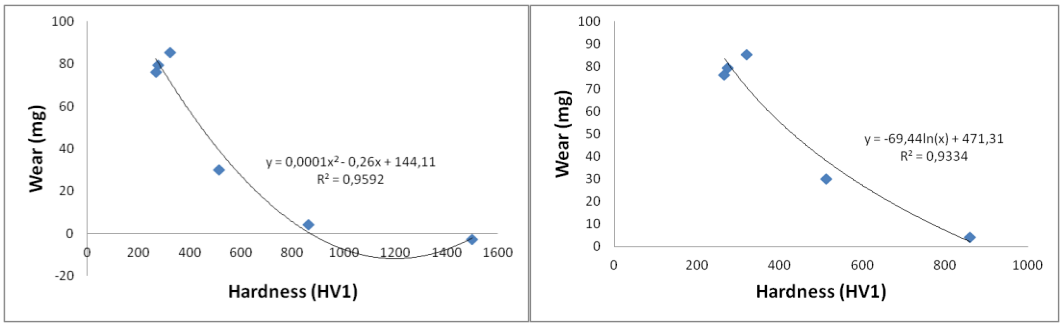

(a) ***(b)***

Figure 119. Correlation between Hardness and wear during the tests for all the surfaces (a) and without TiN (b)

3.5.3.2 Influence of different injection parameters on erosive wear for PIM and HPDC

The conclusions regarding the dependence of injection parameters as injection speed, impact angle and mould temperature have been considered valid for both High Pressure Die Casting solid particle erosion and Plastic Injection Moulding erosion, due that the H13 and H11 steels used in HPDC, have similar properties than 2738 HH and 2738BM steels. In this case 50µm alumina powder has been considered as erodent.

The DOE for this test have been the one of table 17, which has been fully repeated for both 2738 HH and 2738BM steels.

Temperature (ºC)	Angle (º)	Speed (m/s)
25	15	32
100	15	32
25	45	32
100	45	32
25	90	32
100	90	32
25	15	64
100	15	64
25	45	64
100	45	64
25	90	64
100	90	64

Table 17. DOE table for erosive tests

The erosion test results in the Air Jet erosion tester showed that the different microstructure and grain size of steels and mould temperature were negligible compared to the impact angle and impact speed.

The figure 120 shows the influence of the angle (coded as X2) and speed (coded as X3) on wear. Speed shows a more important influence on wear than impact angle when regarding the maximum wear depth.

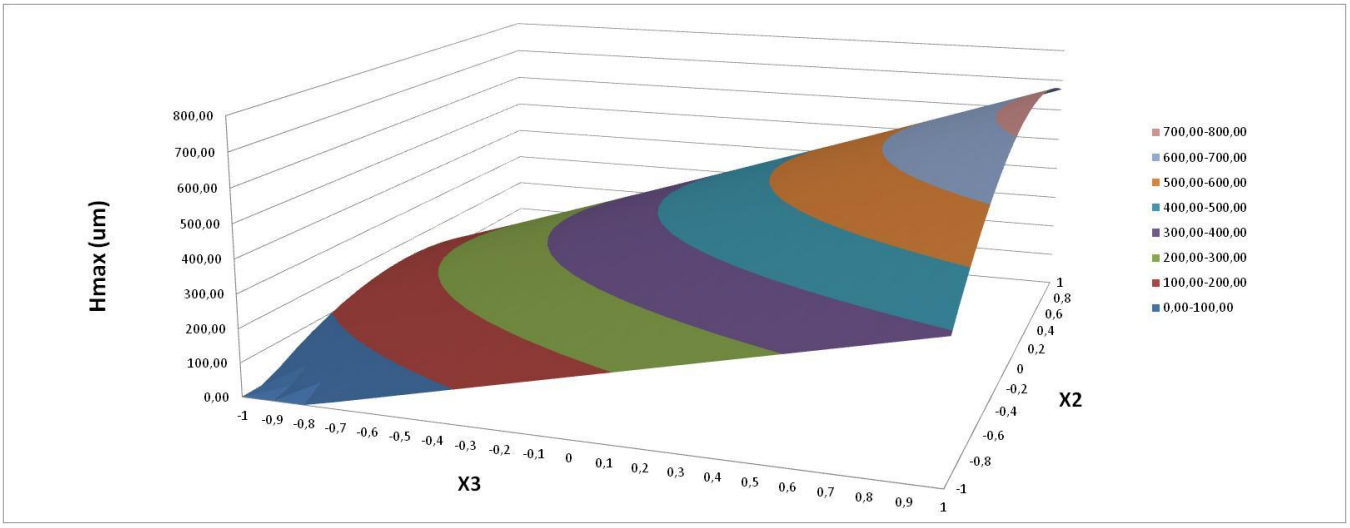

Figure 120. Surface response of wear depending on impact angle (X2) and impact speed (X3)

The influence of impact angle was different regarding maximum wear depth and mass lost (or volume lost), as shown in figure 121. The mass loss is almost linear decreasing with impact angle increase, while wear depth has a parabolic shape where maximum is at around 45º.

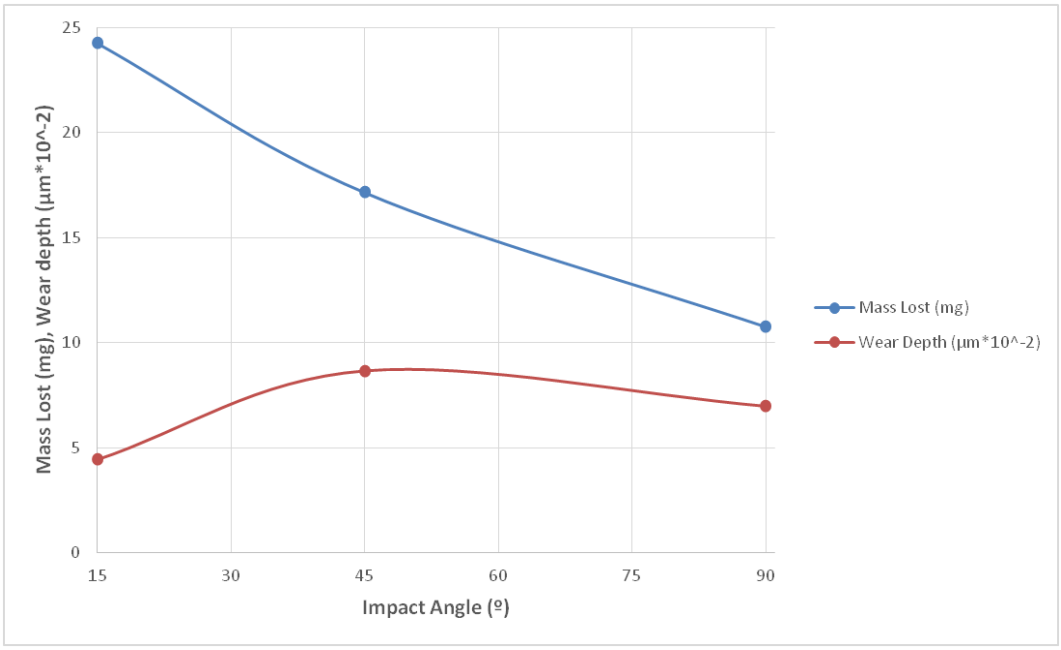

Figure 121. Influence of impact angle on wear depth and wear mass (or volume)

The explanation of this behaviour, it is easy to visualize since the wear shape generated when test is performed in each of the impact angles is very different as shown in figure 122. The wear shape at 15º is

wide and not very deep while at 90º is short and much deeper. The deepest one is achieved at 45ºC with an average scar diameter.

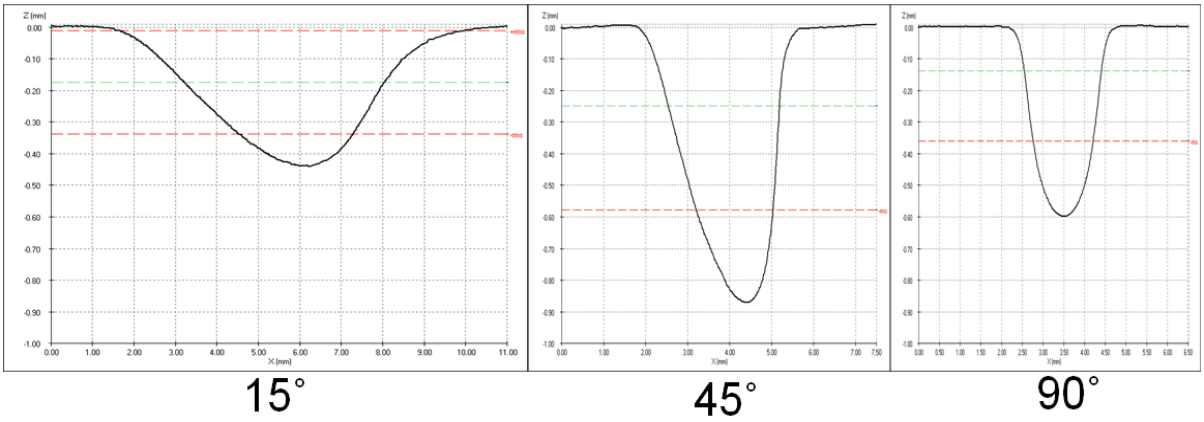

Figure 122. Wear shape of three tests in similar conditions and different contact angles

For the application of mould, the wear depth is probably the critical value since it is what will be copied in the injected/casted part. This dependence on speed and impact angle shown in figure 120 can be written in an equation as follows:

$W_{Hmax}(\mu m)=-607.68+10.27ANG+12.09VEL+0.1ANGVEL-0.13ANG^2$

Where:

VEL: flux speed in m/s (tested from 32 to 64m/s)

ANG: impact angle in º (tested from 15 to 90º)

3.5.4 Model assessment

Similarly to the abrasive wear case, the final erosion wear model will include three parameters, in this case also speed and hardness, but impact angle instead of pressure. The following equation results after the combination of the different parameters:

$W_{Hmax}(\mu m/h)=(-607.68+10.27ANG+12.09VEL+0.1ANGVEL-0.13ANG^2)*(33.24-4.92\ln(H))$

Where:

VEL: flux speed in m/s (valid from 32 to 64m/s)

ANG: impact angle in º (valid from 15 to 90º)

H: Hardness in HV (valid from 200 to 900HV, above wear is 0)

Analysis of variance of the model: $R^2=0.8053$

As an application example for HPDC mould of 43 HRC, in an area where the impact angle is 30º and the flux speed is 50m/s, and supposing that the direct erosion is performed until the first solidification skin is

formed (0.3s), would result in a wear rate of 0.0375μm/cycle, and at 26674 cycles would have already around 1mm wear depth. For this case, a reduction of flux speed or increase of hardness would be needed.

For the case of PIM even if these tendencies are expected to be the same, as the flux speed values are far from the actual PIM speeds. Speed values are necessary to calibrate to convert from PIM range, to the ones measured on the tests.

3.6 Corrosion in PIM and HPDC moulds

3.6.1 Objective

The objective of this test is to simulate the corrosion wear mechanism that occur in moulds of Plastic Injection Moulding and High Pressure Die Casting at laboratory scale, to be able to evaluate the behaviour of the mould materials, and have a better insight of the phenomena.

3.6.2 Materials and methods

Accelerated corrosion tests have been performed in different materials immersed in NH_4Cl 0.5%. The electrolyte has been selected to simulate the effect of the possible NH_3 gases that could release the Polyamide when overheated, and the Cl to simulate the possible halogens that have the plastics as fire resistance additives or for example the PVC that contains Cl-R in its chain. The same electrolyte has been selected for HPDC mould materials. The exposed surface was of 625 mm^2 for all the test samples.

The test materials were the following:

- 1.2343 steel (H11)
- 1.2344 steel (H13)
- 1.2738 BM steel
- 1.2738 HH steel
- Ni-PTFE applied on 2738 BM
- Ni-PTFE applied on 2738 HH
- Salt Nitriding applied on 2738 BM
- Salt Nitriding applied on 2738 HH
- Ionic Nitriding applied on 2738 BM
- Ionic Nitriding applied on 2738 HH
- TiN applied on 2738 BM
- TiN applied on 2738 HH

For this aim, Electrochemical Impedance Spectroscopy (EIS) measurements have been performed at different immersion times.

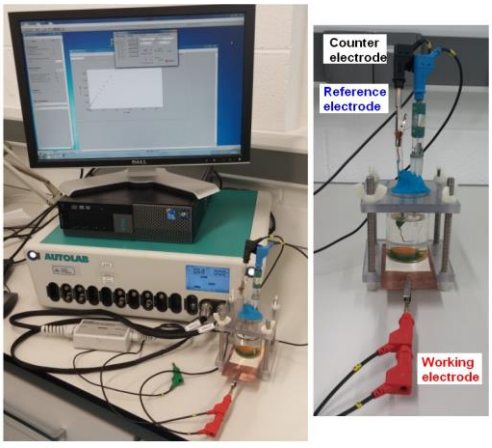

Figure 123. Experimental Setup, the three electrodes, the electrochemical cell and potentiostat

The electrochemical setup consisted of a three electrode cell, connected with an Autolab-Metrohm PGSTAT30 potentiostat shown in figure 124. A commercial Ag/AgCl (KCl 3M) electrode and a platinum wire were used as the reference and the counter electrodes, respectively. The test sample corresponding to each material was connected as the working electrode. The potential of the reference electrode is of 0.207 V vs Standard Hydrogen Electrode (SHE), and all the potentials registered in this document are referred to this electrode. The EIS measurements were performed under a sinusoidal perturbation of ±10 mV amplitude and at a frequency range from 100 kHz to 1 mHz. Four EIS measurements were carried out at different immersion times: 24 h, 72 h, 168 h and 336 h. After, the last data was obtained at 336 h, the samples were removed from the electrochemical cell.

The electrochemical behaviour of the studied surface can be described by means of electrical equivalent circuits. For this aim, the experimental data was fitted by using the Randles equivalent circuit in figure 125, where Rs represents the electrolyte resistance between the reference electrode and the working electrode and Rp correspond to the polarization resistance. The Constant Phase Element (CPE) represents the double layer capacitance at the electrolyte/steel interface. This element is used for replacing the simple capacitances for a better fit quality of the experimental data. The impedance of a CPE element can be represented by the following expression:

$$Z_{CPE} = 1/Y_0 (i\omega)^n$$

where ω is the angular frequency, and i the imaginary number. Y0 and n (n≤1) are the admittance and the empirical exponent of the CPE, respectively. When the surface acts as an ideal capacitor n is equal to unity and Y0 is identical to the double layer capacitance. The Rp values of the ten materials at the different immersion times are also calculated.

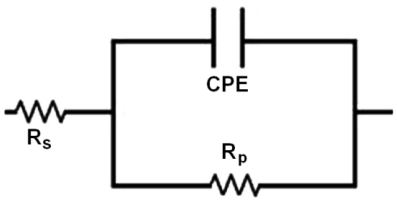

Figure 125. Randles equivalent circuit used for the impedance data fitting

For the comparison of the corrosion resistance this circuit is represented as a Nyquist diagram, where the imaginary impedance and the real impedance are plotted.

An example of the behaviour of two different materials cast iron and aluminium is shown in figure 125 to facilitate the interpretation of these graphics. If the graphic has only one semicircle, it can be modelled as a circuit with only a unique time constant. This is the case of cast Iron material in figure 125a. In this case there is not any protection layer. If the Niquist plot, can be identified 2 semicircles, it can be defined 2 time constants in the equivalent circuit. This is the case of aluminium represented in figure 125b, we can find that it is formed a passivation layer. The intersection of the curve with x axis, gives information about the corrosion resistance, that in the case of cast iron, it decreases when increasing the exposition time to the medium. As it can be seen, from 108 hours to 252 hours, its resistance was reduced about 30%. In the case of aluminium due to the surface passivation, the resistance to corrosion increases with time [72].

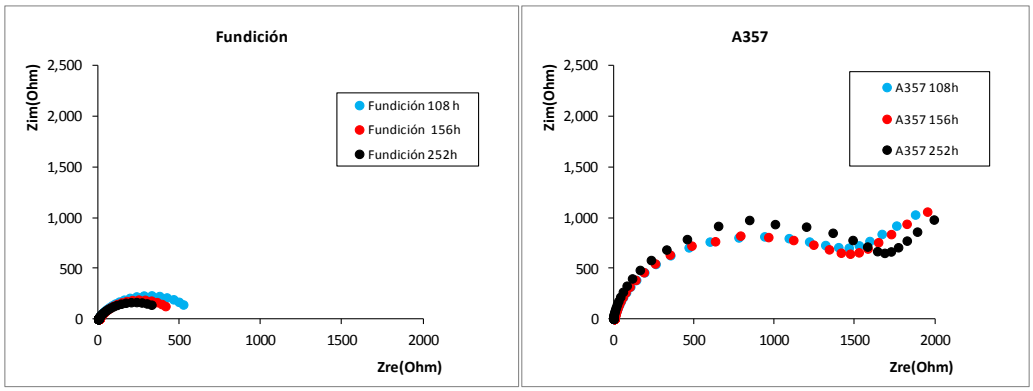

Figure 125. Nyquist of cast iron (without protective layer) and aluminium (with protection layer)

3.6.3 Results and discussion

In the following points, firstly the evolution of the corrosion resistance with immersion time is presented for each test material, and then the results of all the materials are compared for each immersion time.

3.6.3.1 Effect of material and surface treatment on corrosion wear in PIM moulds

Results obtained for 2738 BM and HH samples

Figure 126 show the results of the two typical PIM mould steels 2738BM and 2738HH samples. Both materials exhibited a very low corrosion resistance in the simulated aggressive media composed by NH_4Cl 0.5%.

Maximum corrosion resistance registered in case of 2738 BM after 336 h of immersion is around 326Ω, which indicates an active behaviour and samples dissolution in the aggressive media.

The increase of corrosion resistance with immersion time in case of 2738 BM is associated to the formation of a film of corrosion products on the steel surface that act as a barrier preventing its surface from further dissolution. In the 2738 HH material, the corrosion resistance is increasing at the beginning of the test due to protection by surface oxidation but after 168 hours the corrosion resistance decrease showing still more active behaviour than the BM steel.

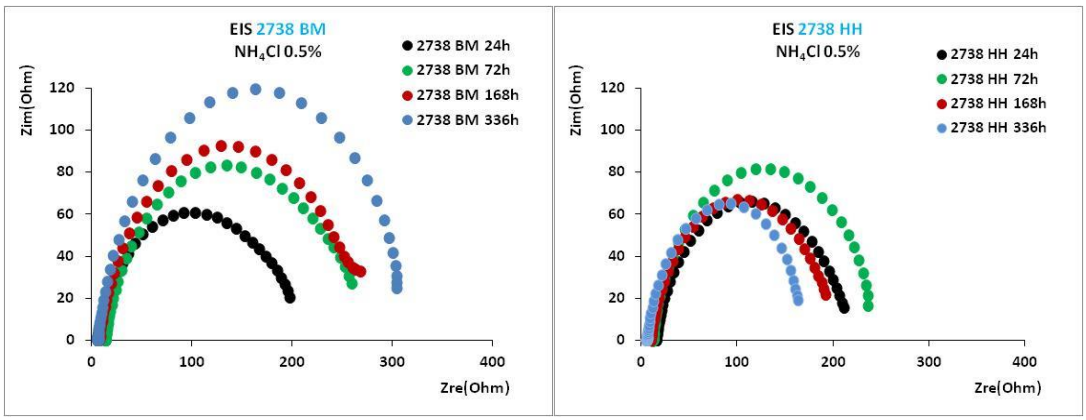

Figure 126. Evolution of the corrosion resistance of 2738BM (left) and 2738HH (right) samples with immersion time

Results obtained for the Ni-PTFE 2738 BM and HH samples

Figure 127 depicts the results of the Ni Teflon 2738 BM and HH samples. In both cases, the highest corrosion resistance value corresponded to that obtained after 24 h of immersion, and the lowest value was registered after 72 h. The resistance of the samples increased again after 168 h, and the values obtained after 336 h were between those at 72 h and 168 h for both samples. The corrosion resistance of 2738 HH+Ni-PTFE was higher than 2738 BM+ HH+Ni-PTFE.

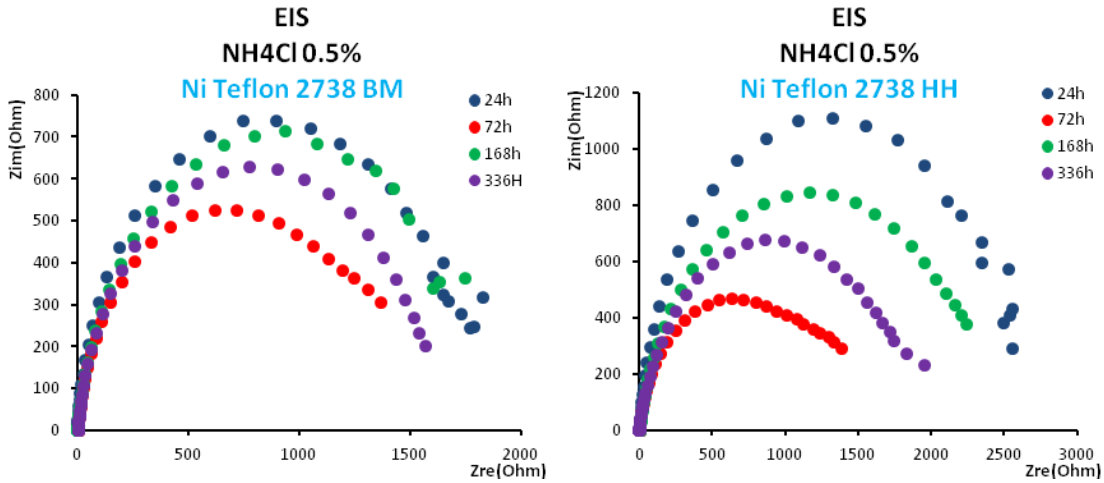

Figure 127. Evolution of the corrosion resistance of Ni-PTFE 2738 BM (left) and HH (right) samples with immersion time

Results obtained for the salt nitriding 2738 BM and HH samples

The results obtained for the salt nitriding 2738 BM and HH samples are shown in the following figure 128. In the case of the BM, the corrosion resistance increased with increasing time until 168 h of immersion and then decreased. With respect to the HH, the resistance values are considerably higher in all the immersion times.

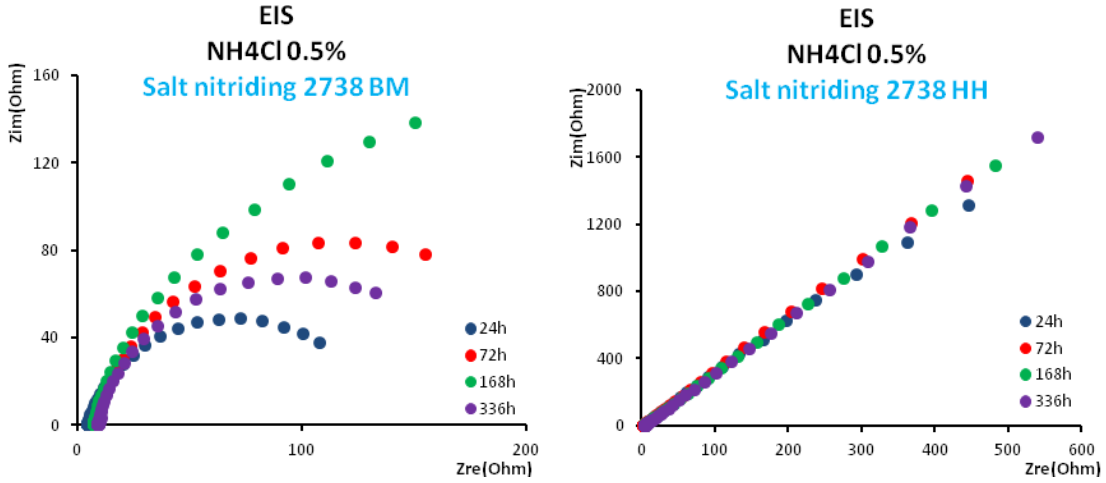

Figure 128. Evolution of the corrosion resistance of salt nitriding 2738 BM (left) and HH (right) samples with immersion time

Results obtained for vacuum nitriding 2738 BM and HH samples

Figure 129 plots the results of the tests performed for the vacuum nitriding 2738 BM and HH samples. The resistance of the BM increased until the 72 h of immersion, and then decreased to reach the lowest values registered. In the case of the HH, the resistance remained more constant during the whole immersion time.

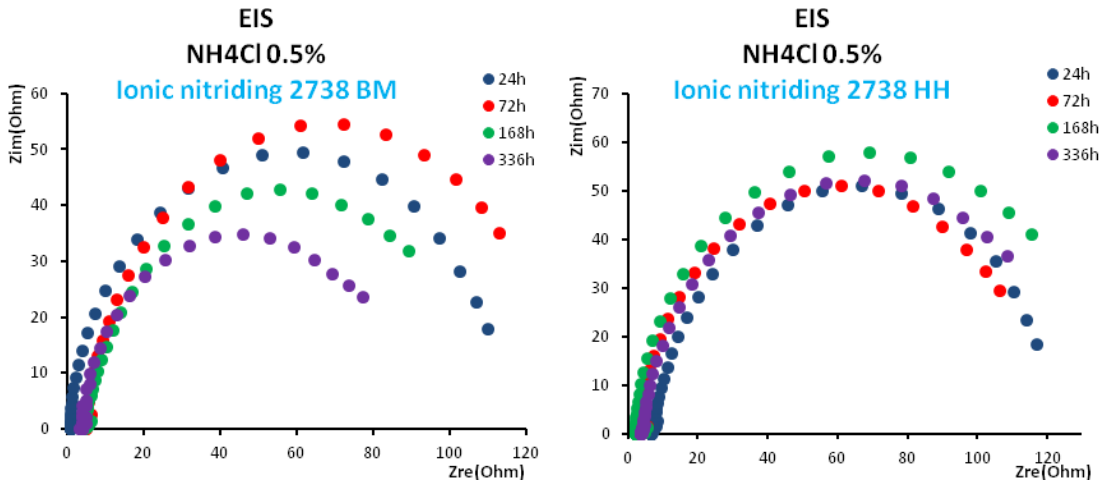

Figure 129. Evolution of the corrosion resistance of vacuum nitriding 2738 BM (left) and HH (right) samples with immersion time

Results obtained for TiN 2738 BM and HH samples

The following figure 130 shows the resistance of the TiN BM and HH samples for the different immersion times. The corrosion resistance of the TiN BM decreased after 72 h of immersion and then increased again. The corrosion resistant is high in comparison with other surface treatments. In the case of the HH, the corrosion resistances registered at 24, 72 and 336 h were very similar, and the higher resistance was registered at 72 h. The corrosion resistance is higher with HH substrate.

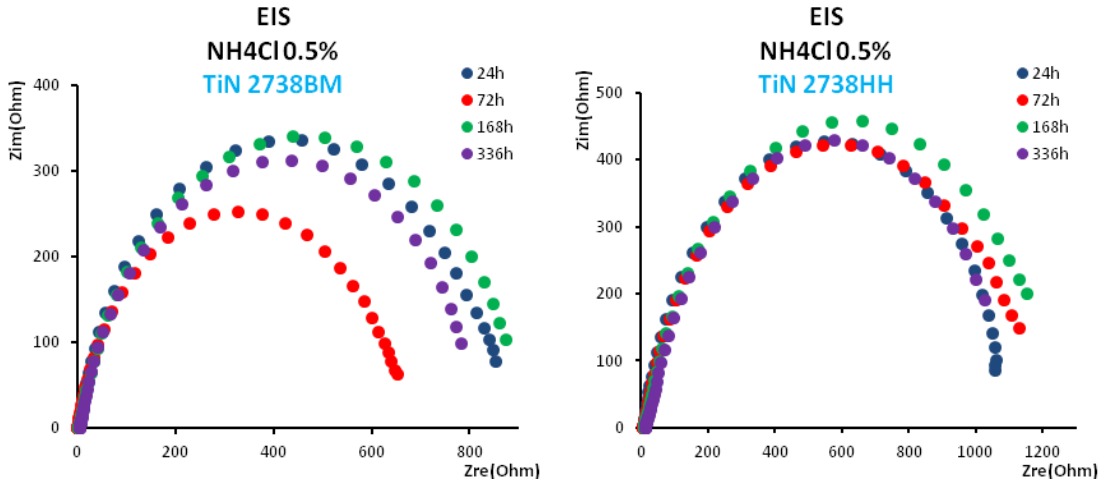

Figure 130. Evolution of the corrosion resistance of TiN Steel no. 1 (left) and no. 2 (right) samples with immersion time

Comparison of all the materials for each immersion time

In the following figure, it has been represented the comparison of the corrosion resistance for the different material solutions in NH_4CL, in function of the immersed time.

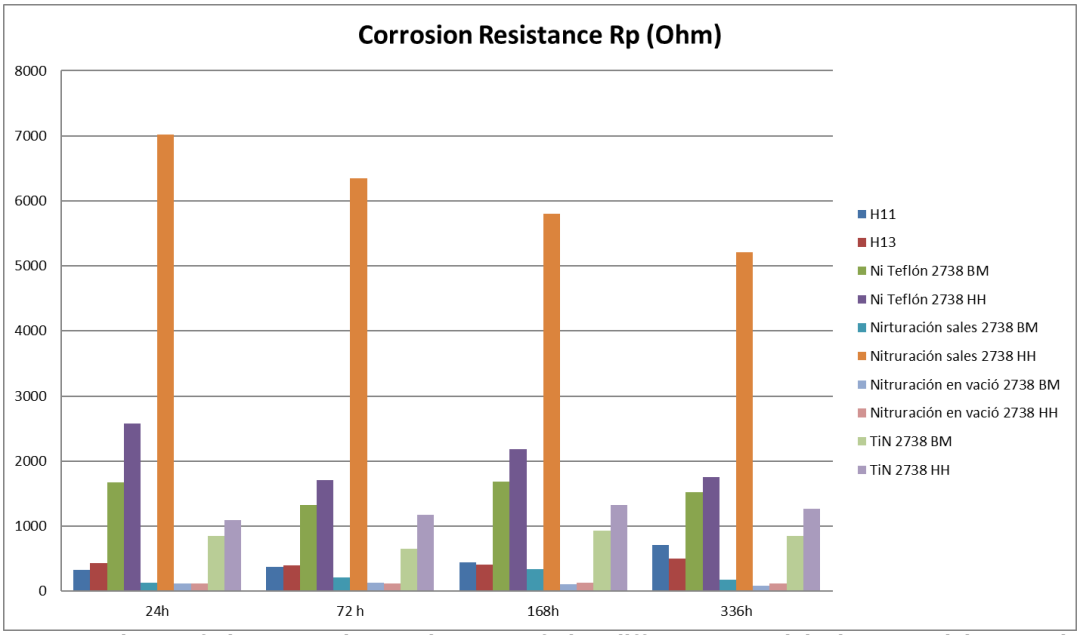

Figure 131. Comparison of the corrosion resistance of the different materials immersed in NH_4Cl at each immersion

After 24 h of immersion in the NH_4Cl solution, the highest resistance was that of the salt nitriding HH, followed by the Ni-PTFE HH and BM, following by TiN HH and BM respectively. In general corrosion resistance of the HH substrate is higher than BM.

The resistance of the salt nitriding HH remained similar after at 72 h of immersion, and the values registered for the Ni-PTFE samples decreased, reaching very close values between HH and BM substrates. The resistance of the TiN 2738 HH sample was closer to those of the Ni-PTFE samples after the 336h of immersion time, since TiN did not changed much the corrosion resistance with the exposition time. The values registered for the rest of the materials were considerably smaller, especially those of the salt nitriding BM and the two ionic nitriding samples. The great difference between the salt nitriding applied to BM and HH is not considered to be related to the nitriding process, that has not very homogeneous appearance, resulting in a very good corrosion inhibitor of the white layer when is properly applied, but when have some small areas worse applied and the diffusion region is exposed, it has very similar corrosion resistance as the substrate. The second highest resistance was for all the exposure times the Ni-PTFE HH followed by BM and the third TiN HH followed BM, but their values registered at high immersion times were unless 3 times smaller in comparison with the salt nitriding HH sample.

On the other hand, the smaller corrosion resistances corresponded to the ionic nitriding BM and HH samples, with values below 130 Ohm after 336 h of immersion.

The high resistance of the HH sample is probably associated with the formation of oxidation films in the surface of the material, which inhibits the corrosion of the bare material by acting as a barrier to the electrolyte; whereas the small resistance of the BM indicates an active behaviour of the material that

undergoes corrosion processes since no oxide protective layer is formed in the surface. The differences in microstructure from both steels could also be influencing their corrosion behaviour. 2738BM showed a sorbobainitic aspect while 2738HH present a sorbitic aspect. 2738BM showed grain size number of 4-5 while 2738 HH of 9-10 (see section 4.4.2), thus 2738HH had smaller grain size. The smaller the grain size the higher the corrosion resistance was obtained. From literature, it is know that the microstructure was expected to have influence on the corrosion resistance of steels [73, 74].

3.6.3.2 Effect of material and surface treatment on corrosion wear in HPDC moulds

The evolution of the corrosion resistances of the H11 and H13 samples with immersion time are presented in figure 132. The corrosion resistance of the H11 was found to increase with immersion time, whereas in the case of the H13, the corrosion resistance seemed to slightly decrease after 72 h, but then increased again to reach the higher value registered at the end of the test. In this case also the grain size of the H13 is smaller than the H11 as shown in the chapter 3.2.2.3.

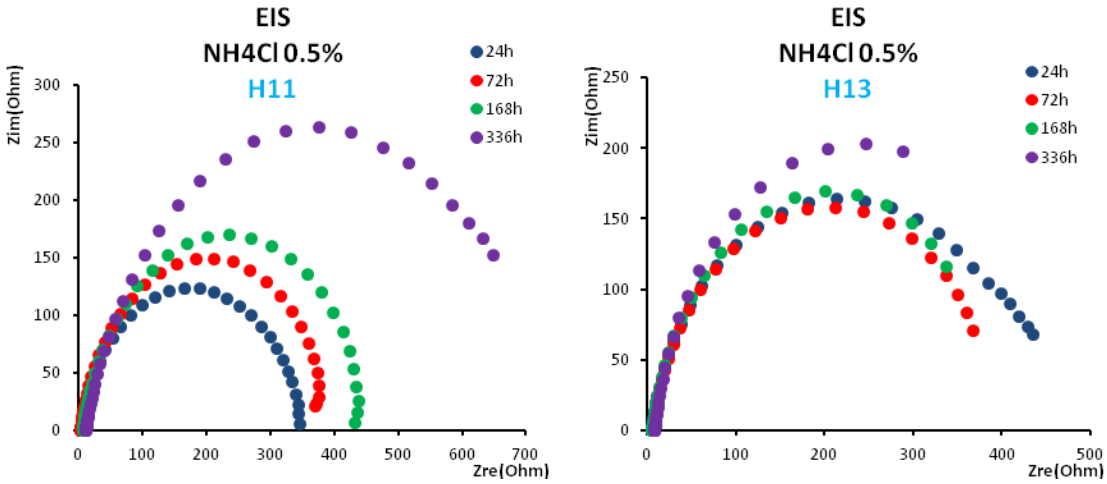

Figure 132. Evolution of the corrosion resistance of H11 (left) and H13 (right) samples with immersion time

3.6.4 Model assessment

In this case, instead of an equation, the model is a table of the risk of corrosion appearance on mould surfaces, presented in table 18. Typically 10,000 Ω is the limit above which a surface is considered non corrosive for NaCl solution. From measured resistance of the surfaces, it is calculated a percentage of risk of corrosion appearance, as a ratio from this limit value. Depending on this value the software user must decide on the appropriate counter measures on material selection or maintenance scheduling.

Corrosion risk (%) = measured Rp (Ω)*100 / limit value (Ω)

H11	95.36%
H13	95.65%
2738BM	97.17%
2738HH	98.04%
Ni-PTFE 2738 BM	84.47%
Ni-PTFE 2738 HH	79.44%

Salt Nitriding 2738 BM	97.87%
Salt Nitriding 2738 HH	39.04%
Vacuum Nitriding 2738 BM	98.93%
Vacuum Nitriding 2738 HH	98.79%
TiN 2738 BM	91.80%
TiN 2738 HH	87.83%

Table 18. Final table of corrosion appearance risk

An alternative model proposal would be possible when the model user has the knowledge of the basic steel corrosion resistance in cycles to corrosion appearance, the safety factor from this data can be calculated as in tables for PIM solutions and HPDC solutions.

Safety factor = measured Rp of the surface (Ω) / measured Rp of the reference material (Ω)

2738BM	1.00
2738HH	0.69
Ni-PTFE 2738 BM	5.48
Ni-PTFE 2738 HH	10.47
Salt Nitriding 2738 BM	0.75
Salt Nitriding 2738 HH	31.05
Vacuum Nitriding 2738 BM	0.38
Vacuum Nitriding 2738 HH	0.62
TiN 2738 BM	2.89
TiN 2738 HH	6.20

Table 19. Safety factors referred to the basic 2738 for PIM solutions

H11	1.06
H13	1.00

Table 20, Safety factors referred to the basic H13 for HPDC solutions

For example, once the PIM mould surface for the process have to be selected, and it is known that with 2738BM is possible to make 400 cycles without surface cleaning and anti-oxidant application, these safety factors can help to select an appropriate maintenance scheduling, according to the corrosion resistance and production needs. For example if production stop for maintenance would be acceptable each 1,000 cycles, TiN application on 2738 BM would be a nice solution, since it would last for 2.89*400=1,156 cycles. Instead, if 2,000 cycles would be needed, Ni-PTFE on 2738 BM or TiN on 2738HH would work. Ni-PTFE 2738 HH would allow to achieve around 4,000 cycles, and Salt Nitriding 2738HH up to 12,000 cycles.

4 Wear modelling implementation

The global picture of the studied wear mechanisms and their model implementation with related inputs and outputs is shown in the table 21. In this chapter, the equations presented through the previous chapters will be recalled and an example from the point of view of final user will be presented.

Process	Wear Mechanism	Input	Output
HPDC	THERMAL FATIGUE	Thermal stress, die material	Cycles to Failure
HPDC	DIE SOLDERING-LUBRICANTS	Lubricant, temperature, pressure	LFP, CA, lub thickness, cycles to failute
HPDC+PIM	EROSION	Impact angle, impact speed, die material, mould temperature	wear
HPDC+PIM	CORROSION	Mould material	corrosion resistance
PIM	ABRASION	Mould material, speed, pressure	wear, friction

Table 21. Overview of generated models with inputs and outputs

HPDC - Thermal Fatigue

For the thermal fatigue prediction in the mould surface, the thermal stress in each location have to be calculated in a software (for example Magmasoft), as an input for the S-N cuve, in order to identify the risk of failure for the different areas of the mould. The equation created in this study has been carried out for H11 and H13 at 43 HRC, in the range of temperatures between 300 and 500ºC and stress range between 820 and 900 MPa. For other materials or other working conditions, it would be needed to measure experimentally their specific fatigue lifetime equation.

$$N\ (cycles) = -200.66*S + 180861$$

Where

S (MPa): thermal stress calculated from simulation in MagmaSoft (tested from 820 to 900 MPa, and valid for die temperatures between 300 and 500 ºC)

Analysis of variance of the model: $R^2=0.8267$

If the approach to be used is to connect directly the thermal fields and cycles to failure, the following equations have been created from the unique two experimental values available. One is related to the thermal gradient into the surface (TG) and the other to the temperature differences during the cycle (ΔT). They should be further improved with more experimental data from the newly developed thermal fatigue machine:

$$N\ (cycles) = -338.24*TG + 55441$$

Where

TG: thermal gradient (in ºC per mm of depth into the surface during spray cooling) measured in the mould or calculated from simulation in MagmaSoft or other software's (valid for thermal gradients between 90 and 160 ºC per mm of depth).

$$N\ (cycles) = -377.05*\Delta T + 192787$$

Where

ΔT: accumulated temperature difference during the cycle, as the sum of the temperature difference while heating and temperature difference while fast spray cooling, measured in the mould or calculated from simulation in MagmaSoft or other software's (valid for temperature differences between 445 and 505 ºC).

Analysis of variance of the model: it has not sense evaluate the R^2 coefficient of the equation created from 2 experimental values which would result in $R^2=1$.

HPDC- Die Soldering

For the die soldering wear mechanism, the equation that gives the number of HPDC cycles before part sticking, preventing mould damage has been defined as the following equation. This forecast would need as inputs the type of used lubricant, the mould surface temperature and pressure from performed simulation on experimental measurements in the mould.

$$N(cycles)= 27.1*10^6*exp(-0.0198*T)-5432.5*Ln(P)+ 7587-6149*K$$

Where:

T: Mould surface temperature in ºC (measured between 350 and 450ºC)

P: Pressure in the mould surface in MPa (measured between 0 and 7 MPa)

K: depending on lubricant (see next table 22). It can be measured at the laboratory by means of Pin on disc test, as defined in Section 4.3.2.

Lubricant type	K
A	1
B	4.49
C	1.96
D	2.68
E	4.48

Table 22. Coefficients for die soldering equation

Analysis of variance of the model: $R^2=0.6148$

PIM - Abrasion

For PIM mould abrasion, the equation for wear generation is shown below. This forecast would need as inputs the mould material surface hardness, and flow speed and pressure. In order to get the cycles to failure, an assumption of how many seconds is sliding the polymer in each cycle has to be revised in each case (or

take the filling time of 5 seconds as reference value) and the unaccepted wear depth on the mould have to be also defined by the user.

*Wear (µm/h)= 5.0918-0.0597*P-0.0262*v+0.0031*P*v-0.8128*ln(H)*

Where:

P: Pressure in MPa (applicable from 8 to 18MPa, below not expected any wear)

v: Speed in mm/s (applicable from 20 to 50 mm/s, below not expected any wear)

H: Hardness in Vickers, HV (applicable up to 900HV, above not expected any wear)

Analysis of variance of the model: $R^2=0.9811$

PIM&HPDC - Erosion

The prediction of the PIM and HPDC mould erosion wear, can be described by the equation below. This forecast would need as inputs the mould material surface hardness, and flow speed and pressure. In order to get the cycles to failure an assumption of how many seconds is impacting the flux against the mould surface (for HPDC for example until the first solidification skin is formed -0.3s-), and the unaccepted wear depth on the mould have to be also defined by the user.

*Wear(µm/h)=(-607.68+10.27*ANG+12.09*VEL+0.1ANG*VEL-0.13*ANG^2)* (33.24-4.92*ln(H))*

Where:

VEL: flux speed in m/s (valid from 32 to 64m/s)

ANG: impact angle in º (valid from 15 to 90º)

H: Hardness in HV (valid from 200 to 900HV, above wear is 0)

Analysis of variance of the model: $R^2=0.8053$

PIM&HPDC - Corrosion

Corrosion has been found dependent mainly on the surface characteristics, and also would be necessary to calibrate a base material first (i.e. 2738 BM for PIM and H13 for HPDC), to have a base value from which the need of cleaning/maintenance will be needed.

2738BM	1.00
2738HH	0.69
Ni-PTFE 2738 BM	5.48
Ni-PTFE 2738 HH	10.47
Salt Nitriding 2738 BM	0.75

Salt Nitriding 2738 HH	31.05
Vacuum Nitriding 2738 BM	0.38
Vacuum Nitriding 2738 HH	0.62
TiN 2738 BM	2.89
TiN 2738 HH	6.20

Table 23. Safety factors referred to the basic 2738 for PIM solutions

H11	1.06
H13	1.00

Table 24. Safety factors referred to the basic H13 for HPDC solutions

4.1 Example of use in HPDC

Taking account the input needs of each wear mechanisms, a HPDC software user could fill the following input table 24. To get some of them (e.g. Thermal stress level) a simulation tool would be needed or perhaps experience based decision can be also made.

INPUT		
MaxT	450	ºC
Thermal stress level	840	Mpa
Pressure	1	Mpa
Impact speed	50	m/s
Impact angle	30	º
Lubricant	1	A
Die material	1	H13

Table 25. Inputs necessary for the HPDC wear prediction

For the defined cycle the user would receive the forecast of the wear in order to schedule the maintenance work, or take counter measures if the wear is unacceptable. In the tool, process parameters or surface material characteristics can be changed.

OUTPUT		
Thermal Fatigue	13763	Cycles
Die Soldering	5097	Cycles
Erosion	17269	Cycles

Table 26. Outputs of the model of HPDC moulds wear prediction

4.2 Example of use in PIM

The user of the mould lifetime model would need to introduce in the software the next input data of table 26. To get for example the impact angle, velocity and applied pressures simulation tools would be needed.

INPUT		
Pressure	18	Mpa
Impact speed	50	mm/s
Impact angle	30	º
Die material	2738BM	Ni-PTFE
Surface Hardness	321	HV
Basic maitenance	600	cycles
Unaccepted wear	100	µm

Table 27. Inputs necessary for the PIM wear prediction

For the defined cycle the user would receive the forecast of the wear in order to schedule the maintenance work and take counter measures if the wear is unacceptable. In the tool, process parameters or surface material characteristics can be changed.

OUTPUT		
Abrasion	89311	Cycles
Erosion	19961	Cycles
Corrosion	3288	Cycles

Table 28. Outputs of the model of PIM moulds wear prediction

Calibration of the obtained model with the general end users experience (e.g. adding a weighting factor), and when possible with experimental trials, will be needed in the future.

5 Conclusions

In this Doctoral Thesis, the wear of HPDC and PIM have been studied. As first step the different wear mechanisms have been identified based on a literature review. For HPDC, thermal fatigue, die soldering, solid particle erosion and corrosion have been selected for investigation, leaving other minor mechanisms apart from the study. For PIM, abrasion, erosion and corrosion have been studied.

A complete literature review have been performed about the nature of these wear mechanisms, the main factors affecting them, laboratory test devices that have been used in literature to simulate the wear, and the models existing in literature to predict moulds wear. The partial conclusions coming from this literature review and the innovative aspects of the Doctoral Thesis compared to the literature have been detailed in the sections 2.4 and 2.5 of this document.

For each of these wear mechanisms a strategy have been selected to simulate them at laboratory scale. The objective has been to study the influence of different casting / injection process parameters or materials to generate a model in order to predict the lifetime. With these models, a final user could predict the wear of the mould after collecting the necessary inputs for the model. With this forecast of the number of cycles before an acceptable wear amount, in the future, it might possible to schedule the maintenance work and take counter measures if the wear is unacceptable. Since the models have been built through laboratory simulated tests, a calibration might be necessary when monitoring the real mould. In the model itself, process parameters or surface material characteristics can be changed.

The activity about **Thermal Fatigue** lead to the following main **conclusions:**

- A new original and fully automated testing machine to reproduce the thermal fatigue failure mechanism has been recently built in IK4-TEKNIKER with joint specifications from AUDI and IK4-TEKNIKER. The machine is able to simulate the thermal cycle of HPDC dies. The activity described in this Doctoral Thesis, represent their first setup. The machine is based in induction heating, and includes features like the internal cooling and external spraying of HPDC moulds.
- The temperature profiles created in the test plate have been validated by a multi-depth thermocouple in order to understand and control heating and cooling propagation.
- It has been considered proved that the test procedure of the thermal fatigue test is able to simulate both the cracking appearing in HPDC dies and the temperature fields in the dies. The testing conditions can be tailored to reproduce a typical durability of the mould of about 10,000 cycles before first cracking appearance. For now the number of valid tests are sparse and a reliable equation connecting the temperature differences and cycles to cracking appearance will need further testing.
- Nowadays, the state of the art of the prediction of thermal fatigue appearance is based on the casting process simulation tools. These tools are able to calculate the casting and mould temperature fields during the cycle. The evolution of temperature fields in the surface and into the surface of the mould during the cycle can be translated to stress evolution in the surface. Afterwards, S-N (Wohler) curves that connect stress and cycles to failure, can be applied to estimate the cycles to failure, but they are hardly available in open literature. In this work S-N curves have been built for the typical HPDC steels (H11 and H13 at 43HRC in the temperature range of 300-500ºC and stress range between 820 and 900 MPa).
- This approach has been used to calculate the stress level appearing in the test plate of thermal fatigue machine, replicating the base thermal cycle generated in the test. Some variants of cooling parameters have been varied, and the following conclusions can be highlighted: The range of minimum die life of this kind of test is estimated between 6,000 and 17,000 shots. The strongest effect on die life has the spray intensity, described by the used spraying. All the other considered parameters have minor effect (the position of the cooling channel below the spray spot improves die

life a little bit, a larger Cooling Channel radius improves die life, cooling channels closer to the die surface, having a positive effect on die life).

Future steps for improvement of the **Thermal Fatigue** appearance prediction:

- Up to now, few test plates have been possible to be tested in the Thermal Fatigue machine. The use of this machine in the near future is expected to lead to a much improved forecast of cycles to failure.
- These data of the Thermal Fatigue machine will be used to further validate the approach presented to model the fatigue behaviour in HPDC moulds. This can be made both, validating the calculation through previous stress calculation or directly connecting temperature field and cycles to failure.
- The S-N curve generated to connect the calculated stresses in the mould and the cycles to cracking appearance resulted in a quality of a R^2 coefficient of 0.8267. Even if this result is not bad taking into account that the scattering of the fatigue phenomena is big, this equation should be improved in the future as well to increase data reliability. It has been observed that the equation might be applied for H13 and H11 moulds of the same hardness (43HRc) but it should be studied the influence of different materials microstructures, hardness and surface treatments.
- Once a considerable experimental information has been collected and a definitive reliable model has been built, it should be validated or calibrated with real mould's wear monitoring.

The activity about **Die Soldering** lead to the following main **conclusions**:

- The die soldering has been simulated as the failure of lubricant protection, an approach never used before in literature. A reciprocating pin on disc at different temperature, pressure and speed levels has been performed, where the hardened H13 steel has been coated by different HPDC lubricants, and the pin is manufactured of an aluminium alloy. The results have been used to build a model of the lubricant failure in function of these variables.
- Depending of the conditions, the cycles to failure can range from very few cycles to several thousand of cycles. It has been shown that the temperature is very critical as it has an exponential influence and pressure plays also a role as it has logarithmic influence. It was found that an appropriate lubricant chemistry improves up to 5 times the soldering resistance, while the speed influence was found negligible.
- The coefficient of friction measured during the pin on disc, which would be related to the capacity of the lubricant to facilitate the aluminium flux into the mould and their behaviour as lubricating agent to release the part, didn't show big differences between lubricants.
- The measurement of the thickness of the lubricant and the behaviour on the differential scanning calorimeter test, showed the possibility to correlate different physical parameters with lubricant properties, chemical and mechanical die soldering appearance. In fact the lubricant that generated higher thickness and have higher temperature resistance, presented also better die soldering prevention.
- The improvement of the wettability of the lubricant in the mould surface is possible by reducing the contact angle and increasing the Leidenfrost point. Practical and useful guidelines for effective selection and optimization of die lubrication has been suggested. It consists of two steps: first, the CA is minimized by selection of the lubricant and the steel grade at given temperature, and the second, the LFP is maximized by tuning two surface-related and three lubricant-related parameters. The optimal configuration for the given ranges of the parameters is the following: aged H13 steel grade lubricated with the A lubricant diluted at 3% using hard water and pulverized by a larger nozzle. The LFP has been significantly increased (from 145 to 165ºC) in comparison with non-optimal configuration.

Future steps for improvement of the **Die Soldering** appearance prediction:

- The prediction based on the model of the lubricated pin on disc test has a lot of limitations, mainly due to the big difference of conditions between this laboratory test and real die casting conditions. In fact in this test the aluminium instead of being in melt conditions, it is at semi-solid state. It has to be remembered that the model, is modelling the die soldering behaviour of a pin on disc test. The main step that would be needed to validate this testing protocol and the related model, it would be to calibrate the connection between the test conditions (especially the pressure of pin on disc test to which pressure can be translated in die casting, and each cycle of the test how many cycles means in die casting). Even though, the prediction of the cycles to die soldering appearance is already in the range of durability of real moulds.
- Another suitable improvement of the reciprocating test protocol would be to improve the pin geometry. Due to restrictions of availability of the aluminium alloy, the pins manufactured have a surface contact with the disc. It would be better to use spherical pins in order to have a point contact and avoid the possibility of appearance of the border effect.
- It has been assumed that the pressure, the speed, the temperature and chemical composition haven't a reciprocal interaction. This assumption should be further confirmed by testing the cross relation between these parameters.
- As last future step, it would be of interest to broaden the pin on disc, TGA, wettability tests and film thickness, to different types of lubricants. In fact, there are several suppliers offering different types of lubricants (not hydrosoluble or even dry powder lubricants) and testing the influence of different aluminium alloys and engineered surfaces like nitridings or PVD coatings.

The activity about **Abrasion** lead to the following main **conclusions**:

- A reciprocating block on plate test at different pressure and speed levels has been performed, where the 1.2738 mould steel, prehardened (HH) and not prehardened (BM), has been located as plate. In some cases this material has been coated by surface treatments (TiN, Salt Nitriding, Ionic Nitriding, and electrolytic Ni-PTFE). The mould material plate has been heated to 100ºC to be near of PIM manufacturing conditions. The 4x4x4 mm^3 block was made of PA+25%GF material for most of the tests. The results have been used to build a model of the wear of mould material, in function of these variables (pressure and speed level and the type of mould material). This and other two plastic materials (PMMA and PC) results were used to evaluate the anti-adherent performance of mould surfaces through friction measurements of the block on plate test. PMMA and PC, even if they generate high friction with mould surfaces, they don't create measurable wear.
- Friction reduction of PMMA and PC has been mainly achieved by using an electrolytic Ni-PTFE coating protection, reducing significantly the friction coefficient under sliding conditions, especially at the beginning of the test, which is expected to be related to the performance as release agent. TiN was the most effective for the friction reduction in the case of PA+25%GF. These results agree with industrial observations of MAIER S. COOP.
- The abrasive wear protection is necessary when using glass fiber 25% reinforced polyamide (PA+25%GF), in this case Vacuum ionic nitriding and TiN physical vapour deposition are the most promising surface alternatives. The wear resistance of mould materials is closely related to the hardness. Ni-PTFE treatment doesn't improve the wear resistance of the substrate. The surface treatments behaved very similarly applied in both of the substrates, 2738 HH and BM.
- The application of surface treatments increase the roughness of the mould surface, which could be translated to an increase of final part roughness and influence its aspect. The Ra roughness ranking from lowest to highest is the following (1.2738 substrate 0.55 μm, Ni-PTFE 0.6 μm, TiN 0.7 μm, Ionic Nitriding 0.75 μm, Salt Nitriding 0.8 μm).
- The mould wear prediction model generated, shows the huge influence of the relative speed and pressure apart from Hardness, as mentioned before, so these manufacturing parameters have to be carefully selected as well. Regarding friction values were not very sensible to speed, while the increase of pressure reduces slightly friction values.

- The wear model created includes the influence of the referred parameters (pressure, speed and hardness) in the wear of mould. A model for friction prediction makes no sense, but a table of friction coefficient values for plastic and mould materials is available to implement in a software, in order to select suitable solutions for moulds where this feature is critical.

Future steps for improvement of the **Abrasion** appearance prediction:

- The wear model presented is suitable to be improved. In fact, testing wider range of pressures and speeds would be of interest. Other plastic materials with different fibre % composition could be also tested.
- The block on plate approach presented in this Doctoral Thesis is quite far from PIM moulds conditions. The possibility of creating a new device able to deal with plastic in melt condition should be open for the future.
- Similarly to the other wear mechanisms, the main future step will be related to the validation / calibration of the model created. A suitable procedure for this step could be to track the wear evolution of real moulds at areas where abrasion mechanisms is present, and of different pressure and speed conditions, and with inserts of different mould materials. Afterwards, the wear amount predicted by the model and the wear of the mould should be compared. The calibration would mean to check if the cycles of the tribological test is one to one compared to the injection cycles. If they are not, it should be calibrated by a coefficient. Similarly, speed and/or pressure could be calibrated. Afterwards this procedure should be iteratively repeated with mould observations.

The activity about **Erosion** lead to the following main **conclusions:**

- The combination of air jet erosion test and gravelometer test results have been used to create a model behaviour of the HPDC and PIM moulds wear. The most influencing parameters, that have been reflected in the model are the particle speed, impact angle and mould material hardness.
- Similarly to abrasion tests, it was found that plastic materials that are not reinforced didn't generate measurable wear in the mould. From the different surface solutions tested against PA+25%GF, they performed similarly to the abrasion test. TiN and Vacuum Ionic Nitriding are the most adequate surface treatments. It is interesting to remark that the Salt Nitriding underwent most of the wear in the first discharge, and progressively less in the rest of the discharges, which would be due to the inhomogeneous nature of this treatment (outer compound layer and inner diffusion layer).
- The erosion test results in the Air Jet Erosion tester showed that the different microstructure and grain size of steels and mould temperature were negligible compared to the impact angle and impact speed.

Future steps for improvement of the **Erosion** appearance prediction:

- Similarly to the abrasion wear mechanisms, the main future step will be related to the validation / calibration of the model created. The procedure would be similar, by tracking the wear of real moulds in areas where erosion mechanism exist, and checking areas with different impact angles and different speeds, and inserts with different hardness's.

The activity about **Corrosion** lead to the following main **conclusions**:

- Accelerated corrosion test have been performed on different steels and surface treatments, in a NH_4Cl electrolyte simulating the harsh conditions of PIM process. For corrosion protection, it seems that salt nitriding provides good protection on 2738HH steel, but this coating is not very homogeneous and it is not so reliable, showing a low corrosion resistance in the sample applied on 2738BM. Furthermore, its corrosion resistance was reduced when increasing time, and it is not environmentally friendly since production process generate contaminants such as cyanides. Next

options to enlarge lifetime against corrosion are the Ni-PTFE coating (2738HH and BM steel) followed by the TiN (2738HH and BM steel).

- In general, the corrosion resistance of treatments applied on 2738HH steel were found slightly higher than the ones applied on 2738BM steel. 2738BM had higher corrosion resistance than 2738HH and in case of HPDC steels, H11 present higher corrosion resistance than H13. Both H11 and 2738BM steels have lower hardness and bigger grains than H13 and 2738HH steels respectively.
- Instead of an equation, a corrosion risk or a safe factors have been proposed to model the mould behaviour, in order to be implemented in software for an appropriate selection of surfaces, in the cases that corrosion risk is high.
- TiN when applied on 2738HH steel present the most suitable surface coating solutions for PIM of glass reinforced polymers generating a minimum friction coefficient of 0.4 and a minimum wear in abrasion tests, and a relatively high corrosion protection, providing a safety factor 6 times higher than reference steel 2738BM.

Future steps for improvement of the **Corrosion** appearance prediction:

- Similarly to the other wear mechanisms the main future step would be to validate the corrosion prediction. Once identified the corrosion resistance of the reference material, it would be necessary to evaluate some of the surface treatments to validate the safety factors defined as corrosion prediction model.

In the chapter 4 of this document, an example of the model implementation for HPDC and PIM mould designer has been presented, to visualize how these kind of models would be useful in the future through implementation in software's, and improve the decision taking for mould design, maintenance scheduling or corrections to be taken. Relatively few work have been published in the topic of moulds wear before, and the multiple innovative aspects of this work are a small step forward in the increase of mould's life, with the aim of increasing the quality of the parts, reducing production stops, reparation and maintenance costs, and increase resource efficiency by reducing material scrap, the use of raw materials and energy consumption.

6 Bibliography

1. Yulong Zhu, David Schwam, John F. Wallace, Sebastian Birceanu, Evaluation of soldering, washout and thermal fatigue resistance of advanced metal materials for aluminum die-casting dies, Materials Science and Engineering A 379 (2004) 420–431
2. Alastair Long, David Thornhill, Cecil Armstrong, David Watson, Predicting die life from die temperature for high pressure dies casting aluminum alloy, Applied Thermal Engineering 44 (2012) 100-107
3. A. Srivastava, V. Joshi, R. Shivpuri. "Computer modeling and prediction of thermal fatigue cracking in die-casting tooling". Wear 256 (2004) 38–43.
4. D. Klobcar, L. Kosec, B. Kosec, J. Tušek, Thermo fatigue cracking of die casting dies, Engineering Failure Analysis 20 (2012) 43–53
5. Ruben Heid, "IFS-Report", 8, Jahrgang, Ausgabe 1, Jahr 2013, Seite 6-9.
6. K. Van Acker, K. Vercammen, Abrasive wear by TiO2 particles on hard and on low friction coatings, Wear 256 (2004) 353–361
7. E.J. Bienk, N.J. Mikkelsen, Application of advanced surface treatment technologies in the modern plastics moulding industry. Wear 207 (1997) 6–9
8. M. Heinze, G. Mennig, G. Ballet, Wear resistance of PVD coatings in plastics processing, Surface and Coatings Technology 74-75 (1995) 658-663
9. Bohai He, Research on the failure and material selection of Plastic mould, Procedia Engineering 23 (2011) 46 – 52
10. Dong-Cherng Wen, Erosion–corrosion behavior of plastic mould steel in solid/aqueous slurry. J Mater Sci (2009) 44:6363–6371
11. Anders Persson, Sture Hogmark, Jens Bergström. "Thermal fatigue cracking of surface engineered hot work tool steels". Surface & Coatings Technology 191 (2005) 216– 227.
12. Ruben Heid, "Unveröffentlichte" Untersuchung, Technische Universität Braunschweig, Institut für Füge und Schweißtechnik, 2012.
13. K.Domkin, J.H.Hattel, J.Thorborg. "Modelling of high temperature and diffusion controlled die soldering in aluminum high pressure die casting", Journal of Materials Processing Technology 209 (2009) 4051–4061.
14. Joshi, V., Srivastava, A., Shivpuri, R. "Intermetallic formation and its relation to interface mass loss and tribology in die casting dies". Wear 256 (2004) 1232–1235.
15. Shankar, S., Apelian, D. "Investigation of Die Soldering Characteristics of Aluminum Die Casting Alloys". http://www.wpi.edu/academics/Research/ACRC/index3.html (2012).
16. Venkatesan K, Shivpuri R. "A study of erosion in die casting dies by a multiple pin accelerated erosion test". J. Mater Eng. Performance (1995) 4:145-153.
17. Zackery Gay. "Benefits of Surface Engineering for Aluminum die Casters". Die Casting Engineering (September 2012) 24-26.
18. ASM Handbook Volume 18, Friction, Lubrication, and Wear Technology, ASM International (1992) 221-231
19. Z.W. Chen, M.Z. Jahedi. "Die erosion and its effect on soldering formation in high pressure die casting of aluminum alloys". Materials and Design 20 (1999) 303-309
20. J.V. Skoff. "A New Approach to the Cause of High Pressure Die Steel Erosion", Pitting, and Breakout. NADCA Expo 2010, Paper T10-051.
21. N. Nagai, S. Nishio, "Leidenfrost temperature on an extremely smooth surface", Exp. Therm. Fluid Sci.12, 1996, pp.373-379
22. D. Owens; R. Wendt, Estimation of the Surface Free Energy of Polymers. In: J. Appl. Polym. Sci 13 (1969), P. 1741-1747.
23. L. Andreoni, M. Casè, G. Pomesano, "Lubrificazione della cavità dello stampo", Quaderni della colata a pressione delle leghe di alluminio 7, 1996, pp.9-26.
24. L. Baraldi, C. Raone, "Relazione tra la lubrificazione e lo stampo - Lubrificazione in funzione delle fasi di processo", La Metallurgia Italiana 3, 2004, p.37
25. L. Andreoni, M. Casè, G. Pomesano, "Il lavoro termico dello stampo", Quaderni della colata a pressione delle leghe di alluminio 5, 1995, p.9.
26. Ewelina Pochec, Stanisław Jozwiak, Krzysztof Karczewski, Zbigniew Bojar, Maps of Fe–Al phases formation kinetics parameters during isothermal sintering, Thermochimica Acta 545 (2012) 14– 19
27. M. Fazarinc, R. Turk, G. Kluger, P. Mrvan, M.Tercelj, "Development of test rig for thermal fatigue testing – preliminary results", RMZ Materials and Geoenvironment, Vol. 54, No 1,pp 33-48, 2007
28. Gary L. Halford, Low cycle thermal Fatigue, Nasa technical memorandum 87225, 1986
29. Rafael Áviles, Análisis de Fatiga en Máquinas, ISBN 8497323440, 2005

30. N.J. Mikkelsen, J. Pedersen, C.A. Straede, Ion implantation—the job coater's supplement to coating techniques, Surface and Coatings Technology 158 –159 (2002) 42–47
31. J. Bergstrom, F. Thuvander, P. Devos, C. Boher, Wear of die materials in full scale plastic injection moulding of glass fibre reinforced polycarbonate, Wear 251(2001) 1511-1521
32. M. Peggiato, F. Bonollo, B. Zabala, Master Thesis 2014, Experimental study about the aluminum-iron interaction in presence and absence of lubricant, with a tribological Pin on Disc test and DSC/TGA chemical analysis.
33. K. Venkatesan, R. Shivpuri, Experimental and Numerical investigation of the Effect of Process Parameters on the Erosive Wear of Die Casting Dies, Journal of Materials Engineering and Performance, Volume 4(2) April 1995 145-153
34. I. Martínez-Mateo, F.J. Carrión-Vilches, J. Sanes, M.D. Bermúdez, Surface damage of mold steel and its influence on surface roughness of injection molded plastic parts, Wear 271 (2011) 2512– 2516
35. F.J.G. Silva, R.P. Martinho, R.J.D. Alexandre, A.P.M. Baptista, Increasing the wear resistance of molds for injection of glass fiber reinforced plastics, Wear 271 (2011) 2494– 2499
36. T. Nishimura, K. Yasuda, K. Nakamura, Orientation behaviour of fibres in suspension flow through a branching channel, J. Non-Newtonian Fluid Mech. 73 (1997) 279–288.
37. S.C. Lee, D.Y. Yang, J. Ko, J.R. Young, Effect of compressibility on flow field and fibre orientation during the filling stage of injection molding, J. Mater. Process. Technol. 70 (1997) 83–92.
38. NADCA Product Specification Standards for Die Castings / 2015 (Tooling for Die Casting, Section 2)
39. Anders Persson, Sture Hogmark, Jens Bergstrom, Simulation and evaluation of thermal fatigue cracking of hot work tool steels, International Journal of Fatigue 26 (2004) 1095–1107
40. A. Abuin, H. Galarraga, I. Crespo, L. M. Plaza, P. Carnicer, I. Vicario y J.C. García, Equipamiento y metodología para la determinación de la vida de materiales para moldes, Revista de Metalúrgia, vol. 46 Número Extraordinario, 101-105, 2010
41. J.R. Laguna-Camacho, L.A. Cruz-Mendoza, J.C. Anzelmetti-Zaragoza, A. Marquina-Chávez, M. Vite-Torres, J. Martínez-Trinidad, Solid particle erosion on coatings employed to protect die casting molds, Progress in Organic Coatings 74 (2012) 750– 757
42. A. Mohammed, M.B. Marshall, R. Lewis, Development of a Method for Assessing Erosive Wear Damage on Dies used in Aluminium Casting, Volumes 332–333, May–June 2015, Pages 1215–1224
43. Q. Han, H. Xu, P. P. Ried and P. Olson, Accelerated method for testing soldering tendency of core pins, International Journal of Cast Metals Research, 2010, Vol 23, Nº 5
44. Q. HAN and S. VISWANATHAN, Analysis of the Mechanism of Die Soldering in Aluminum Die Casting, Metallurgical and Materials Transactions A, Volume 34A, January 2003—139
45. M. Yu, R. Shivpuri, R.A. Rapp, Effects of Molten Aluminum on H13 Dies and Coatings, Journal of Materials and Engineering Performance, Volume 4, April 1995-175
46. Anders Persson, Jens Bergstrom, Christer Burman, Sture Hogmark, Influence of deposition temperature and time during PVD coating of CrN on corrosive wear in liquid aluminium, Surface and Coatings Technology 146 –147 (2001) 42–47
47. S. Shankar and D. Apelian, Die Soldering: Mechanism of the Interface Reaction between Molten Aluminum Alloy and Tool Steel, Metallurgical and Materials Transactions B, Vol 33B, June 2002-465
48. Eduardo K. Tentardini, Augusto O. Kunrath, Cesar Aguzzoli, Maria Castro, John J. Moore, Israel J.R. Baumvol, Soldering mechanisms in materials and coatings for aluminum die casting, Surface & Coatings Technology 202 (2008) 3764–3771
49. V. Joshi, K. Kulkarni, R. Shivpuri, R.S. Bhattacharya, S.J. Dikshit, D. Bhat, Dissolution and soldering behavior of nitrided hot working steel with multilayer LAFAD PVD coatings, Surface and Coatings Technology 146 –147 (2001) 338–343
50. J. Jerina, M. Kalin, Aluminium-alloy transfer to a CrN coating and a hot-work tool steel at room and elevated temperatures, Wear, Volumes 340–341, 15 October 2015, Pages 82–89
51. Jaume Pujante, Montserrat Vilaseca, Daniel Casellas, Maria Dolors Riera, The Role of Adhesive Forces and Mechanical Interaction on Material Transfer in Hot Forming of Aluminium, Tribol Lett (2015) 59:10
52. M. Vilaseca, S. Molas, D. Casellas, High temperature tribological behaviour of tool steels during sliding against aluminium, Wear 272 (2011) 105– 109
53. http://music.eucoord.com/
54. J. C. Berg, "Wettability", Ed. Marcel Dekker, ISBN: 0824790464.
55. J.D. Bernardin, C.J. Stebbins, I. Mudawar "Mapping of impact and heat transfer regimes of water drops impinging on a polished surface", Int. J. Heat Mass Transfer 40, 1997, pp.247-267
56. A. Guzanová, J. Brezinová, Influence of Reinforced Plastomers on Injection Moulds Wear, Journal of Metals, Materials and Minerals, Vol.18 No.2 pp.7-13, 2008

57. A. Guzanová, J. Brezinová, The wear of injection mould functional parts in contact with polymer composites, Materials Engineering, Vol. 16, 2009, No. 1
58. C. Kerschenbauer, M.O. Speidel, G. Lichtenegger, J. Sammer and K. Sammt, Plastic Mould steels- wear resistant and corrosion resistant martensitic chromium steels, 6th International Tooling Conference (2002)
59. P. Boey, W. Ho, S.J. Bull, The effect of temperature on the abrasive wear of coatings and hybrid surface treatments for injection-moulding machines, Wear 258 (2005) 149–156
60. Orhan Öztürk, Ortaç Onmus, D.L. Williamson, Microstructural, mechanical, and corrosion characterization of plasma-nitrided plastic injection mould steel, Surface & Coatings Technology 196 (2005) 341– 348
61. R.G. Bayer, Wear analysis for engineers, HNB (2004)
62. H.C. Meng, K.C. Ludema, Wear models and predictive equations: their form and content. Wear 181-183 (1995) 443-4
63. Guobin Li, Xiangzhi Li, Jianjun Wu, Study of the thermal fatigue crack initial life of H13 and H21 steels, Journal of Materials Processing Technology 74 (1998) 23–26
64. Hanliang Zhu, Jingjie Guo, Jun Jia, Experimental study and theoretical analysis on die soldering in aluminum die casting, Journal of Materials Processing Technology 123 (2002) 229–235
65. Patrick Alan Hogan, Die Solder Prediction and Reduction, a thesis submitted to the faculty of the Worcester polytechnic institute, 2008
66. Pereira, A.; Hernández, P; Martínez J.; Pérez, J.A.; Mathia, T.Study of morphology wear model of moulds from alloys of aluminium EN AW-6082 in injection process., Key Engineering Materials Vols. 554-557 (2013) pp 844-849
67. http://www.academia.edu/2187669/Methodology_to_measuring_wear_molds_Poster_
68. I.M. Hutchings, Tribology, Friction and Wear of Engineering Materials, Butterworth-Heinemann, Cambridge, 1992.
69. A. Long, D. Thornhill, C. Armstrong, D. Watson, Stress correlation between instrumentation and simulation analysis of the die for HPDC, International Journal of Metalcasting/Spring 2013
70. Long AD. Extending life of high pressure die casting dies. Ph.D. thesis (Faculty of Engineering and Physical Sciences, Queen's University, Belfast); July 2010. 11706.
71. F. Bonollo, N. Gramegna, A. Igartua, The MUSIC guide to key-parameters in High Pressure Die Casting, ISBN 978-88-87786-10
72. A. Igartua, R. Bayón, R. Zabala, P. Zabala, V. País, J. Damborenea, J.-P. Celis, "Comparative corrosion wear behavior of cast iron and aluminium", Proceedings from the congress 2006
73. Jia Guo, Shanwu Yang, Chengjia Shang, Ying Wang, Xinlai He, Influence of carbon content and microstructure on corrosion behaviour of low alloy steels in a Cl− containing environment, Corrosion Science, Volume 51, Issue 2, February 2009, Pages 242–251
74. D.A. López, S.N. Simison, S.R. de Sánchez, Inhibitors performance in CO2 corrosion: EIS studies on the interaction between their molecular structure and steel microstructure, Corrosion Science, Volume 47, Issue 3, March 2005, Pages 735–755
75. Douglas C. Montgomery, Design and Analysis of Experiments, ISBN 978-1118-14692-7

7 Acknowledgments

This work was developed within the European Project MUSIC (MUlti-layers control & cognitive System to drive metal and plastic production line for Injected Components, FP7-FoF-ICT-2011.7.1, under Contract nº 314145). I would like to thanks all the Music coordinator Nicola Gramegna from EnginSoft s.p.a, all the consortium partners, and especially the close collaboration of industrial partners MAIER S. Coop (Plastic Injection), Motultech-Baraldi (lubricant supply for HPDC), AUDI AG (collaboration in thermal fatigue Machine in HPDC), MAGMA Giessereitechnologie GmbH (collaboration in simulation of thermal fatigue), SAEN s.r.l. for supplying materials and for their kind suggestions. Also, we would like to thanks to Padova University, Prof. Franco Bonollo and Prof. Giulio Timelli for their kind collaboration specially for sending to IK4-TEKNIKER, 4 students to make a stage under my supervision to fulfil their Master Thesis on the subject of moulds wear: Valeria Scarpis, Matteo Peggiato, Tonino Cundari and Irene Bramati.

My training in modelling activity was also supported by Powerful EU project that was carried out during a period of 3 Months in the company AVL in Austria with the support from RENAULT Company.

I would like to thank my supervisors and all the laboratory colleagues from IK4-Tekniker that have contributed to the success of this work, offering personal and professional support.

8 Annexed articles

In the frame of this investigation, different articles have been published in journals or presented in congresses.

The first article *Friction and wear of a piston ring/cylinder liner at the top dead centre: experimental study and modelling* is the research that has been performed in the stage performed by this doctoral student in the AVL List GmbH in Graz (Austria), that enables the International mention of this Thesis. In this publication, the use of experimental results of tribological tests has been used to generate wear and friction model, and was the first necessary learning steps for the generation of moulds wear models. This article has been published in Tribology International (2017), pp. 23-33 DOI information: 10.1016/j.triboint.2016.10.005.

The second article *On the nature of high pressure die casting die failures* was published in the World Foundry Congress 2014, and is based on the bibliography analysis of the nature wear mechanisms and the parameters influencing them.

The third and fourth article are created from different results that have been presented in this document. The third article *Multiparametric study of Leidenfrost point and wettability of lubricants on high-pressure die-casting dies* has been submitted to the International Journal of Thermal Sciences, and has been revised and has been resent after performing a major revision as recommended by the journal. The fourth article *Evaluation HPDC Lubricant Spraying for Improved Cooling and Die Protection* was presented in the Lubmat 2016 congress.

It is of interest to mention that apart from these articles, a presentation of some of the results were presented in the congresses Tribo Lyon 2013, Lubmat 2014, Euroguss 2016, and also an article is expected to be presented in the Fracture Fatigue and Wear FFW 2017.

8.1 Friction and wear of a piston ring/cylinder liner at the top dead centre: experimental study and modelling

B. Zabala[1], A. Igartua[1], X. Fernández[1], M. Hernaiz[1], C. Priestner[2], H. Ofner[2], O. Knaus[2], M. Abramczuk[3], P. Tribotte[3], F. Girot[4], E. Roman[5], R. Nevshupa[6]

[1] IK4-TEKNIKER, Calle Iñaki Goenaga 5, 20600 Eibar, Spain

[2] AVL List GmbH, Hans-List-Platz 1, 8020, Graz

[3] RENAULT, Direction de la Recherche, des Etudes Avancées et des Matériaux. SCE 68530. FR TCR LAB 0121, Avenue du Golf 78288 Guyancourt Cedex, France

[4]University of the Basque Country, UPV-EHU, Faculty of Engineering, Department of Mechanical Engineering, IKERBASQUE, Basque Foundation for Science, Alameda Urquijo s/n 48013 Bilbao, Spain.

[5] Spanish National Research Council, Institute of Materials Science of Madrid, C/Sor Juana Inés de la Cruz 3, Madrid 28048, Spain

[6] Spanish National Research Council, Institute «Eduardo Torroja» of Construction Sciences, C/Serrano Galvache 4, Madrid 28033, Spain

ABSTRACT

Wear assessment of critical components subjected to relative sliding is a key factor for the development of advanced materials and surface treatments in automotive industry. Simulation of wear process of the engine components is considered as a good alternative for experimental testing which is costly and time-consuming, but it requires a reliable experimental data for model fine-tuning. Friction and wear of cylinder liner against a piston ring were experimentally studied in simulated laboratory tests. The parameters which were controlled in these tests included oil type, lubrication starvation, surface finishing and surface coatings. The obtained experimental data was fed into a specific simulation model (AVL Excite-Power Unit). The error between experimental and simulation results on total wear was below 5 %.

Keywords: c*ylinder liner; piston ring; boundary friction; modelling; surface coatings*

1 INTRODUCTION

Important advancements in performance of reciprocating combustion engines are linked with tribological topics including improvements in lubrication, optimization of surface geometry of individual contacts, application of advanced materials and coatings, etc. Among various engine components, the piston group, i.e. pistons, rings and cylinder liners, is of special concern in passenger car engines since up to 50% of the total energy is lost due to friction of these components. Optimization of friction and wear characteristics of the piston–liner contact is always a trade-off with many other requirements: efficient heat transfer from the piston to the engine structure, sealing against oil flow into and gas leak from the combustion chamber and so on [1-3]. In literature, enhancement of tribological performance of a piston group is usually sought through optimization of the surface topography of the honed surfaces [4-7], lubrication regime [8] and surface modification [9-11].

The most critical zone prominent for intensive wear is located at the top dead centre (TDC) because of the combination of various factors: alternating acceleration from and deceleration to complete stop, the highest temperature and lubrication starvation under mixed or boundary regime. However, there are only few studies

aimed at wear mitigation at the TDC [9, 12], while the main dependencies under these conditions remain poorly understood. Recently, a cylinder-on-plane reciprocating test and scuffing test have been employed for screening tribological characteristics of a number of candidate coatings including thermal sprayed micro- and nanocermets (Cr_3C_2–NiCr, WC86–Co10Cr4) [10, 13], bi- and multilayer coatings (TiN-Ti/CrN-CrN, a-C:W) obtained by physical vapour deposition (PVD) [10], electroless nanocomposites (NiP–Si_3N_4), etc. Taking traditional chromium plating as a benchmark it was found that tungsten-doped carbon coatings (a-C:W) enhanced friction behaviour and the bilayer coating (TiN-Ti/CrN-CrN) enhanced the wear resistance, whereas WC86–Co10Cr4 did not. When tested in a turbodiesel engine, a-C:W PVD coatings showed a good compromise between reduction of wear, friction and fuel consumption [10]. Furthermore, 19 fully-formulated alternative engine oils with different base stocks were tested pursuing improvement of their lubricating capability under hydrodynamic and mixed regimes [9], although boundary regime that is typical for TDC has not been sufficiently addressed.

Today, there is a strong demand from the industry for cost-effective but realistic semi-quantitative simulation test procedures that can rapidly screen potential lubricants, materials and coatings before expensive as well as time-consuming component testing in engines or field testing system-level are performed [3, 14, 15]. Combination of experimental simulation and computational modelling can be a good alternative to the real-life testing because it allows learning about the model more efficiently, finding out quickly which factors are unimportant, building simple proxy models of complicated, expensive simulation models and then optimizing the system performance.

The present work is focused on coupling the experimental simulation of a ring-on-liner contact at the TDC with computational modelling of wear and friction as function of various factors that are crucial for tribological performance: (i) type of the lubricating oil, (ii) lubrication starvation/plenty, (iii) type of the surface finishing: fine or plateau honing; and (iv) surface coatings. Considering that ceramic and carbon PVD coatings showed good results in cylinder-on-plane and real engine experiments, in this work two different CrN PVD coatings as well as self-lubricious diamond-like carbon and MoS_2 coatings have been studied under simulated experimental conditions at TDC. This selection is based on the authors experience as well as literature review. [10]

For computational modelling a specific AVL Excite-Power Unit model that linked advanced lubricated surface contact and wear models and contained all the information related to the studied contact, i.e. geometry, profiles, roughness, material and lubricant properties, etc. was used. For the sake of model validation, the obtained volume of systematic experimental data was correlated with the results of modelling. In addition, the sensitivity of the model regarding various parameters such as coatings/surface treatments, oil properties/additives, surface finishing's or texturing was studied. Validation of the computational model and its fine-tuning has been an important step towards development of a numerical tool for simulations of piston group wear.

2 Experimental study of a piston ring/ cylinder liner friction and wear

2.1 Experimental set-up

Reciprocating linear motion tribometer schematically shown in Figure 1 was used to simulate TDC friction conditions. A ring-to-liner contact was simulated by using parts cut from a real piston and a cylinder liner.

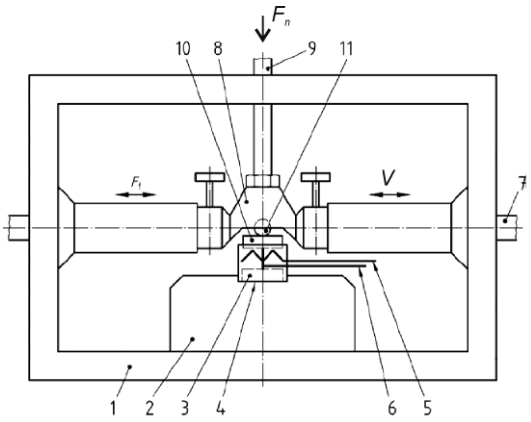

Fig. 1. Schematic view of the experimental test rig: 1 – the fixture; 2 – the receiving block; 3 – the piezoelectric measuring device; 4 – the sample holder; 5 – the electrical resistive heater; 6 – resistive thermometer; 7 – the oscillating drive rod; 8 – the counterpart holder; 9 – the loading rod; 10 – the sample; 11 – the counterpart (reprinted from [10] with permission).

The liner (10) was fixed to the base (4). A piston ring holder was attached to the machine head (8) that applied the movement and load. The ring (11) was attached to the holder (8). This configuration ensures good line contact between the bodies under applied loads. A more detailed description of this setup was given elsewhere [11].

The stroke of reciprocating motion was set 4 mm that is representative for simulation of TDC conditions (see Figure 2). Motion frequency was selected to reproduce the sliding conditions in the engine taking as a benchmark the engine with 90 mm stroke operating at 1000 rpm. The relative speed of the piston at 2 mm from the top dead centre for this case is 0.1 m/s that corresponds to the motion frequency 25 Hz at the stroke length 4 mm.

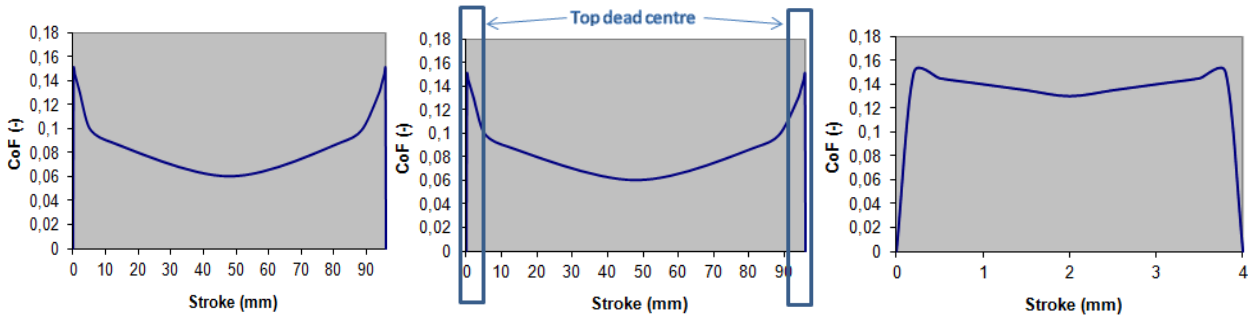

Fig. 2. Friction coefficient evolution during the engine cycle: a) the total stroke of 96 mm stroke; b) the zones of interest for tribological simulation; c) friction coefficient evolution during simulated tribo-test with 4 mm stroke.

In order to have the same contact pressure as under real working conditions (20 MPa) the normal load was set at 616 N. In addition, to determine the load at which scuffing occurred, extreme pressure tests were conducted for various lubricants and surface coatings following ASTM D5706 standard. The chosen load was much below the scuffing load, so normal engine operation could be reproduced with 616 N. As the lubrication regime is mixed/boundary conditions, a drop of 1 ml proved enough to maintain this lubrication regime for the whole testing time as the acquired friction signals showed. The temperature during the test

was 180 ºC. Duration of each trial was 12 hours. After the tests, the wear scars were examined by optical and confocal microscopy. Wear was evaluated from the geometry of the worn surfaces and by mass loss.

Comparative study of friction and wear for two fully formulated lubricating oils: 5W30 and 15W40 was done following standard procedure DIN 51834-2. The experimental conditions of this test were: reciprocating frequency 50 Hz, 1 mm stroke, normal load on the ball 300 N, temperature of the of the oil 180º C, test duration 2 hours.

Chemical composition of some of the worn surfaces was analysed using X-ray Photoelectron Spectrometry (XPS). The angle between the hemispherical analyser (Specs-PHOIBOS100) and the surface was 60º. An X-ray radiation source with MgK_a line (1253.6 eV) was used. The survey spectra were obtained with electron energy step of 0.25 eV and pass energy 40 eV. Fine core level spectra were measured with electron energy step 0.1 eV and pass energy 15 eV. Before the analysis of the obtained data the contribution of the MgK_a satellite line was subtracted and the spectra were subjected to Shirley background subtraction formalism [16].

2.2 Materials

The base materials were different types of cast iron for the ring and the cylinder liner. Reference samples of the cylinder liner were finished using a standard plateau honing. In addition, samples with fine honing surface finishing were used to study the effect of surface micro-geometry on tribological performance at TDC. The texture and roughness of honing is believed to be important for oil retaining and distribution on the surface [17]. Figure 3 shows reconstructed 3D images of samples with fine and plateau honing surface finishing. Grey scale defines heights of surface features.

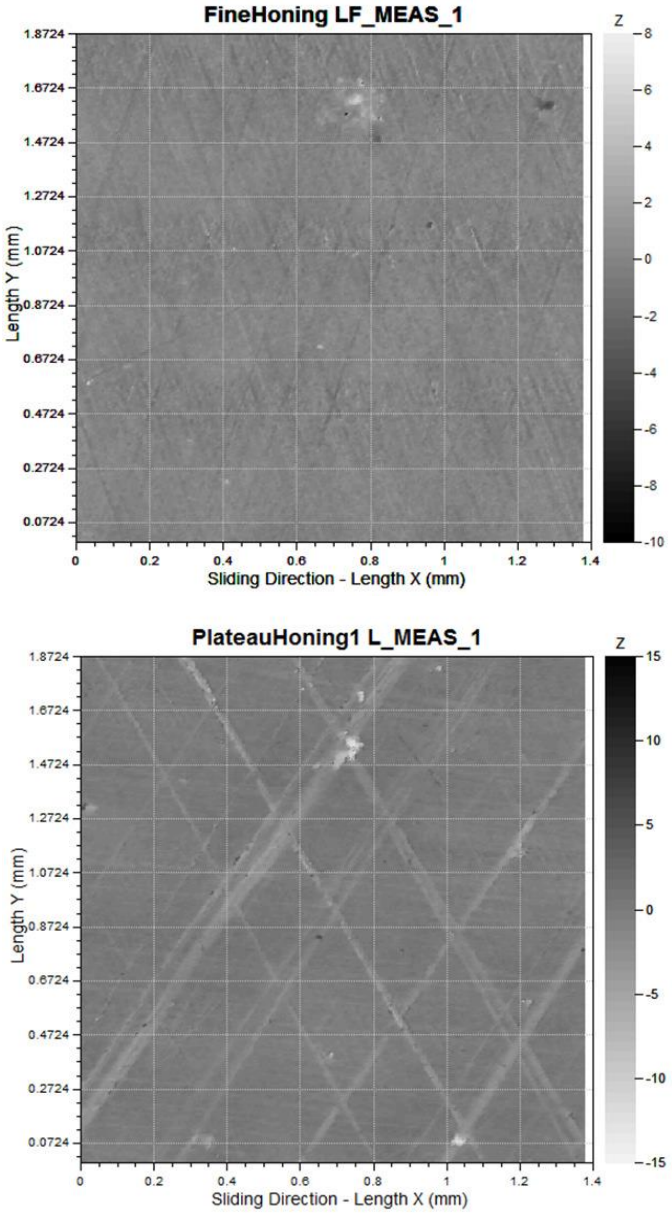

a) **b)**

Fig. 3. Reconstructed 3D surface of cylinder liner obtained by confocal microscopy: a) fine honing surface finishing, Rq=0.511, Ra=0.374; b) plateau honing surface finishing Rq=0.936, Ra=0.619.

Several coated piston rings were tested against uncoated cylinder liner. The coatings were produced either by Physical Vapour Deposition technique at IK4-TEKNIKER or by a third company. The most relevant parameters for tribological performance – microhardness and roughness – are shown in Table 1. Surface roughness of the coatings was measured using confocal microscopy as well as contact profilometer. The main difference between the two CrN coatings is the increased thickness for CrN_2 up to 20µm. It was found that coating deposition have not big effect on the surface roughness that remained very similar to the bare rings.

Table 1. Microhardness of piston rings with various surface coatings

Coating	Hardness (GPa)	Roughness Ra (µm)
DLC	30.4	0.165
MoS_2	6.8	0.167
CrN_1	14.0	0.164
CrN_2	10.5	0.257
Cast Iron	3.8	0.155

For lubrication two fully formulated commercial oils 15W40 and 5W30 were used. Both oils were characterized using Fourier Transformed Infrared (FTIR) spectrometry, Differential Scanning Calorimetry (DSC), Thermogravimetry analysis (TGA) and Inductively Coupled Plasma Optical Emission Spectroscopy (ICP-OES). Degradation temperature was determined through DSC using heating rate 10 ºC/min in the temperature interval from 50 to 500 ºC. Oxidation behaviour was studied using isothermal DSC at 180 ºC in O_2 atmosphere under

20 bar pressure. Additionally, thermal conductivity, heat capacity and viscosity were determined. The results are given in Table 2.

Table 2. Elemental chemical composition of additives and physic-chemical properties of two fresh oils

Property		15W40	5W30
Elemental chemical composition of additives (ppm) [1)]			
	B	129	0
	Ca	32	1100
	Mg	1473	6
	P	893	455
	Zn	992	505
	Mo	105	212
	Si	2682	1196
	S	6	3
Degradation temperature (ºC)		213	215
Oxidation time (min.)		47.4	80.0
Specific Heat, C_p (J/g K)			

	25 ºC	1.61	1.91
	195 ºC	2.33	2.58
Thermal conductivity, *k* (W/m K)			
	40 ºC	0.132	0.142
	100 ºC	0.142	0.14
Viscosity h HTHS @ 150°C (mPa s) [2)]		3.9	3.2

[1)] According to ASTM D 5185-09 mod.

[2)] According to ASTM D445-12

The oils have very similar base stock formulation as could be inferred from the almost indistinguishable FTIR spectra of these oils. Their thermal properties were very similar as well. As it could be expected, viscosity for 5W30 was lower, than for 15W40. Also, 15W40 showed slightly better degradation behaviour and the oxidation resistance that could be associated with higher concentrations of Zn, S and P.

3 Experimental Results and discussion

3.1 Friction and wear tests of uncoated samples

Figure 4 shows friction behaviours of two oils under standard translatory oscillation test (DIN 51834-2). After short running-in friction coefficient stabilized at 0.1 and 0.05 for 15W40 and 5W30, correspondingly. Although for 15W40 friction was slightly higher, friction behaviour was much smoother than for 5W30. For the latter some considerable spikes could be observed in the course of the test, that are probably related to some adhesions between surfaces. These results have been adopted as a benchmark for further simulation tests.

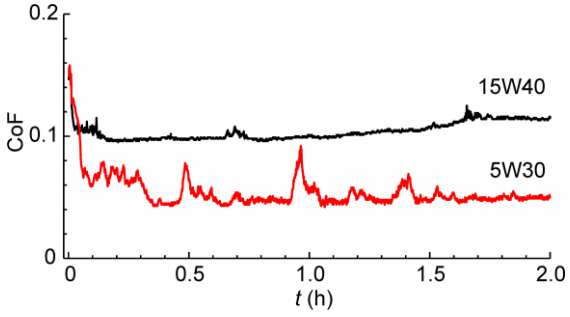

Fig. 4. Friction behaviour for two oils under standard translatory oscillation test DIN 51834-2 (ASTM D6425).

The effect of lubrication starvation was studied under simulated ring-liner contact. In the lubrication starvation tests, a drop of the oil was added only at the beginning of the test. Friction behaviours for these tests for both oils are shown in Figure 5. Running-in phases in these and the benchmark tests were quite similar. After running-in a low friction regime was established (plots S). The lowest friction force corresponded to the steady friction in the benchmark test. Duration of the low-friction regime was about 30 min for 15W40 and almost 1.5 hour for 5W30. Then, friction force gradually increased to a steady starvation value that was close to 0.15 for both oils. This behaviour is similar to that reported in [18] where transition of

friction coefficient from 0.05 to 0.14 was associated to oil oxidation. For 5W30, this regime lasted till the end of the test for more than 7 hours, whereas for 15W40 it was suddenly interrupted after 5 hours and switched to irregular growing trend that is characteristic to severe wear.

For comparison, in another test 1 ml of fresh oil was added periodically during the test (re-oiling, plots X) without rubbing interruption. Every time fresh oil was added friction coefficient slightly increased and then returned to a steady value. For 5W30 a steady value restored in approximately 0.5 h, while for 15W40 it took much longer time: between 1.5 and 2 hours. For 5W30 steady friction coefficient was close to 0.05 during 12 hours of the tests that was in accordance with the benchmark test. For 15W40 steady value decreased in each consecutive re-oiling cycle and stabilized at 0.05 that was three-fold below the steady value in the benchmark test.

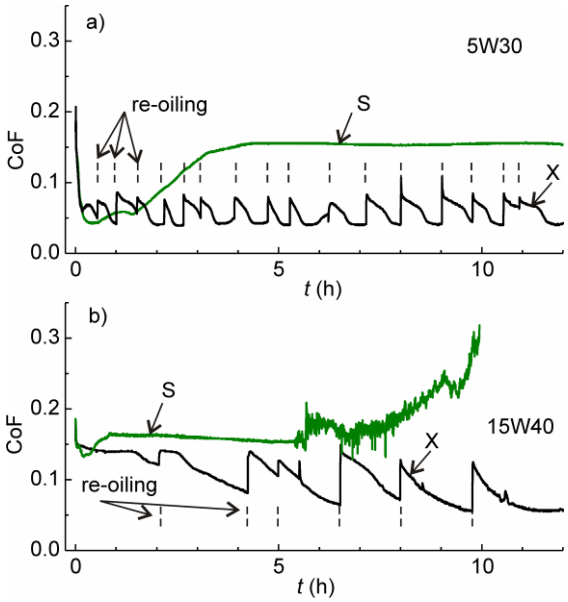

Fig. 5. Friction behaviour for ring-liner contact with a liner finished by fine honing and for two oils: a) 5W30 and b) 15W40. Plots S – oil drop was added at the beginning of the tests. Plots X – oil was added periodically at the moments shown by vertical dashed lines.

3.2 Surface chemical analysis

Instantaneous increase in friction coefficient that occurred when fresh oil was added could be ascribed to the change in lubrication regime from boundary to hydrodynamic one, recovering the boundary condition almost instantaneously. This hypothesis is supported by the fact that the lip was stronger for higher viscosity 15W40 oil, than for the lower viscosity 5W30 one. The steady friction coefficient in lubrication starvation tests had to depend on a tribofilm formation, whereas the duration of steady friction regime depended on the rate of the tribofilm wear/degradation. Failure of the tribofilm was associated with gradual increase in friction coefficient (15W40/S in Figure 5 b). Chemical analysis of worn surfaces after these tests was analysed by XPS and is shown in Figure 6. The main elements found on the surfaces were C and O. In all tests where the tribofilm was not severely damaged, i.e. 5W30/S, 5W30/X and 15W40/X, C and O concentrations were almost the same. In test 15W40/S C was slightly higher and O slightly lower, than in other tests. Fine structure of C 1s peak revealed that the main component corresponded to C-C/C-H bonds with a smaller contribution from C-O in all tests. These findings are in line with literature [19, 20]. It should be stressed that Zn, Mo, S and P derived from the oil additives as well as iron were found on the sample surfaces in low proportion, typically below 4 at. %. From the comparison of the additive elemental concentrations (Figure 6

b), it was found that lubrication starvation for both oils led to significant decrease in Mo, S and Si. Regarding the chemical bonding shown in figure 7, some difference in the oxidation state of sulphur was found for 5W30. Under re-oiling, the dominant component corresponded to metal sulphide/thiol (S^{-2}). Under lubrication starvation, a contribution of metal sulphate (S^{+6}) in S 2p spectra increased for both oils, but most significantly for 5W30, for which it became the predominant peak. Appearance of sulphates indicated thermal transformation of the tribofilm containing components of zinc dialkyl dithio phosphate and molybdenum dialkyl dithiocarbamate as it was recently reported [21, 22]. It can be suggested that this reactivity consume energy and decrease the contact temperature, increasing lifetime of 5W30 oil under oil starvation. Gradual decrease of the total S and increase in sulphate/sulphide proportion in oil with oxidation time was also reported in [18]. In case of 15W40/S S^{-2} component slightly shifted to higher bonding energy that might be related with higher contribution from thiols, than from metal sulphides. This could be a consequence of Mo dithiocarbamate decomposition [21].

Zn concentration, C(Zn), showed different behaviours: $C(\mathrm{Zn})_{5W30/S} > C(\mathrm{Zn})_{5W30/X}$, but $C(\mathrm{Zn})_{15W40/S} < C(\mathrm{Zn})_{15W40/X}$. This might indicate that Zn-rich compounds were responsible for long-term wear resistance of a tribofilm (5W30/S). When a tribofilm was gone, surface Zn concentration decreased. P/S ratios for 5W30 and 15W40 were not significantly affected by the lubrication starvation and were 0.8 and 0.3, correspondingly. Nevertheless, the ratio P/Zn was lower in case of the lubrication starvation. This might point on the continuous depolymerisation of zinc metaphosphate in the presence of goethite and preferential elimination of phosphorous during the friction test [23]. Possible presence of iron hydroxide in our tests could be inferred from the binding energy of Fe 2p at 710.9 eV. O 1s peak could be fitted with three components with binding energies at about 530.0, 531.8 and 533.4 eV ascribed to metal oxide, iron oxy-hydroxide and adsorbed water, correspondingly [23]. The structure of O 1s was very similar in three tests: 5W30/S, 5W30/X and 15W40X, but an increase in the component of O 1s at 533.4 was observed for 15W40/S. For other elements no significant variation in binding energy was observed.

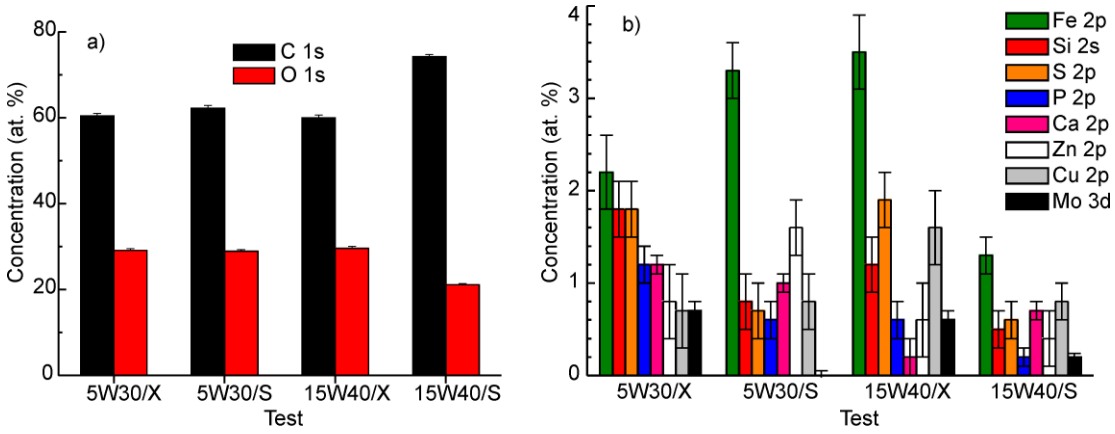

Fig. 6. Concentrations of various elements on the worn surfaces after the tests with 5W30 and 15W40 oils: a) C and O determined from corresponding 1s peaks; Fe, Si, S, P, Ca, Zn, Cu and Mo. The energy level used for calculation of the corresponding atomic concentrations are shown on the legend.

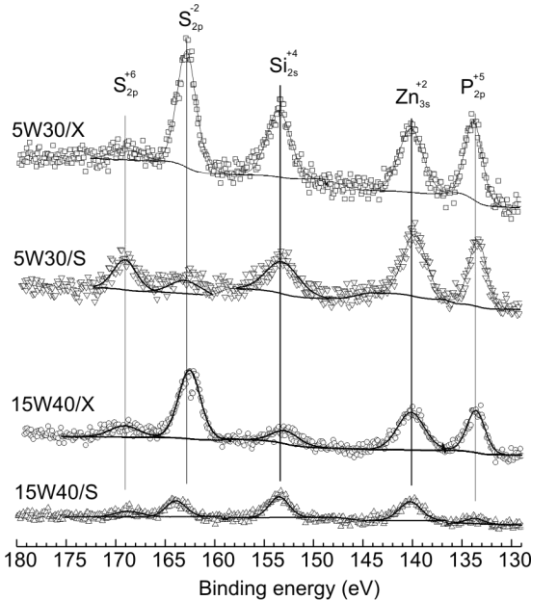

Fig. 7. Fine structures of S 2p, Si 2s, Zn 3s and P 2p peaks of XPS spectra for the samples used in lubrication starvation and re-oiling tests.

3.3 The effect of the surface finishing

The effect of surface finishing of the cylinder liner on friction behaviour under lubrication starvation conditions was of little importance (Figure 8). Generally, friction coefficient was slightly lower for plateau honing (PH) surface finishing for both oils. However, plateau honing led to significant increase in mass wear (Table 3). Such a contradictory effect of surface finishing on friction and wear was related with better oil distribution on the fine honed surface. The values obtained for fine honing (FH) are consistent with literature data [15].

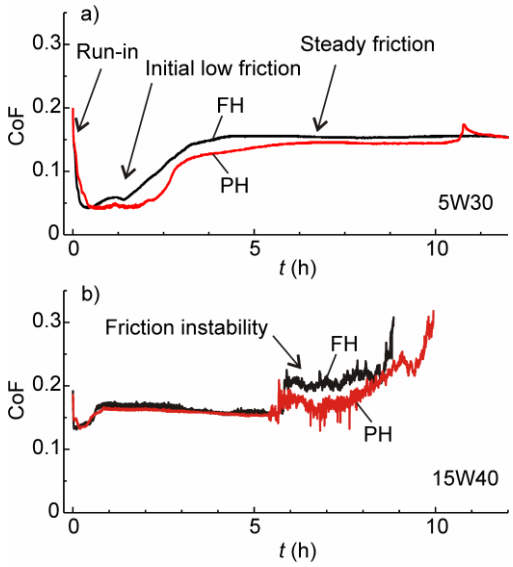

Fig. 8. Friction coefficient evolution for the two oils: a) 5W30, b) 15W40. FH – fine honing of the cylinder liner; PH – plateau honing of the cylinder liner.

Table 3. Mass wear (mg) of the ring and the cylinder liner as function of the oil type and liner surface finishing

		Fine honing	Plateau honing
5W30	ring	0.02	-0.04
	liner	0.46	1.60
15W40	ring	0.01	0.03
	liner	5.66	7.02

3.4 Friction and wear tests of the coated samples

Finally, the effect of surface coatings on friction was studied for 15W40 oil under lubrication starvation. Both self-lubricating coatings: MoS_2 and DLC showed quite stable friction behaviour during whole test (Figure 9 a). The lowest friction coefficient achieved for MoS_2 was below 0.07. These values are in accordance with literature data obtained under plenty lubrication [24]. The steady friction values were 0.15 and 0.13 for MoS_2 and DLC, correspondingly. The results of the tests for ceramic PVD coatings are shown in Figure 9 b. Friction coefficient for the harder CrN_1 coating was around 0.15 and stable throughout the test. The softer, slightly rougher and thicker CrN_2 coating experienced increase in friction coefficient up to 0.22 half an hour after the beginning of the test. Then, it followed by a slow transition to the steady value close to 0.15. The wear measured from this test followed the trend of the friction coefficient behaviour. The results are shown in table 5, Section 4.

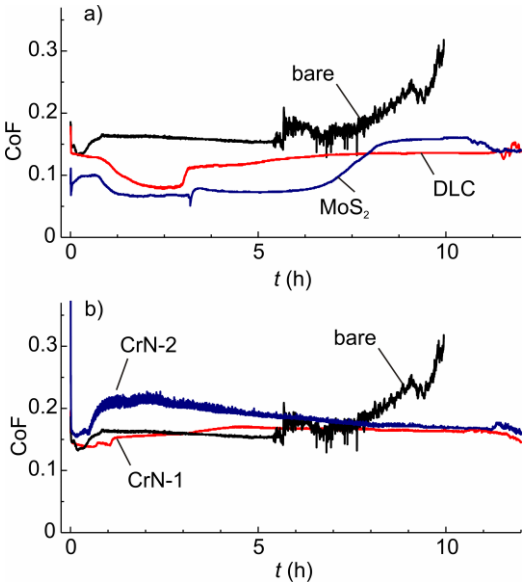

Fig. 9. Friction coefficient under lubrication with 15W40 for piston rings coated with self-lubricious DLC, MoS2 and the ceramic coatings compared to the base materials

4 Modeling

4.1 General characteristics of the model

AVL Excite Power Unit and its hydrodynamic and asperity contact models included in EPIL joint (Elastohydrodynamic (EHD) mesh that contains tribological information, and simulates the performance of the lubricated surfaces) were used to simulate the Tribological behaviour of ring against cylinder materials,

achieving the same results measured during laboratory test rigs. The mathematical models applied by AVL Excite-Power Unit and related tools are explained elsewhere [27].

The approach presented here is for piston ring to cylinder liner contact. This approach has been similarly applied for other tribo-tests results in order to represent piston skirt to cylinder liner contact and also ball-on-disc test.

The 2D schema of the model of reciprocating movement between two bodies is presented in Figure 10, where the bodies can be others like piston skirt.

It has been represented 360º of the body and then defined the contact only for the section of ring in contact in the test of an angle of 23.2º. This value is due to the section cut from ring for experimental tests.

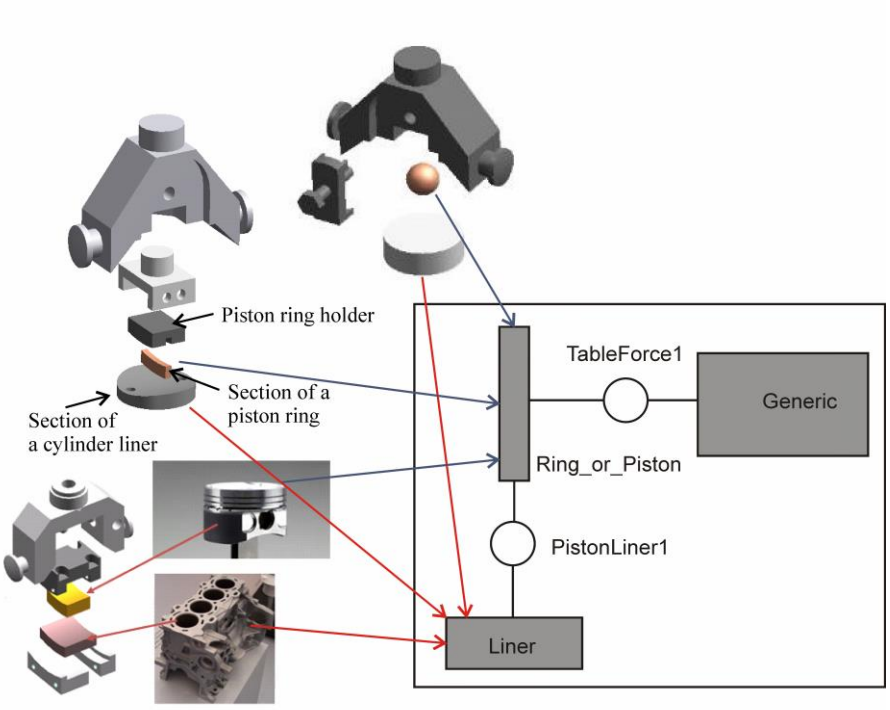

Fig. 10. 2D schematic representation of the contacting bodies

In this model, both bodies are assumed to be rigid. Their condensed meshes include: 772 and 1273 nodes, correspondingly. The model includes a generic body that define the ring reciprocating movement (speed, stroke). The liner is constrained (0 active degrees of freedom - DOF). The ring includes 3 translational DOF. The EPIL joint is the EHD mesh that contains all the information related to tribology (surface contact model for friction and wear, lubrication and body profiles). Load of 616 N concentrated in one point was applied in radial direction. The contact is distributed in the 23.2°, as it is in the actual tribotest.

4.2 Model inputs

Once the model defined above has been built up, it is necessary to obtain some values from experimental data or bibliography, in order to have the model as near from reality as possible. Other model default parameters or recommended values, that are not measurable physical parameters, have been validated in this work based on tribotest results.

To define the Finite Element mesh, body geometry and materials characteristics are necessary to collect, including dimensions of the bodies, their mass and stiffness matrix, profiles of ring and piston surfaces, and material properties as hardness or young modulus. The stroke, speed and load and the length of the contact were defined as it was in the tribotest,

The roughness's three dimensional pattern were measured by confocal microscopy, and treated with MicroSlideAnalysis in order to obtain a compliance - pressure relationship based on Greenwood and Tripp model [25] as well some parameters influencing EHD lubrication, based on "Patir and Cheng" model [26]. 3 different surface areas were measured and treated for averaging.

Regarding the oil properties, the viscosity in function of temperature of the lubricant tested was measured and included. The temperature of the lower sample in the tribotest was kept constant at 180ºC, and the contact temperature is estimated as 184.5ºC.

The key input values for tribological performance are the following:

- *Boundary lubrication value of friction coefficient* of the studied pair,
- *Archard wear factor*.

The values of these parameters can be obtained from basic tribo-tests with pin-on-disc or ring-on-liner configuration. The measured friction coefficient is used as initial value. Its evolution during the cycle was calculated as a sum of viscous shear stress and asperity friction influenced by micro-hydrodynamics. The wear factor is defined for each element of the tribo pair. It is a dimensionless constant calculated from the experimental results applying the Archard law. The calculation of the Archard wear factor has been made through the following equation:

$$k(-) = \frac{H(MPa) \times V(mm^3)}{F(N) \times L(mm)}$$

where:

H (MPa): hardness

V (mm^3): wear volume

F (N): applied load

L (mm): sliding length between bodies during the test

The parameters used in the reference model are listed in Table 4.

Table 4. List of input parameters

Ring Surface	Standard Ring
Liner Surface	Fine Honing
Ring Profile	Standard Ring
CoF	0.13

Wear Factor (Ring)	2.01×10^{-9}
Wear Factor (Liner)	2.47×10^{-8}
Oil groove angle (deg.)	23.2
Oil Type	5W30, viscosity dependence with temperature
Oil Temperature (ºC)	184.5
Protection Pressure (MPa)	0
EHD Mesh	91×361
Wear Time Steps	0.6 min, 1.5 min, 3 min, 9 min, 18 min, 36 min, 1 h, 2 h, 4 h, 6 h, 12 h
Lubricated asperity friction and wear constants	
a	2.71828
b	10000
c	100
Ls (μm)	25
Grinding wear model	Not included
Nominal radial clearance (μm)	1
Stroke (mm)	4
Speed (rpm/Hz)	1500/25
Load (N)	616 (concentrated)
Rigid/Flexible Bodies	Liner_Rigid, Ring_Rigid
Control parameters:	
end initial phase (deg.)	30
start of evaluation (deg.)	360

To have correct results, it has been highlighted that the EHD mesh is critical. It is important to define the grid points of EHD mesh on based on the Ring body FEM mesh. This means coincidence between ring grid points and with some of the EHD mesh grid points in axial direction, as it is shown in Figure 11.

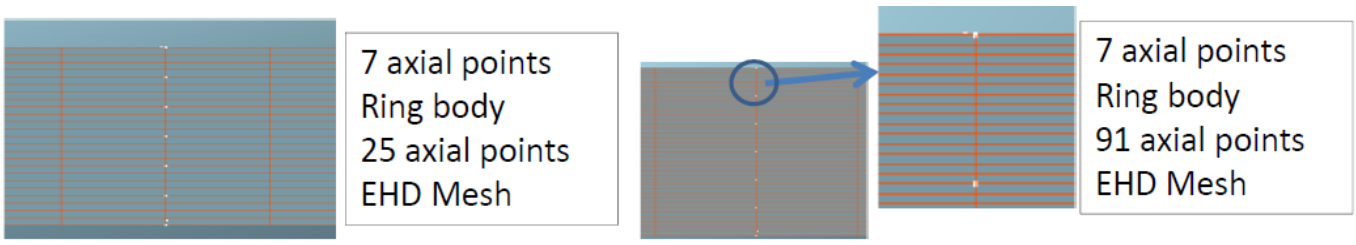

(a) **(b)**

Fig. 11. EHD mesh (red grid) superposed on the ring FEM mesh (white grid). It is shown a case of 4 EHD elements for each FEM element, resulting in total 25 axial points of the EHD mesh in axial direction (a) and 15 EHD elements for each FEM element, resulting in total 91 axial points of the EHD mesh in axial direction (b)

It has been identified that the wear result is very dependent of EHD Mesh. At the beginning 25 axial × 361 radial was selected, what it was right for ring wear calculation. This proved not enough as shown for the liner wear in Figure 12b. Consequently, the core of the simulation work was performed for 91 axial × 361 radial, in order to get good accuracy.

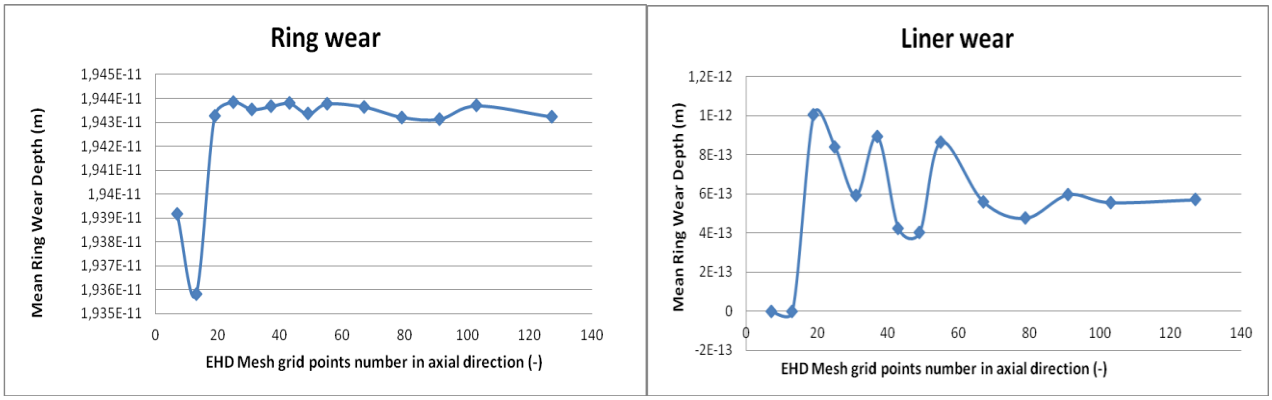

(a) **(b)**

Fig. 12. EHD mesh grid points related to wear calculation. Wear of Ring (a), Wear of Liner (b)

4.3 Model outputs

The main outputs given by the calculation, and selected for the validation and evaluation of this work are:

- Minimum oil thickness in the contact
- Asperity and Hydrodynamic Friction Power Loss
- Asperity contact percentage
- Peak pressures: asperity contact pressure, oil film pressure, total pressure
- Shear stress (Hydrodynamic and Asperity)
- CoF = Friction Force / Load
- Wear mass = average wear height × total area × specific mass

These parameters have shown that the contact is mainly influenced by the asperities with almost no Hydrodynamic influence. In consequence, the wear and coefficient of friction are influenced by the oil only

at micro-Hydrodynamics. Figure 13 shows some of these results. The X axis (0-720º) in this figure refers to 2 full cycles of translational movement, so travelling 4 times the stroke. The relationship between Hydrodynamic and Asperity Friction Power Loss (Figure 13 a) shows that almost nothing is related to Hydrodynamics, since green curve is all over the cycle at 0W, while Asperity Friction (blue) and Total Friction (red) Power loses are superposed. Asperity contact percentage (Figure 13 b) was 6.4%.

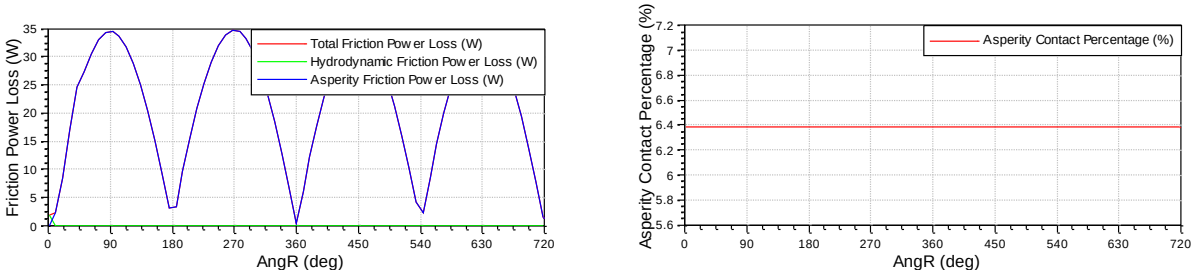

(a) **(b)**

Fig 13. Friction Power losses (a) and asperity contact percentage (b)

4.4 Comparison between experimental and model results

The coefficient of friction during the simulated cycle of reciprocating movement changes from a maximum (input based on experimental data) when the speed is cero to a minimum value when the speed is higher during the movement along the stroke. A more hydrodynamic lubrication will represent a higher reduction of friction coefficient for the values at higher speed.

The measured friction forces in this project have a low resolution since the data recorded is the average during 12 hours. To correlate the friction coefficient behaviour during a cycle, a higher resolution friction force data were taken from another tribometer working at similar conditions. The qualitative correlation was good as shown in Figure 14, meaning that the lubrication regime has been modelled correctly.

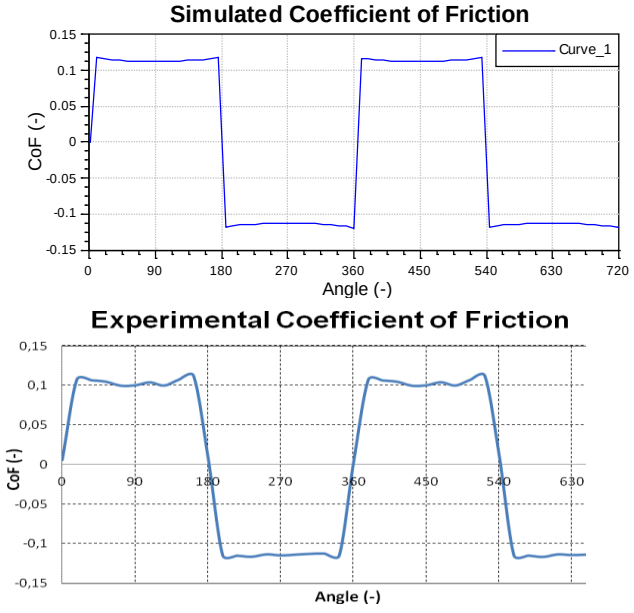

(a) **(b)**

Fig. 14. Friction coefficient resulted in simulation (a) Friction coefficient resulted at high CoF resolution tribotests (b)

During model tests it is important to notice that the mean friction coefficient is used as input for initial friction coefficient (CoF=0.13 in Figure 14, which refers to the standard non coated case). In the test result shown in Figure 8, even if the mean values is 0.13 a lower value of the friction coefficient was recorded at the beginning of the test (0.042), which has been referred to the formation of a tribofilm that reduces the friction coefficient when enough lubricant is on the contact and additives are still working. This region can be related to an engine working conditions where oil is continuously supplied and additives would not be vanished.

Regarding *wear*, the calculated data match well with the experimental data (Table 5), achieving in general errors in the range of 5%. The experimental differences shown for different materials, roughness´s or oil types from a chemical point of view are included in the wear factor, and the calculated wear have been found to be strongly dependent on this factor.

Table 5. Simulation results compared to Quantitative experimental Wear. (Negative value is due to mass increase due to adhesion, instead positive values correspond to mass loss due to abrasion phenomena)

	Ring wear (mg)		Liner wear (mg)		Error (%)	
	experiment	simulation	experiment	simulation	ring	liner
DLC_B03+Fine Honing+15W40	0.02	0.019	0.15	0.156	4.91	4.01
CrN_1+Fine Honing+15W40	0.05	0.048	2.44	2.470	4.92	1.35
CrN_2+Fine Honing+15W40	0.22	0.208	15	13.04	5.53	13.05
MoS_2+Fine Honing+15W40	0.10	0.094	0.45	0.460	5.58	2.4
Standard+Fine Honing+5W30	0.02	0.019	0.46	0.477	4.92	3.76
Standard+Plateau Honing+5W30	-0.04	-0.038	1.60	1.670	4.05	4.44

In Figure 15 wear scar on the actual piston ring and the calculated wear scar are shown, in order to evaluate qualitatively the wear of them. The images of the different wear scars of ring and liner of the different alternatives have been inspected. Good correlation was found of both width and length wear scars between experiments and simulations for all the cases.

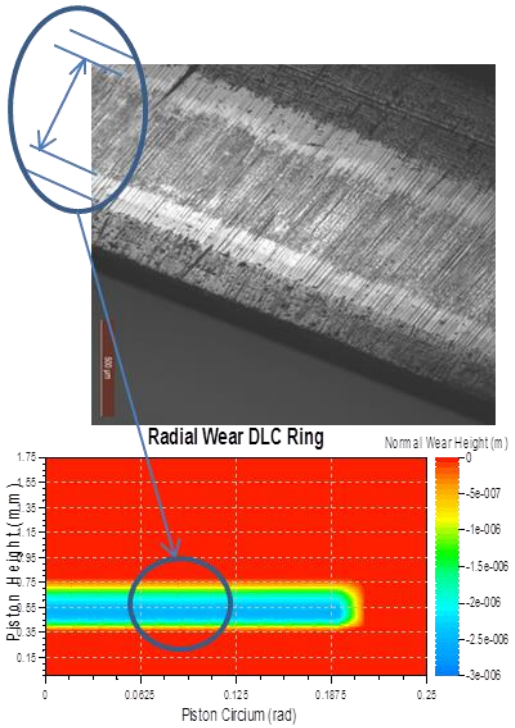

Fig. 15. Qualitative comparison between simulation results and experimental wear for the DLC coating

4.5 Effect of surface roughness

To include the roughness effects, the Micro Slide Analysis tool is used. It gives for a pair of surface roughness´s the relation between the separation (*Hs*) and the contact pressure or the real contact area. This tool gives additional information related to the Hydrodynamics via Flow Factors, detailed elsewhere [27]. See Figure S1 in supplementary materials for the definition of different variables.

One of the outputs of the model is the real contact area through contact of body asperities. All the studied cases resulted in asperity contact percentage of 6.4%. In Figure 16b it is possible to see the relation between this contact ratio and the separation *Hs* between the two contact bodies (liner honing's and different ring surfaces). Once the separation is obtained for each case, in Figure 16a the relationship between contact pressure and *Hs* separation gives the value of the overall contact pressure.

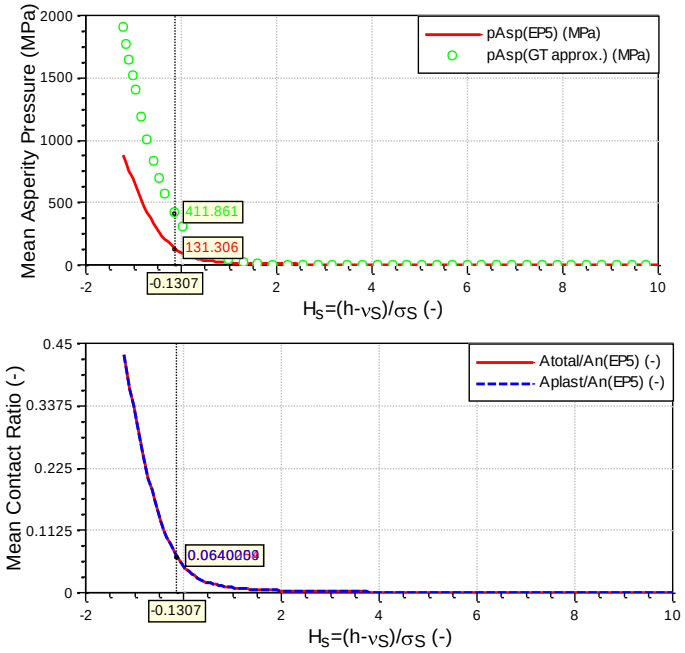

(a) **(b)**

Fig. 16. Relation between the separation and contact pressure related to the model (EP5, in red) and according to Greenwood Tripp approximation (GT, in green) (a), and between the separation and the real contact area to nominal area ratio (b)

This workflow has been repeated for some case studied, and results are shown in Table 6.

Table 6. List of input parameters

	Contact Ratio (-)	*Hs* (-)	Pressure (MPa)
standard ring - plateau honing	0.064	(-)0.131	131.306
standard ring - fine honing	0.064	(-)0.138	131.391
DLC ring - plateau honing	0.064	0.185	131.683
DLC ring – fine honing	0.064	0.155	131.973
CrN ring - plateau honing	0.064	0.141	130.69
CrN ring - fine honing	0.064	0.101	130.9

It is concluded, that the influence of roughness on wear is not due to a higher contact pressure since a similar contact pressure was observed for fine and plateau honing. The reason seems to be related with the lubrication effectiveness for various surface structures, which is taken into account only through the *wear factor*.

The pressure distribution is also affected by the ring profiles that are the same at the beginning of the test for all cases. In each case different wear factor were used, therefore, the wear profiles were updated during simulation resulting in varying contact pressure in each EHD cell.

5 Conclusions

Piston rings coated with various coatings showed good performance in tribotests. DLC coatings yielded the lowest friction and wear rate among the studied coatings. It was found that when 5W30 oil was used for lubrication a protective tribolayer was spontaneously formed on uncoated rings. This layer with antiwear properties was responsible for significant friction reduction. The most probable precursors of the tribofilm were the components of mating surfaces and the oil additives including zinc dialkyl dithio phosphate and molybdenum dialkyl dithiocarbamate. Regarding the liner surface finishing, it didn't show significant influence on friction and wear under boundary lubrication. It could have some influence on friction under hydrodynamic conditions, which, however, were not studied in the present work, since the most critical wear is generated at the Top dead center.

A model of the pin-on-disc reciprocating tests was developed. The qualitative evolution of the friction coefficient during a cycle and the regime modeled were validated. The values of the friction coefficient were compared with the experimental friction coefficient for boundary lubrication showing good correlation between them. The results of the simulated wear tests match well the experimental data, both qualitatively and quantitatively. Increase in roughness during wear didn’t lead to increase in a contact pressure, but it influenced the lubrication effectiveness.

Some conclusions related to the ring/ liner contact that were obtained by simulation as well as recommendations for using AVL Excite software as a tool for friction and wear simulation are shown in Table 7.

Table 7. List conclusions and recommended actions when using AVL Excite for friction and wear simulation

	Conclusions	**Recommended actions**
1	Changing the surface finishing from plateau to fine honing, doesn´t has influence on contact pressure. The influence of the change in texture and roughness is in oil distribution or oil retention capacity.	The latter effect is taken into account using **the wear factor**
2	Asperity friction and wear model constants default parameters have been validated for the studied cases.	If it is necessary to validate them for further projects, it is possible to rely on detailed CoF measurements for 1 cycle.
3	The wear factor of Liner and Ring is for a unique pair. If it changes the Ring material or roughness, it is necessary a new value for Liner and Ring wear factor value.	Create a **wear factor library of material pair, oil type, roughness** combinations based on tribotests.
4	In boundary lubrication, the friction coefficient is very dependent on material type and lubricant characteristics (viscosity, thermal resistance,	Create a **coefficient of friction library of material pair, oil type** combinations based on tribotests. If possible for material pair, oil type, roughness

	additives). Also influences a bit the type of honing, but it is not as much as in wear behaviour.	combination. Use the CoF value in the moment when additives are still active.
5	EHD Mesh has influence in wear calculation. To have accurate values is important to check at what values, steady state is achieved.	Use around 100 grid points in axial direction and 360 in radial. Take into account to have coincidence between ring grid point and EHD grid points in axial direction (as Figure 8). Alternatively check for the steady state in the studied model.
6	The wear rate at the beginning of the test, is much higher than after a running in, where a linear steady state is reached.	The resolution in wear time steps for wear accumulation calculation have to be higher at the beginning. In the tribometer model for 12 hours was: 0.6, 1.5, 3, 9, 18, 36 min, 1, 2, 4, 6, 12h

ACKNOWLEDGEMENTS

The authors acknowledge the European Commission for funding of the European Project "Powerful" under Contract 234032.

REFERENCES

[1] Tian T. Dynamic behaviours of piston rings and their practical impact. Part 1: Ring flutter and ring collapse and their effects on gas flow and oil transport. Proceedings of the Institution of Mechanical Engineers, Part J: Journal of Engineering Tribology. 2002;216:209-28.
[2] Tian T. Dynamic behaviours of piston rings and their practical impact. Part 2: Oil transport, friction and wear of ring/liner interface and the effects of piston and ring dynamics. Proceedings of the Institution of Mechanical Engineers, Part J: Journal of Engineering Tribology. 2002;216:229-48.
[3] Kapsiz M, Durat M, Ficici F. Friction and wear studies between cylinder liner and piston ring pair using Taguchi design method. Advances in Engineering Software. 2011;42:595-603.
[4] Profito FJ, Tomanik E, Zachariadis DC. Effect of cylinder liner wear on the mixed lubrication regime of TLOCRs. Tribology International. 2016;93, Part B:723-32.
[5] Mezghani S, Demirci I, Yousfi M, El Mansori M. Mutual influence of crosshatch angle and superficial roughness of honed surfaces on friction in ring-pack tribo-system. Tribology International. 2013;66:54-9.
[6] Tomanik E. Modelling the hydrodynamic support of cylinder bore and piston rings with laser textured surfaces. Tribology International. 2013;59:90-6.
[7] Keller J, Fridrici V, Kapsa P, Huard JF. Surface topography and tribology of cast iron in boundary lubrication. Tribology International. 2009;42:1011-8.
[8] Morris N, Rahmani R, Rahnejat H, King PD, Fitzsimons B. Tribology of piston compression ring conjunction under transient thermal mixed regime of lubrication. Tribology International. 2013;59:248-58.
[9] Igartua A, Fernández X, Areitioaurtena O, Luther R, Seyfert C, Rausch J, et al. Biolubricants and triboreactive materials for automotive applications. Tribology International. 2009;42:561-8.
[10] Igartua A, Fernandez X, Woydt M, Luther R, Illaramendi I. Tribological Tests to Simulate Wear on Piston Rings. In: Lakshminarayanan PA, Nayak NS, editors. Critical Component Wear in Heavy Duty Engines. Singapore: John Wiley & Sons Ltd.; 2011. p. 167-95.
[11] Igartua A, Nevshupa R, Fernandez X, Conte M, Zabala R, Bernaola J, et al. Alternative eco-friendly lubes for clean two-stroke engines. Tribology International. 2011;44:727-36.

[12] Igartua A, Fernandez-Pérez X, Illarramendi I, Luther R, Rausch J, Woydt M. Biolubricants and Triboreactive Materials for Automotive Applications. In: Carmo JP, Ribeiro JE, editors. New Advances in Vehicular Technology and Automotive Engineering. Zagreb: Intech; 2012. p. 119-46.
[13] Fedrizzi L, Valentinelli L, Rossi S, Segna S. Tribocorrosion behaviour of HVOF cermet coatings. Corrosion Science. 2007;49:2781-99.
[14] Johansson S, Nilsson PH, Ohlsson R, Rosén B-G. Experimental friction evaluation of cylinder liner/piston ring contact. Wear. 2011;271:625-33.
[15] Truhan JJ, Qu J, Blau PJ. The effect of lubricating oil condition on the friction and wear of piston ring and cylinder liner materials in a reciprocating bench test. Wear. 2005;259:1048-55.
[16] Martinez L, Nevshupa R, Felhoes D, de Segovia JL, Roman E. Influence of friction on the surface characteristics of EPDM elastomers with different carbon black contents. Tribology International. 2011;44:996-1003.
[17] Spencer A, Almqvist A, Larsson R. A semi-deterministic texture-roughness model of the piston ring–cylinder liner contact. Proceedings of the Institution of Mechanical Engineers, Part J: Journal of Engineering Tribology. 2011;225:325-33.
[18] De Barros Bouchet MI, Martin JM, Le Mogne T, Bilas P, Vacher B, Yamada Y. Mechanisms of MoS2 formation by MoDTC in presence of ZnDTP: effect of oxidative degradation. Wear. 2005;258:1643-50.
[19] Rusanov A, Nevshupa R, Martin J-M, Garrido MÁ, Roman E. Tribochemistry of hydrogenated amorphous carbon through analysis of Mechanically Stimulated Gas Emission. Diamond and Related Materials. 2015;55:32-40.
[20] Lenauer C, Tomastik C, Wopelka T, Jech M. Piston ring wear and cylinder liner tribofilm in tribotests with lubricants artificially altered with ethanol combustion products. Tribology International. 2015;82, Part B:415-22.
[21] De Feo M, De Barros Bouchet MI, Minfray C, Le Mogne T, Meunier F, Yang L, et al. MoDTC lubrication of DLC-involving contacts. Impact of MoDTC degradation. Wear. 2016;348–349:116-25.
[22] Morina A, Zhao H, Mosselmans JFW. In-situ reflection-XANES study of ZDDP and MoDTC lubricant films formed on steel and diamond like carbon (DLC) surfaces. Applied Surface Science. 2014;297:167-75.
[23] Berkani S, Dassenoy F, Minfray C, Belin M, Vacher B, Martin JM, et al. Model formation of ZDDP tribofilm from a mixture of zinc metaphosphate and goethite. Tribology International. 2014;79:197-203.
[24] Komori K, Umehara N. Effect of surface morphology of diamond-like carbon coating on friction, wear behavior and tribo-chemical reactions under engine-oil lubricated condition. Tribology International. 2015;84:100-9.
[25] Greenwood JA, Tripp JH. The Contact of Two Nominally Flat Rough Surfaces. Proceedings of the Institution of Mechanical Engineers. 1970;185:625-33.
[26] Patir N, Cheng HS. Application of Average Flow Model to Lubrication Between Rough Sliding Surfaces. Journal of Lubrication Technology. 1979;101:220-9.
[27] Mahmoud KG, Knaus O. Micro Contact Analysis in Hydrodynamic Joints. 5th World Tribology Congress (WTC 2013) Proceedings of a meeting held 8-13 September 2013, Torino, Italy. Torino: Politecnico di Torino (DIMEAS); 2013. p. 173-6.

8.2 On the nature of high pressure die casting die failures

B. Zabalaa*, A. Igartuaa, F. Paganoa, M. Contea, Harald Eibischb, Ruben Heidc

a) IK4-TEKNIKER, Tribology Department

b) AUDI AG Ingolstadt, Technologieentwicklung Gießen

c)Technische Universität Braunschweig, Institut für Füge- und Schweißtechnik

e-mail: borja.zabala@tekniker.es

ABSTRACT

High pressure die casting (HPDC) is a single step and high production rate manufacturing process of light alloy castings. The resulting pieces have close dimensional tolerances and smooth surface finish. HPDC is a very cost efficient method, however, the maintenance and initial costs of the mould (around 20% of the total) limits the competitiveness of the process seriously.

Another limit is due to wear of the devices, therefore, a better understanding of the wear mechanisms nature and the main parameters affecting them are needed.

In this document, the main wear mechanism related to HPDC, such as thermal fatigue, erosion, die soldering and corrosive wear are analyzed according to literature.

Keywords: die failure, thermal fatigue, die soldering, erosion, corrosion, washout

INTRODUCTION

HPDC is an important metallurgical process for the production of complex metallic pieces. The molten metal is forced, under high pressure, to flow through some ducts and to fill a mould with the finished shape. Since the operational temperature should be over the melting point, it is easier to use this technique for metals with relatively low melting point. Typical metals used for HPDC are aluminium or magnesium but there are also many other non ferrous materials that could be used as zinc, tin, etc.

The die casting process is characterized by four main steps: - Die preparation: the cavity of the mould is prepared by spraying a water-based lubricant that has two main functions. It facilitates the removal of the piece from the mould and it helps in the operation of cooling the mould.- Filling: the melted metal is injected into the mould with an extremely high pressure between 20 MPa and 100 MPa. In these conditions the melt can enter in the die cavity with speed of 60 m/s in the area of the gate [Modern High Pressure Die-casting Processes for Aluminium Castings]. The pressure is maintained until the casting has reached a proper solidification condition.- Ejection: the castings are ejected thanks to ejector pins.- Shakeout: the different parts of the casting are separated and the scrap is removed (gate, runners, sprues and flash) [1].

Permanent moulds (dies) are usually made of hard materials, such as tool steels, and should endure several hundreds of thousands of casting cycles They are subjected to harsh working conditions like high temperatures (up to 715ºC), high injection velocities (up to 60m/s) and chemical attack by molten alloys. Die-casting dies are prone to surface damage, what influence the resulting casting quality or even force to stop the production process. Visual inspection of damaged mold allowed identifying the most common failure mechanisms. Even if they are connected to each other's, here following a short list is proposed:

1. Thermal fatigue: Cracks generated due to alternate heating and cooling of the die during the die-casting cycle. Involves two different failure types named heat checks and corner cracking.
2. Erosion wear: Loss of material due to mechanical interaction between surface and the casting fluid flow. An extensive erosion wear does not allow die soldering to develop. Involves three different failure types: liquid impingement erosion, solid particle erosion and cavitation erosion.
3. Die soldering: Intermetallic chemical and mechanical reactions in the die surfaces generating adhesion of the casting fluid to the die.
4. Corrosion wear: Diffusion or dissolution of the die in the melt.

There are less common catastrophic failures due to thermal shocks (gross fracture) or over-heating of die material, which causes instability of mechanical properties [2]. It is commonly used the term washout to refer a combination of mechanical and chemical wear, so contribution of erosion, die soldering and corrosion.

Material washout is mainly observed in regions close to the ingate where high melt velocities are achieved.

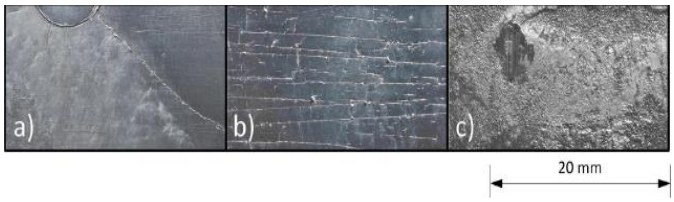

Fig 1. Detailed picture from tension cracks (a), heat checks (b) and washouts (c). [3]

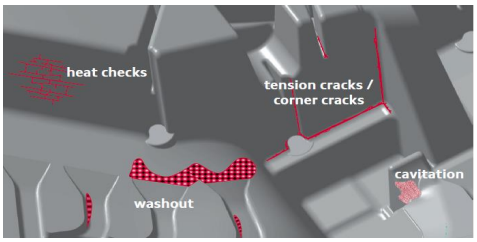

Fig. 2. Schematic picture of the different damage in a die. [3]

1 THERMAL FATIGUE

Thermal fatigue cracking is a major mode of failure of hot working tool steel dies in die-casting and forging applications. In literature, two different failure groups have been identified ([2], [4], [5]): *Heat checks* and *corner cracking.*

HEAT CHECKS

Heat checks are normally observed on the flat die surface, where normally stress concentration does not take place. Because of the large thermal gradients, during heating, the die steel surface is under compression and it is in tension during cooling. This leads to die surface cracks, which are popularly known as 'heat checks'. The direction of cracking depends on which component of strain is dominant, but could exist a point in the die where there are two directions of maximum strain because of symmetry, thus the cracking can occur in both directions [2]. This phenomenon deteriorates the surface but can also initiate crack propagation, leading to gross failure of the die. An example of thermal fatigue cracks in a large transmission die is shown in figure 3:

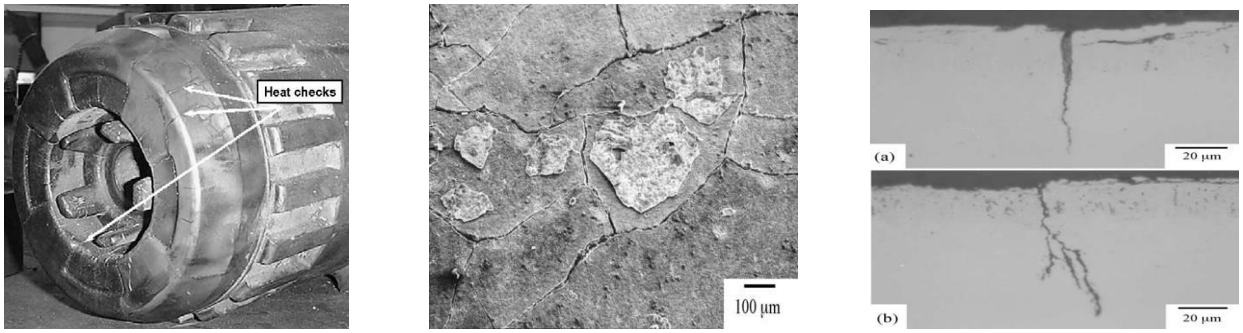

Fig.3. a) Cracks in transmission die [2], b) surface cracking detail [5] and c) polished cross-section revealing typical thermal cracks [5]

CORNER CRACKS

Cracks may appear in corners, in presence of sharp edges or abrupt transitions.

Corners are more susceptible to crack. At corners like in the figure 4b, cracking can take place in two directions, perpendicular to the edge, because of cyclic strain in direction 1, and along the edge (dotted line) because of cyclic strain in direction 2. In most of the laboratory tests, cracks perpendicular to the edges are observed more often.

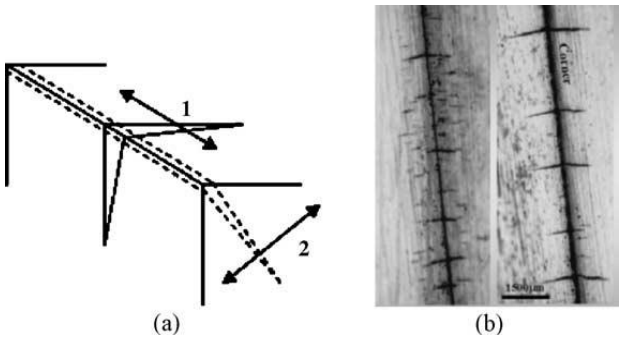

Fig. 4. (a) Schematic of crack direction and stress direction and (b) corner cracking.[2]

In serial production dies, it is observed corner cracks:

- In positive edges, they can be found just perpendicular to the edges.
- In negative edges, they can appear both along the edges and perpendicular to the edges.

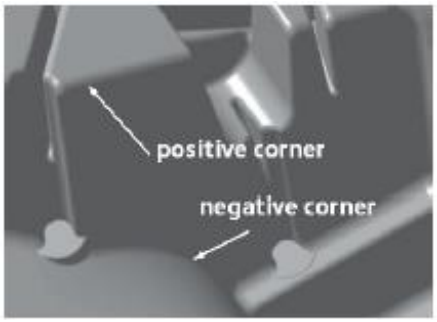

Fig. 5.- Corner cracks observed in serial production dies. [6]

DEFECT GENERATION

The formation of thermal cracks can be divided into three stages; (1) nucleation, (2) initial growth, and (3) crack propagation. [4]

(1) The crack nucleation is associated with the accumulation of the local plastic strain in the surface material due to fatigue cycles. During the hot phase of the die casting cycle, high compressive stresses are produced in the surface material. The temperature in the surface is higher than in the bulk, subsequently the material does not expand homogeneously leading to deformations in the plastic region. In general, compressive stresses avoid crack nucleation and crack growth.

Instead, at working temperature a local plastic deformation occurs as a consequence of exceeding local material yield strength. During the cold phase of die casting cycle high tensile stresses are produced on the surface of the material, increased by their plastic deformation. When these stresses exceed the local yield strength and sometimes ultimate tensile strength of the surface material at working temperature, failure is produced.

Crack nucleation could be also due to aluminum alloy soldering to the mold surface, followed by the material washout, since it could produce sharp surface corners with subsequent stress concentration and crack nucleation.

(2) At cyclic loading, low cycle fatigue occurs, producing nucleation and initial crack growth (i.e not big enough to have influence of the melt introduction of crack surface oxidation). This behaviour could be simulated by classical low cycle fatigue Coffin-Manson equation or an equivalent one.

(3) Crack propagation is facilitated by cast material infiltration into the cracks, by oxidation (due to the presence of oxygen in high temperature environment) of the working surface and surface of the crack, and by softening of the tool material due to tempering or aging of surface layer.

- During the cold phase of the cycle, the presence of nitrogen and aluminum alloy inside the cracks increases the tension at the crack tip, causing the growth of cracks.

- The oxide layer has lower thermal expansion, higher volume and fragility than the mold material. Oxides may be formed from iron, aluminium, silicon, cobalt or nickel, in case of maraging steels.

- The undesired softening also affects to material yield strength causing rapid progression of the crack length to a depth of soft layer. Another reason for rapid crack length growth is the local stress relive of areas along the thermal cracks, which delays the growth of adjacent cracks as larger once propagate into the tool material.

2 EROSION WEAR

Erosion is a progressive loss of material from solid surface due to the mechanical interaction between that surface and impinging fluid flow, resulting in washout of the die surface. [7]

Erosion begins in the die with the physical removal of the lubricant and natural oxide film, but once the iron is exposed directly to the melt, it dissolves into aluminum (corrosion) or solidifies into an intermetallic compound. This is the onset of soldering. Experimentally it is difficult to pounder how much damage is due to erosion and how much is caused by soldering or corrosion, or to measure directly the erosion.

According to literature, three main mechanism of erosion involved in die casting can be recognized: Liquid impingement erosion, solid particle erosion and cavitation erosion.

LIQUID INPINGEMENT EROSION AND SOLID PARTICLE EROSION

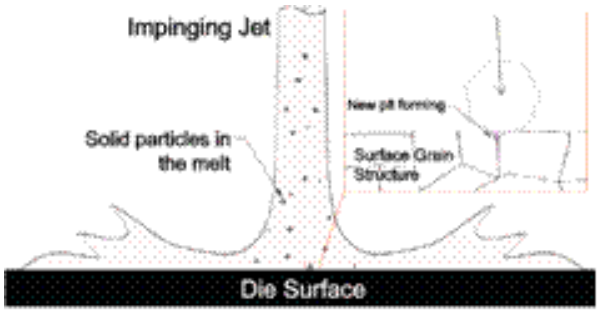

Fig 6. Representation of high angle impinging jet molten aluminum, and (Inset) pit formation through erosive wear and local deformation [8]

Liquid impingement erosion has been defined as "progressive loss of original material from a solid surface due to continued exposure to impacts by liquid drops or jets"[9]. Sometimes the fluid can contain also solid particles that could increase the erosion rate (Figure 6).

Research on liquid impingement erosion have been conducted using liquid impact velocities much higher than the upper end of the filling velocities usually used in HPDC [10]. It could be expected a quadratic/cubic dependence between wear and velocity.

Erosion rate due to a continuous melt jet can be from one to five orders of magnitude lower than that due to the same quantity of liquid impinging at the same velocity but in the form of droplets.

Hardness is one of the key properties a material needs to resist this type of erosion, and the ingate is often the most damaged zone. H13 is the most popular and most versatile hot work tool steel providing a good balance of toughness, heat check resistance and high temperature strength in addition to moderate wear resistance. It may BE used for tool temperatures up to about 1000ºF and it is useful to examine the hardness of H13 and melt metals (silicon, aluminum) particles at temperatures relevant to die filling (30HRc *vs* <20HRc). In Figure 7, it can be seen the ranges of temperatures corresponding to mentioned hardness.

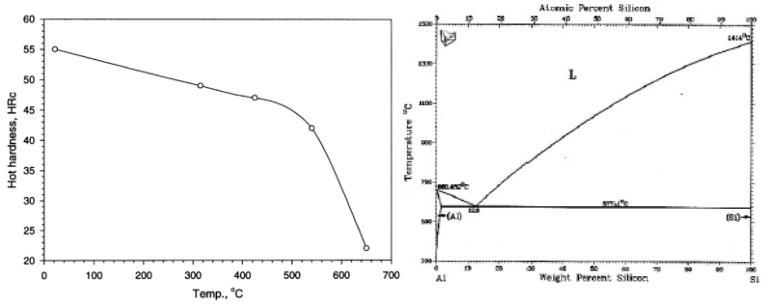

Fig 7. Evolution of hardness of H13 in function of the temperature and Al-Si phase diagram.[10]

Repeated impacts may result in erosion in a long-term through fatigue-like phenomena but it may require a long incubation stage for both impingement and solid particle erosion. Analysis based on existing theories on erosion has suggested that severe forms of liquid impingement and solid particle erosion are not likely to occur in HPDC, before soldering develops (short-term). However, the mechanisms of long-term erosion in HPDC are not well understood.[10]

CAVITATION EROSION

Any device handling liquid can be subjected to cavitation. Local pressure falls below saturated vapor pressure causing cavitation to occur. Resulting vapor bubbles collapse on surface material with high energy and heat. The casting metal vapor pressure could be around pure aluminum vapor pressure (2.42E-06Pa at 660°C [11]).

In HPDC, a sudden change of pressure is experienced due to melt flow direction changes generating pressure variations and cavitation. In figures 8, 9, 10 are represented some examples of these failures.

These phenomena (pitting, breakout, erosion and washout) may also occur on the high pressure side where the melt hits directly on the surface. [3]

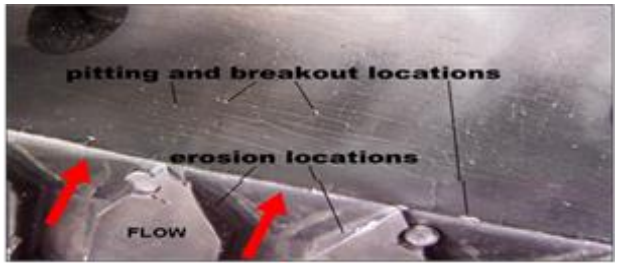

Fig 8. Breakout, erosion, and washout appears in the opposite locations of where they would be expected - on the low pressure side of the flowing liquid. [11]

Fig 9. Typical Cavitation phenomena in High Pressure Die Casting of Aluminium Dies [6]

Fig 10. Exhibited sheet or cloud and vortex cavitation effect [11]

Thermal fatigue can lead to breakout without incipient inertial cavitation, but breakout lead to heat checking of the die's surface [11]. The last can lead also to die soldering.

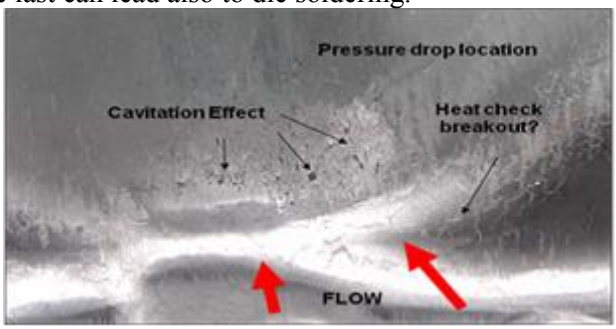

Fig 11. Cavitation effect exacerbates itself when lower vapor pressure develops from the disrupted flow patterns [11]. This kind of failure could be also related to washout [3]

The calculation of the boundary conditions for the cavitation, specially the saturated vapor pressure of the liquid melt between 600 – 700 °C, have been considered in the reference [11] as:

Aluminum Vapor Pressure = 2,42E-06Pa@660°C (1220°F)

The available data are for pure aluminum in literature are the following:

Table 1. Vapor pressure of pure aluminium [12]

Temperature, ºC	Vapor Pressure, kPa
2517	100
2091	10
1781	1
1544	0,1
1359	0,01
1209	0,001

Despite the lack of data at lower temperature, it could be expected values around 10^{-6}Pa (see graph below that for 950ºC is 1.28E-06Pa). To calculate it could be used Antoine Equation:

$\log_{10}(P) = A - (B / (T + C))$
P = vapor pressure (bar)
T = temperature (K)),

The difficulty is to find the right constant for different aluminum alloys. The available data correspond to pure aluminum in the range between 1284-2056ºC:

Table 2. Antoine equation constants for pure aluminium [12]

Temperature (K)	A	B	C	Reference	Comment
1557. - 2329.	5.73623	13204.109	-24.306	Stull, 1947	Coefficents calculated by NIST from author's data.

3 DIE SOLDERING

The losses from soldering do not provoke such an important damage to the die as for example large cracking, but affect the die casting production seriously due to the interruption for cleaning (remove chemically, re-melt or mechanically polished) and ejection problems (more force is needed to separate a soldered casting, or bent/broken pins).

Die soldering can be subdivided in two categories: mechanical and metallurgical-chemical.

Mechanical soldering takes place when sticking of the melt to the die happens after a few shots. Sticking is not related to any metallurgical-chemical reaction because there is not time/temperature to form intermetallic layers, but could be related either to high pressure or to an error in the design of the mould [13].

Metallurgical-chemical soldering is preceded by mechanical erosion since chemical interactions between the die and the melt are possible only when any protective skin layer separating the die surface from the melt (including iron oxide film and lubricant, or coating) is removed by erosion. Reactions between the melt and the die substrate are responsible for the die corrosion. These interactions could be due to the dissolution of iron of the die material into the melt or to the cast alloy elements diffusing into the die. As result, intermetallic layers are formed on the die surface like shown in figure 12.

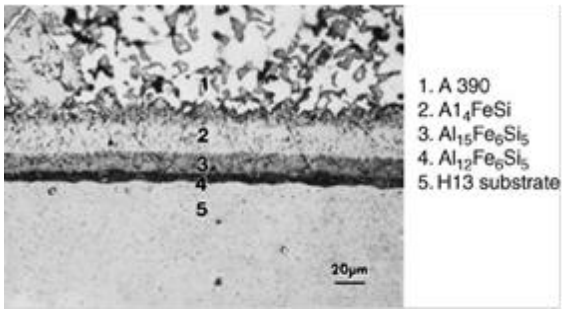

Fig 12. Intermetallic layers formed after dipping H13 steel for 2 hours in liquid aluminum (390) at 680 ºC [14]

The resulting formation of a layer of the cast alloy that occurs on the interface is called soldering. The distinction between corrosion and soldering has its roots in the die-casting engineering practice. The term corrosion emphasizes the undesirable removal of the die material due to a chemical deterioration of the die surface, while soldering refers to the effect of adhesion (sticking) of cast material to the die surface.

Several approaches to the modeling of die soldering have been suggested in literature based in damaged molds or laboratory tests at different temperature ranges, and most agree in that the diffusion processes on the die surface and the formation of the intermetallic layer play a major role in die soldering. Here, it is presented the most complete model found in literature, including both dissolution (corrosion) and diffusion (soldering) behavior, explained in 5 stages, in the absence of a oxide layer.[14]

Stage 1: During melt injection and solidification, diffusion of aluminum and iron atoms occurs to form $Fe_xAl_ySi_z$ intermetallic at the interface. Silicon changes the kinetic rate and the solubility of iron into aluminum.

Stage 2: A new die casting cycle begins and fresh melt enters the die cavity. The driving force for diffusion is slightly lower due to the presence of previous intermetallic layer. There is enough driving force for the

intermetallic layer to continue to grow. The driving force for dissolution in this stage is high but still lower than that for diffusion.

Stage 3: In the next cycle, the thickness of the $Fe_xAl_ySi_z$ intermetallic layer reaches a critical limit, the driving force for diffusion has decreased to become negligible and the driving force for dissolution becomes the dominating force. The soldering dissolves in the melt.

Stage 4: Mass loss has taken place on the die surface but is free of intermetallic layer. Driving force for diffusion increases due to loss of Fe_xAl_y to the melt but is still negligible compared to the driving force for dissolution. The driving force for dissolution decreases with increasing intermetallic thickness.

Stage 5: The cyclic process of soldering growth and dissolution continues while the die surface continuously loses iron to the melt.

The interesting schematic illustration of the die soldering mechanism proposed by Shankar and Apelian is presented [15].

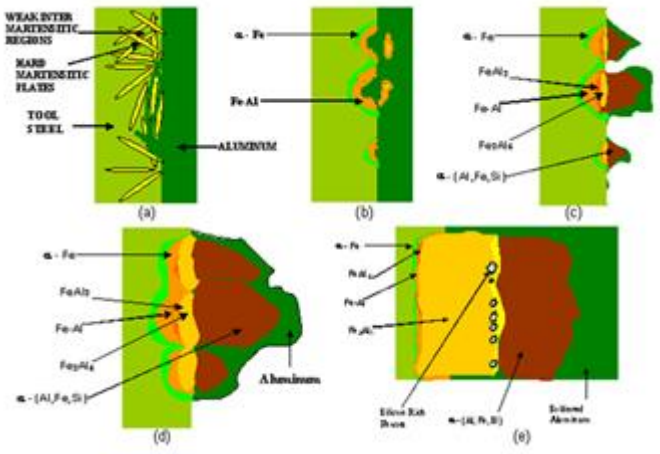

Fig 13. Modeling of die soldering [15]:

(a) Initial attack of the grain boundaries by aluminum to loosen up the hard grains and martensitic plates to cause pitting on the die surface.

(b) Formation of the iron-aluminum intermetallic phases inside the pits and around the broken grains close the die surface.

(c) "Pyramid' growth of the ternary -(Al,Fe,Si) phase on the pits over the -Fe2Al5. In addition, the pits expand laterally and in depth. Aluminum begins tostick after this layer structure is formed resulting in the beginning of soldering.

(d) Shows the growth of intermetallic layers and merging of neighboring pits. Molten aluminum encounters the die surface only through the cracks and gaps present between adjacent pits.

(e) Straightening out of the pits and closing of the gaps between the adjacent pits. The ratio of the intermetallic layer thickness and the soldered aluminum is ~1:5. The reaction mechanism becomes very slow. Silicon is precipitated in the grain boundaries of the -Fe2Al5 phase and at the intersection boundaries between the two intermetallic phase layers

4. CORROSIVE WEAR

As explained in the previous paragraph, corrosion means dissolution of the die material in the melt. In literature soldering and corrosion are not always separated. Although the behavior is already explained in the model of soldering it is important to clarify two aspects.

The high temperature corrosion (or oxidation) is the formation of an iron oxide layer with no chemical reaction and is beneficial to protect the die from damage.

The chemical (or electrochemical) corrosion is closely related with die soldering, and it could have also influence on thermal fatigue or erosion because of the changes of mechanical properties of the corroded die.

CONCLUSIONS

In this paper the main failure mode of the High Pressure Die casting dies have been defined according to most recent bibliographical data. There is created a classification of terms and tried to explain the nature of them. In the frame of the EU project MUSIC "MUlti-layers control & cognitive System to drive metal and plastic production line for Injected Components" the main wear mechanism of HPDC dies will be simulated in the laboratory in order to predict lifetime and find the best solutions to increase the durability of the molds and dies. This paper is the first step to achieve this objective.

ACKNOWLEDGMENTS

The partners would like to acknowledge the financing of the European Project MUSIC, under Contract FoF-ICT-2011.7.1.

REFERENCES

1. R. Shivpuri, M. Yu, K. Venkatesan, and K-L. Chu, "A Study of Erosion in Die Casting Dies by a Multiple Pin Accelerated Erosion Test". Journal of Materials Engineering and Performance, (1995) 4:145-153
2. A. Srivastava, V. Joshi, R. Shivpuri. "Computer modeling and prediction of thermal fatigue cracking in die-casting tooling". *Wear* 256 (2004) 38–43.
3. Ruben Heid, "IFS-Report", 8, Jahrgang, Ausgabe 1, Jahr 2013, Seite 6-9.
4. D. Klobcar, L. Kosec, B. Kosec, J. Tušek. "Thermo fatigue cracking of die casting dies". *Engineering Failure Analysis* 20 (2012) 43–53.
5. Anders Persson, Sture Hogmark, Jens Bergström. "Thermal fatigue cracking of surface engineered hot work tool steels". *Surface & Coatings Technology* 191 (2005) 216– 227.
6. Ruben Heid, "Unveröffentlichte" Untersuchung, Technische Universität Braunschweig, Institut für Füge und Schweiβtechnik, 2012**.**
7. Venkatesan K, Shivpuri R. "A study of erosion in die casting dies by a multiple pin accelerated erosion test". *J. Mater Eng. Performance* (1995) 4:145-153.
8. Zackery Gay. "Benefits of Surface Engineering for Aluminum die Casters". *Die Casting Engineering* (September 2012) 24-26.
9. ASM Handbook Volume 18, Friction, Lubrication, and Wear Technology, *ASM International* (1992) 221-231
10. Z.W. Chen, M.Z. Jahedi. "Die erosion and its effect on soldering formation in high pressure die casting of aluminium alloys". *Materials and Design* 20 (1999) 303-309
11. J.V. Skoff. "A New Approach to the Cause of High Pressure Die Steel Erosion", *Pitting, and Breakout*. NADCA Expo 2010, Paper T10-051.
12. NIST Chemistry web book.
13. K.Domkin, J.H.Hattel, J.Thorborg. "Modelling of high temperature and diffusion controlled die soldering in aluminum high pressure die casting", *Journal of Materials Processing Technology* 209 (2009) 4051–4061.
14. Joshi, V., Srivastava, A., Shivpuri, R. "Intermetallic formation and its relation to interface mass loss and tribology in die casting dies". *Wear* 256 (2004) 1232–1235.

15. Shankar, S., Apelian, D. “Investigation of Die Soldering Characteristics of Aluminum Die Casting Alloys”. *http://www.wpi.edu/academics/Research/ ACRC/index3.html* (2012).

8.3 Multiparametric study of Leidenfrost point and wettability of lubricants on high-pressure die-casting dies

Borja Zabala[a,c*], Amaya Igartua[a], Valeria Scarpis[a,b], Giulio Timelli[b], Frank Girot[c,d], Roman Nevshupa[e]

[a)] IK4-TEKNIKER, Parque Tecnológico de Eibar, C/Iñaki Goenaga 5, 20600 Eibar, Spain.
[b)] University of Padova, Department of Management and Engineering, Stradella S. Nicola 3, I-36100 Vicenza, Italy.
[c)] University of the Basque Country, UPV/EHU, Faculty of Engineering, Department of Mechanical Engineering, Alameda de Urquijo s/n, 48013 Bilbao, Spain.
d) IKERBASQUE, Basque Foundation for Science, Bilbao, Spain
e) Spanish National Research Council, Institute "Eduardo Torroja" (IETCC-CSIC), C/Serrano Galvache 4, 28033 Madrid, Spain
**Corresponding author Borja Zabala, Tel.: 0034943206744; E-mail: borja.zabala@tekniker.es.*

Abstract
This work is aimed at improving the lubricant film formation on the die surfaces in high-pressure die-casting (HPDC) pursuing enhancing cooling, temperature homogenization and casting release. An original test procedure was employed to study the Leidenfrost point (LFP) and the contact angle (CA) of various lubricants on die steel grades in the temperature range from 20 to 320 ºC. The effects of various parameters such as steel grade, surface roughness, ageing, temperature, droplet size, water hardness and lubricant concentration on LFP and CA were isolated and analyzed. It was found that the LFP remarkably increased for aged die surface with fine grains and relatively high roughness. The CA was affected mainly by the type of the lubricant. These findings lay the ground for optimal selection of the HPDC lubrication depending on the specific operating conditions.

Keywords
High-pressure die-casting; lubrication; Leidenfrost point; contact angle.

Highlights

- The contact angle (CA) depended mainly on the lubricant type and the die steel grade and varied with temperature
- The Leidenfrost point (LFP) was the highest for rough and aged H13 steel grade
- The Leidenfrost point was the highest for synthetic lubricant diluted in hard water at 3% and pulverized with a large nozzle
- Practical guidelines for effective multiparametric optimization of the CA and the LFP was developed

1. Introduction

High-pressure die-casting is a single step process producing accurate, thin-walled and very detailed light alloy parts at high productivity. Typically, molten light metal alloy (Al-, Zn-, Mg-based, etc.) is injected at high pressure into a steel die where it is solidified. After cooling down to certain temperature, the die is opened and the die casting is ejected mechanically [1].

Quality remains an important issue for HPDC, which parameters must be optimized to completely exploit its technological potential [2]. Usually during the casting cycle the temperature on the die surface can vary between 80 ºC and 500 ºC [4]. Various researchers argued that sharp changes of the die surface temperature and its uneven distribution can be the reason of thermal cracking, soldering and thermal distortions of the die as well as lamination, shrinkage, cold laps and other defects of the casting [2-5]. Controlling the die surfaces temperature during the lubricant spraying within a narrower band around 200 ºC [6] would be beneficial for increasing the useful die life and the surface quality of the casting. This also will contribute to reduce scrap, manufacturing cost and energy consumption [7]. For this purpose, lubricant is usually sprayed onto the inner contour of the die cavities at the beginning of each cycle pursuing to improve the temperature uniformity, create a film that facilitates the filling and the extraction of cast components (release agent) and, together with the surface oxide layer, prevent die soldering and adhesion [8].

Much effort has been focused on investigating the heat removal capability of lubricants sprayed onto a die casting dies [6, 9-11] as well as on the behaviour of drop splashing [12, 13]. The efficient heat transfer and wetting can be achieved at the temperatures below the Leidenfrost point (LFP) which serves as the temperature boundary between the transition and film boiling regimes [11, 14-16]. Various experimental investigations of the effects of droplet diameters and fluid properties on the Leidenfrost temperature of polished and nano/microstructured surfaces of aluminium, stainless steel, copper, nickel, silver and ceramics were carried out [10, 11, 17-21]. It was found that fluid properties, surface roughness of textured surface, and surface contamination were the most influential parameters for the LFP, whereas the surface roughness on the polished level and the contact angle (CA) had weak correlation with the LFP. The effect of additives and lubricant dilution on the LFP is not straightforward. Addition of surfactants to the lubricant can influence the dynamics of a bouncing droplet [18]. However, low dilution of lubricant provided lower heat transfer coefficient, than pure water [14]. The optimal formulation of the lubricant and its dilution must be experimentally found for each specific die casting conditions.
Increasing randomly distributed surface roughness is usually beneficial for both heat transfer and wetting on hydrophilic surfaces since it leads to biasing the LFP to higher temperature [11, 22] and decreasing the CA of hydrophilic surfaces, in accordance with Wenzel's model [23, 24]. It was also reported that the temperature of the LFP for superhydrophobic surfaces (CA>150º) could be significantly lower, than for hydrophilic ones (CA<90º) [25]. In contrast, developing regular microstructures on hydrophilic surface may notably reduce the LFP [26].
Among the parameters of the spray the following are the most relevant for controlling the heat flux removed: the dimensionless droplet Webber number (*We*), liquid Jacob number, volumetric flow rate, fluid composition, spray angle, droplet diameter, and subcooling [10, 27]. The Weber number being 12 times the ratio of the kinetic energy of a droplet to its surface energy [28], defines the breakup behaviour of liquid droplets impinging the hot surfaces. The following three general cases can be distinguished [25, 29]: $We<30$ – a droplet bounces without disintegration; $30<We<80$ – a droplet disintegrates in several fragments after bouncing; and $We>80$ – a droplet breaks up into smaller droplets while splashing on the surface. The dependence of the LFP on *We* is still under debate. Some authors argued that maximizing the *We* could be effective for shifting the LFP to higher temperature [25, 29, 30], whereas other reported little sensitivity of the LFP to the droplet velocity and *We* [19].
The analysis of the literature showed that the LFP and the CA being the indicators of the performance of spray lubrication depend non-linearly on the technological parameters. This considerably hinders optimization of spray lubrication since extrapolation of the available data, incomplete and mainly disembodied, is related with significant uncertainties. Therefore, in this study, the conditions at a liquid droplet/die material interface were experimentally simulated and the dependence of the LFP and the CA on various characteristics of the die surface (material type, roughness, temperature and ageing) and the liquid spray (lubricant type, dilution, water hardness and nozzle diameter) were isolated and analyzed. The obtained results lay the ground for the methodology of the optimal selection of the HPDC lubrication depending on the specific operating conditions.

2. Materials, experimental set-up and procedure

2.1 Materials

Five different concentrated HPDC lubricants in the form of 20-30 % emulsion were supplied by Motul-Baraldi and denoted hereafter as A, B, C, D and E, correspondingly. The lubricants contained oil blends, polysiloxanes, polymers and film forming additives. Emulsifiers and surfactants were added to stabilize the emulsion and to enhance the filming power on the die surface [31].

The B, D and E could be classified as semi-synthetic lubricants, since they contained mineral oil with viscosity index around 90. The A and C were synthetic lubricants with viscosity index approximately 180. The A and C had a very high releasing power and were intended for large weight die castings. The B was particularly indicated for thin-walled components of low weight, whereas the D and E were the general purpose HPDC lubricants.

The lubricants were prepared by dilution of the concentrates with water. The reference dilution rate was 1:50 (2%). Other dilution ratios between 1% and 20% were also screened.

Tap water (7.52 ^{o}dH German grade, 53.6 mg/l Ca^{+2}, <1 mg/l Mg^{2+}) and artificially prepared hard water (17.9 ^{o}dH, 96.8 mg/l Ca^{+2}, 18.7 mg/l Mg^{2+}) were used for dilution the concentrates.

Two common HPDC die steel grades – AISI H13 and H11 – were chosen for the study. The chemical compositions of the steel grades were determined using optical emission spectroscopy and are shown in Table 1. Both steel grades had very similar composition except V, which higher content in H13 leads to higher temperature resistance as well as higher resistance to wear and softening. Thermal conductivity and specific heat capacity: 28 W/(m K) and 460 J/(kg K), correspondingly, were also very similar for both steel grades as reported by the manufacturer. The steel samples were supplied quenched and tempered.

Table 1. The measured and nominal (according to AISI) chemical compositions (wt. %) of H13 and H11 steel grades

Steel grade		C	Si	Cr	Mo	V	Mn
H13	Nominal	0.39	1.00	5.10	1.35	0.90	0.40
	Measured	-*	0.91	4.85	1.33	0.96	0.35
H11	Nominal	0.38	1.00	5.10	1.35	0.40	0.40
	Measured	-*	0.99	4.90	1.20	0.31	0.40

* not measured by optical emission spectroscopy

2.2 Experimental set-up and procedure

A universal goniometer "SURFTENS" was used for the measurement of the LFP, the CA and the surface energy. This set-up based on the experimental device described by Nagai et al. [22] was modified to allow measuring both the LFP and the CA.

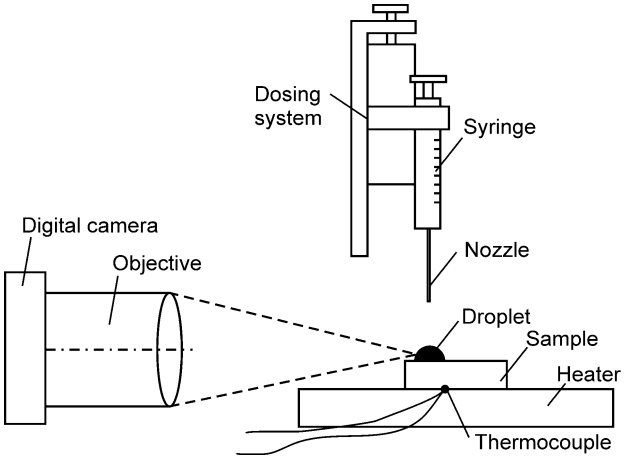

Fig. 1. The experimental set-up used for measuring the LFP and the CA.

The set-up (Fig. 1) consisted of a heater, a syringe with a connected nozzle and a dosing system. The sample was fixed to a hot plate of the heater, which temperature was controlled using a K-type thermocouple. The image of the droplet was acquired sideward using a digital camera. Two nozzles with the diameters of 0.5 and 0.9 mm were used.
For measuring the LFP the sample temperature was scanned in the range from 320 ºC doewn to 80 ºC in 20 ºC steps. At each fixed temperature a drop of the selected lubricant was let fall onto a fresh surface of the sample, while the boiling regime was analyzed using a camera. Then, a repeated experiment was done in a narrow temperature range with finer temperature steps. The lowest temperature in the studied range at which film boiling was observed was accepted as the Leidenfrost point. The uncertainty of the LFP was approximately ±0.5 ºC (for the temperature step of 1 ºC).
The CA was determined using a sessile drop method at three temperatures: 25, 50 and 80ºC. The CA was determined from fitting the droplet circumference at five points. Several images of the droplet were taken during 30 seconds after it was put on the surface. The mean value was determined averaging the CA obtained from various images of each droplet as well as between at least four repetitive tests.
The surface free energy of the die samples was determined using Wu's method [23] based on measuring the CA of distilled water (polar component) and diiodomethane (disperse component).
The surface tension of the lubricants at 2% dilution was measured using the du Noüy ring method (Krüss K20 Easydyne).
The Rockwell C Hardness was measured according to UNE-EN ISO 6508-1:2015.
The surface roughness was measured by a stylus profilometer "Perthometer M2". The R_a values were determined following DIN EN ISO 4288 and 4287 standards.

3. Results and discussion

3.1 Materials characterization

Table 2 shows the measured surface tension of the five lubricants at 2 % dilution. Even at such high dilution the surface tension of all lubricants was significantly lower than for pure water, which surface tension is 72 mN/m.

Table 2. Mean values and standard errors (±se) of surface tension of the lubricants at 2% dilution

Lubricant	Surface tension (mN/m)
A	48.7±0.60
B	53.2±0.66
C	35.1±0.43
D	33.9±0.42
E	31.5±0.39

The microstructure of the steel grades is shown in Fig. 2. Both steel grades had tempered martensitic structure. For the H11 few precipitated carbides were found. The H13 steel had finer grain structure, than the H11 grade. This could be the reason for the higher hardness of H13: 47 ± 1 HRC against 40 ± 1 HRC of the H11.

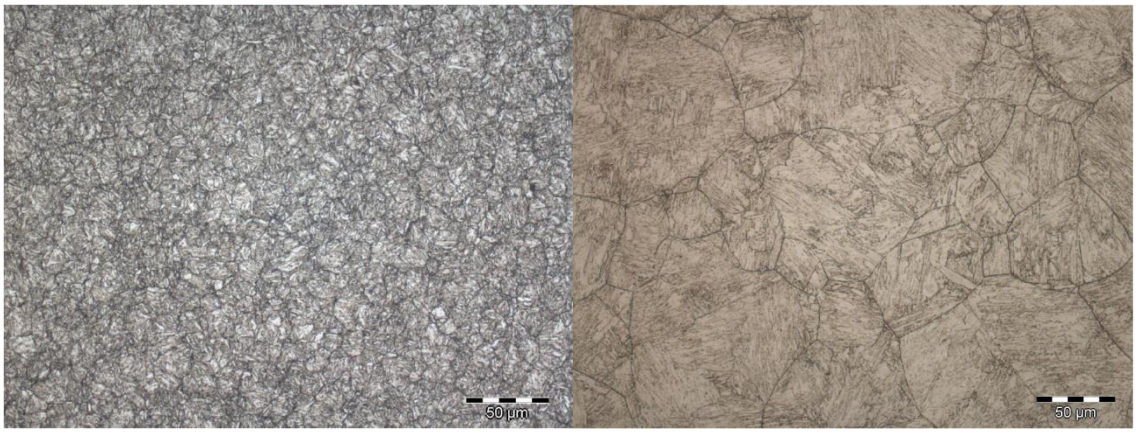

a) **b)**

Fig. 2. Microstructures of the steel samples: a) H13 and b) H11.

The effect of surface finishing and in-service conditions on the surface roughness, R_a, of a real HPDC die was studied pursuing adequate simulation of surface microgeometry in our experiments. The following three types of surface finishing of a new die were chosen: (*i*) electrical discharge machining (EDM), (*ii*) milling using two different tools referred to as "a" and "b" hereinafter, and (*iii*) polishing. In addition, two zones of the die which were subjected to 15000 casting cycles were analyzed: the one, where the metal flow was smooth, and another where the metal flow was turbulent. The results are summarized in Table 3.

Table 3. Roughness of the dies with surface finishing obtained using various methods as well as of the die subjected to 15000 casting cycles.

Surface finishing	R_a (µm)
EDM	2.02±0.04
EDM and milling (tool "a")	1.22±0.07
EDM and milling (tool "b")	0.80±0.12
EDM, milling and polishing	0.66±0.07
The die after 15000 casting cycles:	
zone of smooth flow	0.88±0.11
zone of turbulent flow	0.91±0.12

There are clear evidences that the die's roughness increased during the service life, and that this increase can be related with the severity of the operation conditions. On the basis of this analysis the R_a values of the samples for the simulation tests were selected between 0.02 and 1.8 µm.

In order to reproduce the real surface conditions of the die, the H11 and H13 samples were subjected to ageing for 5 hours at 600 ºC in normal atmosphere. The analysis carried out after the ageing did not reveal any notable variation in microstructure and surface hardness, but in surface free energy (Table 4). The polished samples of both steel grades had nearly the same surface free energy, whereas ageing led to different behaviour: for the H13 the surface free energy notably decreased, while for the H11 it slightly increased. The reason for this behaviour is not clear from this study and could be related with such factors as conceivable segregation of doping elements at the surface and microgeometry changing, among others.

Table 4. Surface free energy of polished and aged H13 and H11 steel samples

Steel grade	Surface finishing	Surface free energy (mJ/m^2)
H13	polished	39.9±0.49

H11	aged	23.3±0.29
	polished	40.7±0.50
	aged	46.3±0.57

3.2 The effect of temperature and steel grade

The behaviour of a bouncing droplet was screened for diluted lubricants and pure water at various surface temperatures in the wider temperature range from 320ºC down to 80ºC in 20°C steps. The *We* in this study varied between 9 and 64 depending on the surface tension of the liquid and the size of the droplet. The lower values corresponded to the lubricants A and B and the smaller droplet size. The findings of this preliminary experiment are the following:

- for both water and the lubricants the LFP was found in the range 140-160ºC;
- above the LFP, the film boiling regime and the droplet behaviour were similar for all lubricants and water;
- below the LFP, the droplets of the lubricants and of water had different behaviour after impinging the surface. The droplets of the lubricants flattened and spread on the surface. The CA decreased until the droplet evaporated. Water droplets did not spread, but maintained the shape with the CA nearly constant in time. This difference could be attributed to the additives and surfactants which adhere to the die surface and pin the droplet. This, apparently, enhanced the contact angle hysteresis at the receding phase. In addition, migration of the lubricants on the surface contributed to the spread of the droplets. Considering variations of the droplets size and shape, and in order to reduce data scattering, all the measurements were done during 30 s after putting the droplet onto the surface.

Then, an accurate measurement of the LFP was carried out in the temperature range from 140 to 160 ºC. Fig. 3 shows the LFP for the lubricants diluted in soft water on aged H13 and H11 steel grades.

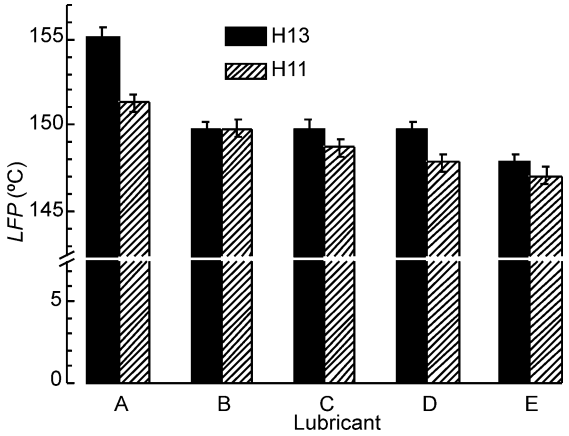

Fig. 3. The LFP for the lubricants dissolved in soft water on aged H13 and H11 steel grades.

For both types of the substrate the LFP decreased in the following order: A>B>C>D>E. The H13 steel grade samples yielded slightly higher LFP values for all lubricants. This could be due to the differences in the surface microstructure such as finer grain structure of the H13, since thermal properties of both steel grades were very similar. The variation in the LFP between the lubricants should be attributed to the compositional differences.

The dependence of the CA on surface temperature is shown in Fig. 4. At 20 ºC the mean CAs of the lubricants were in the range 44-67 and 38-47 degree for the H13 and H11 substrates, correspondingly. When temperature increased from 20 to 50 ºC the CAs of the lubricants showed different behaviour, although with certain tendency to decrease. When the temperature further increased to 80 ºC the CAs of all lubricants significantly decreased, while the E reached the minimal value of the CA among the lubricants. The higher CAs found for the H13 agreed with its lower surface free energy. The decrease in the CA with increasing temperature has been tentatively ascribed to partial water evaporation and the contact angle hysteresis.

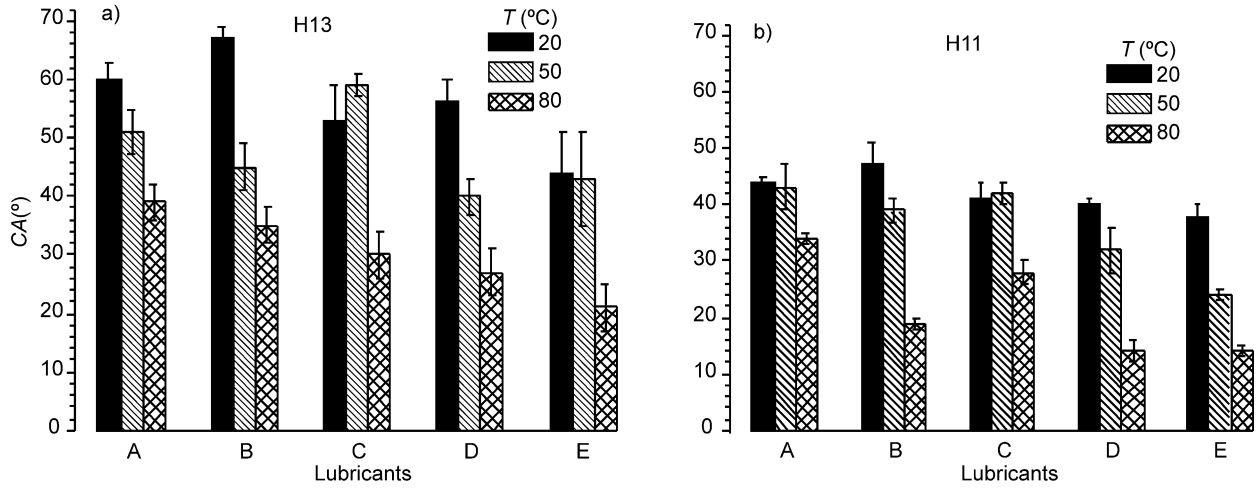

Fig. 4. The CA at 20, 50 and 80°C on (a) H13 and (b) H11 steel samples.

Fig. 5 shows the LFP of the five lubricants plotted against the corresponding CAs measured at various temperatures. For the H13 steel grade (Fig. 5 a) the LFP was not very well correlated with the CA at 20 and 50 ºC. At 80 ºC as well as at all temperatures for the H11, the data could be fitted by a linear function moderately well (R^2_{adj} in the range 0.5276 – 0.6006). The slope was positive in all cases and ranged between 0.15 and 0.38 ºC/degree. These results demonstrated that the LFP and the CA cannot be optimized individually through tuning the lubricant composition since improvement of the LFP (higher values) leads to worse wetting (higher CA).

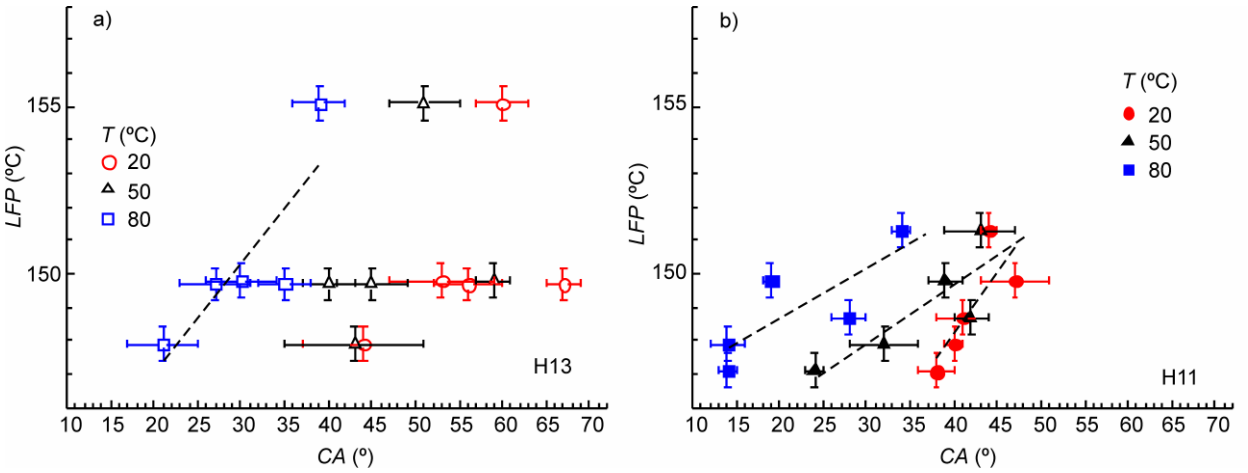

Fig. 5. The correlation of the LFP with the CA for steel grades: a) H13 and b) H11.

Notable decrease of the CA was observed during the 30 s after the droplet placement (Fig. 6). After the initial transition period the rate of the CAs decrease stabilized. This rate was influenced by temperature. Apparently, the decrease of CA of the lubricants could be due to the two processes. On the one hand, migration of the lubricant along the surface could lead to the deformation of the initial shape of the droplet and it's flattering. On the other hand, water evaporation, which should be especially intensive at 80 ºC, could produce receding of the pinned droplet. In order to evaluate the contributions of each of these two processes the measured data were fitted to the Tanner's model of the droplet spreading, which predicts that "the edge velocity is approximately proportional to the cube of the slope at the inflection" near the edge of the droplet [32]:

$$-\frac{1}{3}\ln\left(\beta(t)\right) \propto \ln(t), \quad (1)$$

where β is the slope, t is the time. The slope can be satisfactorily approximated by a tangent of the CA. The function $y = -\frac{1}{3}\ln(\beta(t))$ was calculated for the data shown in Figs. 6 a) and b) and is plotted versus ln(t) in Figs. 6 c) and d), correspondingly. For all lubricants at 20º C, y could be perfectly fitted by linear functions in the whole range of t. High fitting quality is evidenced from the adjusted coefficient of determination, $R^2_{adj.}$, which ranged between 0.9575 and 0.9915. The slopes differed for synthetic and semi-synthetic lubricants: for the A and C they were $(47.9\pm1.1)\times10^{-3}$ and $(49.0\pm0.8)\times10^{-3}$, correspondingly, whereas for the B, D and E they were $(67.9\pm1.3)\times10^{-3}$, $(61.2\pm1.3)\times10^{-3}$, and $(64.9\pm2.5)\times10^{-3}$, respectively. For water, fitting quality was not satisfactorily ($R^2_{adj.}<0.6$) due to large dispersion of the data. At 80 ºC y maintained the linear behaviour during the initial 15 s, although with considerably larger slopes (between 0.100 and 0.155), than at 20 ºC, and then upturned. For water the plot significantly deviated from linear function.

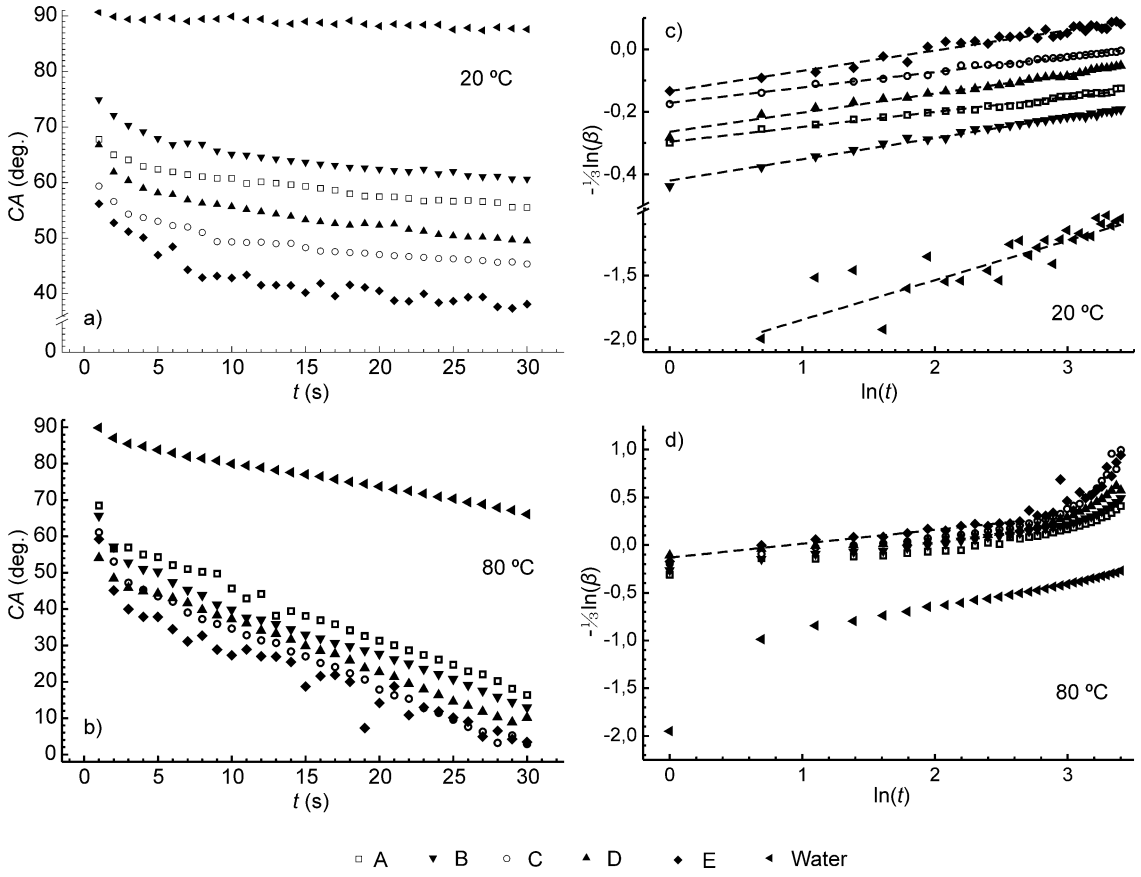

Fig. 6. The dependence of the CAs of the lubricants and water on time on H13 steel grade at 20 ºC (a) and 80 ºC (b). Plots c) and d) show fitting of the data from a) and b), correspondingly, by Tanner' model.

These findings suggest that at 20º C as well as during the initial period at 80º C the CA of all lubricants was controlled mainly by migration on the surface. This process is influenced by the oil viscosity: the slope of y increases with decreasing viscosity [32]. This explains the increase of the slope of the plots in Fig. 6 c) and d) with increasing temperature. There should be also some influence of the type of the base oil, since the slopes differed for the synthetic and semi-synthetic oils. After the initial period at 80 ºC (non-linear part of the plots in Fig. 6 d) the CA of the lubricants had to be controlled mainly by evaporation as in the case of water droplets, which shrank with time rather than spread on the surface.

3.3 The influence of water hardness and dilution rate

The effect of the hardness of water used for preparation of the lubricant emulsions is shown in Fig. 7. The lubricants mixed with hard water tended to have slightly higher LFP (an increase by 0.8±0.22%), than the

same lubricants mixed with soft water. This effect was the same for both steel grades. Increasing water hardness can enhance the LFP, while maintaining unchanged the CA.

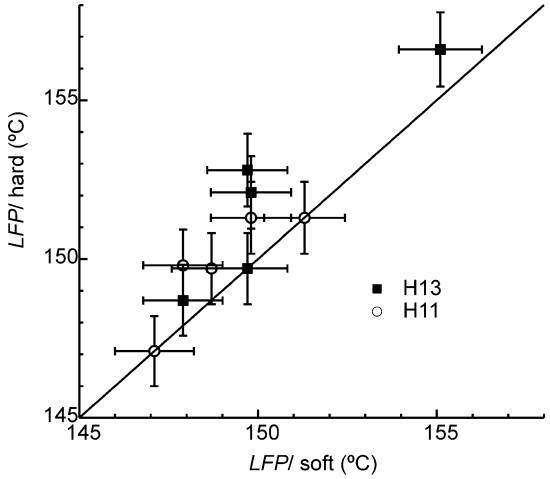

Fig. 7. The correlation of the LFP values for the lubricants mixed with hard and soft water on H13 and H11 steel grades.

The effect of the dilution rate in the range 1-3 % was examined for some of the lubricants. Additionally, a higher dilution rate (up to 20 %) was investigated for the A/H13 lubricant/steel grade combination, which showed the highest LFP in the previous tests. The results are shown in Fig. 8. The behaviour of all lubricants was the same. The LFP steeply increased (on 4.6 to 7.0 %) when the dilution rate increased from 1 to 3 % and stabilized. The increase of the dilution rate above 5% led to small decrease in the LFP. These results are in line with literature [29]. Plausible explanation of the initial improvement in the LFP is based on the consideration that a droplet with higher lubricant concentration requires higher surface temperature to produce the critical vaporization rate and to overcome the weight of the droplet to lift out from the die surface [14]. Stabilization of the LFP at the lubricant concentration higher, than 3% can be related with the saturation of the droplet surface with the surfactants, so that additional amount of the lubricant has no effect on the surface tension.

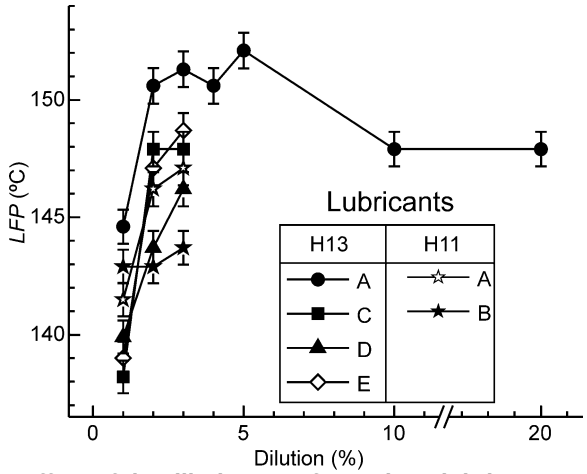

Fig. 8. The effect of the dilution rate for various lubricants on the LFP.

3.4. The influence of surface roughness and ageing

The tests were performed with the A and B lubricants on various ground or polished steel samples. The LFP increased with the surface roughness for both lubricants and both steel grades. These findings are in line with the published results on the surfaces with irregular microgeometry [22]. The increase in surface roughness leads to decrease in the real contact that hinders heat transfer between a droplet and the surface. So, higher temperature is needed to create sufficient vapour layer and establish the Leidenfrost effect.

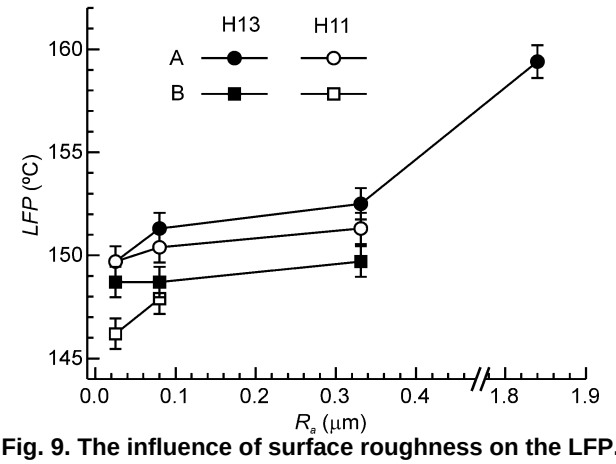

Fig. 9. The influence of surface roughness on the LFP.

In the range of R_a from 0.022 to 1.84 μm no definite correlation of the CA with the surface roughness was found. This could be due to large scattering of the experimentally measured values of the CA that ranged between 57 and 67 degrees for the H13 and between 44 and 49 for the H11. The scattering was especially notable on the samples with higher roughness.

Fig. 10 shows the effect of ageing on the LFP for the A and B. For all studied combinations of the lubricants and steel grades ageing led to considerable increase of the LFP. This effect was more pronounced for the H13. The effect of ageing can be interpreted in terms of lowering thermal conductivity of the surface oxide layer in comparison with the bare steel.

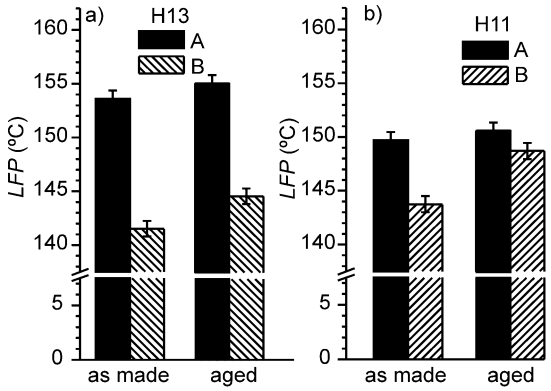

Fig. 10. The LFP for the A and B lubricants on as made and aged steel samples: (a) H13 and (b) H11.

3.5 The influence of the droplet size

Droplets of different size were obtained by varying the nozzle diameter. The LFP increased with the nozzle size for both steel grades as shown in Fig. 11. This finding is consistent with literature [25, 29, 30]. The larger droplets impinge the hot surface at higher *We* that provides better conditions for heat transfer. In addition, the larger droplets requires higher evaporation rate to produce Leidenfrost effect.

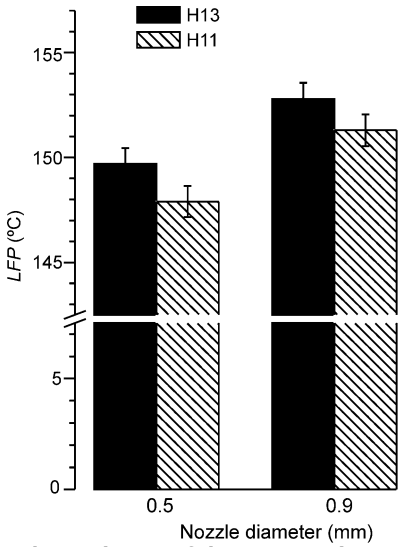

Fig. 11. The dependence of the LFP on the nozzle diameter.

As expected, the droplet size had no effect on the CA as shown in Table 5.

Table 5. Mean CA (deg.) and standard error (±*se*) for droplets obtained with different nozzle diameter on H13 and H11 steel surfaces.

Surface	0.5 mm	0.9 mm
H13	57±3	59±1
H11	59±2	56±1

Tuning the lubricant droplet size is critical for optimization of the HDPC process in terms of quality and efficiency. This is schematically shown in Fig. 12. At higher die temperature the lubricant must provide effective cooling that could be achieved by increasing the droplet size, which tend to shift the LFP to higher values. At low temperatures, typically below 180 ºC smaller droplets size may avoid working below the temperature of critical heat flow, where the risk of porosity formation in castings due to vapour bubbles is high. A lower temperature leads to faster solidification of metal, enhancing its mechanical properties due to decreasing the grain size, and improving the overall casting quality. However, the energy efficiency is low due to the need of intensive cooling of the dies.

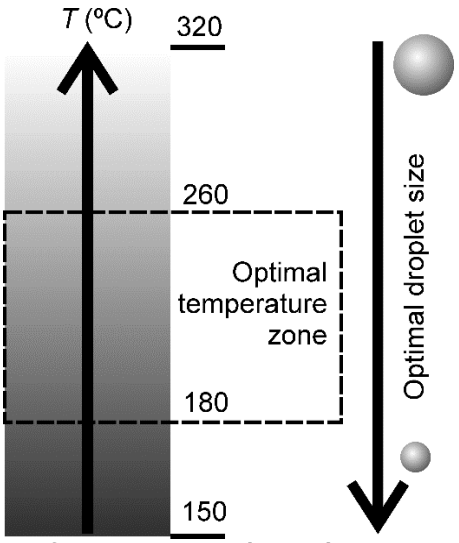

Fig. 12. Schematic drawing of temperature region and corresponding optimal droplet size.

3.6 Considerations for lubrication optimization

Simultaneous maximizing of the LFP and minimizing of the CA is the objective of the lubrication optimization pursuing to improve the heat exchange and capacity to create a film. These two characteristics are tightly and non-linearly linked, so the LFP and the CA cannot be isolated and optimized individually through tuning the lubricant composition. The present study has elucidated the dependencies of the LFP and CA on various technological parameters that lays the ground for development of practical guidelines of effective lubrication optimization. It is suggested to carry out the optimization in two steps (Fig. 13). At the first step, the CA can be minimized with respect to the possible combinations of the die material (steel grade) and the lubricant. This should be done in the temperature range corresponding to real service conditions since the CA is heavily influenced by temperature. At the second step, the LFP can be maximized through tuning the parameters which affect the CA only slightly. These parameters include the surface-related properties (surface roughness and surface oxidation state) and the lubricant-related ones (water hardness, dilution rate and the droplet size).

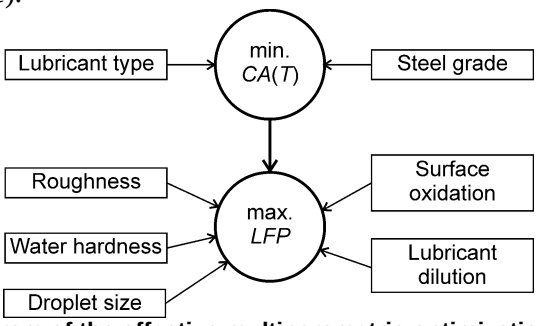

Fig. 13. Schematic diagram of the effective multiparametric optimization of the die lubrication.

For instance, for the ranges of parameters in this study the optimal configuration is the following: aged H13 steel grade lubricated with the A lubricant diluted at 3% using hard water and pulverized by a larger nozzle. In comparison with nonoptimal configuration, the LFP could be raised from 145 to 165°C, while maintaining low CA.

4. Conclusions

Multiparametric study of the LFP and the CA of five types of lubricants on two steel grades has shown that the LFP can be raised from 145ºC to 165ºC by optimization the lubricant-related and the surface-related parameters. This improvement is significant for the HPDC. The studied lubricants has been ranked according their performance with respect to the LFP in the following order (from best to worst): A, B, C, D, and E. The CA decreased with temperature for all lubricants. The synthetic lubricants A and C had a lower variation of CA with temperature, probably due to the higher viscosity index. Certain degree of positive correlation between the CA and the LFP was observed for the H11 steel grade, while for the H13 these parameters were generally uncorrelated. An optimal dilution ratio was in the range 1-3%. Above 3%, the LFP levelled out and its further improvement could not be achieved. The water hardness had positive effect on the LFP for both steel grades. This effect was especially significant for the lubricants C and D. The droplet size should be optimized considering *We* number and the temperature. Bearing in mind that the CA is not influenced by the droplet size, this parameter could be effectively utilized for tuning the LFP independently from the CA. Surface migration of the lubricants seemed to control the CA behaviour at lower temperature as well as during the initial period after placing the droplet at higher temperatures. After the initial period the decrease of the CA was ascribed to receding contact angle due to water evaporation from a pinned droplet.

The H13 steel graded tended to have better performance in terms of the CA and the LFP that could be tentatively associated to its finer microstructure. Oxidized surfaces show higher LFP, since the oxide layer, has a lower thermal conductivity that promotes surface temperature protection. The increase in surface roughness had positive effect in the LFP for both steel grades. However, no definite correlation of the CA with the surface roughness was found.

A practically significant guidelines for effective optimization of die lubrication has been suggested. It consists of two steps: first, the CA is minimized by selection of the lubricant and the steel grade at given temperature, and the second, the LFP is maximized by tuning two surface-related and three lubricant-related parameters. The optimal configuration for the given ranges of the parameters is the following: aged H13 steel grade lubricated with the A lubricant diluted at 3% using hard water and pulverized by a larger nozzle. The LFP has been significantly increased (from 145 to 165ºC) in comparison with non-optimal configuration.

Acknowledgments
The authors acknowledge the collaboration of the industrial partners from Motultech-Baraldi and SAEN s.r.l and their valuable suggestions and supplying the lubricants and the die materials. This work was funded through the European Project MUSIC (FP7-FoF-ICT-2011.7.1, under Contract nº 314145) and supported in part by the Spanish Ministry of Economy and Competitiveness (project BIA2016-79582-R) with contribution of the European Regional Development Fund.

Bibliography

[1] Zhu Y., Schwam D., Wallace J.F., Birceanu S., Evaluation of soldering, washout and thermal fatigue resistance of advanced metal materials for aluminum die-casting dies, Materials Science and Engineering: A, 379 (2004) 420-431.
[2] Bonolo F., Gramegna N., The MUSIC guide to key-parameters in High Pressure Die Casting, in, Assomet Servizi S.r.l., EngineSofft Spa, Milan, 2015, pp. 128.
[3] Muhič M., Tušek J., Kosel F., Klobčar D., Pleterski M., Thermal fatigue cracking of die-casting dies, Metalurgija, 49 (2010) 9-12.
[4] Lumley R., Deeva N., Gershenzon M., An Evaluation of Quality Parameters for High Pressure Die Castings, International Journal of Metalcasting, 5 (2011) 37-56.
[5] Fiorese E., Bonollo F., Timelli G., Arnberg L., Gariboldi E., New Classification of Defects and Imperfections for Aluminum Alloy Castings, International Journal of Metalcasting, 9 (2015) 55-66.
[6] Liu G.W., Morsi Y.S., Clayton B.R., Characterisation of the spray cooling heat transfer involved in a high pressure die casting process, International Journal of Thermal Sciences, 39 (2000) 582-591.
[7] Long A., Thornhill D., Armstrong C., Watson D., The Impact of Die Start-Up Procedure for High Pressure Die Casting, SAE Int. J. Mater. Manf., 6 (2013) 416-426.
[8] Fiorese E., Bonollo F., Battaglia E., Cavaliere G., Improving die casting processes through optimization of lubrication, International Journal of Cast Metals Research, 30 (2017) 6-12.
[9] Pautsch A.G., Shedd T.A., Spray impingement cooling with single- and multiple-nozzle arrays. Part I: Heat transfer data using FC-72, International Journal of Heat and Mass Transfer, 48 (2005) 3167-3175.
[10] Hassebrook A., Kruse C., Wilson C., Anderson T., Zuhlke C., Alexander D., Gogos G., Ndao S., Effects of Droplet Diameter and Fluid Properties on the Leidenfrost Temperature of Polished and Micro/Nanostructured Surfaces, Journal of Heat Transfer, 138 (2016) 051501-051501-051507.
[11] Bernardin J.D., Mudawar I., The Leidenfrost Point: Experimental Study and Assessment of Existing Models, Journal of Heat Transfer, 121 (1999) 894-903.
[12] Xu L., Zhang W.W., Nagel S.R., Drop Splashing on a Dry Smooth Surface, Physical Review Letters, 94 (2005) 184505.
[13] Josserand C., Thoroddsen S.T., Drop Impact on a Solid Surface, Annual Review of Fluid Mechanics, 48 (2016) 365-391.
[14] Yang L., Liu C., Shivpuri R., Physiothermodynamics of Lubricant Deposition on Hot Die Surfaces, CIRP Annals - Manufacturing Technology, 54 (2005) 253-256.
[15] Saha S., Mandal M.K., Nonami H., Hiraoka K., Direct analysis of anabolic steroids in urine using Leidenfrost phenomenon assisted thermal desorption-dielectric barrier discharge ionization mass spectrometry, Analytica Chimica Acta, 839 (2014) 1-7.
[16] Ng B.T., Hung Y.M., Tan M.K., Suppression of the Leidenfrost effect via low frequency vibrations, Soft Matter, 11 (2015) 775-784.
[17] Patterson C.J., Shiri S., Bird J.C., Macrotextured spoked surfaces reduce the residence time of a bouncing Leidenfrost drop, Journal of Physics Condensed Matter, 29 (2017).
[18] Chen S., Bertola V., Jumps, somersaults, and symmetry breaking in Leidenfrost drops, Physical Review E - Statistical, Nonlinear, and Soft Matter Physics, 94 (2016).
[19] Bernardin J.D., Stebbins C.J., Mudawar I., Mapping of impact and heat transfer regimes of water drops impinging on a polished surface, International Journal of Heat and Mass Transfer, 40 (1997) 247-267.
[20] Avedisian C.T., Koplik J., Leidenfrost boiling of methanol droplets on hot porous/ceramic surfaces, International Journal of Heat and Mass Transfer, 30 (1987) 379-393.
[21] Tran T., Staat H.J.J., Susarrey-Arce A., Foertsch T.C., van Houselt A., Gardeniers H.J.G.E., Prosperetti A., Lohse D., Sun C., Droplet impact on superheated micro-structured surfaces, Soft Matter, 9 (2013) 3272-3282.
[22] Nagai N., Nishio S., Leidenfrost temperature on an extremely smooth surface, Experimental Thermal and Fluid Science, 12 (1996) 373-379.
[23] Nevshupa R., Martinez L., Alvarez L., Lopez M.F., Huttel Y., Mendez J., Roman E., Influence of Thermal Ageing on Surface Degradation of Ethylene-Propylene-Diene Elastomer, Journal of Applied Polymer Science, 119 (2011) 242-251.

[24] Martínez L., Román E., Nevshupa R.A., X-Ray Photoelectron Spectroscopy for Characterization of Engineered Elastomer Surfaces, in: Spectroscopy, InTech, Zagreb, 2012, pp. 165-194.
[25] Clavijo C.E., Crockett J., Maynes D., Hydrodynamics of droplet impingement on hot surfaces of varying wettability, International Journal of Heat and Mass Transfer, 108, Part B (2017) 1714-1726.
[26] Arnaldo del Cerro D., Marín Á.G., Römer G.R.B.E., Pathiraj B., Lohse D., Huis in 't Veld A.J., Leidenfrost Point Reduction on Micropatterned Metallic Surfaces, Langmuir, 28 (2012) 15106-15110.
[27] Hsieh S.-S., Fan T.-C., Tsai H.-H., Spray cooling characteristics of water and R-134a. Part I: nucleate boiling, International Journal of Heat and Mass Transfer, 47 (2004) 5703-5712.
[28] Ciofalo M., Caronia A., Di Liberto M., Puleo S., The Nukiyama curve in water spray cooling: Its derivation from temperature–time histories and its dependence on the quantities that characterize drop impact, International Journal of Heat and Mass Transfer, 50 (2007) 4948-4966.
[29] Wachters L.H.J., Westerling N.A.J., The heat transfer from a hot wall to impinging water drops in the spheroidal state, Chemical Engineering Science, 21 (1966) 1047-1056.
[30] Staat H.J.J., Tran T., Geerdink B., Riboux G., Sun C., Gordillo J.M., Lohse D., Phase diagram for droplet impact on superheated surfaces, Journal of Fluid Mechanics, 779 (2015).
[31] Baraldi L., Raone C., Relazione tra la lubrificazione e lo stampo - Lubrificazione in funzione delle fasi di processo, La Metallurgia Italiana, 3 (2004) 37.
[32] Tanner L.H., The spreading of silicone oil drops on horizontal surfaces, Journal of Physics D: Applied Physics, 12 (1979) 1473.

8.4 Evaluation HPDC Lubricant Spraying for Improved Cooling and Die Protection

B. Zabala[1], A. Igartua[1], C. Raone [2], G. Timelli[3], F. Bonollo[3], V. Scarpis[1,3], M. Peggiato[1,3], F. Girot[4]

[1]Fundación TEKNIKER, Parque Technologikoa, c/ Iñaki Goenaga, 5, 20600 Eibar, Spain

[2]Motultech Baraldi, S.r.l. - Via Lombardia 2/I-2/L - 40024 Osteria Grande - Castel San Pietro - Bologna (BO) - Italy

[3]University of Padova, Dep. of Management and Engineering, Strad. S. Nicola 3, I-36100 Vicenza, Italy.

[4]University of the Basque Country, UPV-EHU, Faculty of Engineering, Department of Mechanical Engineering, IKERBASQUE, Basque Foundation for Science, Alameda Urquijo s/n 48013 Bilbao, Spain.

Abstract

This study tries to find out a better cooling and temperature homogenization as well as better die protection on high-pressure die-casting (HPDC) spray lubrication. Test procedures have been set up to study the Leidenfrost point (LFP), contact angle (CA), film thickness and protection from die soldering of lubricants typically applied into the die surfaces during HPDC process.

Five different lubricants have been studied as well as the influence in different controllable process parameters (type of die material, oxidation of the surface, temperature, roughness, droplet diameter, water hardness and lubricant concentration).

The increase of the LFP, avoiding film boiling regime, and a reduced CA, improve the cooling and film ability of die surface during spraying. The best chemistry exhibits high LFP, shows an increased thickness of the formed film and is more effective preventing the sticking of the aluminum part to the die surface. Thermogravimetric analysis shows better thermal properties for lubricants with anti-sticking performance. The study performed and the test protocols set up result in a better insight of the involved phenomena and allow selecting the most favorable operating window for HPDC lubrication.

Keywords:
HPDC, lubrication, Leidenfrost Point, Contact Angle, Film Thickness, Die soldering, thermogravimetry

1. Introduction

High-pressure die-casting is a single step process producing accurate, thin walled and very detailed light alloy parts at high productivity. Typically molten Al alloy is injected into a steel die at high speed and solidified under high pressure. When the solidification is completed and the casting cooled sufficiently, the die is opened and the diecasting is mechanically ejected by activated pins. The die surfaces are then cooled by lubricant spraying [1]. Die lubricants are sprayed onto the inner contour of the die cavities for many reasons [2]:

- to cool and balance the die temperature;
- to create a lubricating film that facilitates the filling and the extraction of the part acting as release agent;
- to create a protecting film that, together with the surface oxide layer, prevents die soldering phenomena.

The temperature variation on the die surface during spraying operation ranges from a maximum of 300ºC to a minimum of 80ºC [3]. In this range, the heat flux depends on the boiling regime as shown in Figure 1. In order to achieve optimum cooling conditions, the die surface should be able to work at temperatures below the LFP, where the heat transfer is higher. At the LFP, a vapour film forms a continuous barrier over the die surface that lubricant cannot penetrate, and the formation of the protective film that prevents die soldering is not formed. The *wettability* is the ability of a liquid to cover a solid surface, assuring full contact. This physical property is measured by the CA between the die surface and the lubricant droplet. Covering a larger area through reduced contact angle, the heat transfer capacity is improved and a wider lubricant film is formed at the die surface.

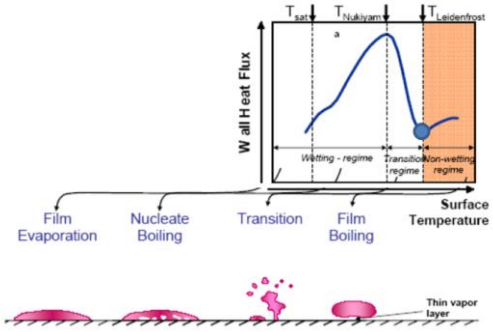

Figure 1: The boiling curve of a droplet, where the heat flux dependence on the surface temperature due to the boiling regime is shown [4].

Once the correct filming of the die surface is achieved, the chemistry and the thickness of the film are also important on the performance as release agent and protective film against die soldering. Other requirements can be requested to lubricants, for example they don't have to disturb post processes of the castings such as welding or sticking with glue, but these aspects have not been studied.

In this study, a new testing device has been setup to measure the LFP and the CA in order to understand individually the effect of different surface status (materials, roughness, oxidation), lubricant characteristics (mineral, synthetic, dilution, water hardness), temperature, spray properties (nozzle diameter). In the protocol setup, the measured LFP differs slightly from the

one in HPDC, but this procedure provides certainly independent, relative and valuable information on the nature of this phenomenon. For evaluation of the effectiveness of the formed film, film thickness measurements have been carried out, and a tribological test to evaluate the capability of the lubricant to prevent die soldering and the frictional behaviour as release agent has been set up. Finally, differential scanning calorimetry and thermogravimetric (DSC/TGA) tests have been performed to the lubricants.
The results and test procedures are expected to be useful for improving the lubricant selection and film formation, the cooling and the temperature homogenization of the spraying process during HPDC.

2. Materials and methods

2.1 Materials

Five different lubricants for HPDC applications have been used for this study, supplied by Motul-Baraldi in the form of concentrated lubricant and hereafter named A, B, C, D, E. The lubricants are generated from a concentrated solution composed by a 20-30% of an anhydrous part that is usually diluted in water once time more with a rate from 1:50 to 1:100 [2]. The active part, made of a blending of oils, polysiloxanes, polymers and many additives, gives the main characteristics to the film that forms on the die cavity after water vaporization. Together with the anhydrous part, there are the emulsifiers, normally surfactants, which have the aim to join the oil and water and to increase the filming power on the die surface [5].
Based on the typical classification of metal working fluids [6], the B, D and E lubricants could be classified as semi-synthetic lubricants, since they contain mineral oil with a viscosity index estimated around 90; the A and C lubricants are synthetic ones with a viscosity index estimated around 180. The A and C lubricants offer a very high releasing power for average to big weight diecastings. The B lubricant is particularly indicated in the case of thin walled components with a low weight, and the D and E lubricants for general purpose, not recommended to any specific kind of diecast parts.
The reference dilution was 1:50 (2%) but other ratios were studied as well, from 1% up to 20%. The surface tension of lubricants diluted at 1:50 was measured according to the ASTM D-971-99 standard. The dilution were made mostly with tap water (7.52 ºdH German grade, 53.6 mg/l Ca^{+2}, <1 mg/l Mg^{2+}) and artificially generated hard water (17.9 ºdH, 96.8 mg/l Ca^{+2}, 18.7 mg/l Mg^{2+}).
Table 1 shows the measured surface tension values for the analysed lubricants. It is important to highlight that these HPDC lubricants at such a small dilution rate as 2% drastically reduce the water surface tension from 72 mN/m to around the half of this value.

Lubricant	Surface Tension (mN/m)
A	48.7
B	53.2
C	35.1
D	33.9
E	31.5

Table 1. Measured surface tension of the analysed lubricants at 2% dilution ratio.

Two different type of steels, AISI H13 and H11, were selected for the study, since they are the most common die materials in HPDC [7].

2.2 Leidenfrost point and contact angle measurement

Experimental measurements were carried out by a SURFTENS universal goniometer shown in Figure 2, which was used for the determination of the LFP, as well as the CA. The apparatus used here is similar to that described in [8] used for the similar purpose, but its main advantage is the capability of measuring both the LFP and CA. The universal goniometer was modified by IK4-Tekniker from original version to be able to measure CA at high temperature and the LFP.

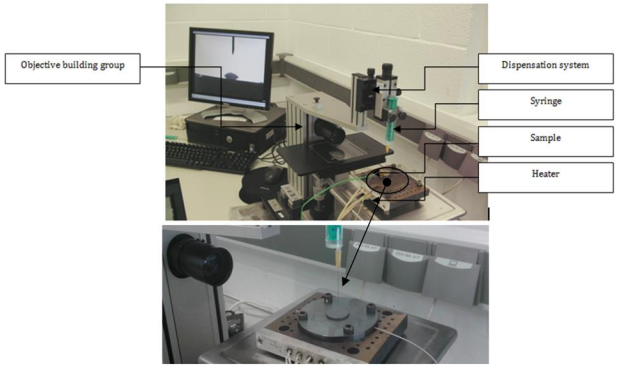

Figure 2. The universal goniometer modified by IK4-TEKNIKER to carry out high temperature measurements.

The equipment is composed by a fixed structure with an objective building group, an illumination unit and a droplet dispensation system, which was here used with two different nozzle diameters, 0.5 and 0.9 mm respectively. Most of cases were performed with the 0.5 mm diameter, except for dedicated tests used to study the influence of the droplet size. The sample is located over an electrical resistance heater fixed to a mobile structure. In order to check the temperature, a K-type thermocouple is placed into the sample and connected to a control unit.
The criterion used to identify the LFP was to increase the temperature progressively, in order to identify the temperature when the film boiling regime began. A screening of the lubricant impact behaviour at the surface was recorded. After each droplet falls to the hot surface, the sample is rotated to carry out further test in a new area that is not contaminated by previous lubricant droplets.
The same system is used to evaluate the contact angle. When the droplet falls from the dispensation system onto the surface, automatic measurement and data recording of CA is made from identification of 5 points of the droplet shape, and a CA value is reported as the mean given by the data acquired during 30 seconds. Each measurement was repeated at least four times. The heating device was used to heat the surface at 25, 50 and 80ºC, respectively, in order to evaluate the CA at different temperatures.

2.3 Die soldering protection measurement

A reciprocating pin-on-disc test, where a cylindrical pin of aluminium EN-AC-43500 is forced to move against a mould material in AISI H13 steel disc, has been used for evaluating the performance of lubricants to prevent soldering and as release agent.

To create good conditions to simulate the presence of the lubricant film on the disc surface, a procedure to create a lubricant coating on the disc surface has been set up, based on resistance heating. About 1 ml of pure lubricant was progressively deposited on the H13 surface at 130ºC, resulting in a homogeneous and well distributed lubricant film.

The machine used is a SRV©. The testing temperature is selected as close as possible at HPDC die surface. A low temperature condition (~365ºC) has been selected to study the phenomena in a range of temperature that is equal to the average surface temperature in real HPDC process,

and a higher temperature (~450ºC), which is the maximum value of the die temperature during die filling.

The basic normal load and sliding speed selected to reproduce the wear mechanism were 50 N and 25 Hz. The stroke was kept constant at 2 mm. To investigate this effect, different level of pressure and speed were considered: 20-50-125-200-300 N and frequencies of 10-25-35Hz.

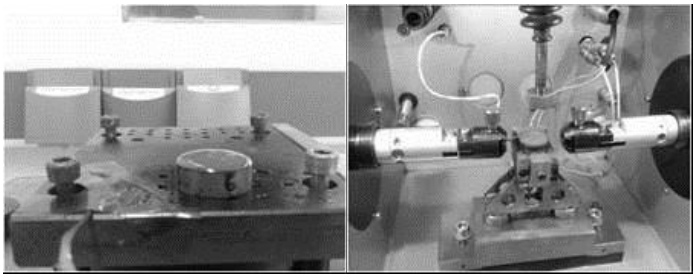

(a) *(b)*

Figure 3. (a) Preparation process of the sample with a ''coating'' of the lubricant and (b) sample that is ready to start the pin on disk test

In order to evaluate the effectiveness as release agent, the stable initial value of friction was considered. It was not not identified a big difference between lubricants friction behavior as shown in the Table 2. As output for die soldering prevention the time to lubricant failure has been identified to be good indicator of lubricant effectiveness. The failure is measured when the friction coefficient rises from the stable value of 0.1-0.2 to a value of around 1 of friction coefficient.

2.4 Film thickness measurement

The procedure for film thickness formation of lubricants is quite simple. A lubricant film is formed similarly to the samples of pin-on-disc tests and leaving drying for 5 hours. Afterwards a general tool for measuring thickness's of non-magnetic coatings, EASY-CHECK FN from NEURTEK Instruments, is used for thickness measurement, shown in Figure 4. About 20 measurements are taken in different points of the sample surface.

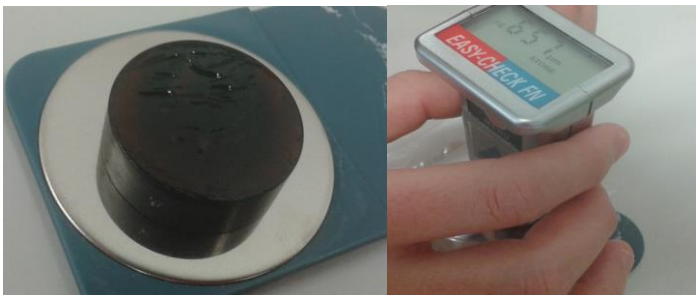

(a) *(b)*

Figure 4. (a) Steel sample coated with a lubricant film and (b) thickness measurement device

2.5 DSC/TGA measurement

This test has been made with a pure lubricant with an initial mass equal to 40 mg. Different lubricants have been tested to evaluate the effect of the temperature in lubricant degradation.

The range of temperatures investigated in the dynamic thermal test were from 50 up to 700°C. The heating rate was 10°C/min using N_2 atmosphere. Isothermal tests have been performed in the range from 350 to 425ºC.

Figure 5. Lubricants ready to be tested in the DSC/TGA test

3. Results and discussion

3.1 LFP and CA measurements

LFP and CA for different water based lubricants in H11 and H13 hot work tool steels

Tests to search LFP were carried out with liquids diluted in soft water, both for H13 and H11 samples. The results are reported in Figure 5.

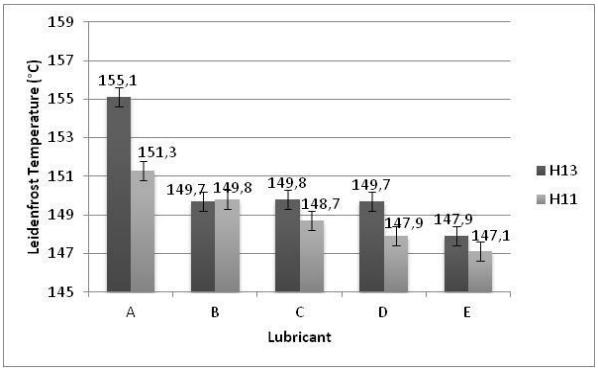

Figure 5. The LFP for soft water-based lubricants on H13 and H11 die materials.

The differences between lubricants, on the value of LFP, are probably due to the different formulations and additives. For both die materials, lubricant A has the highest LFP and lubricant E has the lowest LFP, while B, C and D are similar. The LFP is typically higher for H13 for most of the lubricants.

Regarding the CA values for different lubricants, shown in Figure 6, there is a wide range of values from almost 70º to below 15º depending on lubricant and surface temperature. It is shown, a reduction of contact angle when increasing the temperature, but not all lubricants reduce their values in the same way. The synthetic lubricants A and C, have less differences in contact angle at different temperatures with both steels, H13 and H11. This is probably due to their higher viscosity index due to their synthetic nature that means a lower dependence of the viscosity with the temperature. All the semisynthetic lubricants have a similar behaviour.

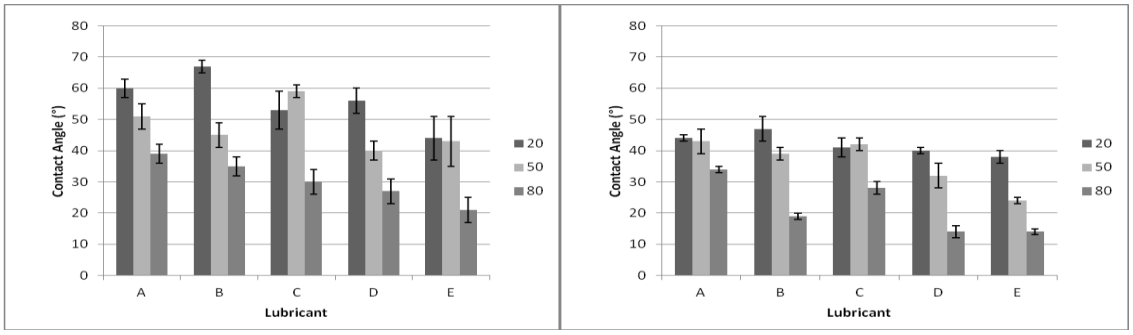

(a) **(b)**

Figure 6. The CA at 20, 50 and 80°C on (a) H13 and (b) H11 steels

The trend of these curves highlight that the LFP decreases with the decrease of contact angle (CA). An explanation for this phenomena could be that a less wettable liquid has less contact area with the surface, but its weight is the same. Thus, the higher pressure makes necessary a thicker vapour layer to sustain the droplet, then this layer will be created at higher temperature.

Study of effect of different parameters on LFP and CA

- A study of the different variables that affect LFP and CA was done and the results can be here summarized.
- The variation range of the LFP for all the studied cases is in the range 140-165ºC. These differences are significant for HPDC.
- The variation range of contact angle for all the studied cases is in the range 15-70 degrees; the repetitions show up to 5 degrees of deviation.
- The lubricant ranking of LFP for all the cases shows: highest value for A, lowest value for E and in the middle similar values for B, C and D.
- The higher the temperature, the lower is the contact angle. In general the lubricant CA values at 80ºC present a similar behaviour to temperatures near LFP.
- The CA decrease is less pronounced for some lubricants. The synthetic lubricants A and C, have a lower variation of CA with temperature, probably due to the higher viscosity index of this type of lubricants.
- The lubricant ranking of CA, even if it is not the same ranking for the 3 tested temperatures, is similar to the LFP ranking. In fact, more hydrophobic combinations (higher contact angle) tend to have higher LFP.
- The LFP and CA for H13 are a bit higher than H11 probably due to their finer grain microstructure.
- The hardness of the water used for the formulation of the lubricant has some influence in the LFP for both steels H13 and H11. In general, the harder the water, the higher was the LFP being this behaviour especially significant for lubricants C and D.
- Oxidized surfaces show higher LFP, since the oxide layer, has a lower thermal conductivity that promotes surface temperature protection.

- A higher lubricant percentage (1-3%) leads to higher LFP. Above 3%, it is not observed further increase.

- Rougher surfaces have higher LFP both for H13 and H11 steels, but the CA variation depends on the type of steel and their microstructure. In the H13 with a finer microstructure, the contact angle increases with the roughness, they present a hydrophobic behaviour and it seems to fulfil Cassie's model [12] where the liquid doesn't penetrate the roughness. The H11 seems to follow the Wenzel's model [12] range where liquid penetrates in roughness grooves, and the contact angle decrease when increasing the roughness.

- Higher droplet size shows higher LFP, in line with prediction from We number [11]. Wettability seems not to be influenced by droplet size, being the droplet size, a parameter that could play a good role trying to maximize LFP keeping low the contact angle.

- Die cast lubricants get lower surface tension, CA and LFP values than water. The droplet of the lubricant flattens after impact and then it evaporates, while water evaporates without an increase of surface contact.

- The combination of several factors make synergic the improvement, increasing further LFP. An increase of 25ºC in LFP relative to the reference, were achieved combining a high droplet size 0,9mm diameter, with 3% of lubricant A, diluted on hard water, on an oxidized sample, with high roughness.

3.2 Time to film failure on pin-on-disc tests

The lubricant behaviour and its tendency to be washed from the steel surface depend on many factors such as: pressure, speed, temperature and surface conditions. The main parameter that affects this tendency isn't a physical variable but it's a chemical parameter. The chemical composition (especially the amount and typology of additives) describes the desorption tendency of the lubricant.

Regarding the physical parameters, as it is shown in the response surface created from experimental results shown in Figure 7, temperature was the most important parameter (as exponential dependence), followed by Pressure (logarithmic dependence), while the speed didn't show any influence. This is in accordance with Fick diffusion law, which also rules die soldering mechanism [21].

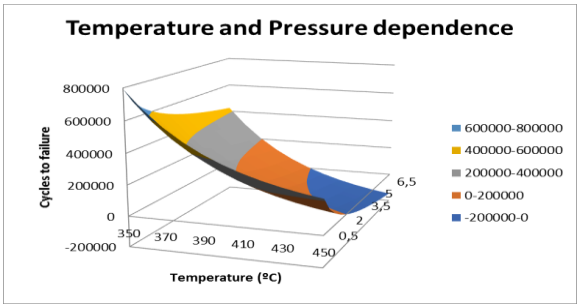

Figure 7. Surface response of time to failure for the A lubricant dependent of Temperature and Pressure

The time to failure ranking of lubricants was similar to the one of LFP. The table 2 shows these results, being A lubricant the one that lasted more followed by C and D, while B and E where the worst.

	A	C	D	E	B
Time to Failure (cycles)	39750	21625	16025	6500	5000
COF (-)	0,167	0,166	0,177	0,155	0,187

Table 2. Time to failure and friction coefficient of the different lubricants in the pin on disc tests at 50N, 25Hz and 365ºC

3.3 Film thickness measurements

The resulting film thicknesses are shown in Figure 8. The scattering of the data is quite big because the film thickness is not totally flat, since it is a curvature of the film and have some irregularities. The mean value shows an important difference between the lubricants. The lubricant A had the highest film thickness (400µm), followed by C (~300µm), D (~250µm), while B and E, have the thinner thickness (<200 µm).

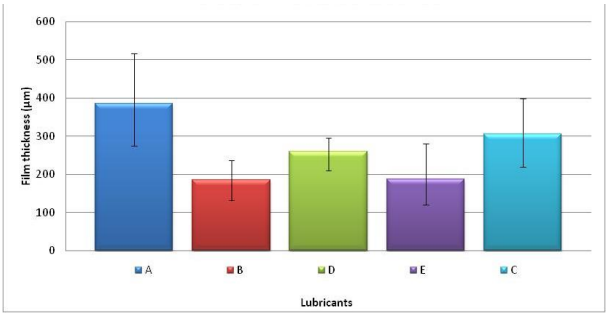

Figure 8. Results of film thickness measurement

3.4 TGA tests

It has been observed that the main element that affects the degradation mechanism of the protective film is the temperature; it leads to an increasing desorption tendency of the lubricant and a chemical degradation of it. These two aspects have been studied with another chemical test, the TGA test. This TGA test has been divided in two different parts: the isothermal and thermal dynamic tests. The first one has the scope to evaluate the effect of the time at high temperature conditions, and the second one has the aim of evaluating the effect during temperature variation.

The dynamic tests have shown that the lubricant has a very high initial degradation (at 100°C) because of the evaporation process. The degradation doesn't carry on until 375°C; above this temperature there's a high degradation process that causes a complete degradation of lubricant above 475°C. In this degradation process it is a difference between the different lubricants (Figure 9).

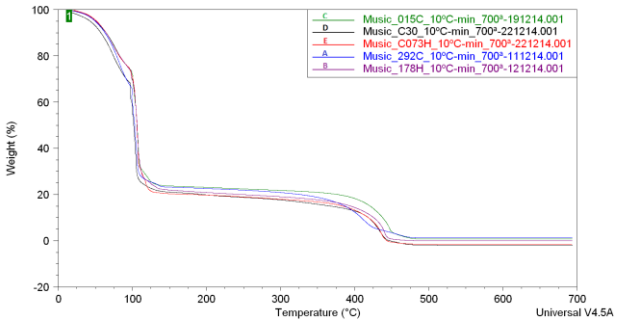

Figure 9. Results of non-isothermal / dynamic test of the analysed lubricants

The isothermal test of the lubricant have been carried out at 350°C and at this temperature, after 3,5 hours, the degradation process isn't complete. At 425°C (Figure 10) the total degradation of the lubricant appears after about 30 minutes of test. The ranking of degradation process in isothermal tests and dynamic tests was the same, and as it is as well coincident, with the already stated at film thickness measurements.

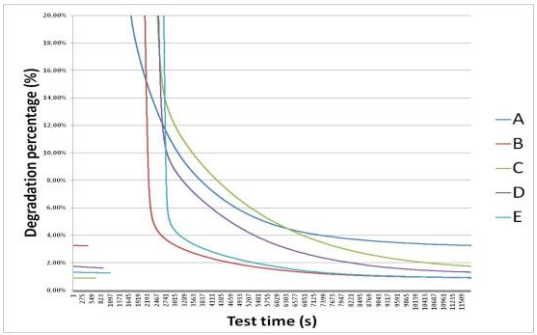

Figure 10. Results of isothermal DSC-TGA tests at 425ºC carried out on the analysed lubricants

4. Conclusions

Taking into account the requirements of lubricants used for the spraying of HPDC die surfaces, different experimental procedures have been set up. It included Leidenfrost point, contact angle and film thickness measurements for the evaluation of filming capacity and effectiveness on heat extraction. Effectiveness for die soldering prevention was tested through pin-on-disc tests. Thermogravimetric TGA tests were performed to evaluate the thermal behaviour of lubricants.

Good correlation was found between filming capacity (Leidenfrost point, contact angle stability at high temperature, film thickness), TGA of lubricants (thermal behaviour) and time to failure during pin-on-disc tests (die soldering prevention).

In these tests the best lubricant is the A followed by the C, both lubricants contains in their formulation synthetic oils with a high viscosity index. Lubricants D, B, and E in this order follow in the best performance ranking.

Isothermal TGA test at 425ºC has been found as a suitable test for screening of big amount of lubricant formulations, which will give an idea of their behaviour on the mould, due to the correlation found between the different tests. The rest of the tests can be used for more detailed studies or when the evaluation of a specific characteristic of the lubricant (i.e. high LFP or high die soldering protection) is needed.

5. Acknowledgments

This work was developed within the European Project MUSIC (MUlti-layers control & cognitive System to drive metal and plastic production line for Injected Components, FP7-FoF-ICT-2011.7.1, under Contract nº 314145). The authors would like to thank other laboratory colleagues that have contributed to the success of this work.

6. References

[1] F. Bonollo, N. Gramegna, The MUSIC guide to key-parameters in High Pressure Die Casting, ISBN 978-88-87786-10-1.

[2] L. Andreoni, M. Casè, G. Pomesano, "Lubrificazione della cavità dello stampo", Quaderni della colata a pressione delle leghe di alluminio 7, 1996, pp.9-26.

[3] J.L. Graff, L.H. Kallien, "The effect of die lubricant spray on the thermal balance of dies", Paper T93-083, NADCA Meeting, Cleveland, 1993

[4] Simultaneous Measurements of droplet characteristics and surface thermal behaviour to study spray cooling with pulsed sprays" by Humberto M Loureiro, Miguel R A Panao, Antonio Luis L Moreira of Mechanical Engg Dept Instituto Superior Tecnico at Lisbon Portugal.

[5] L. Baraldi, C. Raone, "Relazione tra la lubrificazione e lo stampo - Lubrificazione in funzione delle fasi di processo", La Metallurgia Italiana 3, 2004, p.37

[6] P.Bittorf, S.G.Kapoor, R.E.DeVor, "Transiently Stable Emulsions for Metalworking Fluids", Department of Mechanical Science and Engineering University of Illinois at Urbana-Champaign, December 2011

[7] L. Andreoni, M. Casè, G. Pomesano, "Il lavoro termico dello stampo", Quaderni della colata a pressione delle leghe di alluminio 5, 1995, p.9.

[8] N. Nagai, S. Nishio, "Leidenfrost temperature on an extremely smooth surface", Exp. Therm. Fluid Sci.12, 1996, pp.373-379

[9] K. Domkin, J.H. Hattel, J. Thorborg, Modeling of high temperature- and diffusion-controlled die soldering in aluminum high pressure die casting, Journal of Materials Processing Technology 209 (2009) 4051–4061

[12] J. C. Berg, "Wettability", Ed. Marcel Dekker, ISBN: 0824790464.

[11] J.D. Bernardin, C.J. Stebbins, I. Mudawar "Mapping of impact and heat transfer regimes of water drops impinging on a polished surface", Int. J. Heat Mass Transfer 40, 1997, pp.247-267